Modelling, Optimisation and Control
of a
Falling-Film Evaporator

A thesis presented in partial fulfilment of the requirements for the degree of
Doctor of philosophy
in
Production Technology

at
Institute of Technology and Engineering
Massey University
Palmerston North
New Zealand

Shabeshe Paramalingam
2004

Acknowledgements

My primary thanks are to my supervisor, Dr. Huub Bakker, for his support, guidance, friendship, patience and encouragement throughout this project. Without his direction, motivation, committed attitude, help and advice this project would never have succeeded.

I would like to express my appreciation to my second supervisor Dr. Hong Chen, Fonterra-Ingredients, Whareroa, Fonterra Co-operative Ltd, for sharing his wealth of knowledge in evaporation and drying technology and for his support during this project. I thank him also for providing me with the tools, permission to conduct trials in a commercial evaporator and support to complete my project successfully. I really appreciate his encouragement and helpful attitude. My thanks go also to Clive Marsh for his valuable input to this project. I appreciate him spending his valuable time in supporting this project.

I would like to thank many staff at Whareroa with whom I have had the privilege to become familiar during my time at site. Special thanks go to the whey products managers, supervisors and operators for their encouragement, support and involvement during the evaporator trials.

Thanks to the Foundation for Research in Science and Technology for their sponsorship through the Graduate Research in Industry Fellowship programme. I am indebted to the staff of the Institute of Engineering and Technology, Massey University, New Zealand, for assistance with this work and for the facilities provided. Also thanks to my colleges and friends who made my time at Massey very enjoyable.

I would like to thank the Hawera community, in particular Neil and Helen Walker, for their hospitality, support and friendship during my stay. Finally, I would like to express my special thanks to my wife, Ahalya for her encouragement, patience and moral support throughout this project.

Acknowledgements

Contents

PART-3   Model applications

PART-4   Conclusions, recommendations and future work

List of figures

Contents

Contents

List of tables

<u>Summary</u>

Falling-film evaporators are widely used in dairy industry for concentrating products. With increasing demand and competition, there is always a need for process improvement. This is made more difficult when using the same evaporator for concentrating different products. Therefore, it is vital to gain a greater understanding of the industrial falling-film evaporator process. This is possible through process modelling.

The aim of this work was to improve the process of whey products evaporation at Fonterra Ingredients-Whareroa, Fonterra Co-operative Ltd. This was done by an investigation of the evaporation process and optimisation of the operating conditions. Mathematical models were derived for this purpose, including dynamic and steady state models for the evaporator system and models for the physical properties of whey products. Complete evaporator simulations were established for process understanding, optimisation, and control. The steady state model was used for optimisation studies and the dynamic model was used for controllability studies.

Experiments were carried out on the physical properties of whey product. Regression models were developed in relation to the total solids concentration and to the temperature. Physical properties were also estimated from literature semi-empirical models (model constants were identified using the experimental data) and compared with the experimental values. The application of regression models is limited to one product within a predefined operating range with less than 5% error. The semi-empirical models are applicable to a variety of products and in a wider range of operating conditions with less than 10% error. The liquid height above the distribution plate in the evaporator is important to filter high frequency feed disturbances. The discharge coefficient has strong influence on the liquid height prediction but there were no investigation in the literature that applicable to the evaporator. Experiments were conducted to measure the discharge coefficient and to investigate how orifice shape affects discharge coefficient. The distribution plate model

derivation was improved and showed that the distribution plate thickness influences the discharge coefficient and discharge flow calculations.

Trials in a commercial evaporator showed that protein content has no influence on the evaporation process. Protein type, air content and viscosity have a significant influence on the evaporation process. A modified evaporator configuration proved that poor evaporator performance for whey protein isolate is caused by the heat treatment given prior to the evaporation. It was shown that 15% increase in the evaporator capacity can be achieved when operating at optimum operating conditions compared to standard industry practice. The energy savings resulting from the optimisation was about NZ$70,000/season.

The plant controllability studies focused on the disturbance rejection capabilities of current control loops, product density and effect temperature. Experience has shown that the use of a single feedback PI controller for product density control is not sufficient. The applicability of a cascade controller to this problem was tested and was shown that the disturbance rejection properties can be significantly improved.

Overview of work and contribution

A brief overview of the research work and the contributions made to the field of falling film evaporator modelling and control are outlined.

1) Modelling of a two-effect thermal vapour recompression falling film evaporator Fonterra Ingredients-Whareroa, Fonterra Co-operative Ltd.
   a. Dynamic modelling.
   b. Steady state model development and complete evaporator simulation.
   c. Linear dynamic model development and complete evaporator simulation.
   d. Identification of model constants.
   e. Model testing with whey products, water and milk products.

2) Product Property models **("Physical properties of whey product", Journal of Food Technology, February 2003, pp. 8 -15)**
   a. Experimental data on density, viscosity, contact angle and surface tension of whey products.
   b. Calibration data of Refractive Index against the actual total solids concentration of whey products.
   c. Regression equation for actual total solids concentration as a function of Refractive Index of whey products.
   d. Regression equation for density and viscosity as a function of temperature and total solids concentration.
   e. Semi-empirical models for density, viscosity, thermal conductivity and specific heat capacity.
   f. Model testing of whey products, milk products and water.
   g. Investigation and measurements of the discharge coefficient for different products.

3) Optimisation of falling-film evaporator (*Journal of Food Engineering, submitted*))
   a. Determination of the optimum operating conditions for each whey product.
   b. Heat transfer coefficient data for whey products.
   c. Improved preheat condenser performance by re-routing the non-condensable gas line to the vacuum pumps.
   d. Demonstration of the need for correct control valve sizing and control of steam pressure in the falling film evaporator.
   e. Demonstration that the total whey protein content has no influence on the heat transfer coefficient but that the protein type and the product viscosity do.
   f. Demonstration from trials that the heat transfer coefficient of high whey protein content products can be improved with low heat treatment prior to the evaporator.

g. Demonstration of the need for increased feed flows with water pre and post product runs to avoid fouling due to film breakdown.

h. Demonstration of the need for viscosity measurements in the whey evaporator to determine the optimum solids concentration.

4) Cascade controller design for concentration control in a falling-film evaporator (**Journal of Food Control, in press**)
   a. A complete evaporator simulation with one pass model and three pass model.
   b. Demonstration that the feed solids and the 2nd effect temperature have significant influence on the product total solids concentration compared to the feed temperature.
   c. Demonstration that the 2nd effect temperature control is quick and can be tuned so that it can be assumed to be constant.
   d. Demonstration that the product total solids control is slow due to the large falling film residence time and pipe delays.
   e. Demonstration that the use of cascade control for controlling product total solids improved the disturbance rejection bandwidth, allowing the controller to be tuned to correct the disturbances quickly.

5) Recommended future work
   a. Study of the influence of the compositions, component interactions and shear rate on the viscosity of whey products. Development of a generic viscosity model for both milk and whey products.
   b. Measurement of thermal conductivity of whey products, development of a reliable method for measurement of air content in the product and development of a generic model that can calculate the film heat transfer coefficient from product composition.
   c. Study of the influence of whey protein types and their interactions at different temperatures on foaming and its relevance to the film heat transfer coefficient.

Introduction

Falling-film evaporators in the dairy industry are key process units where most of the water is removed in the production of milk and whey powders. Evaporators of two to eight effects are common in the dairy industry. Mechanical vapour recompression is widely used to increase the energy efficiency of the evaporation process. A Thermal vapour recompression is used to control the final total solids concentration exiting the evaporator at Fonterra-Ingredients, Whareroa. Previous research into the performance of dairy evaporators has focused largely on milk evaporators (Choudhary, 1996; Runyon et al., 1991; Quaak & Gerritsen, 1990; Quaak et al, 1994; Winchester, 2000). The performance of the whey evaporator at whey products was completely different (see Chapter-9) to the performance with milk products (Winchester, 2000). This could be due to the difference in the physical and chemical properties (discussed in Chpter-3).The aim of the current study was to apply mathematical modelling to the optimisation and control of a two-effect thermal vapour recompression evaporator for whey products at Fonterra Ingredients-Whareroa, Fonterra Co-operative Ltd. The purpose of this study is to solve the problems (low throughput, fouling due to film break-up, increased energy consumption and unknown running conditions for each product) currently experienced with the evaporator at whey products. Figure 1.0 illustrates a general whey powder process at Whareroa (see section 2.2).

The manufacture of protein ingredients from cheese and casein whey has evolved during the last fifty years into an established part of the world dairy industry (Bylund, 1995). Raw milk is variable in its composition (see Appendix A-3) and most dairy products can be produced in a variety of ways from this milk. Therefore, it is not surprising to find significant variations in reported values for the physical properties of dairy products (Bloore et al., 1981; Snoeren, 1982; Murakami and Okos, 1989; Fernandez-Martin, 1971; Jeurnink and Kruif, 1993; Antonio, 1983; Adam et al., 1994; Middleton, 1996). A major problem in the processing of whey protein ingredients is variation in final product properties (foamability and solubility index) due to factors relating to protein denaturation

during processing and to the high variability of raw material composition. These interrelated factors include the source of raw material (whey), cheese manufacturing practices, heat treatment history, protein fractionation procedures and storage conditions (Bloore et al., 1981). The processing of whey powder, types of whey products and their properties are discussed in Chapter 2.
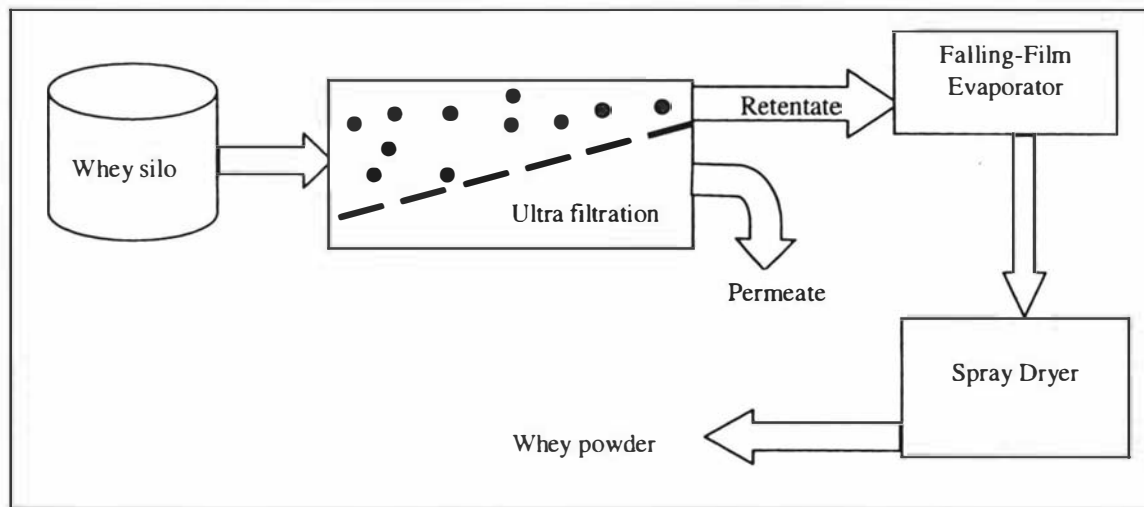
Figure 1.0: Schematic diagram of the whey powder process

The viscosity of whey concentrate after evaporation is one of the most important process input variables in the manufacture of whey powders as it influences the powder quality (Mackereth et. al, 2003). Total solids, temperature, heat treatment, composition, holding time and pH all influence the viscosity of the whey concentrate. The density of whey concentrate is important in the processing and handling of concentrates, as it is an indirect measure of total solids and could be used in estimating the air content of the raw whey. Advancing contact angle and surface tension are also important parameters in the minimum flow calculations in falling-film evaporators. The experimental work discussed in Chapter 3 investigated the effect of temperature and total solids on the physical properties of whey concentrates. Theoretical models were developed to calculate the physical properties of whey concentrates from the properties of individual components comprising the whey concentrates. The discharge coefficient measurements are discussed in Chapter 4.

2

Chapter 5, 6 & 7 discuss the evaporator model derivations and develop improvements to an existing dynamic mathematical model of a falling-film evaporator for milk. The derivations are dealt with under several different areas—preheat condensers, evaporator sub-system and thermal vapour recompression (TVR)—following the sub-system structure introduced by Quaak & Gerritsen (1990).

The tasks involved in this included deriving dynamic evaporator models (Chapter 5 & 6), developing steady state models and identifying all the physical constants in the models (Chapter 7), verifying that the model ran correctly (Chapter 7) and validating the new model against plant data from the new evaporator set (Chapter 7). The purpose of the steady state model development was to investigate the operation of the evaporator systems at different operating conditions for each whey product. In Chapter 8 the linear dynamic models are derived and a complete linear dynamic model is developed for the controllabiliy studies.

The different whey products that are concentrated in the Fonterra evaporator studied in this work are cheese Whey Protein Concentrate (WPC-1), high fat Whey Protein Concentrate (WPC-2), casein Whey Protein Concentrate (WPC-3) and Whey Protein Isolate (WPI). Chapter 9 discusses the optimisation of the evaporator conditions for these different whey products. This involved using the mathematical model plus the product property data to perform sensitivity tests on the evaporator process variables and thereby identify the key variables. Optimisation was then performed on the key variables to maximise throughput subject to final product composition targets, foaming limits, fouling limits and minimum product flows in each evaporator effect.

With the evaporator optimised, the ability of the evaporator to maintain the process variables close to the target value was investigated. Control of total solids concentration exiting the evaporator and the 2nd effect temperature are the crucial control loops in the whey evaporator. To get consistent powder quality, any disturbance that occurs in the process should be rejected before it significantly affects the total solids concentration. A

3

controller with sufficient disturbance rejection bandwidth was therefore required to get better performance out of the control operation. Chapter 10 discusses the controllability studies and the ability of the controller to reject the disturbances. This chapter also investigates the applicability and design of a cascade controller to improve the disturbance rejection bandwidth, for the control of total solids concentration.

2. Background

This chapter introduces whey and whey proteins, how they are separated, their properties and their applications. It then provides information on different types of evaporators, their operating principles and applications. The falling-film type evaporators and the falling-film evaporator used in the whey products application at Fonterra-Ingredients, Whareroa, Fonterra Co-operative Ltd are then described. Finally, the control loops in the Fonterra whey evaporator and the method and importance of the relative gain array (RGA) are discussed.

2.1 Whey and Whey Proteins

2.1.1 Whey

Whey is a valuable by-product resulting from cheese and casein manufacture. Of the total volume of milk that enters the cheese and casein process, 80-90% will leave the process as whey. This contains approximately 50% of the total solids of the original milk. Whey from the manufacture of cheese and rennet casein is "sweet whey" with a pH of 5.5-6.0, whereas the manufacture of casein using acid for coagulation results in "acid whey" with a pH of 4.3-4.6. Whey is a very complex mixture of many constituents and some are highly valuable in their isolated forms (Bylund, 1995).

2.1.2 Whey proteins

Cow's milk contains approximately 3.6% by weight protein. Of the total milk protein, approximately 80% is casein protein and 20% is whey protein (Bylund, 1995). Casein protein is separated from the milk in the cheese and casein processes. The whey from these processes is rich in whey protein. The types of protein present in the whey are β-lactoglobuline, α-lactalbumin, immunoglobulins and minor proteins (e.g. bovine serum albumin, proteose-peptone, lactoferrin and glycomacropeptide). The protein profiles in the final product are very dependent on the source of the whey and on the whey process.

2.1.3 Whey protein denaturation

The majority of the valuable functional properties of whey proteins are associated with a globular native state. The native state of whey proteins can be disrupted physical and chemical factors resulting in denaturation and ultimately aggregation and precipitation under certain conditions. The loss of the native state of the protein reduces the

functional properties (solubility, emulsification and gelation), while the unfolding and precipitation reduces the efficiency of heat exchangers. Therefore, whey protein denaturation (partial unfolding or complete denaturation) should be avoided during whey processing (see Chapter-9).

The denaturation of protein can be defined as any process that causes changes in the structure of a protein without rupturing the covalent bonds in the polypeptide (Fox, 1992). It is restricted to changes in the secondary and tertiary structure. Denaturation is therefore, a process by which hydrogen bonds and hydrophobic interactions are broken and the protein is unfolded.

Denaturing agents can be divided into two classes: physical and chemical. Heat is the most important physical agent. The rate of protein denaturation is highly dependent on temperature, increasing exponentially with increasing temperature. The pH of the medium also has a profound effect on the denaturation of proteins. High concentrations of compounds that tend to break hydrogen bonds, such as synthetic detergents and organic solvents also cause the denaturation of proteins.

Most whey proteins are heat sensitive and undergo a permanent denaturation at temperatures above 60°C; the degree of denaturation depends on the protein component, total protein content, pH, temperature and time of exposure (Oldfield, 1996). The relative heat stability of the individual whey proteins varies as follows: immunoglobulins < bovine serum albumin < β-lactoglobuline < α-lactalbumin (Oldfield, 1996). It was shown (Haggarty, 1995) that changes in the conformation of β-lactoglobuline begin upon heating to 40°C with the complete loss of secondary and tertiary structure above 65°C. The transition temperature could be lower than 40°C for immunoglobulins and bovine serum albumin as these are more temperature sensitive compared to β-lactoglobuline.

2.1.4 Whey protein foaming

Foams are formed by the entrapment of air, which is enveloped by the protein. The foaming ability is an important functional property (see Figure 2.5) of the final product but it is undesirable during processing.

Mechanism of foam formation

Foams are composed of air, water and protein (surface active agent). A thin continuous film envelops the air bubbles with adjacent bubbles separated by lamellae. Lamellae are thin layers of water held within protein film capillaries between adjacent bubbles.

Three sequential stages are involved in protein foaming (German, 1990). Initially, the soluble protein diffuses to the air-water interface, concentrates and reduces the surface tension; then some unfolding occurs at the interface with concurrent reorientation (the hydrophobic amino acids orient towards the non aqueous phase); and finally, interactions between the proteins occur to form a continuous film. The more hydrophobic the protein, the greater the concentration of protein at the interface, the lower the interfacial surface tension and the more stable the foam. The physical stability of the film once foamed is the major determinant of foam stability.

Factors affecting foaming

The quantity of foam and the stability of foam depend on protein concentration, pH, heat treatment, ionic concentration, the presence of sucrose and the presence of lipids (Lakkis & Villota, 1990; Zhu & Damodaran, 1994; German, 1990).

Protein concentration: The volume and stability of foams tends to increase with protein concentration and foams formed with higher concentrations of foaming protein are finer, denser and usually more stable because of the thicker interfacial films.

pH: At the isoelectric point, where electrostatic attractions are maximum, proteins assume a compact state. Provided no coagulation occurs, more protein adsorbs at the interface, resulting in maximal reduction of surface tension.

Heat treatment: Heat treatment and temperature affect foaming via their effects on protein structure and the viscosity of the aqueous phase. Heating that causes partial unfolding of whey proteins without causing coagulation facilitates foam formation.

Ionic concentration: Zhu and Damodaran (1994) showed that calcium and magnesium increase foaming properties via their effects on the structure of water and protein conformation.

Sucrose: Sucrose may improve or impair foaming, though the mechanisms are not clear. However, German (1990) stated that sucrose tends to enhance foam stability, apparently by increasing the viscosity of lamellae and thereby retarding drainage.

Lipids: German (1990) stated that lipids displace the proteins that form the film at the bubble surface, destabilising the foam and leading to collapse.

2.2 Whey Processing

2.2.1 Overall Process (Whey products, Whareroa)

The process steps that cheese and casein whey undergo in an industrial whey powder process are shown in Figure 2.1 and Figure 2.2 respectively. Firstly, both the raw whey from cheese and casein undergo pre-treatment (section 2.2.2) to remove the fat and fines. The whey is then heat treated before being stored in chilled silos. The chilled whey undergoes fractionation in membrane filters (section 2.2.4) and whey protein isolation in ion exchangers (section 2.3.3). The retentate, rich in whey protein, from the membrane filters, is sent to the retentate evaporator (2.2.5) to increase the total solids concentration and is then, spray dried (2.2.6) to obtain the whey powder (WPC and WPI). Permeate, rich in lactose, is concentrated in the permeate evaporator and can be further processed to extract the lactose.

2.2.2 Pre-treatment (Whey products, Whareroa)

Raw whey usually contains fines and varying amounts of fat. In order to obtain the best whey quality for further processing, the raw whey is normally subjected to various pre-treatments whose purpose is to improve the bacteriological quality, remove the fines and reduce the fat content as much as possible (filtration, separation and pasteurisation). However, pre-treatment not only improves the raw material for processes such as membrane filtration and evaporation, it is also important for the quality and composition of the final whey product.
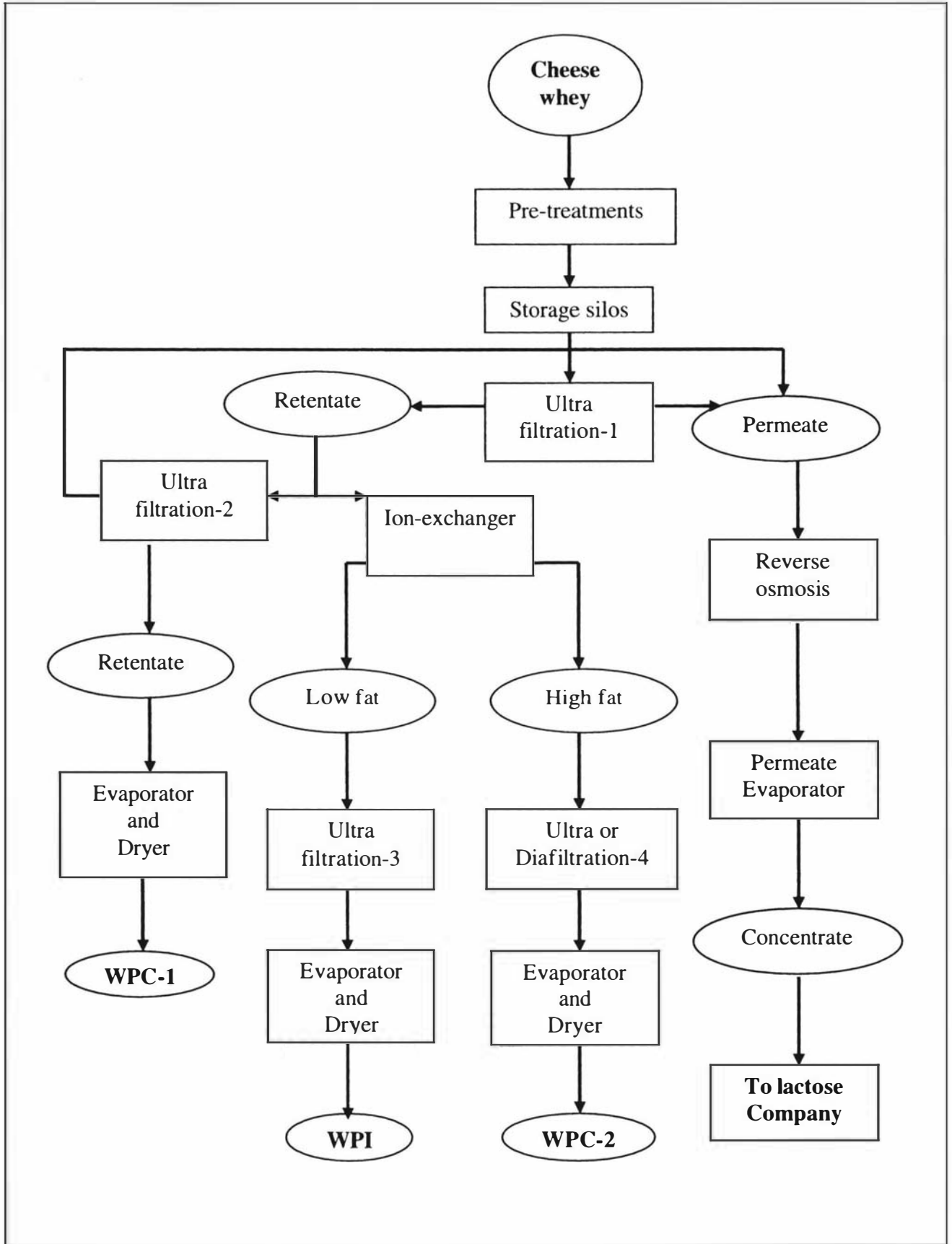
Figure 2.1: Whey process from cheese whey
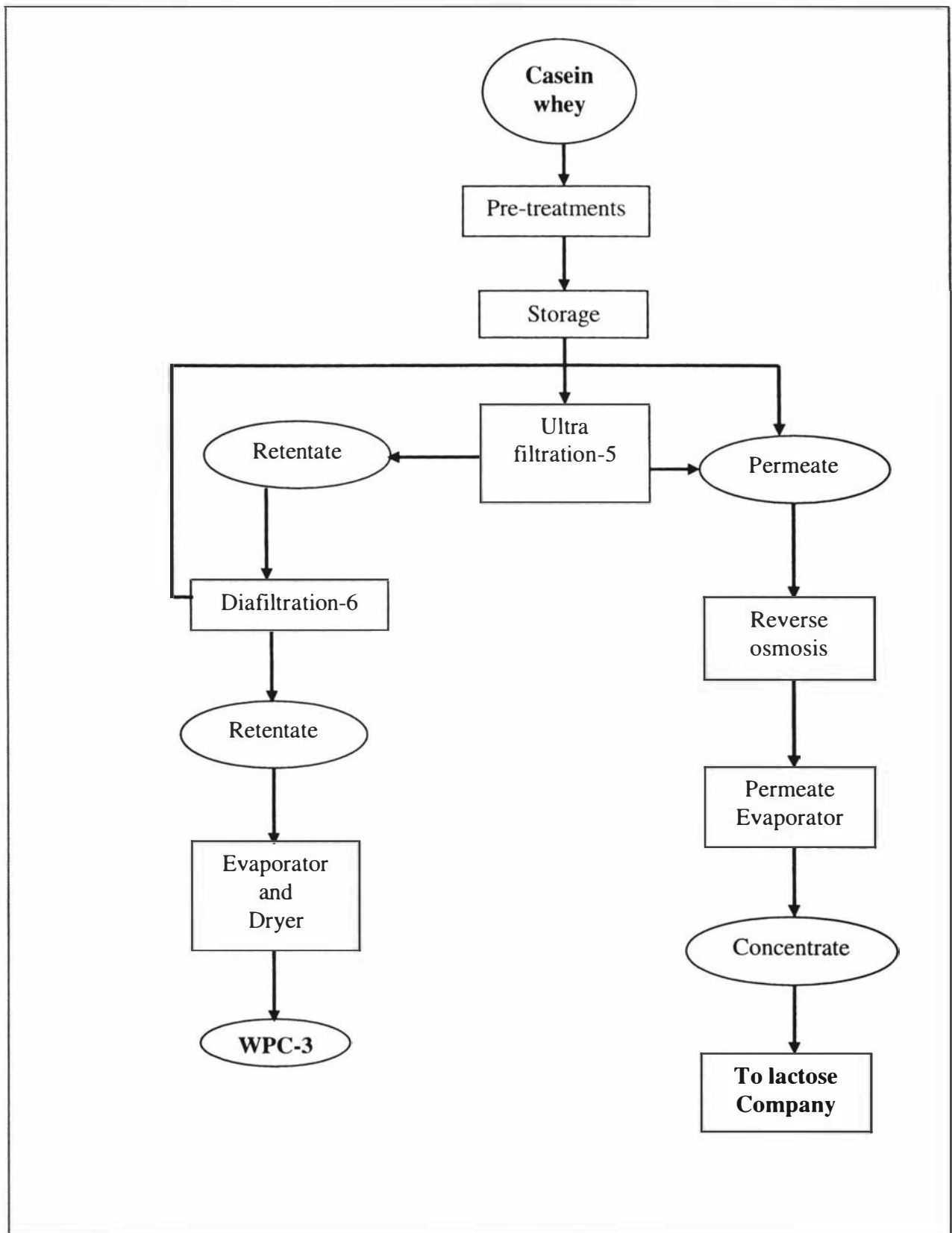
Figure 2.2: Whey process from casein whey

2.2.3 Ion exchange process (Whey products, Whareroa)

The protein ion exchange process is a batch process that extracts the whey protein fractions from the whey stream and minimises the lactose and fat contents. An ion exchanger consists of an insoluble resin to which charged groups have been covalently bound. The charge of the exchanger, whether positive or negative, depends upon the type of whey protein to be extracted. Positively charged exchangers have negatively charged counter ions (anions) available for exchange and so are termed anion exchangers. Negatively charged exchangers have positively charged counter ions (cations) and are termed cation exchangers. Whether or not any given protein will adsorb to a resin depends on the pH and the ionic strength of the solution.

2.2.4 Membrane process (Whey products, Whareroa)

Figure 2.3 is a schematic diagram of the membrane process. The aqueous solution to be filtered flows under pressure along the membrane filter. Water and, depending on the membrane type (microfiltration, ultrafiltration or nanofiltration), some of the smaller molecules and ions pass through the membrane. Larger molecules cannot pass through the membrane and are rejected. They have an increased concentration on the membrane surface. When the liquid flow along the membrane is sufficiently fast, the rejected molecules mix back into the main stream, resulting in cross-flow filtration without the formation of a filter cake. Thus, the feed is divided into the retentate and the permeate streams. The principle of diafiltration is identical to ultrafiltration process except water is added continuously to wash out the lactose and the salts. This process can lead to a high protein content retentate.
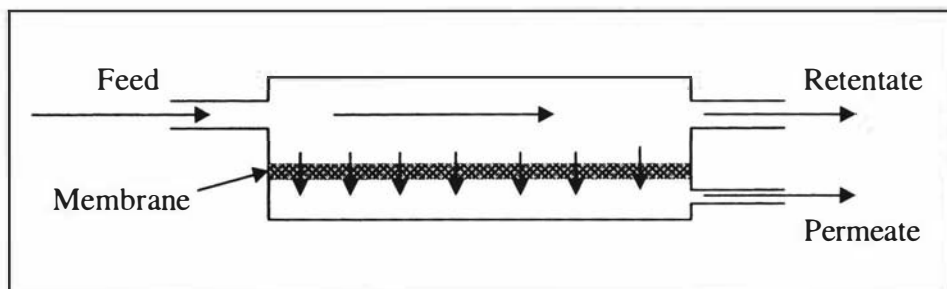
Figure 2.3: Membrane process

In reverse osmosis, solvent molecules (e.g. water) pass from a solution of high concentration on one side of membrane to a solution of lower concentration on the other

11

side. A pressure above the osmotic pressure must be applied to the high concentration side for this process to occur.

2.2.5 Evaporation (Whey products, Whareroa)

Evaporation is defined as the concentration of a solution of solids (non-volatile substances) by evaporation of liquid (volatile substance) in the form of vapours. This process consists of the transition of a solvent to the vapour state and removal of this vapour from the remaining concentrated solution. Evaporation is usually carried out at boiling point, when the vapour pressure over the solution is equal to the pressure in the working volume of the equipment. Evaporation is the major concentrating process used in the dairy industry.

Products intended for powder production are normally concentrated by evaporation before going in to the spray dryer. Evaporation is a necessary production stage for high-quality whey powder and also makes the drying process more economical. Food products are usually heat sensitive and can be destroyed by adding heat. To reduce the heat impact, evaporation takes place under vacuum so that boiling occurs at low temperatures. The product should have the shortest possible residence time in the evaporators.

To evaporate water from the process stream, heat must be supplied. This heat is supplied in the form of steam. To reduce the amount of steam needed, i.e., to reduce energy consumption, the evaporator is designed with multiple-effects. In a multiple-effect evaporator, the vapour produced in one effect is used as the heating medium for the following effect. A schematic diagram of the falling-film evaporator used in Whareroa whey products is shown in Figure 2.4.

2.2.6 Drying (Whey products, Whareroa)

Spray drying is defined as the transformation of a feed liquid from a fluid state to a dried particulate form by spraying the feed into a hot drying medium and effecting the removal of moisture. Drying of the concentrated whey in whey products takes place in two stages: firstly in the dryer chamber and secondly in a vibrating fluidised bed. In the drying process, the whey concentrate from the evaporator is fed to an atomiser system and sprayed downwards in the drying chamber co-currently with hot drying air. The powder from the chamber continues to a vibrating fluidised bed where cooling of the

product takes place. Most of the water is removed in the chamber and the final control of the moisture of the product is achieved in the vibrating fluidised bed.
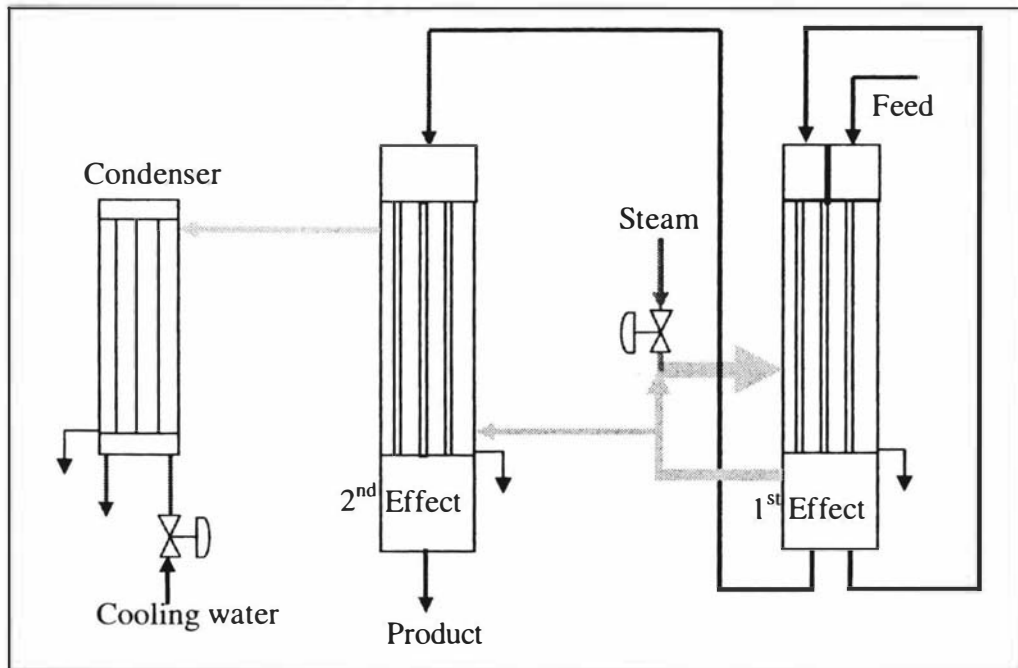
Figure 2.4: Two-effect falling-film evaporator

2.3 Whey Powder

2.3.1 Product types and compositions

The type and the composition of whey powder depend upon the upstream processes and the feedstock. The major components of whey powder are protein, fat, lactose and minerals. The dry basis compositions (w/w%) of each type of whey powder for Whareroa are shown in Table 2.1. The type of protein fractions and their proportions in WPC-1 and WPC-3 are different although the total protein is the same. Different whey source and the process steps are the cause for this difference (see figure 2.1 and 2.2).

Table 2.1: Compositions of whey powder

Product	Protein	Fat	Lactose	Minerals
WPC-1	83.0	5.0	7.0	5.0
WPC-2	75.0	10.5	8.5	6.0
WPC-3	83.0	4.5	7.5	5.0
WPI	98.0	0.3	0.2	2.0

2.3.2 Functional properties

What are functional properties of protein?

Functional properties affect the overall behaviour of proteins in foodstuffs and reflect the various interactions that proteins take part in. The functional properties of a protein are defined by the structure or conformation of the protein and the intermolecular associations of the protein with other proteins and food components. Functional properties vary with protein source, composition, method of preparation, thermal history and the environment. The key functional properties of whey proteins are solubility, viscosity, gelation, water binding, emulsification and foaming.

Functional properties and applications

The applications of whey proteins depend upon their specific functional properties. Figure 2.5 shows the functional properties of whey proteins and their related applications (de Wit, 1988; de Wit, 1989).
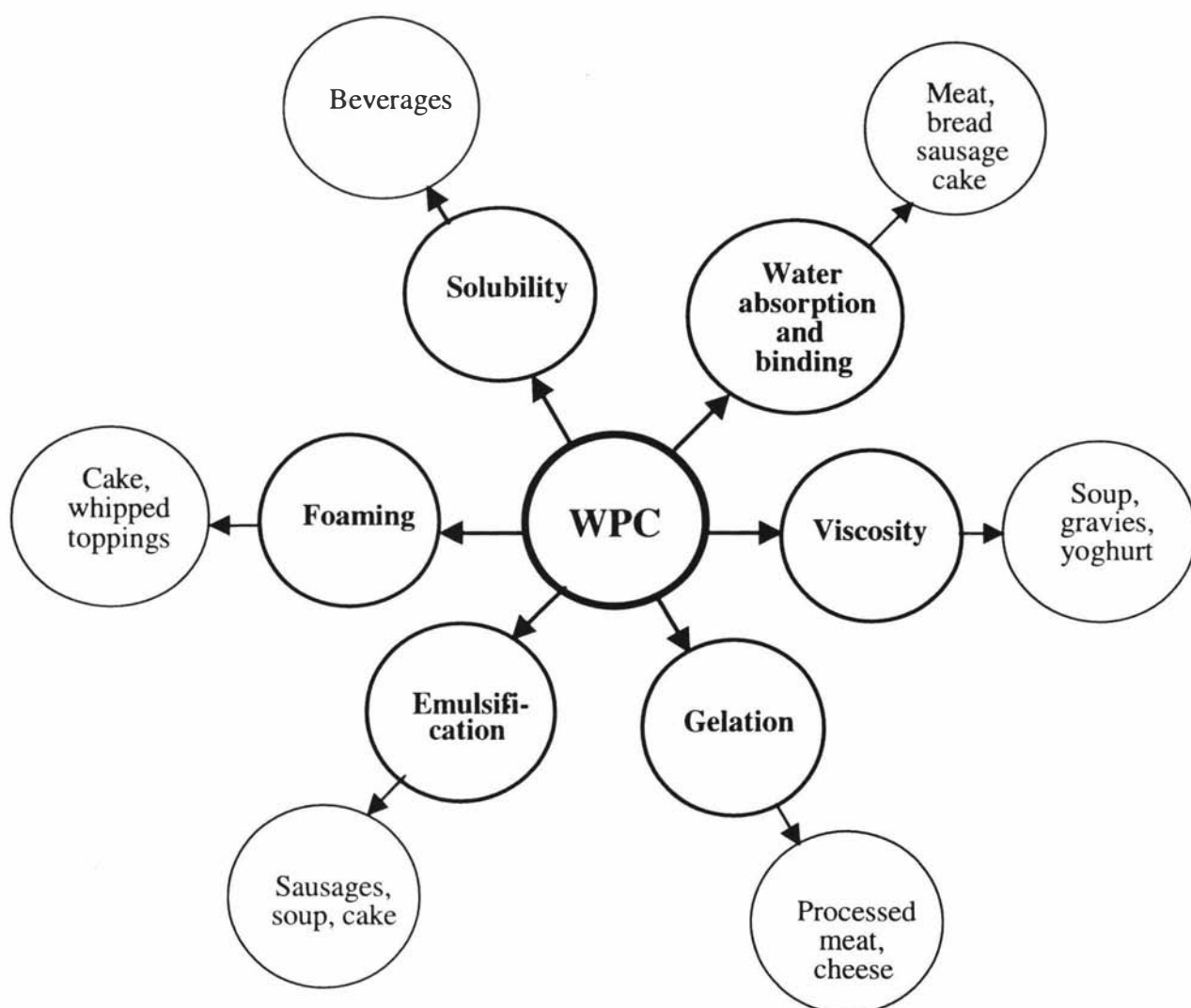
Figure 2.5: Functional properties and application of whey proteins

2.4 Properties

2.4.1 Physical properties

The physical properties -viscosity, density, advancing contact angle (angle that an advancing liquid front makes with the contact surface at rest) and surface tension-of whey concentrates are the most important process input variables in the manufacture of whey powders. The property models as a function of the total solids concentration, temperature and the product composition is needed for the work (i.e. generic model). Many theoretical and semi-empirical models for physical properties (Bloore and Boag, 1981; Snoeren, 1982; Murakami and Okos, 1989; Fernandez-Martin, 1971; Jeurnink and Kruif, 1992; Antonio, 1983; Adam et al., 1994; Middleton, 1996) can be found in the literature for milk concentrates while few can be found for whey concentrates (Adam et al., 1994; Buma, 1980). The regression models developed for milk concentrates are not suitable for whey concentrates as the compositions differ significantly (eg. Protein content of milk powder is in the range of 25% to 37% whereas the protein content of whey powder is in the range of 75% to 98%). The composition of the whey for which the models were developed was not mentioned in the papers referred above. However, the property predictions of the (Adam et al., 1994; Buma, 1980) models are compared with the experimental data in Chapter 3. The literature property models that relate the individual components and the models developed for whey concentrates are listed in Appendix C.

2.4.2 Discharge coefficients

Discharge coefficients are needed to calculate the discharge flow from the distribution plate (see Chapter-4) or to estimate the liquid height above the distribution plate. The discharge coefficient is defined as the ratio of the actual rate of discharge to the ideal rate of discharge, if there were no friction and no contraction. To understand the distribution plate dynamics in a falling-film evaporator, discharge coefficients must be known accurately. Much experimental work has been reported on the discharge coefficients of large orifices with large liquid heads (Mohanty, 1986; Vennard & Street, 1982; Daugherty and Franzini, 1965). A few reports also exist for small orifices with large heads (Trinh et al., 1996; Chee et al., 1988). Many researchers (Mackereth, 1993; Winchester, 2000; Chee et al., 1988) have suggested a value of 0.6 for dairy applications regardless of the orifice size and the liquid head. Mackereth (1997), Vennard & Street (1982) and Daugherty and Franzini (1965) investigated the effect of

orifice shapes on the discharge coefficient for water. Their results are shown in Figures 2.6 to 2.8.
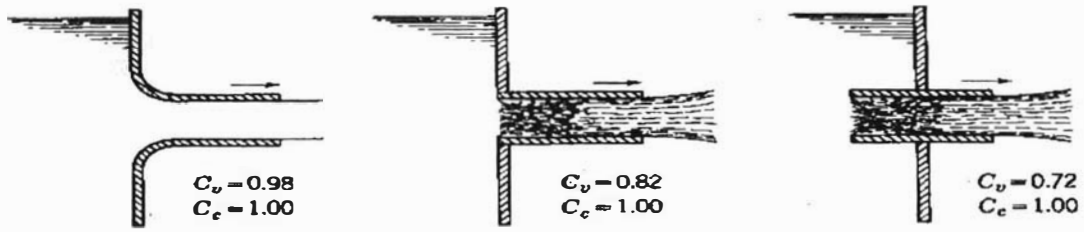
Figure 2.6: Coefficients for tubes

Daugherty and Franzini, *Fluid Mechanics with Engineering Applications, 1965, pp.347*

Orifices and their Nominal Coefficients				
	Sharp edged	Rounded	Short tube	Borda
C	0.61	0.98	0.80	0.51
C_c	0.62	1.00	1.00	0.52
C_v	0.98	0.98	0.80	0.98

Figure 2.7: Discharge coefficients

Vennard & Street, Elementary Fluid Mechanics, 1982, pp.533
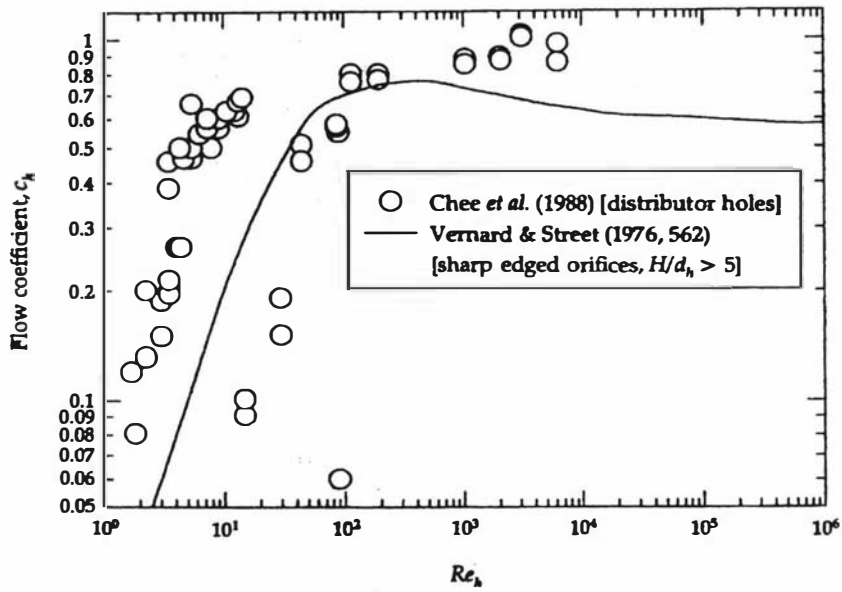
Figure 2.8: Flow coefficient curve for sharp-edged orifices

Mackereth, Milk Powder Technology, 1997, pp.9.1

2.5 Evaporators

2.5.1 Types of evaporators

There are a number of evaporators of various designs and operating characteristics that have been developed to cope with all kinds of products (Billet, 1989; McCabe et. al, 2001; Minton, 1986). Brief descriptions for the common types are given below. Figures 2.6 to 2.12 were taken from Evaporation Technology (Billet, 1989) and from Handbook of Evaporation Technology (Minton, 1986).

Natural circulation

The basic moving force in a natural circulation evaporator (Figure 2.9) is the difference in densities that exist within the system. A vertical-tube heat exchanger is placed inside a cylindrical evaporator body. The liquid rises up through the tubes being heated, boiling as it rises. The decrease in density that occurs as the liquid rises is the source of the difference in head. Steam condensers on the outside of the tubes (in the shell) of the heat exchanger. The most frequent application of this type is where the scaling problem is small and the liquid is relatively viscous.
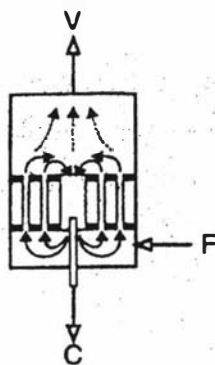
**Figure 2.9: Natural circulation
evaporator**
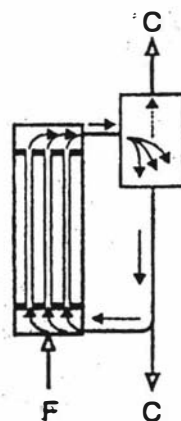
**Figure 2.10: Forced circulation
evaporator**

Forced circulation

In forced circulation type evaporators (Figure 2.10), boiling occurs in the tubes in the same way as with natural circulation. A recirculating pump maintains the desired liquid rate to the heat exchanger. A high circulation rate is maintained to achieve a good heat transfer rate. (Within limits, the higher the velocity across the heat transfers area, the greater the heat transfer rate). These types of evaporators are best applied to crystalline

products, as the solids remain in suspension throughout. This type of evaporator can also be operated as a natural circulating type. The symbols F, C and V in the above figure refer to feed, concentrate and vapour.

Climbing-film

In a climbing-film evaporator (Figure 2.11), feed is pumped into the bottom of the evaporator. The pressure of the feed forces the liquid up the tubes where it is heated until it reaches its boiling point. As the liquid begins to boil, vapours are released from the surface of the liquid. These vapours then rise in the centre of the tube while the liquid is distributed in the form of a film on the tube wall. Steam condensing on the outside of the wall continues to heat the film. The two-phase fluid exits the tubes and enters the vapour body where the vapour and liquid are disengaged. The vapour is removed from the body and the liquid is trapped and removed as product. These evaporators are especially effective in concentrating liquids that tend to foam. Foam breaks when the high-velocity mixture of liquid and vapour impinges against the vapour- head baffle.
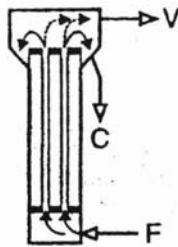
Figure 2.11: Climbing-film evaporator
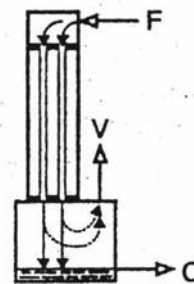
Figure 2.12: Falling-film evaporator

Falling-film

In a falling-film evaporator, the liquid is fed into the top section of the heat exchanger where some form of distribution device distributes the liquid to each tube of the heat exchanger. Heat (steam or vapour) applied to the outside of the tubes causes evaporation of the film of liquid as it travels down the tube. Vapour passing through the centre of the tube accelerates the liquid film because of the drag effect. The two-phase mixture then enters the separator where the liquid drops to the bottom and the vapours rise. These types of evaporators are widely applied with heat sensitive products (e.g. food products) due to short residence time in the tubes and high heat transfer rates.

Thin-film evaporator

This type of evaporator (Figure 2.13) is designed to operate at low boiling temperatures with low residence times. A wiper scraps the feed off the tube walls and maintains a thin film and keeps the wall clean throughout the process. The cleaning action of the wiper enables the use of a high wall temperature, which reduces the wall area required. However, too high a temperature can damage thermally sensitive products.
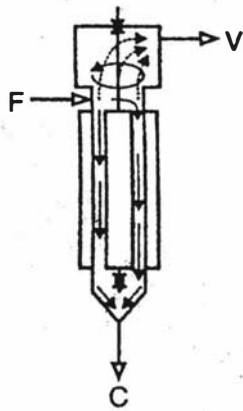
| Figure 2.13: Thin-film wiper evaporator | Figure 2.14: Thin-film centrifuge evaporator |
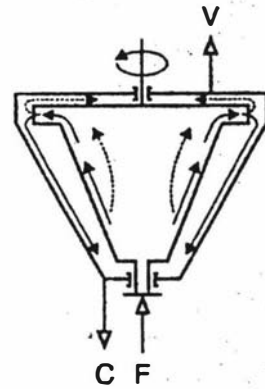
Thin-film centrifuge

In this type of evaporator, the feed is introduced onto the centre of a spinning, upwardly inclined, heated disc. The centrifugal force causes the feed to travel up the inclined surface as a thin film. The rotational speed and the type of product control the thickness of the film. High speed ensures that the steam condensing on the other side of the disc forms droplets that are thrown off. The thin product film and the drop-wise condensation increase the heat transfer rate and enable the use of a low wall temperature. This type of evaporator is best for food products where the thermal damage to the product must be minimal.

Flash

Flash evaporation (Figure 2.15) is simply the process of introducing a hot feed into a low-pressure chamber. The absence of nucleation sites and potential dry surfaces in the heaters allows the use of these evaporators for solutions that are prone to scaling.

Agitated-film

This is a modified falling-film evaporator with a single jacketed tube containing an internal agitator. Feed enters at the top of the jacketed section and is spread out into a thin, highly turbulent film by the vertical blades of the agitator. Concentrate leaves from the bottom of the jacketed section and vapour rises from the vaporising zone. In the separator the agitator blades throw entrained liquid outward against stationary vertical plates. The droplets coalesce on these plates and return to the evaporating section. Liquid-free vapour escapes through outlets at the top of the unit. Agitated-film evaporators are particularly effective with viscous heat-sensitive products such as gelatine, rubber latex and fruit juices. Disadvantages are the high capital cost, high maintenance and small capacity.
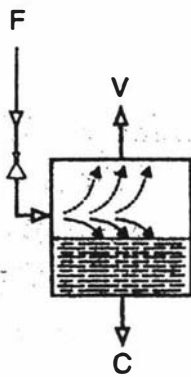
Figure 2.15: Flash evaporator   **Figure 2.16: Agitated-film evaporator**
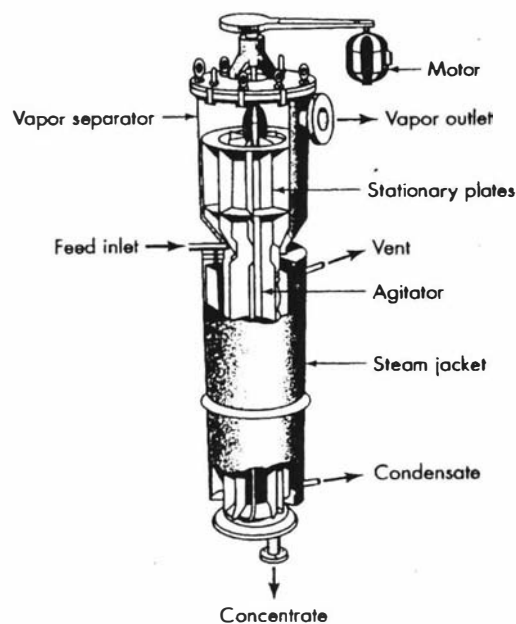
(McCabe et. al, 2001)

2.5.2 Dairy industry falling-film evaporators

The falling-film evaporator is the most widely used in the dairy industry (Fonterra Dairy Co-operative Ltd). This is due to the following features of falling-film evaporators:

- The small liquid content (thin film) and the high flow velocities result in a short residence time beneficial for heat-sensitive products.
- The evaporator can be operated at a low temperature difference and thus can be equipped with many effects.
- The simple construction and the possibility of using long tubes allow the application of the falling-film principle to a wide range of production capacities.
- A large amount of water evaporation is possible due to the high operating heat transfer coefficients and thus energy efficient evaporation process.
- All parts of the stream have an equal time of direct contact with the evaporator tubes, depending on the tube length, the liquid velocity and the viscosity of the product.
- The small liquid content means that only very small amounts of cleaning agent are needed.

In a typical dairy industry falling-film evaporator (shown in the Figure 2.17) the product is introduced at the top (so called falling-film). The liquid flows through a vertically arranged bank of tubes, forming a thin film on the inside surface of the tubes. The product is heated by a heating medium on the outside of the tubes (utilising steam or steam from another effect in multi-effect evaporators). For efficient evaporator performance, it is very important to obtain a uniform distribution of the product over the tube surfaces.

Multiple evaporator effects are generally used in order to increase thermal efficiency and reduce steam consumption. In order for the vapour from the first effect to be used for heating in the second effect, the pressure, and subsequently the boiling temperature, of the second effect must be reduced compared to the first. This arrangement is advantageous when concentrated product would be damaged or would lead to enhanced fouling when exposed to high temperatures. In the dairy industry, between two and seven effects are fairly common.

Multiple effect evaporators are often used with a TVR (Thermo Vapour Re-compressor) or an MVR (Mechanical Vapour Re-compressor) or both, to compress the vapour from the first effect and supply the heat source to the subsequent effects.
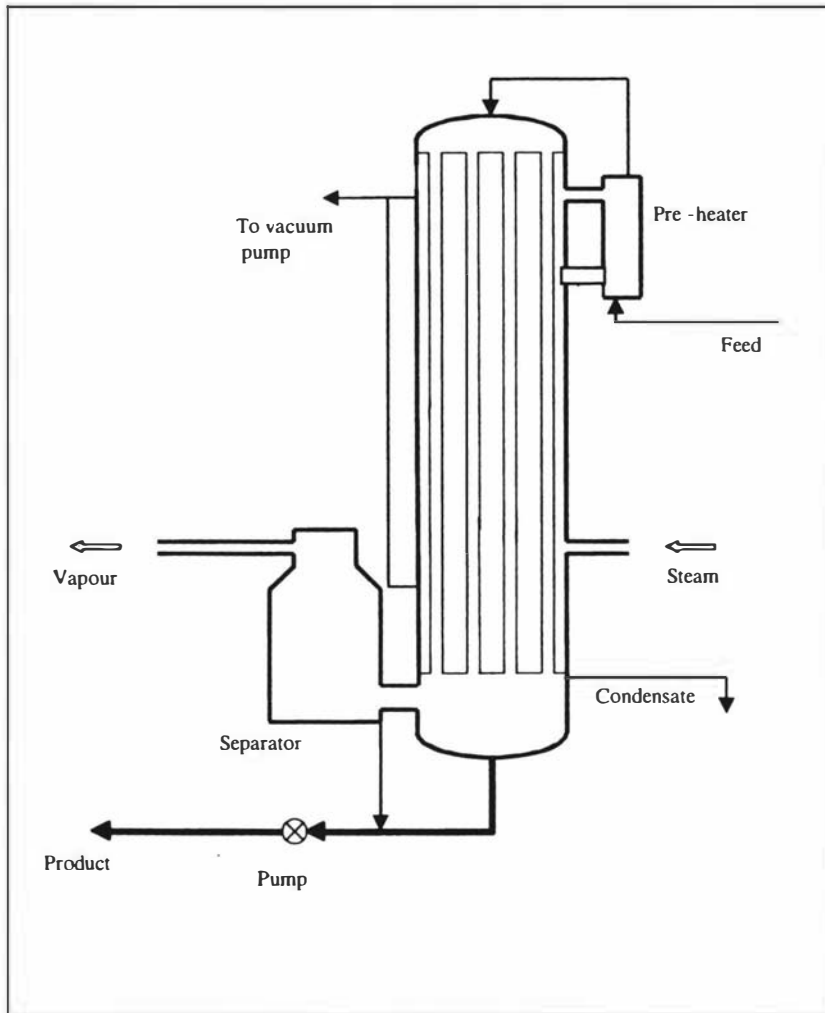
Figure 2.17: Single effect falling-film evaporator

When a TVR is used, a part of the vapour generated from one effect is supplied to the TVR section, to which high-pressure steam is connected. The TVR uses the high-pressure steam to increase the pressure of the low-pressure vapour from the effect. The addition of a TVR section would be as economical as a two-effect unit without vapour compression. For instance, a two-effect falling-film evaporator with TVR requires about 1 kg of steam to evaporate 4 kg of water while the same evaporator without vapour compression would require about 2.4 kg of steam (Bylund, 1995; Minton, 1986). These values may differ in real operations depending upon the product used and the operating

conditions. An MVR uses an electrically-driven mechanical compressor to raise the pressure of the vapour and thus the saturation temperature of the vapour above the product boiling temperature. The thermal efficiency and thus the potential saving is higher with an MVR unit compared to a TVR unit (Winchester, 2000). The use of an MVR evaporator design is therefore common in the dairy industry (Fonterra Dairy sites).

The mass of evaporation and the temperature profile within a falling-film evaporator is determined by the overall heat transfer coefficients between the product to be evaporated and the condensing vapour. The overall heat transfer coefficients vary depending upon the properties of the products to be evaporated, and typically lie between 700 and 4000 W/m^2K (Perry & Green, 1984). The pressure drop is usually small (Mackereth, 1993), so that the evaporation temperature varies little throughout an individual effect. As a result of the parallel flow of liquid and vapour within the tubes, substantial vapour velocities can develop as the product progresses down the tubes. These velocities exert a large shear stress on the liquid film and produce a thin liquid film at the bottom part of the tubes. Many researchers (Winchester, 2000; Choudhary and Das, 1996; Angeletti & Moresi, 1983; Perry & Green, 1984; Chun & Seban, 1972; Murthy & Sarma, 1977) have assumed that the evaporation occurs from the surface of the thin film, that is, the vapour is formed only on the film surface, without any vapour bubbles being formed on the wall. There is little information available in this area. However, some researchers (e.g. Bouman et. al, 1993; Chen and Jebson, 1997) suspect that nucleate boiling starts at very low temperatures for milk products.

2.5.3 Whey evaporator at Fonterra Whareroa

A schematic diagram of the evaporator used in the whey product plant at Fonterra, Whareroa, Fonterra Co-operative Ltd is shown in Figure 2.18. This is a two-effect, three-pass, falling film evaporator with a thermal vapour compression unit (TVR). The first and the second effect have two passes and one pass, respectively. The evaporator uses three preheat condensers (PHC) to heat the feed whey to the 1st effect evaporating temperature (10^oC to 45^oC). The first, second and the third preheat condensers are attached to the 2nd effect, 2nd shell and to the 1st shell of the evaporator respectively.

The whey from the third preheat condenser enters the distribution plate (DP) of the first effect and flows evenly into the evaporator falling-film tubes. The whey then flows down the tubes under gravity and heat is supplied to it from steam condensation in the shell. The heating causes water to evaporate from the whey, thereby concentrating the total solids in the liquid stream. At the bottom of the evaporator tubes the concentrated whey is collected and pumped to the next pass in the first effect. After passing through the second pass, the concentrated whey is pumped to the second effect for the final pass.

The TVR compressor uses motive steam to drive the evaporator. The compressed water vapour condenses at a higher temperature in the shell and provides the driving force for evaporation in the first effect. The whey evaporator contains a vacuum condenser attached to the second effect. Cooling water is circulated in the condenser tubes to maintain the vacuum and thus the temperature profile in the evaporator.

2.6 Evaporator modelling

2.6.1 Mathematical modelling

Mathematical models of industrial processes allow us not only to understand the processes more clearly but also to control them more closely and make predictions about them. A good mathematical model should be realistic, precise, accurate and robust. However, a mathematical model can never be an exact representation of a process, since it would usually be difficult, overly complex or impossible to describe the whole system with exact mathematical formulations (Aris, 1999; Jeffreys and Jenson, 1977; Bender, 1978; Ozilgen, 1998). Instead, the modelling process invariably requires the adoption of various simplifying assumptions to facilitate the model formulation and solution. A common heuristic in process modelling is the 80-20 rule, which holds that 80% of the benefit (in terms of model accuracy) is achieved for the first 20% of the model complexity (Glasscoke and Hale, 1994).

Mathematical models can be categorised as empirical, analogous or phenomenological. An empirical model assumes the form of the functional relationship between the input and the output variables. There is no theoretical background sought when suggesting this relationship. Empirical models are best used within the range of the experimental data they are based on. An analogous model may be suggested for a lesser known
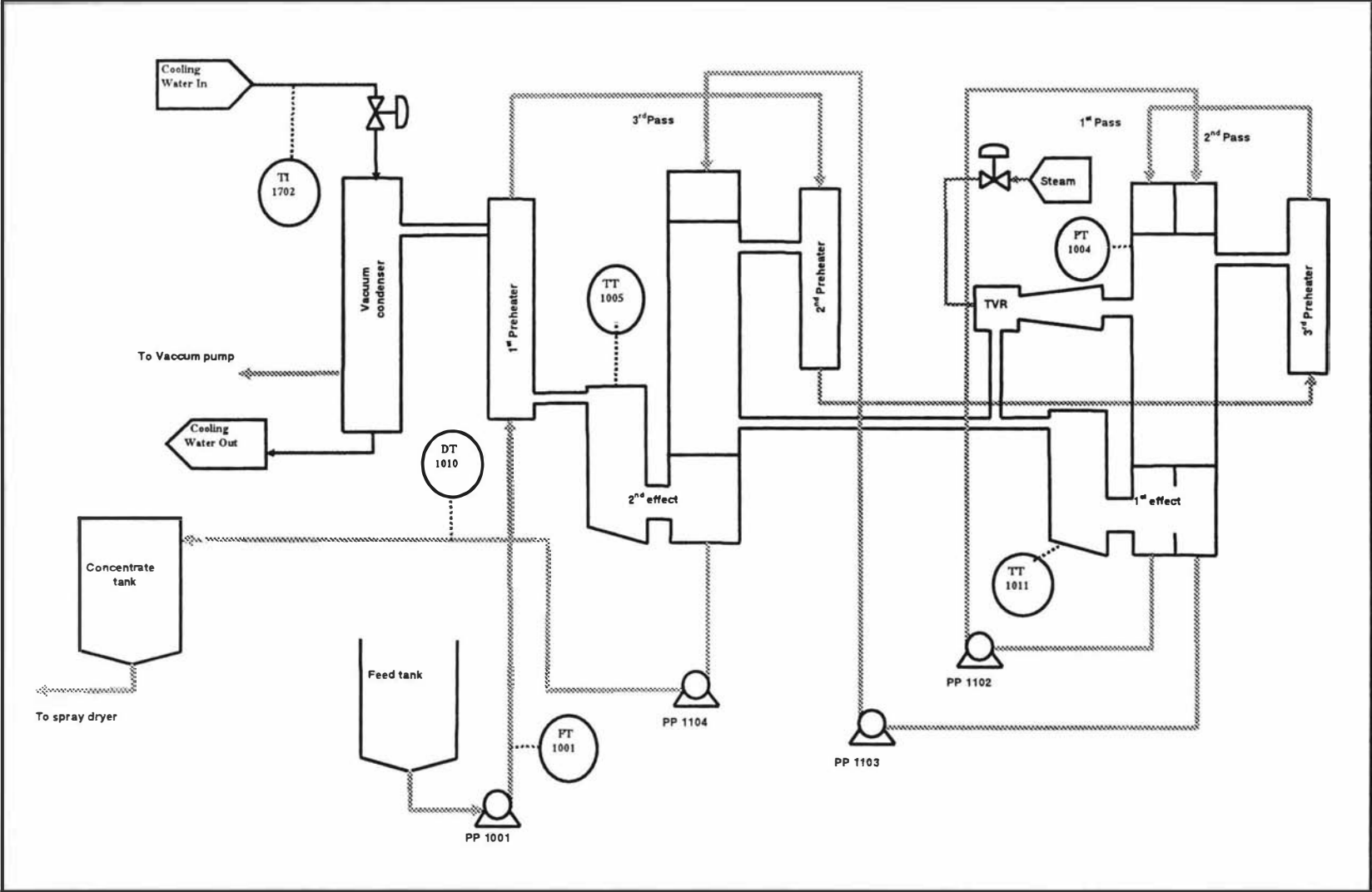
Figure 2.18 :Schematic diagram of the whey evaporator plant at Fonterra Ingredients, Whareroa, Fonterra Co-operative Ltd.

process by considering its similarity to a well-known process. Phenomenological models use a theoretical approach based on conservation laws (mass, energy, momentum, etc.) to describe the transport process characterising the behaviour of a system.

2.6.2 Literature on the modelling of falling-film evaporator

If an evaporation process to be optimised, an accurate model of the process is essential. The models can be generally classified into two groups: *physically modelled* (phenomenological) and *black box modelled* (empirical). Both forms of model have their advantages and limitations.

Physical models based on 'first principles' describe the physical phenomena occurring during the evaporation process. They give insight into the process and often apply over a wide operating range. However they require that many physical quantities be known, such as heat transfer coefficients, physical properties of the fluids and, in some cases, even surface tension and contact angle. Comprehensive, accurate data for these quantities are not available in the literature for most dairy products. The accuracy of physical models is limited by the available data, process knowledge and the model assumptions and simplifications. The mathematical solution of physical models often requires computational resources.

Alternatively a black-box model can be developed by using identification techniques to investigate the relations between process input and output parameters. The black-box model is a model without physical details or theoretical basis. This is an advantage as well as a disadvantage. The regression coefficients have no physical meaning and may change unpredictably if product properties or process conditions are changed. However, black-box models are often particularly accurate in a limited range around a specific operating point; the accuracy of the models is limited mainly by the linear modelling techniques used to formulate the models and the accuracy of the data used for the regression. The mathematical solution of black-box models is usually straightforward and rapid.

In the dairy industry, evaporators of two to seven effects are commonly used. Some researchers (e.g. Choudhary and Das, 1996) have modelled a single-effect evaporator

with recompression unit while others have modelled a double-effect evaporator (e.g. Runyon et al., 1991) or three- or four-effect evaporators. Quaak & Gerritsen (1990) and Quaak et al (1994) conducted comprehensive work on pilot-plant multi-effect evaporators to model the dynamic behaviour of evaporators used in milk powder production plants. Many other researchers (Angeletti and Moresi, 1983; Chun and Seban, 1972; Murthy and Sarma, 1977) have modelled evaporators for non-milk products such as fruit juice and seawater. Winchester (2000) developed a model for a multi-effect falling-film evaporator used for milk powder production at Fonterra Whareroa. Winchester adapted parts of many existing models to the Whareroa evaporator incorporating many improvements. However, there was still much that was left unfinished such as physical properties and TVR models.

One of the most difficult aspects of evaporator modelling is describing the distribution of the falling-film. There has been a lot of work done on characterising the falling-film on vertical tubes, but not specifically for milk products (Bui and Dhir, 1985; Van der Mast and Bromley, 1976; Hirshburg and Florschuetz, 1982). Some researchers (Jebson and Iyer, 1991; Chen and Jebson, 1997; Bouman et al., 1993; Mackereth, 1993) have used theoretical correlations modified with experimental data to suit their particular application. However, these models are product and system specific and do not apply to products or evaporators different from those for which the models were derived.

No work has been done on the modelling of evaporators in the whey products application, although the evaporator configuration is similar to the one in the milk product application. The lack of model development for whey evaporation has been due to insufficient data or models available in the public domain describing the physical properties of whey products.

2.7 Evaporator control

2.7.1 Process control

Process control is a sub-discipline of automatic control that involves the selection and tailoring of methods for the efficient operation of industrial processes. Proper application of process control can improve the safety and profitability of a process while maintaining consistently high product quality. There are two major duties that a control

system is expected to perform in a process, firstly, maintaining the process variable at its desired value when disturbances occur and, secondly, responding to changes in the desired value. Other attributes that desirable for a good control system are robustness and gracefulness.

2.7.2 Loops interaction and Relative Gain Array

Control loops can interact with one another when there is more than one manipulated variable and more than one controlled variable and when a given manipulated variable affects more than one controlled variable. Loop interactions give rise to two potential problems; they may destabilise the closed loop system and they tend to make controller tuning more difficult. One method of analysing these multivariable interactions is the use of the relative gain array (RGA). The RGA provides a measure of process interaction and an indication of control loop pairings. The steps involved in calculating the RGA are shown below for a two input, two output systems (Stephanopoulos, 1984).
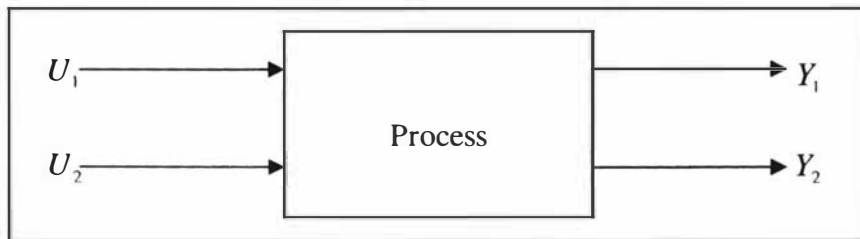
The first step is to calculate the open loop gain matrix. This gives an indication of the influence that each input has on each output. The gain matrix for the above system can be denoted by:

	U_1	U_2
Y_1	$K_{11} = \dfrac{\Delta Y_1}{\Delta U_1}\bigg|_{U_2}$	$K_{12} = \dfrac{\Delta Y_1}{\Delta U_2}\bigg|_{U1}$
Y_2	$K_{21} = \dfrac{\Delta Y_2}{\Delta U_1}\bigg|_{U2}$	$K_{22} = \dfrac{\Delta Y_2}{\Delta U_2}\bigg|_{U1}$

The gain matrix above gives some insight into which pairings have the most influence on each other and whether positive or negative gains are needed in the final controllers. The next stage of the analysis takes into account the interaction when the loops are closed. The relative gain array is given by:

	U_1	U_2
Y_1	$\lambda_{11} = \dfrac{K_{11}}{\left.\dfrac{\Delta Y_1}{\Delta U_1}\right|_{Y2}}$	$\lambda_{12} = \dfrac{K_{12}}{\left.\dfrac{\Delta Y_1}{\Delta U_2}\right|_{Y2}}$
Y_2	$\lambda_{21} = \dfrac{K_{21}}{\left.\dfrac{\Delta Y_2}{\Delta U_1}\right|_{Y1}}$	$\lambda_{22} = \dfrac{K_{22}}{\left.\dfrac{\Delta Y_2}{\Delta U_2}\right|_{Y1}}$

The general interpretation of the relative gain array elements is as follows.

- If $\lambda_{ij} = 1$, open loop gains and closed loop gains are identical and interaction does not affect the pairing.

- If $\lambda_{ij} = 0$, open loop gain is zero and U_j has no effect on Y_i.

- If $0 < \lambda_{ij} < 1$, Closed loop interaction increases the gain and is most severe when $\lambda_{ij} = 0.5$.

- If $\lambda_{ij} > 1$, Closed loop interaction reduces the gain and higher values indicate more interaction.

- If $\lambda_{ij} < 0$, Closed loop gain is in the opposite direction from the open loop gain and these pairings should be avoided.

Therefore, the strategy is to match the variables where λ_{ij} is nearest to 1 while avoiding pairings where λ_{ij} are zero or negative.

2.7.3 Control loops in the whey evaporator

Schematic diagram of the control loops in the whey evaporator at Fonterra Ingredients, Whareroa is shown in figure 2.19. The most important factors in whey evaporation are to produce a concentrate with a consistent total solids concentration and to regulate the level of heat treatment.
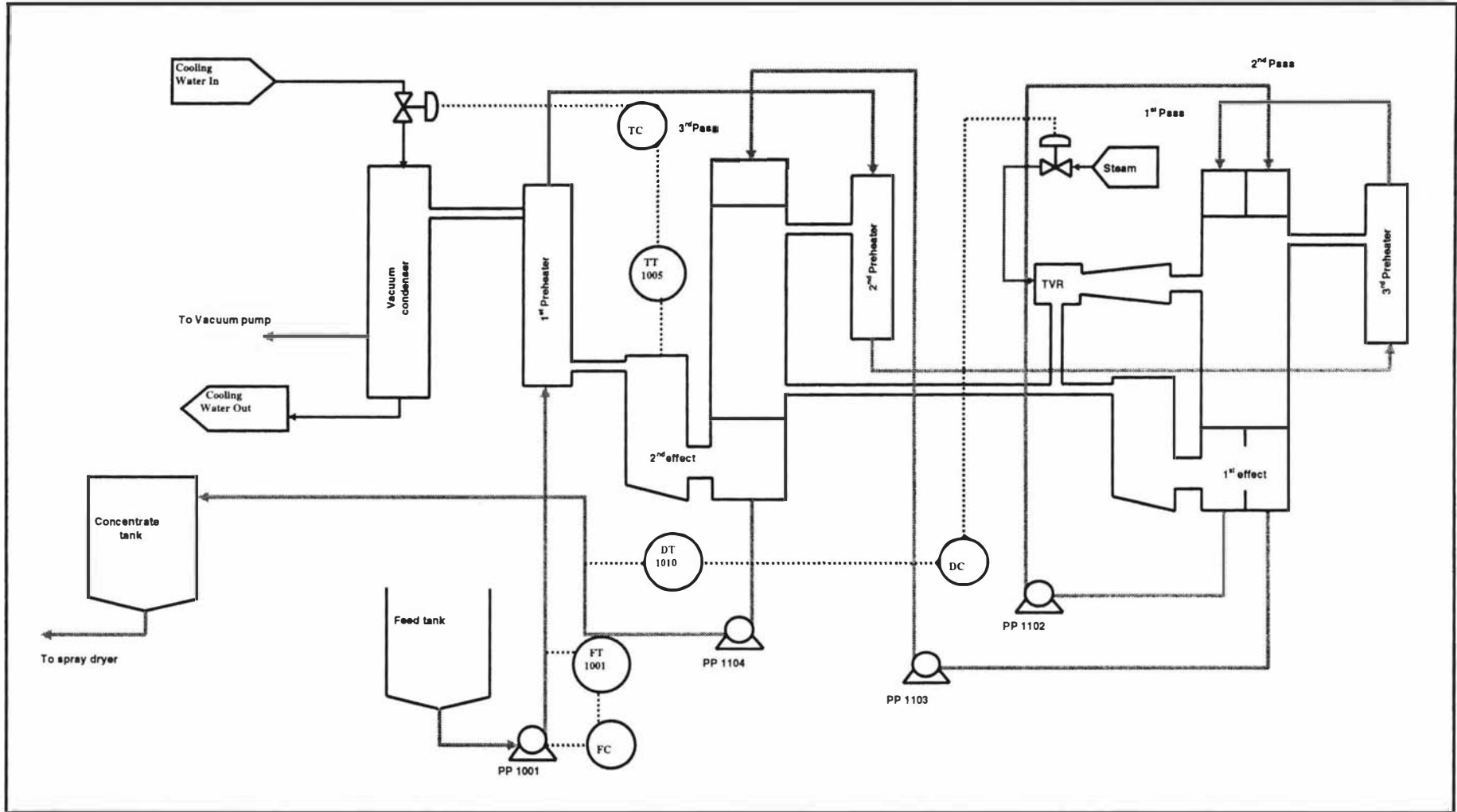
Figure 2.19 : Schematic diagram of the control loops in the whey evaporator plant at Fonterra Ingredients, Whareroa, Fonterra Co-operative Ltd.

Feed flow

A variable speed centrifugal pump controls the product feed flow. This flow is usually pre-set and changed manually when the desired concentrate solids level is reached to match the concentrate flow with the dryer feed.

Second effect temperature

By adjusting the amount of cooling water fed to the vacuum condenser, the rate of condensation can be controlled. This in turn affects the vacuum in the final effect, and is therefore used to control the vacuum and the temperature in the rest of the evaporator.

Product density

Regulating the steam pressure to the TVR (Thermo Vapour Re-compressor) is the most common way of controlling the final total solids concentration of the product from the evaporator. Concentrate density is used as the indication of the product concentration from the evaporator. Adjusting the TVR steam pressure controls the amount of evaporation taking place and therefore the final solids concentration.

2.7.4 Literature on control of solids concentration in falling film evaporators

Product concentration is mainly affected by disturbances in the feed concentration. The disturbance rejection bandwidth achieved by a single feedback PI controller is often found to be inadequate. Winchester and Marsh (1999) studied a single pass falling-film evaporator with mechanical vapour recompression and concluded that it was not controllable (as defined by Skogestad and Postlethwaite, 1996) because it was not possible to achieve a high enough disturbance rejection bandwidth in the concentrate total solids loop. They further concluded that the disturbance rejection bandwidth would become more inadequate for multi-pass evaporators due to the increase in process delay.

Many successful simulations and implementations of control systems for the falling-film evaporator can be found in the literature. Most of these use advanced control strategies. For example, Tade and Page (1998) studied a geometric, non-linear controller implementation, Quaak et al. (1994) carried out work on multivariable, supervisory control design, Lahtinen (2001) studied the application of fuzzy controllers and Lozano

et al. (1984) studied the applicability of model predictive control. However, single feedback controllers are still widely used in Fonterra Dairy Co-operatives Ltd.

PART 1

Parameter estimation and determination

3. Physical properties

In this section the property measurement methods are discussed followed by the regression and semi-empirical model development and the results. Finally, the literature models are compared with the newly developed models and the model applicability to other products is tested.

3.1 Introduction

The major obstacles in the processing of whey protein ingredients are those relating to the high variability of compositions and thus the properties of the products. The variability in the product properties results from many interrelated factors including the source of raw material (whey), cheese manufacturing practices, heat treatment history, protein fractionation procedures and the storage conditions. Many articles describing the physical properties (De Wit, 1989; Bylund, 1995; Middleton, 1996; Velez-Ruiz and Barbosa-Canovas, 1998, Bloore, 1981; Snoeren et al., 1982; Fernandez, 1971) can be found in the literature but these reports contain no useful data of whey concentrates.

Generally, engineers need the physical properties of whey concentrates to perform process calculations in order to optimise and control the plant. This is because most of the models are strongly influenced by the physical properties. All the physical properties (density, viscosity surface tension and contact angle) of whey products depend mainly upon composition and the temperature at which the properties are measured. Experiments were done in the laboratory to measure these physical properties for whey samples collected from the commercial plant at Fonterra Ingredients-Whareroa, Fonterra Co-op Group Ltd. Theoretical models were developed to calculate the physical properties of whey concentrates from the properties of individual components comprising the whey concentrates. The values predicted using the models were compared with values from the experiments.

The density of whey concentrate is important in the processing and handling of concentrates. It is an indirect measure of total solids and could be used in theoretical models to estimate the air content in the liquid whey concentrates. The viscosity of whey concentrate is one of the most important process input variables in the manufacture of whey powders as it influences the powder quality. It is well known that the viscosity of whey concentrates is very complex, as with milk concentrates, and that it changes with a number of factors (Bloore and Boag, 1981; Snoeren et al., 1982)—total solids, temperature, heat treatment, composition, holding time, shear rate and the pH— the most important of these being temperature and composition. Advancing minimum flow and retreating minimum flow are important in dairy evaporator operations to avoid fouling due to film break-up. Since the flow within the evaporator should not allow dry patches to occur, minimum flow estimation should be based on advancing contact angle. Note that using the retreating contact angle will produce a smaller minimum flow below which it is believed (Hartley and Murgatroyd, 1964) dry patches will begin to form spontaneously.

3.2 Methodology

3.2.1 Total solids versus Refractive Index correlations

To facilitate the continuous measurements of whey products total solids in the evaporator at several locations, the total solids of each product was correlated against its refractive index value (RI). There are four sample points available in the falling-film evaporator for whey products: the feed, the first pass, the second pass and the third pass. Four samples per product were taken at each sample location and the total solids contents were determined in the laboratory at Fonterra Ingredients-Whareroa, Fonterra Co-op Group Ltd.

RI measurements were made using two RI meters as shown in figure 3.1 (ATAGO, Japan), one meter having a range of 0-32% Brix and the other a range of 28-62% Brix. For each product, a plot of total solids against RI was constructed to determine the correlation factor. This correlation factor was then used for subsequent physical property measurements and in the heat transfer coefficient calculations to calculate the total solids from RI measurements. The principles of RI measurement, calibration and temperature correction are discussed in Appendix A.1.

1 . Daylight plate
2 . Prism
3 . Scale adjustment screw
4 . Eyepiece

Screw Driver
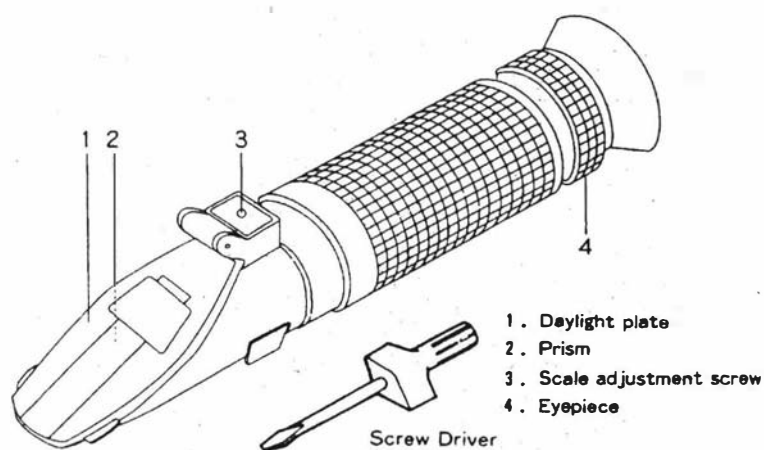
Figure 3.1: Refractive Index meter (*Atago Co. Ltd, Tokyo, Japan*)

3.2.2 Sampling and Sample preparation for physical property measurements

Sampling

Samples were taken from different locations (end of each pass) of the falling-film evaporator to prepare samples of different solids concentrations. To eliminate the variation in the compositions of the solids fraction along the evaporator, samples at various locations were analysed for individual components in the laboratory of Fonterra Marketing and Innovation. The results (Appendix A.2) showed that there was no significant change in the solids composition during the evaporation of whey products. Because the pH of the product WPC-3 was adjusted just before the feed to the evaporator, no sample from the balance tank was taken for sample preparation with WPC-3.

Sample preparation

There were two possible methods of preparing samples to be used in the property measurements. One involved taking the whey powder after it had exited the spray drier and adding different quantities of distilled water to form samples of varying concentration. The second method involved taking the whey concentrate as it was travelling through the falling-film evaporator and diluting it to the required concentrations. The advantage of taking the final powder product and adding water to form a liquid sample is that the concentration that can be achieved by the evaporator is no longer a limiting factor. But difficulties were experienced in mixing the whey powder with water. Whey protein powder, particularly Whey Protein Isolate, has excellent foaming characteristics, which resulted in unwanted air bubbles being introduced into the sample during mixing. The miscibility of whey powder in water is not high and complete dispersion was not achieved in any of the samples prepared, resulting in samples of inaccurate concentration.

Sampling the product at different locations in the falling-film evaporator and diluting to predetermined concentrations was found to give better results compared to the first method. This method involved measuring the refractive index (RI) value and deriving the percentage total solids by using the previously determined correlations for each product.

3.2.3 Experimental design

In order to develop models for the physical properties (density, viscosity, surface tension and contact angle) used in the model developed for the whey evaporator set, one has to consider the factors that would affect these properties in the evaporator. Various factors that influence these properties are temperature, percentage (by weight) total solids, solids composition, pH, storage time and the heat treatment. The pH and the heat treatment history are constants for a given product but differ from product to product. The effect of the feed whey storage time can be ignored, as the storage time is normally less than 12 hours and the storage temperature is 5-10°C (Viscosity measurements with the feed whey over 24 hours show no variation). The effect of feed composition on the physical properties is significant as can be seen from comparisons between the different products but for a particular product this is insignificant (Appendix A.3). The total solids concentration and the temperature vary significantly in the evaporator and thus strongly influence the physical properties during the evaporation process. The models were therefore based on two factors: temperature and percentage total solids. We were not constrained in the choice of temperatures for the samples (the sample temperature could easily be altered). However, the concentration that can be achieved by the evaporator limits the maximum percentage total solids of the product, and samples could not have a higher concentration than that at the end of the last pass.

3.2.4 Methods of measurements

Density

A hydrometer was used to measure the density of whey products in the laboratory. There are hydrometers suitable for measuring a wide range of densities, including the density of concentrated solutions. Hydrometers are typically calibrated at 20°C and the use of these meters at different temperatures requires a correction factor. The principle, calibration and correction factors of hydrometers are discussed in Appendix A.4.

Using the dilution method, 500 ml product samples with concentrations of 5-30% total solids were prepared from different whey products. Each sample was placed in a 500 ml measuring cylinder and density was measured using a hydrometer at room temperature. The hydrometer was lightly dropped into the whey solution, and at the same time it was

given a spin. When it had stopped bobbing up and down the number on the stem that corresponded to the level reached by the liquid was read. Samples were then heated in 10°C increments up to 60°C using the water bath where the density measurements repeated at each 10°C increment. This was repeated with different concentrations of whey solutions.

Viscosity

The viscosity of whey products at different shear rates was measured using a rotational Rheomat viscometer (Mettler RM180 Rheomat, Rheometric Scientific, USA). The open, concentric measurement system of this viscometer allows measurements by immersion (Figure 3.2). The measuring head and measuring tube are rigidly coupled; a direct-current motor drives the measuring head. The measuring head rotates within a fixed surrounding tube, defining a specific geometry. The flow resistance of the sample in the measuring gap causes a retarding torque that is measured electronically from the motor current. The viscosity is the measured torque divided by the applied shear rate. The Rheomat is accurate to 0.5 mPa s, and cannot usually measure below 5 mPa.s. Using the dilution method, 100 ml samples with concentrations of 5-30% total solids were prepared from different whey products. The maximum shear rate one can achieve with the Rheomat viscometer is 1291 s^{-1}. The temperature of the samples was controlled to ± 1°C using a water bath, and the viscosity was measured at 10°C increments between 20°C and 60°C.
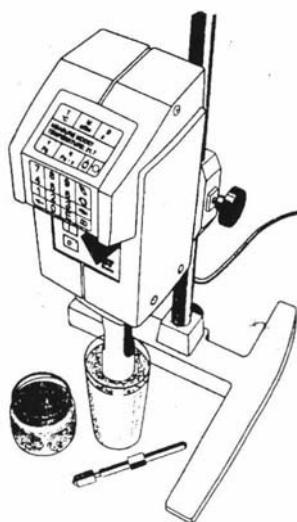
Figure 3.2: Rheomat viscometer (*Rheometric Scientific, Ltd., New Jersey, U.S.A*)

In order to measure the absolute viscosity at low shear rate, a capillary tube viscometer was used (Figure 3.3). This apparatus uses very low shear and operates under gravity. The liquid sample was sucked into the capillary tube until the liquid level was slightly above mark C. The liquid was then allowed to flow freely down from mark C. The time was measured for the meniscus to pass from Mark C to mark E. The viscosity of the sample was then estimated by multiplying the flow time by the viscosity constant. In this procedure, the viscometer was placed in a water bath and heated up in 10°C increments to a maximum of 50°C. The time that the product took to flow between two marks was measured approximately three times at each temperature, or until uniformity in values was observed. The viscometer was calibrated by measurements carried out with water, before performing the measurements with whey products. The principles of the viscometer measurements and calibration tests are discussed in Appendix A.5.
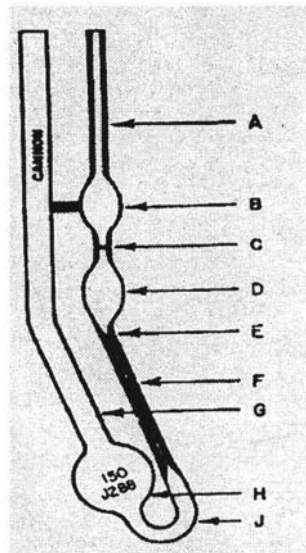
Figure 3.3: Capillary viscometer
(*Gebhard Schramm, 1981*)

Contact angle and surface tension

A technique developed from previous studies (Paramalingam et al., 1999, Paramalingam, 1999) was used to evaluate advancing contact angle and surface tension. The sessile drop profile equation and capillary rise on a vertical plate were simultaneously solved for two unknown parameters, surface tension and advancing contact angle (Appendix-A.6). The measurements were carried out in two steps. Firstly, the sessile drop

height on a flat plate was measured and secondly the capillary rise on a vertical plate was measured. This procedure was repeated with different concentrations of whey products. The principles of this measurement are discussed in Appendix A.6.

3.2.5 Products selected for properties measurements

Two common products, casein Whey Protein Concentrates (WPC-3) and Whey Protein Isolate (WPI) were selected for the physical property measurements for experimental and theoretical model development. The models were then validated for two further products, high fat Whey Protein Concentrate (WPC-2) and cheese Whey Protein Concentrate (WPC-1), using fewer experimental measurements.

3.3 Results and discussion

3.3.1 Regression models

Total solids Refractive Index correlations

There were four whey products for which the total solids and refractive index correlation were obtained. These were WPC-1, WPC-2, WPC-3 and WPI, products whose compositions differ significantly from one another (Appendix A.3). The general correlation equation between the total solids and the refractive index (RI) is shown in equation (3.1) with the coefficients listed in Table 3.1.

$$w_{TS} = r_i \cdot RI + s_i \qquad\qquad (3.1)$$

Where,

w_{TS} - Total Solids concentration (w/w%)
RI - Refractive Index value (%Brix)
r_i - Constants (w/w%/ %Brix)
s_i - Constants (w/w%)

Table 3.1: Correlation factors for each whey product

Product	r_i	s_i	R^2
WPC-1	0.9302	- 2.8314	0.9716
WPC-2	0.8917	-1.098	0.9849
WPC-3	0.8656	-0.3479	0.9744
WPI	0.7654	1.9109	0.9588

Each correlation factor was generated from a graph of total solids vs refractive index (shown in the Appendix A.1). These graphs showed a linear relationship between total solids and refractive index. The four whey products are produced to a number of different specifications. However, the composition of each specification of the same product type is fairly similar. Therefore, the correlations were derived for only one product specification for each product type.

Density

The measured density values of both WPC-3 and WPI are shown in Figures 3.4 and 3.5 respectively, along with the regression models.
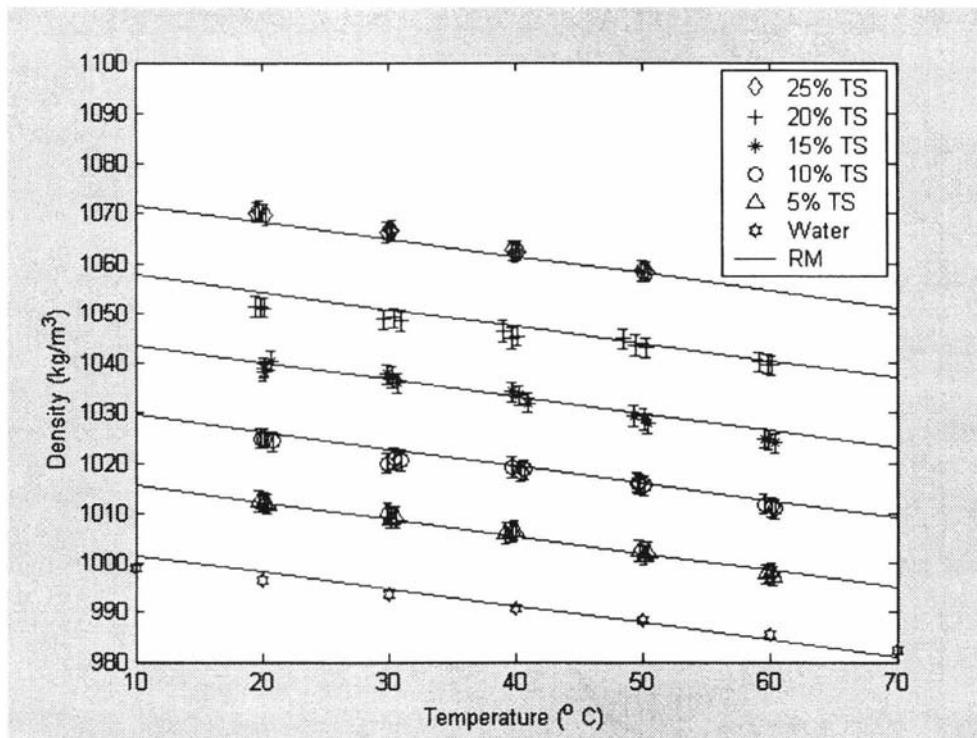
Figure 3.4: The effect of temperature on the density of WPC-3 as a function of total solids concentration (RM- Regression Model)

Density was measured to ± 0.5 kg/m^3 using the hydrometer and the error in sample preparation was $\pm 0.5\%$ total solids which is equivalent to 1.5 kgm^{-3}. The error bars shown in Figures 3.4 and 3.5 represent ± 2 kgm^{-3}. There were difficulties associated with density measurements high total solids (30-35%) at high temperatures (above 50°C) due to the denaturation of whey protein. This is further discussed under the viscosity section.
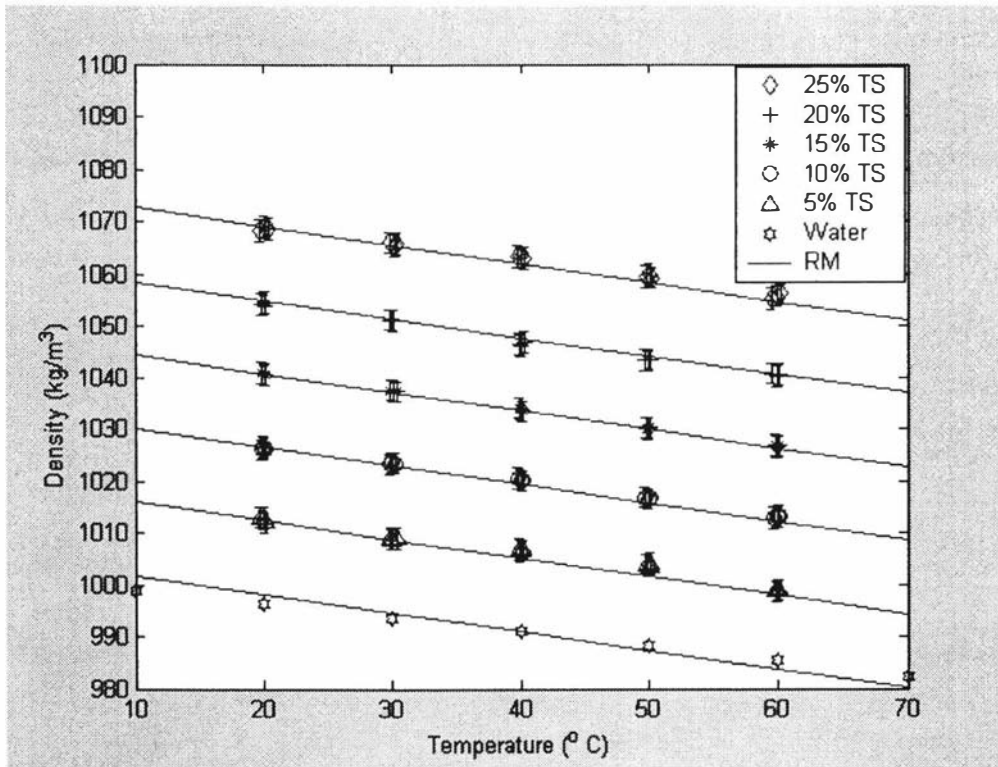
Figure 3.5: The effect of temperature on the density of WPI as a function of total solids concentration (RM- Regression Model)

The density results obtained from the experiments with both WPC-3 and WPI followed a linear trend. Multi-factor regression models were developed with regression factors (R^2) of nearly 1 (Appendix A.4). The regression models for WPI and WPC-3 are given by equation (3.2) and (3.3) respectively.

$$\rho_{wpi} = 1005.3 - 0.359T + 2.837w_{TS} \qquad R^2 = 0.998 \qquad (3.2)$$

$$\rho_{wpc-3} = 1005 - 0.342T + 2.800w_{TS} \qquad R^2 = 0.996 \qquad (3.3)$$

Where,

T - Temperature (^oC)

ρ - Density (kgm^{-3})

The regression models were tested for water ($w_{TS} = 0$) using the data from Perry and Green (1984). The models underestimate the density above 60°C and overestimate the density below 20°C. The density regression models can be considered applicable to whey products if the temperature is in the range of 20°C to 60°C and the total solids concentration up to 25%.

Viscosity

Figures 3.6 and 3.7 show the viscosity of WPC-3 at low and high shear rates while Figures 3.8 and 3.9 show the viscosity of WPI at low (100 s^{-1}) and high (1291 s^{-1}) shear rates, respectively. The regression models are plotted in the same Figures.
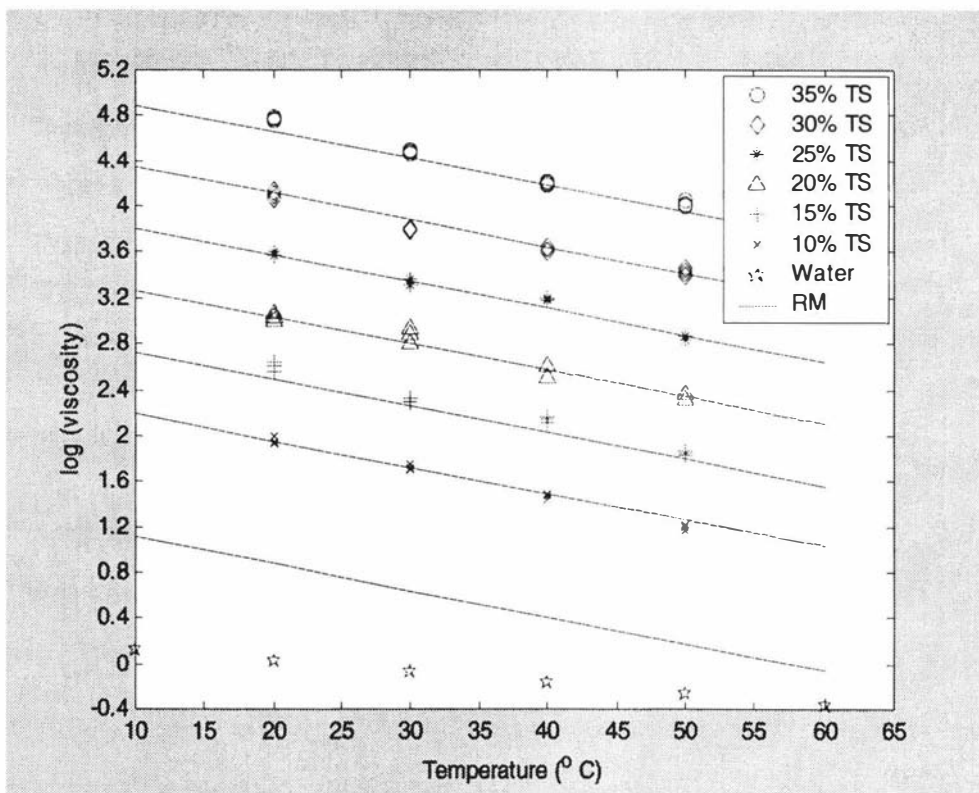
Figure 3.6: Viscosity of WPC-3 concentrates as a function of temperature and total solids concentration at low shear rates (RM-Regression Model)
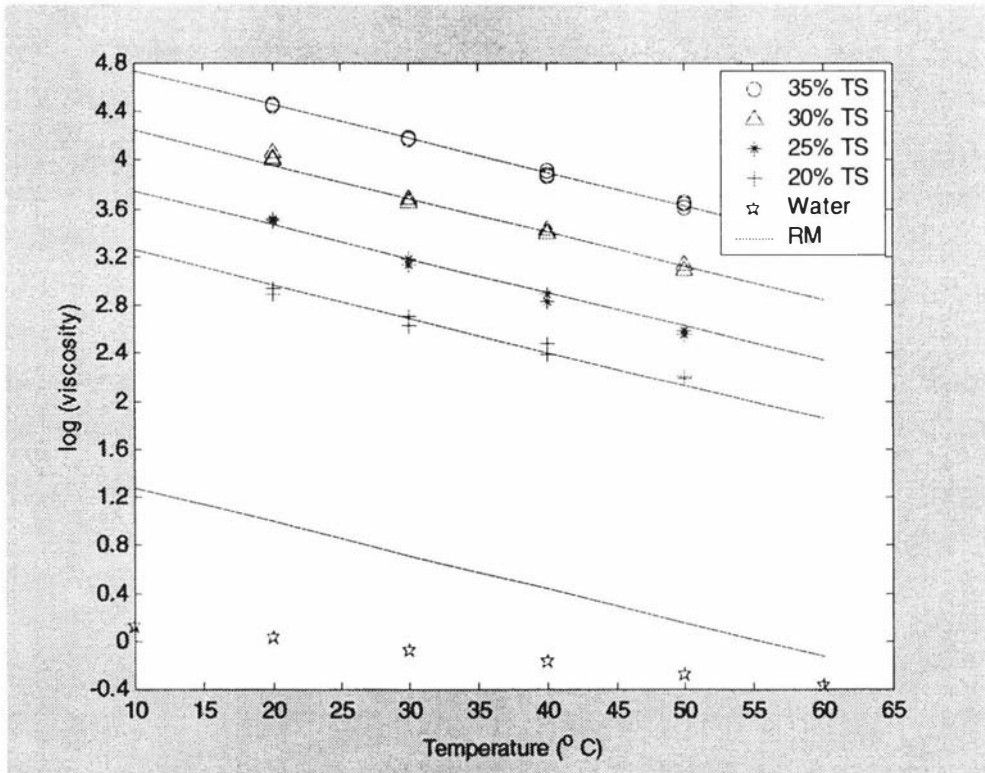
Figure 3.7: Viscosity of WPC-3 concentrates as a function of temperature and total solids concentration at high shear rate (RM-Regression Model)
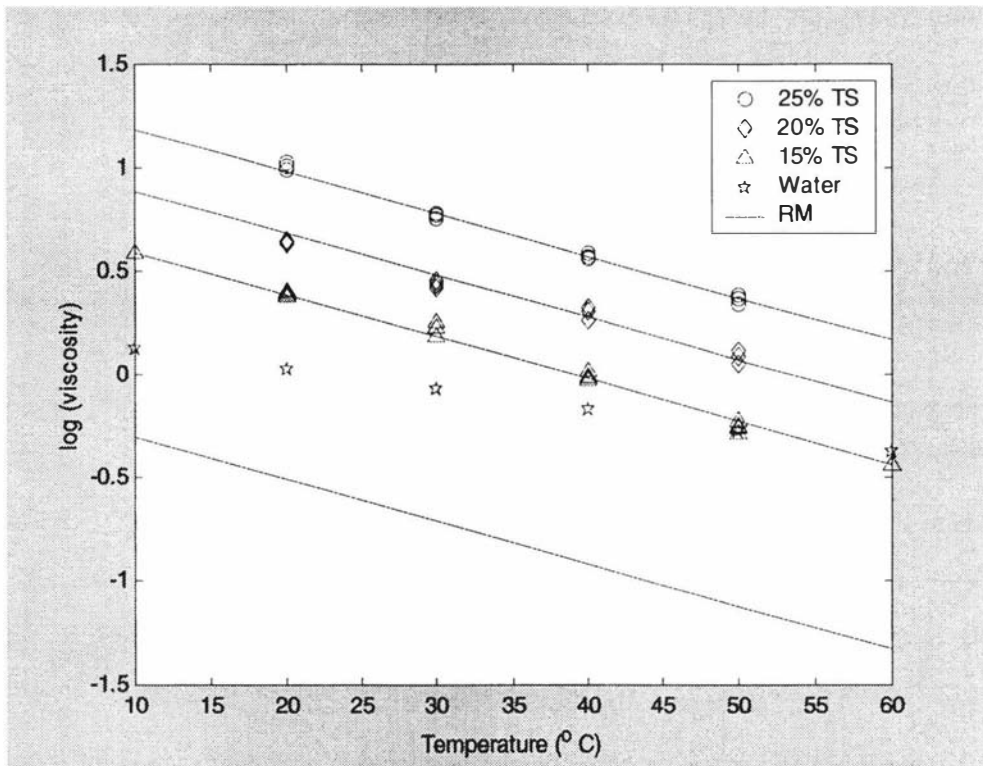
Figure 3.8: Viscosity of WPI concentrates with temperature as a function of temperature and total solids concentration at low shear rates (RM- Regression Model)
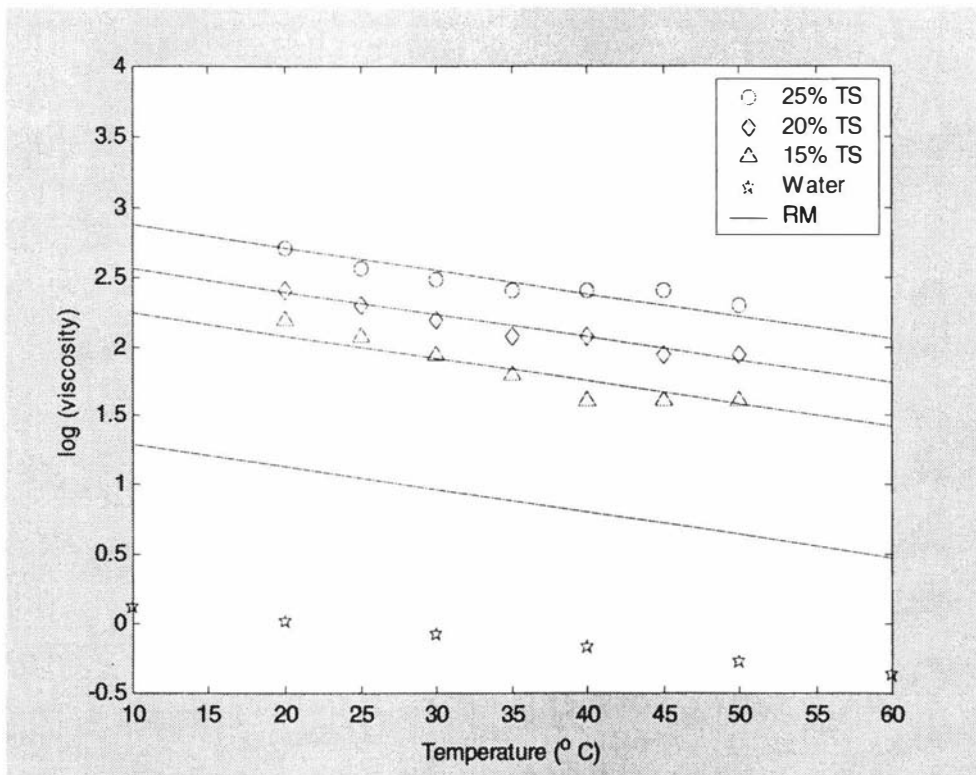
Figure 3.9: Viscosity of WPI concentrates with temperature as a function of temperature and total solids concentration at high shear rates (RM- Regression Model)

It is clear from Figures 3.6 to 3.9 that both products show an increase in viscosity with increasing total solids concentration and decreasing temperature regardless of what shear rate is applied. Significant differences in viscosity between WPC-3 and WPI can be observed from the Figures. The higher viscosity of WPC-3 can be related to the presence of fat, casein and the types of whey proteins. The presence of fat, lactose and types of protein are the difference between WPC-3 and WPI. For WPI, the high shear viscosity was higher than the low shear viscosity. This is due to the shear thickening effect (Pascas, 2002; Appendix A.5). During the measurements, the sample temperature was raised from room temperature to approximately 70°C. In practice, the maximum temperature of the concentrate does not exceed 50°C. The reason for this is to avoid whey protein denaturation. To avoid additional complexity of incorporating protein denaturation in the viscosity models, the regression model was limited to the temperature range 20 to 50°C. The range of total solids concentrations of the prepared samples varied between products. This was due to the difference in total solids concentration exiting the evaporator for different products.

Experimental data for the temperature range 20 to 50°C and total solid concentrations between 10 and 35% (WPC-3) or 10 and 25% (WPI) were satisfactorily described by equation (3.4). The regression coefficients are listed in Table 3.2. The models are not valid below 10% total solids because viscosity data for water and solids below 10% were not included when creating the regression models.

$$\ln(\mu) = e_1 + e_2 T + e_3 w_{TS} \qquad R^2 = 0.99 \qquad (3.4)$$

Where, μ is the dynamic viscosity of the product (cp) and e_1, e_2, e_3 are constants (-)

Table 3.2: Viscosity regression coefficients

Products	Shear rate (s^{-1})	e	f	g
WPC-3	Low (100 s^{-1})	1.3400	-0.0233	0.1080
	High (1291 s^{-1})	1.5500	-0.0281	0.0993
WPI	Low (100 s^{-1})	-0.1000	-0.0204	0.0595
	High (1291 s^{-1})	1.4600	-0.0163	0.0630

Contact angle and surface tension

Figures 3.10 and 3.11 show the advancing contact angle and surface tension of WPC-3 concentrates while Figures 3.12 and 3.13 show the advancing contact angle and surface tension of WPI concentrates.
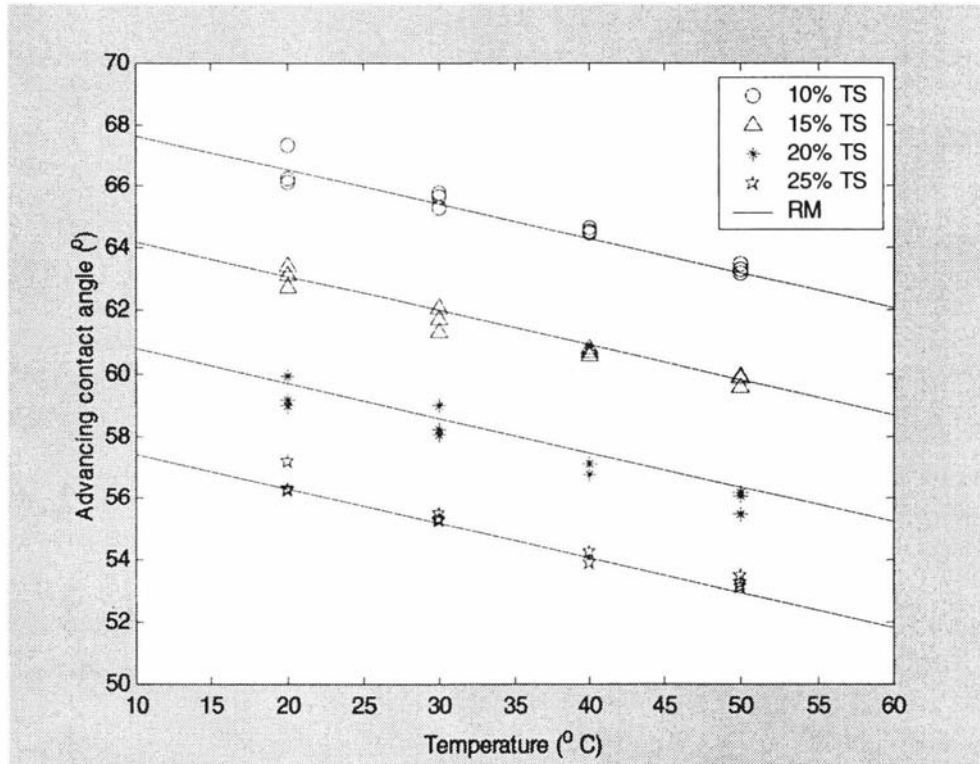
Figure 3.10: Advancing contact angle of WPC-3 concentrates as a function of temperature and total solids concentration (RM-Regression Model)

47
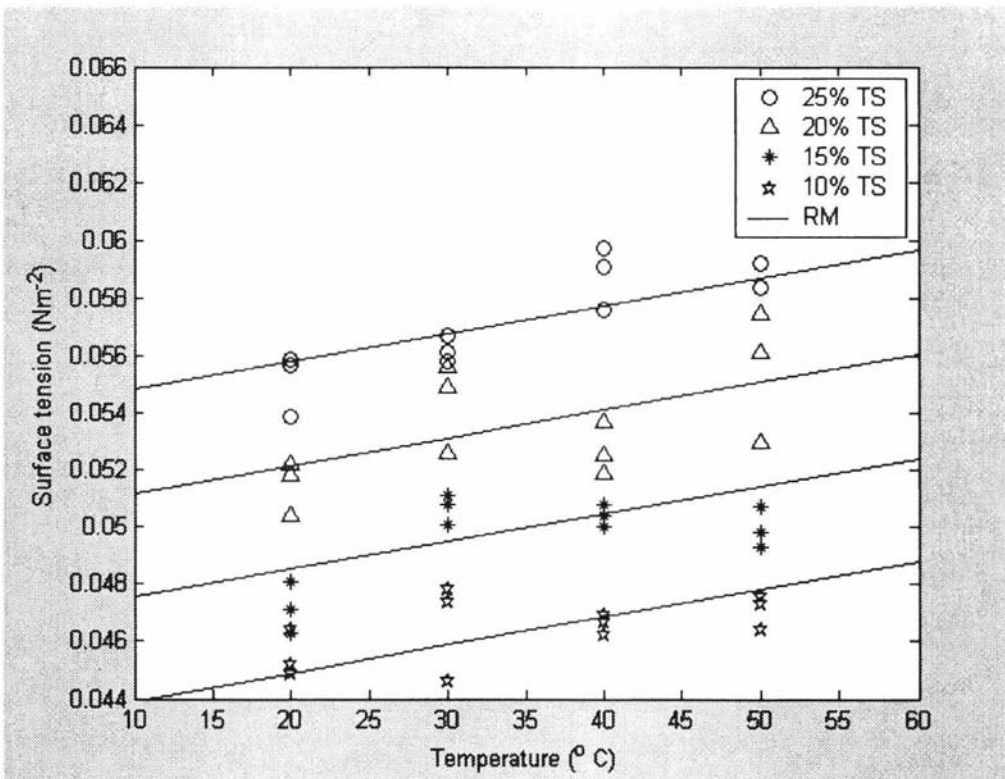
Figure 3.11: Surface tension of WPC-3 concentrates as a function of temperature and total solids concentration (RM- Regression Model)
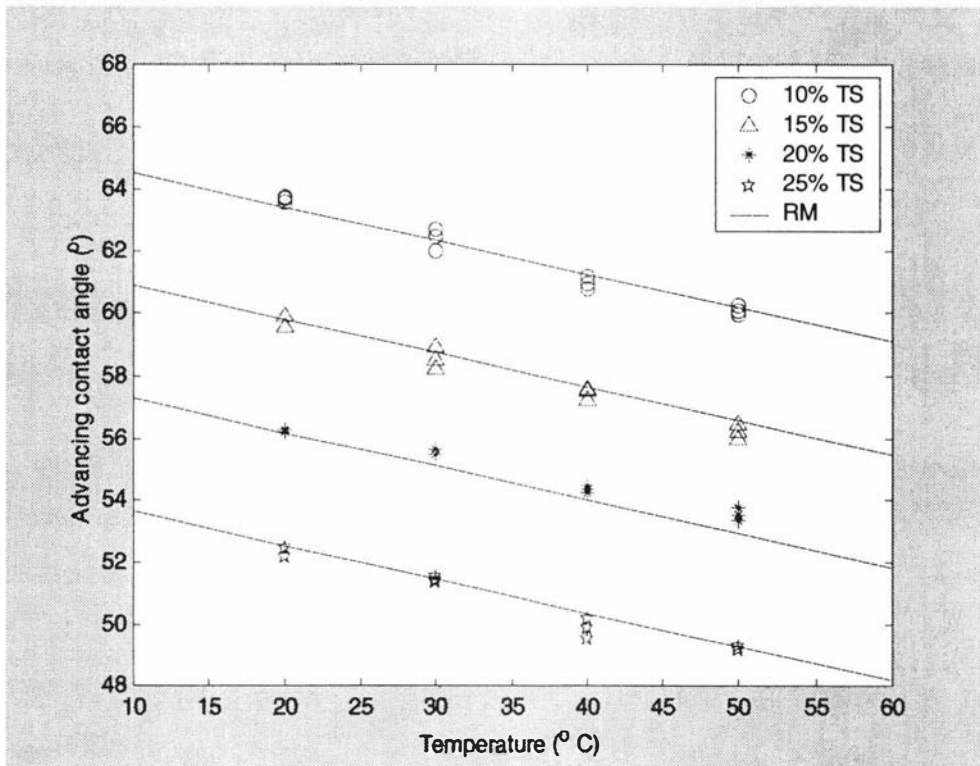
Figure 3.12: Advancing contact angle of WPI concentrates as a function of temperature and total solids concentration (RM-Regression Model)
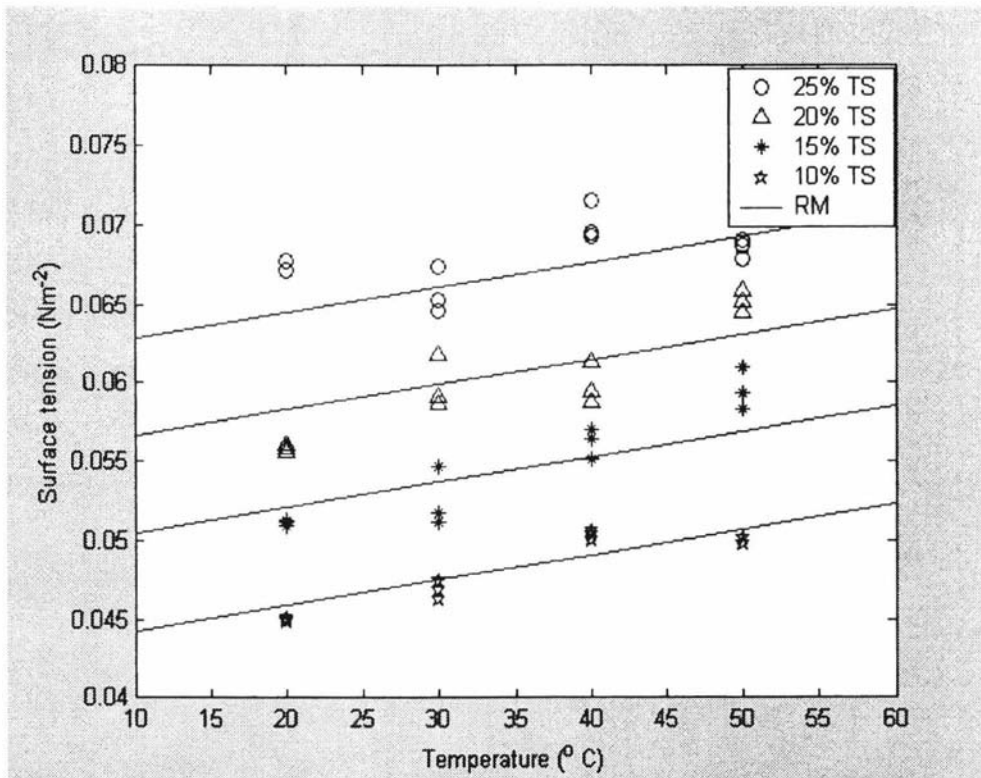
Figure 3.13: Surface tension of WPI concentrates as a function of temperature and total solids concentration (RM- Regression Model)

The uncertainties associated with contact angle and surface tension measurements were $\pm 0.34°$ and $\pm 0.016 \mathrm{Nm}^{-1}$, respectively. The literature (Paramalingam et al., 2001; Hartley and Murgatroyd, 1964) suggests that the retreating contact angle for water is $40°$ and this value can be used in retreating minimum flow calculations with milk or whey products. The regression model for the advancing contact angle and surface tension is given by equation (3.5). The regression coefficients are listed in Table 3.3.

$$\theta_a = a_{oc} + a_{Tc}T + a_{TSc}w_{TS} \ (R^2 = 0.99), \quad \sigma = a_{os} + a_{Ts}T + a_{TSs}w_{TS} \ (R^2 = 0.91) \tag{3.5}$$

Where, θ_a - Advancing contact angle (°) and σ - Surface tension (Nm^{-1})

Table 3.3: Regression coefficients for advancing contact angle and surface tension

Product	Advancing contact angle (θ_a)			Surface tension (σ)		
	a_{oc}	a_{Tc}	a_{TSc}	a_{os}	a_{Ts}	a_{TSs}
WPC-3	75.6	-0.111	-0.685	0.0357	0.000097	0.000726
WPI	72.9	-0.109	-0.727	0.0303	0.000160	0.001240

3.3.2 Semi-empirical models

Density, specific heat capacity and thermal conductivity

The semi-empirical models of physical properties (density, specific heat capacity and thermal conductivity) developed by Murakami and Okos (1989) are applicable to milk concentrates but not to whey concentrates since the dominant components in milk products are different from those of whey concentrate. Casein protein, fat and lactose are the major components of milk concentrates whereas whey proteins are the major components of whey concentrates. The effects of individual proteins- casein, α-Lactalbumin and β-Lactoglobuline- must be included to make the models of Murakami and Okos applicable to both milk and whey concentrates. Density of α-Lactalbumin and β-Lactoglobuline are calculated using physical property software (G&P Engineering physical property, 2001) and with whey protein chemical structure information given in Appendix A.4.7 (Bylund, 1995; Robert and Don, 1997; Fox, 1992). The ideal mixture formula was used to estimate the concentrate property as it is with Murakami's model.

Density

The density of the whey concentrate is given by equation (3.6) and the density models for each component are given as a function of temperature.

$$\frac{1}{\rho} = \sum_{i=1}^{n} \frac{w_i}{\rho_i} \qquad (3.6)$$

Where, ρ_i- Density of ith component (kg m^{-3}) and w_i - Weight fraction of ith component. The density of water is given by $\rho_w = 1001.3 - 0.2423 \times T - 0.0004 \times T^2$ (G&P Engineering physical property, 2001) and the density of whey components is given in the form of $\rho_i = a_i + b_i T$. The model coefficients for each component are given in Table 3.4.

Table 3.4: Density model coefficients

Constant	Salt	Lactose	Fat	α-Lact albumin	β- Lacto globuline	Casein
a_i	2800.0	1599.1	925.58	1464.4	1378.1	1317.3
b_i	-0.28063	-0.31046	-0.1553	-1.2103	-1.1451	-0.4141

Specific heat capacity

The specific heat capacity of the whey concentrate is given by equation (3.7) and the specific heat capacity for each component expressed as a function of temperature.

$$Cp = \sum_{i=1}^{n} w_i Cp_i \tag{3.7}$$

Specific heat capacity of water is given by

$Cp_w = 4226.6 - 2.4917 \times T + 0.0354 \times T^2 - 0.0001 \times T^3$ and the specific heat capacity of

whey components is given in the form of $Cp_i = c_i + d_i T + e_i T^2$. The model coefficients

for each component are given in the Table 3.5.

Where,

Cp - Specific heat capacity of product (J kg^{-1} K^{-1})

Cp_i - Specific heat capacity of ith component (J kg^{-1} K^{-1})

Cp_{water} - Specific heat capacity of water (J kg^{-1} K^{-1})

Table 3.5: Specific heat capacity model coefficients

Constant	Salt	Lactose	Fat	α-Lact albumin	β- Lacto globuline	Casein
c_i	2930.1	1256.0	1848.533	2630.3	2592.8	2183.8
d_i	-	-	8.25885	-2.4668	-2.3420	-2.7901
e_i	-	-	-0.04977	0.0116	0.0118	0.0140

Thermal conductivity

The thermal conductivity of the whey concentrate is given by the equation (3.8) with the thermal conductivity for each component expressed as a function of temperature.

$$k_p = \sum_{i=1}^{n} \phi_i k_i = \frac{w_i \rho_p}{\rho_i} k_i \tag{3.8}$$

Thermal conductivity of water is given by $k_w = 0.5672 - 0.0017 \times T - 0.000006 \times T^2$

and of whey components is given in the form of $k_i = f_i + g_i T + h_i T^2$. The model

coefficients for each component are given in Table 3.6.

Where,

k_p - Thermal conductivity of product (W m^{-1} K^{-1})

k_i - Thermal conductivity of ith component (W m^{-1} K^{-1})

k_w - Thermal conductivity of water (W m^{-1} K^{-1})

Table 3.6: Thermal conductivity model coefficients

Constant	Salt (10^{-3})	Lactose (10^{-3})	Fat (10^{-3})	α-Lact albumin	β- Lacto globuline	Casein
f_i	329.600	201.400	180.700	0.20240	0.19970	0.17970
g_i	1.40110	1.38740	0.27604	-0.0003	-0.0003	-0.0003
h_i	-0.00291	-0.00433	-0.000178	0.0000	0.0000	0.0000

Viscosity

Snoeren et al. (1982 & 1983) carried out experiments with skim milk to find the volume fractions in the empirical viscosity model shown in equation 3.9. Winchester (2000) has used Snoeren's model for milk concentrates without any modifications. Because of difficulties in finding the viscosity of the components separately the maximum total solids concentration (w_{max}) and model constant (k_v) in model (3.9) were identified from the experimental data for whey concentrates. The solvent viscosity, μ_s, was replaced by the viscosity of lactose plus salt solution.

$$\mu = \mu_s \left[1 + \frac{1.25 k_v \phi_t}{\left(1 - \frac{\phi_t}{\phi_m} \right)} \right]^2 \qquad (3.9)$$

Where,

$\phi_t = \left(x_{cp} V_{cp} + x_{wp} V_{wp} + x_f V_f \right) w_{TS} \rho$ and $\phi_m = \left(x_{cp} V_{cp} + x_{wp} V_{wp} + x_f V_f \right) w_{max} \rho_{max}$

The regression model for the viscosity of lactose solution was developed from the experimental data of Buma (1980) and is given by equation (3.10).

$$\ln(\mu_s) = 0.326 - 0.0226 \times T + 4.57 \times w_{ls} \qquad (3.10)$$

Where,

$$w_{ls} = \frac{x_l w_{TS}}{(1 - w_{TS} + x_l w_{TS})}$$

Voluminosity is defined as the effective volume occupied by 1kg of the component. Experimental and theoretical voluminosities (v) of whey components are given in Table 3.7. The theoretical values obtained from the inverse density of each component and the experimental values from Snoeren's work.

Where,
v_i - Voluminosity of ith component (m^3 kg^{-1})
ϕ_i - Volume fraction of ith component (-)
ϕ_t - Total volume fraction (-)
ϕ_m - Maximum volume fraction (-)
μ_s - Viscosity of lactose solution (cp)
w_{max} - Maximum concentration before gel (w/w)
ρ_{max} - Density of the maximum concentration (kg/m^3)
w_{ls} - Concentration of the lactose solution if it were the only component (w/w)
x_l - Dry matter fraction of the lactose in the whey concentrate (w/w)
x_{cp} - Dry matter fraction of the casein protein in the whey concentrate (w/w)
x_{wp} - Dry matter fraction of the whey protein in the whey concentrate (w/w)
x_f - Dry matter fraction of the fat in the whey concentrate (w/w)

Table 3.7: Voluminosity of whey components

	Native			Denatured whey	Casein	Fat
	whey	α	β			
Theoretical $v \times 10^3$ (m^3/kg)	1.17	0.706	0.751	1.17	0.769	1.11
Experimental $v \times 10^3$ (m^3/kg)	1.07	-	-	3.09	3.57	-

Maximum concentration (w_{max}) *and model constant* (k_v) *identification*

The concentration, above which concentrated whey starts to form a gel, (w_{max}) was identified using the regression model developed from the experimental data for WPC-3. The viscosity of the milk concentrate at maximum solids is approximately 200 cP (Snoeren et al., 1982) and it is assumed to same with whey concentrates. The data set available for WPC-3 was sufficient to identify both the maximum concentration and the model constant, (k_v) for this product. However, the data set available for WPI was not sufficient for this purpose (low viscosity data involved in the regression model development). Thus, w_{max} and k_v were first identified for WPC-3 (Figures 3.14 and 3.15). The value of k fitted for WPC-3 was then used together with the experimental data for WPI to determine the maximum volume fraction (ϕ_m) for WPI. (Figure 3.16). The values of w_{max} and k_v for WPC-3 and WPI are tabulated in Table (3.8). All these constants were identified at 40°C, as the temperature of the final effect of the whey evaporator is 40°C. The w_{max} and k_v for WPI would need correction if more viscosity data were are available with higher total solids concentrations.
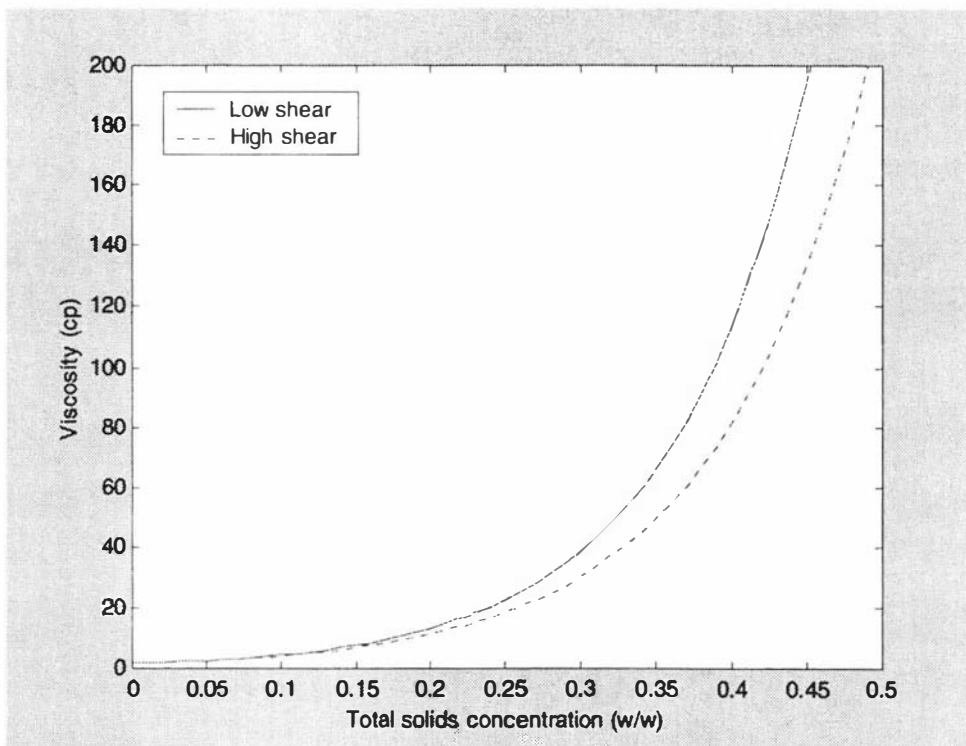
Figure 3.14: Regression model for viscosity of WPC-3 as a function of total solids concentration at low and high shear rates
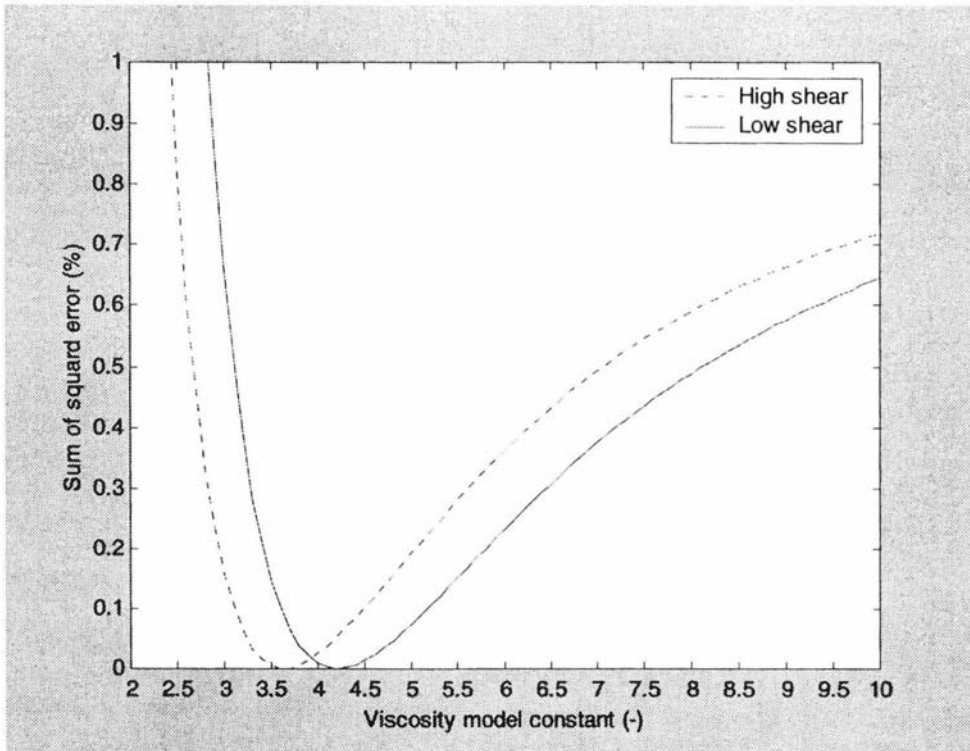
Figure 3.15: Optimum value of k for WPC-3
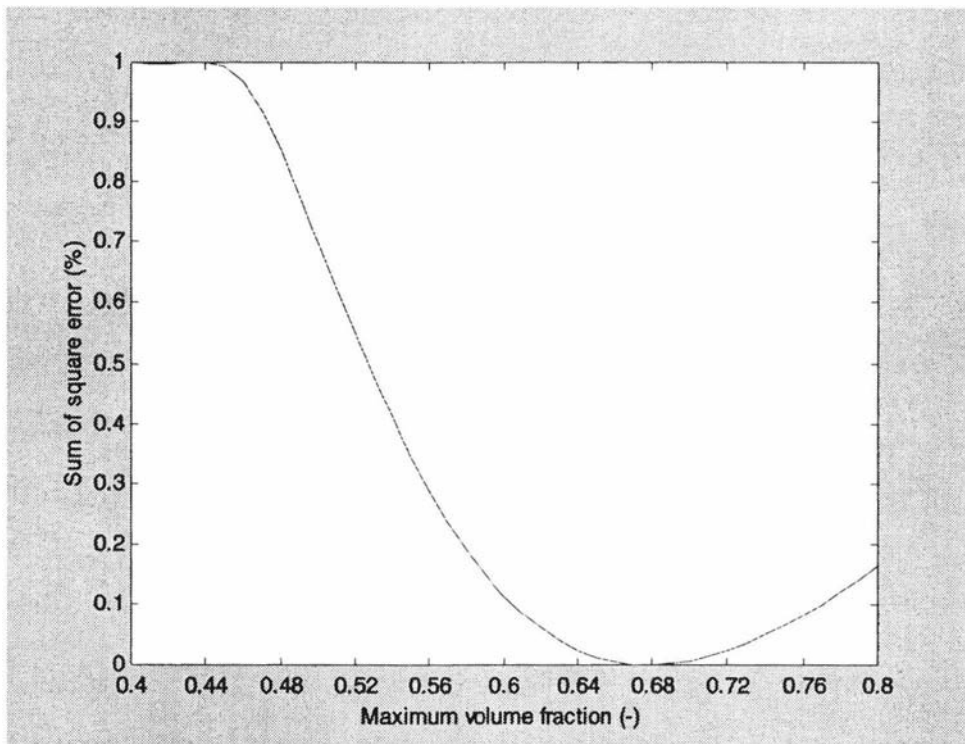
Figure 3.16: Optimum value of ϕ_m for WPI

Table 3.8: Viscosity model constants

Products	Shear rate	w_{max} (w/w)	k_v
WPC-3	Low	0.45	4.2
	High	0.50	3.6
WPI	Low	0.55	1
	High	0.55	4.2

3.3.3. Models testing and comparison

Calibration correlations

Whey samples diluted using the RI calibration equations were sent to the laboratory for an accurate verification of percentage total solids. The total solids concentrations predicted from RI measurements showed good agreement with laboratory-determined percentage total solids (Figure 3.17 and 3.18).
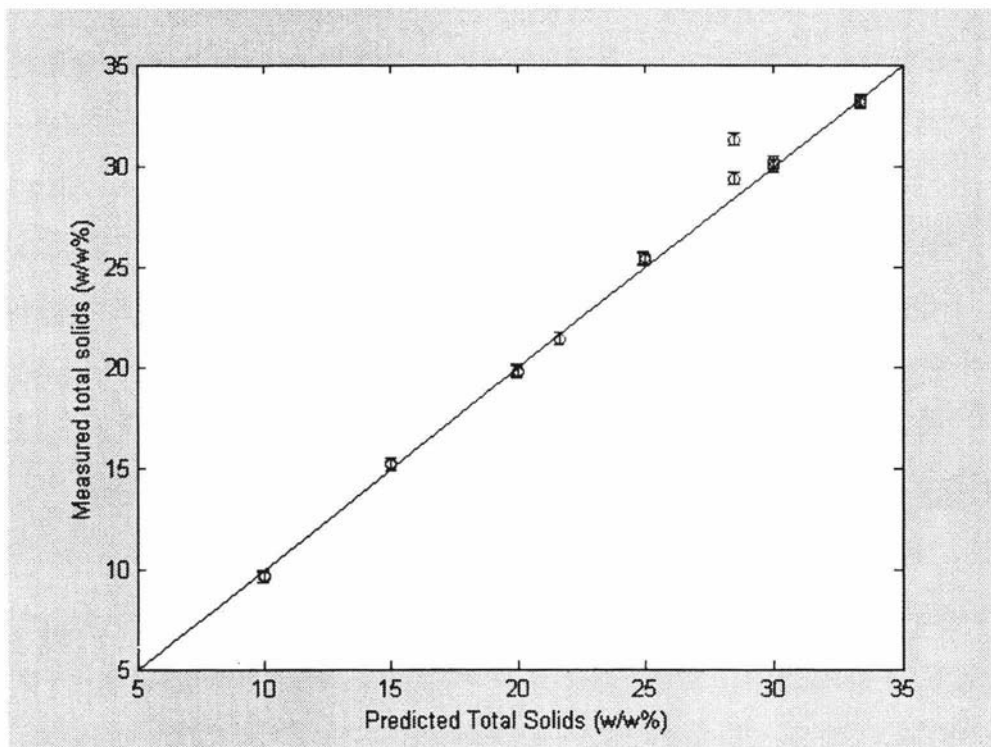
Figure 3.17: Laboratory-determined percentage TS versus percentage TS predicted from RI measurements for WPC-3
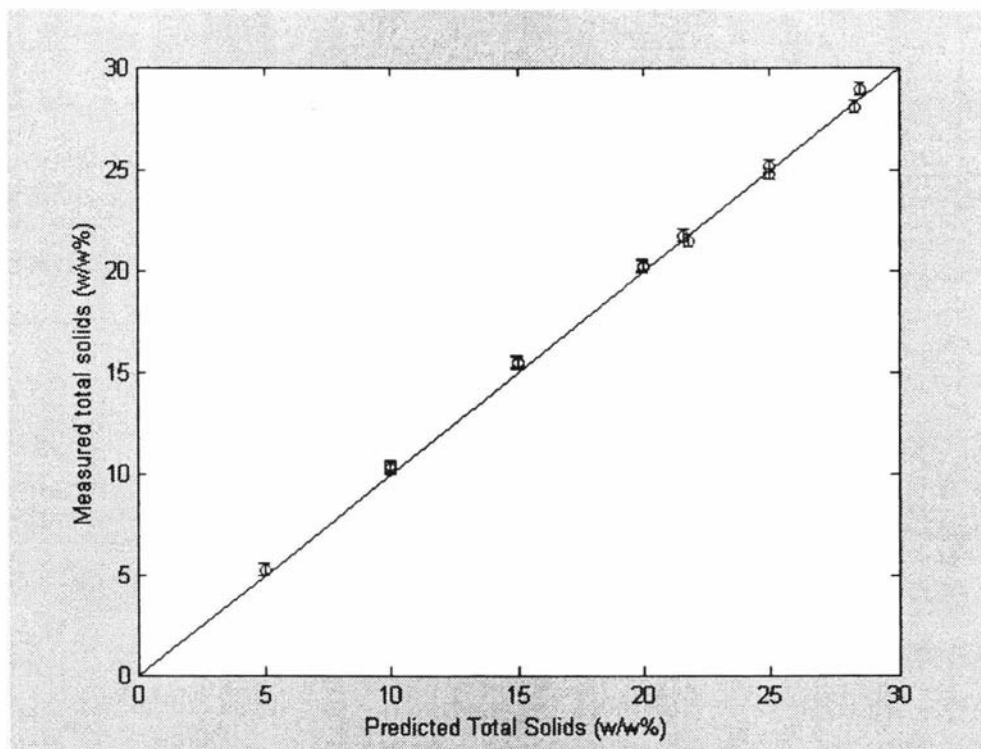
Figure 3.18: Laboratory-determined percentage TS versus percentage TS predicted from RI measurements for WPI

Density

Figures 3.19 and 3.20 compare the semi-empirical and regression models against commercial plant data for WPI and WPC-3 respectively. The density of the feed and the final product were measured using the Micromotion (DL200, Rosemount) density meter in the whey evaporator plant at $10^{\circ}C$ and at $40^{\circ}C$. The feed density (low TS) predictions for WPI differ from the plant data, in contrast with closer agreement for WPC-3. This could be due to the quantity of air present in the WPI. The high feed densities predicted by the regression model for WPI could be due to a partial release of entrained air from the feed during the sample preparation and the regression model's deviation below $20^{\circ}C$. The regression model for WPC-3 shows good agreement with the plant data up to 25% solids content but deviates at higher solids contents (Figure 3.20). The semi-empirical model predicts well the final product solids and shows deviation in the feed density predictions. This is due to the presence of air in the feed product which was not considered when developing the models. The air content in the feed product was estimated from the theoretical and measured density difference. The air content was high for WPI and is approximately 0.001% (w/w).

57
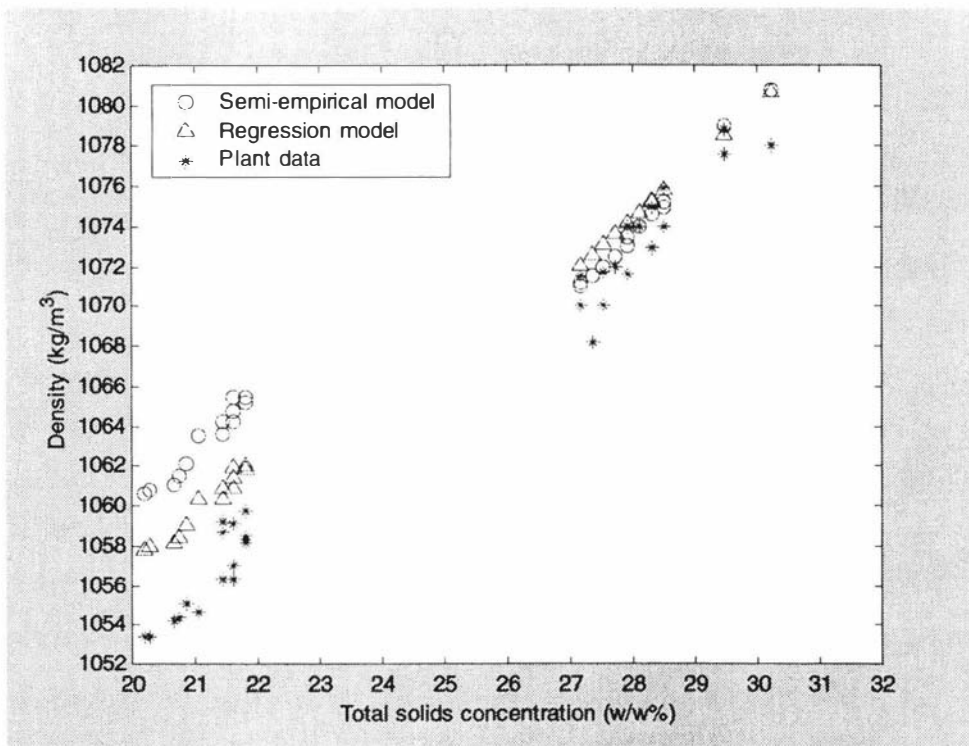
Figure 3.19: Comparison of regression and semi-empirical density model predictions against plant data for WPI
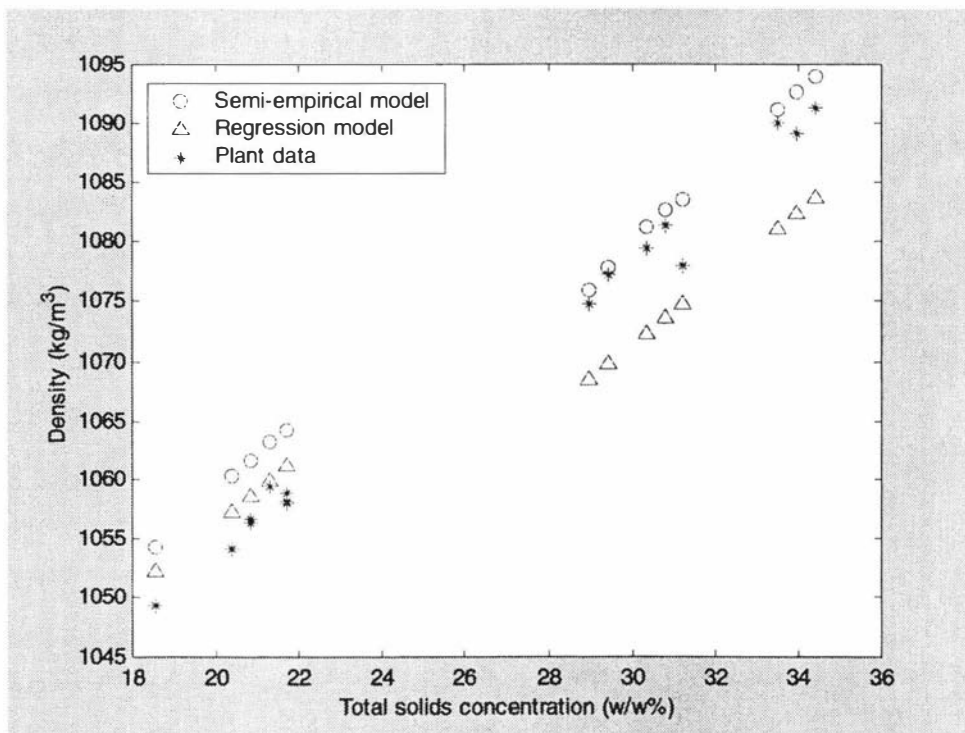
Figure 3.20: Comparison of regression and semi-empirical density model predictions against plant data for WPC-3

The applicability of the semi-empirical density model to other whey products (WPC-1 and WPC-2) was tested. Plant data were used to check the model predictions as for WPI and WPC-3. Figure 3.21 shows this comparison. The model predictions for WPC-1 and WPC-2 were better than for WPI and WPC-3 for both feed and product. Because the semi-empirical model is an extension of Murakami's model, the new semi-empirical model can be applied to milk products as well.
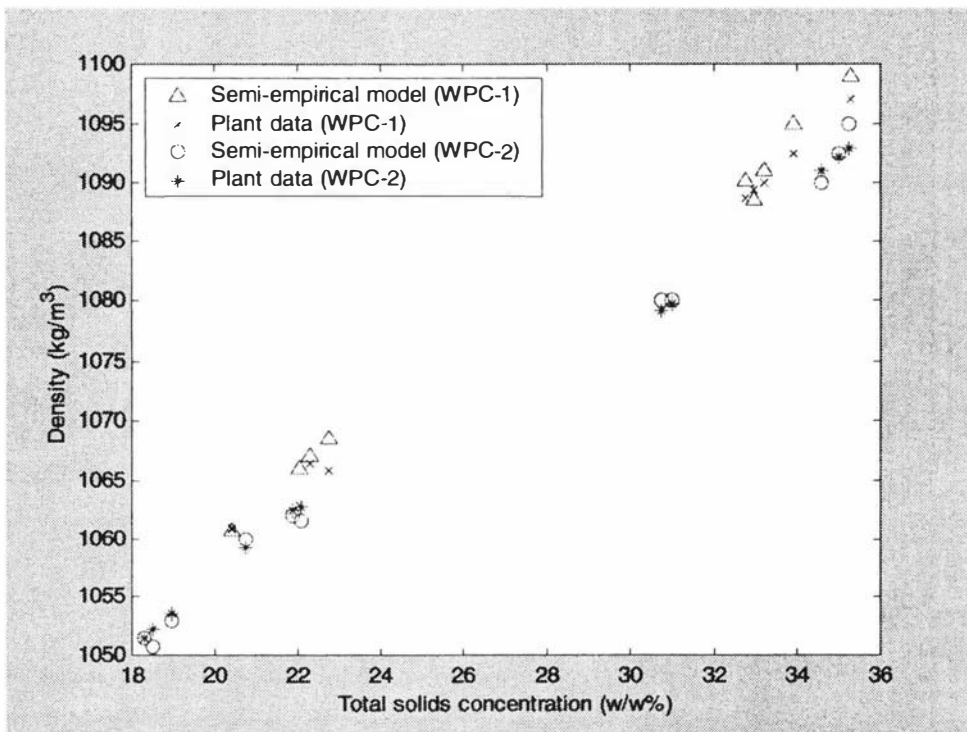
Figure 3.21: Comparison of semi-empirical density model predictions against plant data for WPC1 and WPC-2

Figure 3.22 compares the new semi-empirical model developed in this work based on product compositions with literature models (Heldman and Singh, 2001; Buma, 1980; Murakami and Okos, 1989) for predicting the evaporator exit density of WPI at various total solids concentrations. The accuracy of the semi-empirical model with the new model constants identified for concentrated WPI is shown in Figure 3.19. The literature model predictions deviate from the new-empirical model as the total solids concentration increases (Heldman and Murakami's model deviation is 10 kg/m^3 at 30% total solids). Thus, the accuracy of the literature models decrease as the total solids concentration increases.
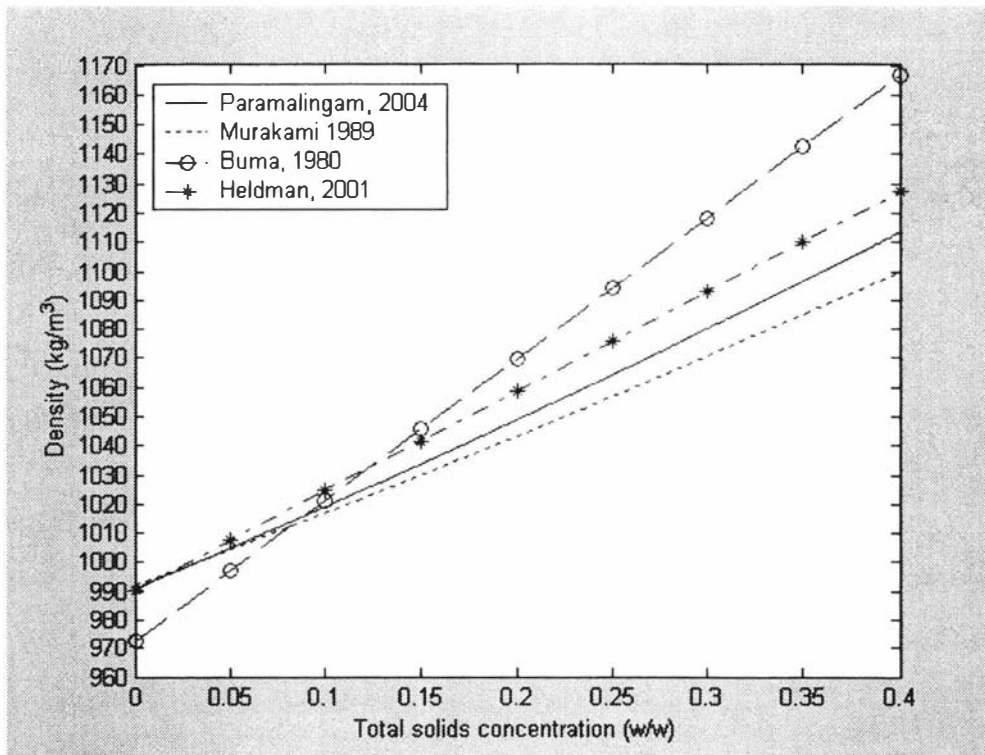
**Figure 3.22: Literature density model predictions comparison with
new semi-empirical model for WPI**

Viscosity

Because the semi-empirical model coefficients were determined using the experimental
data, the predictions of the two models (semi-empirical and regression) were not
compared. The applicability of the semi-empirical model to other whey products (WPC-
1 and WPC-2) was tested. The experimental data collected for WPC-1 and WPC-2
(smaller data sets than for WPC-3 and WPI) were used to test the semi-empirical model
predictions for these products (Figure 3.23). The high shear model predictions match
the experimental data well at all concentrations. The low shear model predictions match
the data well at low concentrations but deviate at high concentrations. This could be due
to the fact that the maximum volume fractions for WPC-1 and WPC-2 are not exactly
the same as for WPC-3. However, the accuracy of this estimation is adequate to
determine the optimum final total solids concentration from the evaporator. An
advantage of the semi-empirical model is that the concentrate viscosity of a new
product can be estimated whereas the regression models are limited to one product.
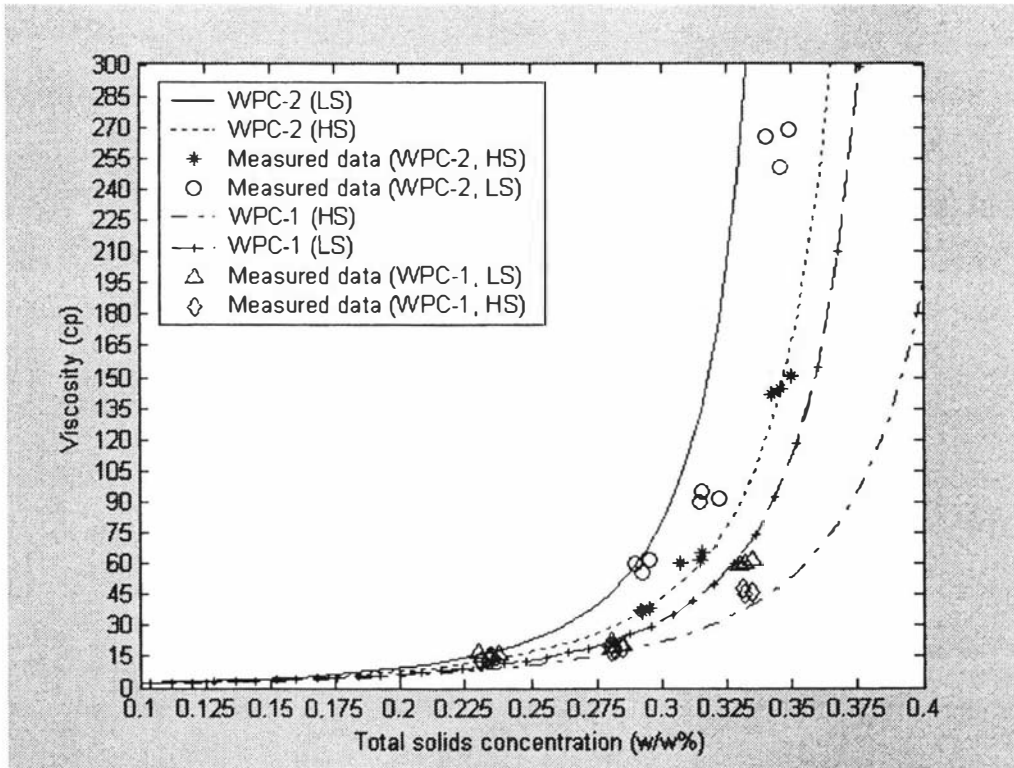
Figure 3.23: Semi-empirical viscosity model predictions compared with experimental data for WPC-1 and WPC-2 at 30°C
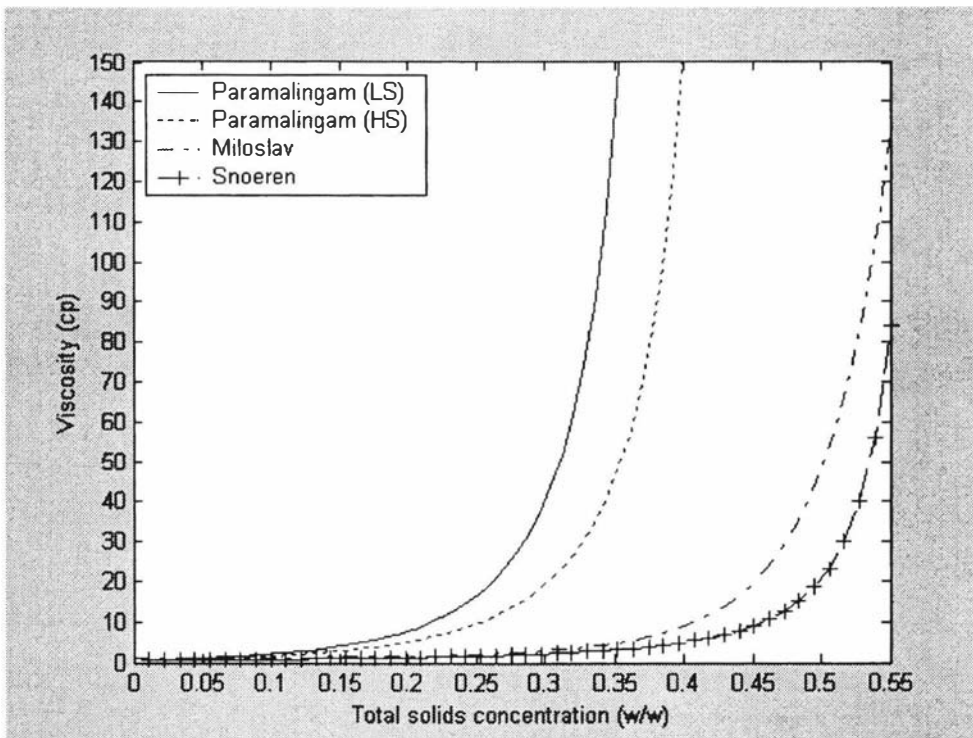
Figure 3.24: Comparison of semi-empirical viscosity model with literature viscosity models for WPC-3 at 40°C

The semi-empirical viscosity models were compared with literature models developed for whey products (Adam et. al, 1994) and milk concentrates (Snoeren, 1982). The comparison of these models was made for WPC-3 product and is shown in Figure 3.24. The literature models differ and cannot be applied directly to whey products. There was insufficient information on the compositions and the heat treatment history of the whey concentrates for which Miloslav's model was developed, and the maximum volume fraction used in Sneoren's model was for skim milk concentrates.

Specific heat capacity

Figures 3.25 and 3.26 show comparisons of the semi-empirical models developed in this work with literature models for WPC-3 (Heldman, 2001; Adam et. al, 1994; Murakami, 1989) and whole milk (Murakami, 1989; Fernandez-Martin, 1971) respectively. The difference between the specific heat capacity models for WPC-3 increases as the total solids concentration increases (Figure 3.25). As there was no experimental data available for whey concentrates against which the model predictions could be validated, the models were instead validated by comparison with the regression model developed by Fernandez-Martin (1971) for whole milk concentrates (figure 3.26). Figure 3.26 shows that both Murakami (1989) and new semi-empirical model predictions were close to Fernandez-Martin's experimental model. The effect of 0.001% (w/w) air in the product on the specific heat capacity is insignificant and therefore not shown in any of the figures.
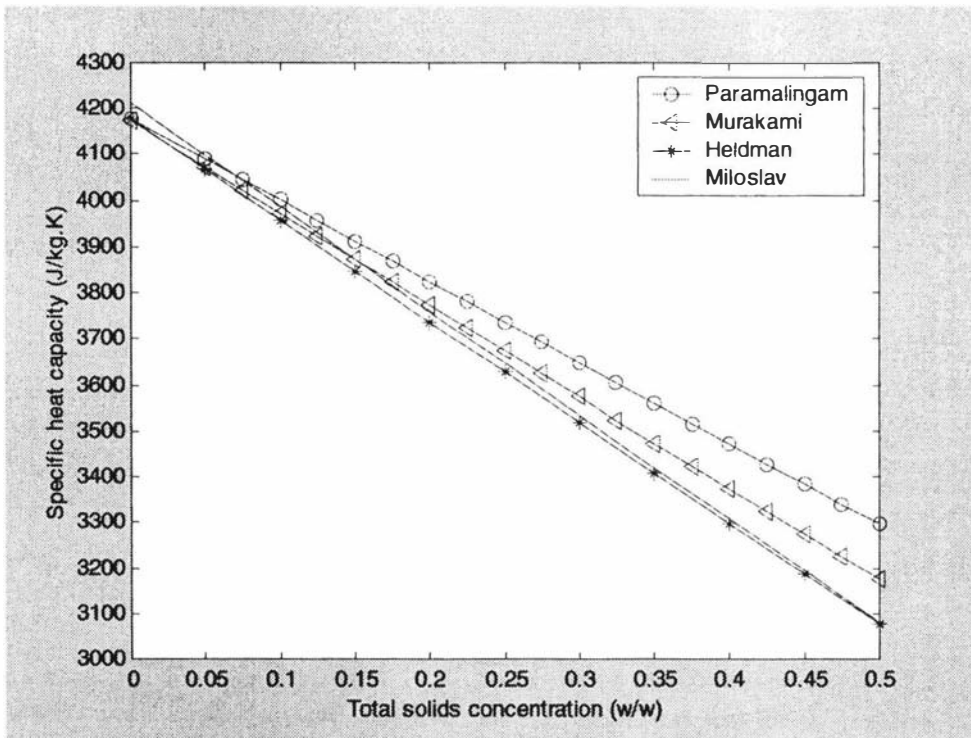
Figure 3.25: Comparison of the Semi-empirical and literature models for the specific heat capacity of WPC-3
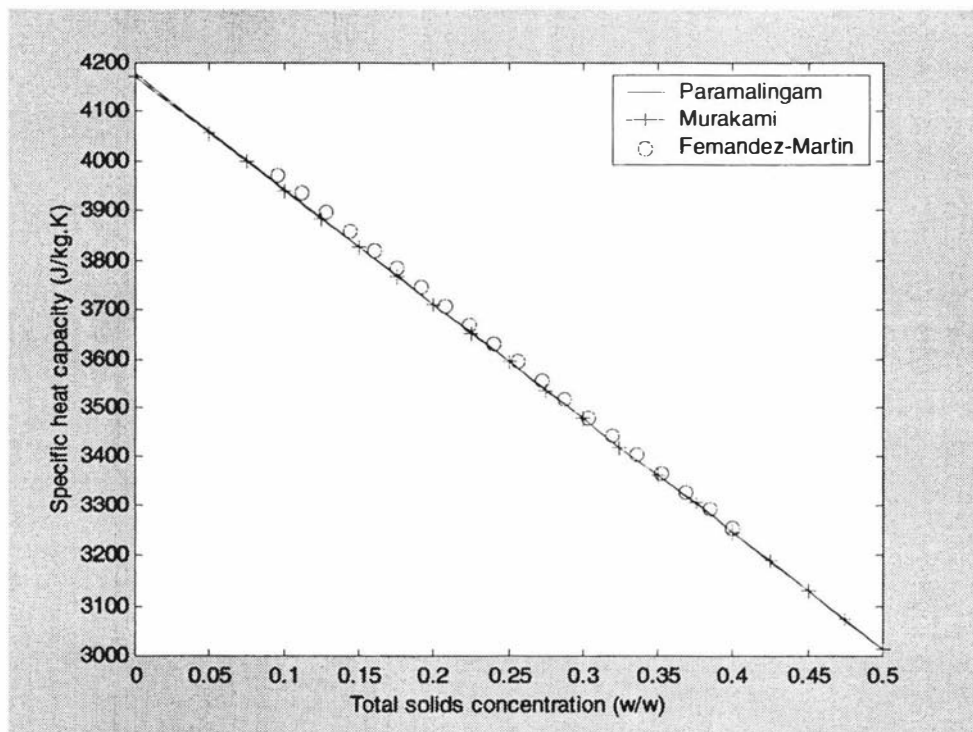
Figure 3.26: Comparison of the Semi-empirical and literature models for the specific heat capacity of whole milk

Thermal conductivity

Figure 3.27 compares the semi-empirical thermal conductivity model with literature models (Heldman, 2001; Murakami, 1989) for WPC-3. The difference in the thermal conductivity model predictions increases as the total solids concentration increases. The difference in the thermal conductivity value at 40% solids content is 0.02W/m. K. The effect of air content (0.001%) on the thermal conductivity was less than 1% (shown in Figure 3.27).
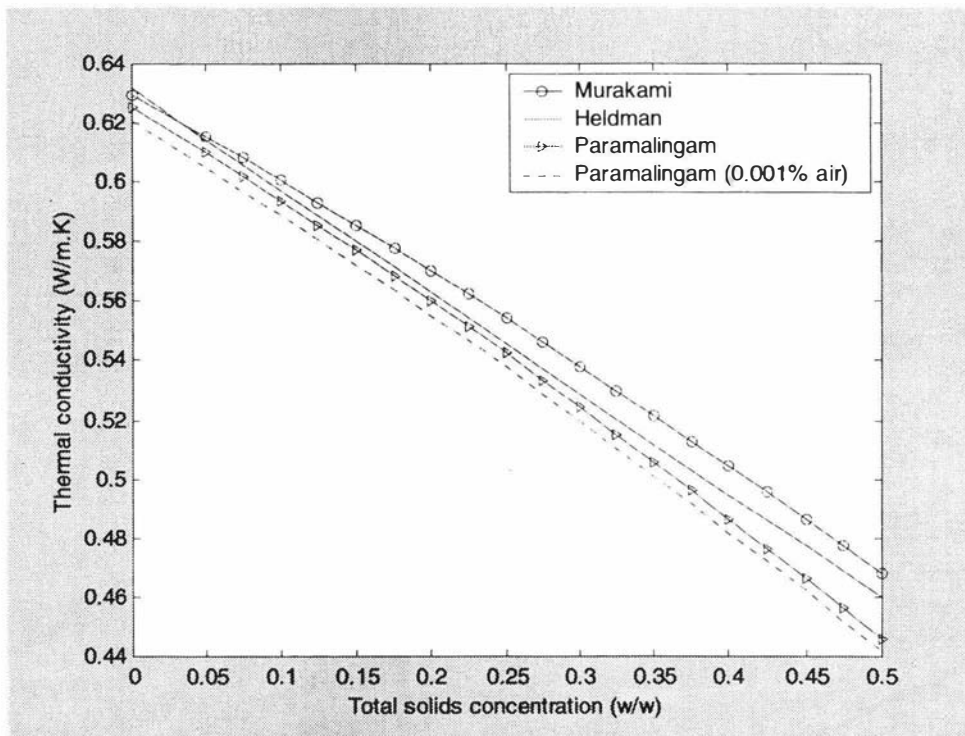
Figure 3.27: model prediction of thermal conductivity with literature model predictions with WPC-3

3.4 Conclusions

The physical properties of WPC and WPI concentrates produced in a two-effect falling film evaporator were investigated. As all other external factors (pH, heat treatment and holding time) except composition, temperature and total solids are fairly constant in the whey evaporation process, the effects of temperature and total solids on these properties were examined. Whey products were prepared to different concentrations and the properties were measured at different temperatures at each concentration.

The regression models developed for density are applicable for concentrates up to 25%w/w and temperatures between 20 and 60°C. A semi-empirical model was also developed for density to extend the limited application range of the regression models. The semi-empirical model was tested for whey products and milk products. The model can be applied to both whey and milk products in a wide range of temperatures and solids with less than 5% error. Difference was observed for model predictions of feed density for whey products, due to the air content of the whey feed. This effect is more significant for whey products than for milk products and can be corrected if the air content in the product is known.

Regression models were developed relating the viscosity of the concentrate to the total solids and to the temperature. These are applicable for concentrates between 10 and 35%w/w and temperatures between 20 and 50°C. The difference in viscosity between WPC-3 and WPI indicate that composition and constituent interactions significantly influence concentrate viscosity. It was difficult to carry out testing on the individual effect of each milk component on the concentrate viscosity and this presents an area for further investigation in the future.

The task of developing a mechanistic model that can accurately explain the effect of composition on viscosity is too complex to attempt at present. Therefore an empirical model developed by Snoeren (1982) for milk was modified for whey concentrates. The model coefficients for whey concentrates were determined by fitting the model to experimental data.

Viscosity model coefficients identified at low and high shear rates enable us to apply the models for different purposes in the evaporator. The low shear data are useful for the evaporator calculations, while the high shear data are useful for optimisation work with the spray dryer. The semi-empirical viscosity model predicts the viscosity with less than 10% error.

Regression models were developed for both contact angle and surface tension with prediction errors less than 5% and 10% respectively. The surface tension of whey products is less than that of milk products or water (This is also evidenced by the foaming properties of whey products, which are attributed to the low surface tension). Therefore, the minimum flow necessary to wet a dry surface is less for whey products. This suggests that film breakdown is less likely in whey products evaporators than in milk evaporators.

No measurements were conducted on the thermal conductivity and specific heat capacity of whey products. Semi-empirical models developed by Snoeren (1982) were modified and tested for whole milk and whey products. It was shown to predict well not only for milk products but also for whey products.

4. Discharge coefficient

In this section the importance of the discharge coefficient is discussed. Then the apparatus and method for measurements of the discharge coefficient are discussed. Finally, the discharge coefficient results are presented and discussed.

4.1 Introduction

The major key to success with falling-film evaporators is to maintain uniform distribution of the product over the heating surface and to filter high frequency disturbances. The distribution plate is assumed to be an ideally mixed vessel with variable product level. Figure 4.1 shows the distribution plate arrangement employed in the whey evaporator at Fonterra, Whareroa. The product accumulates several millimetres above the perforated plate and flows through the holes under its own weight. A dynamic model of the distribution plate was developed (Chapter 6) and the height of the liquid above the distribution plate was found to be influenced by the coefficient of discharge ($h_d \alpha \dfrac{1}{C_d^2}$).
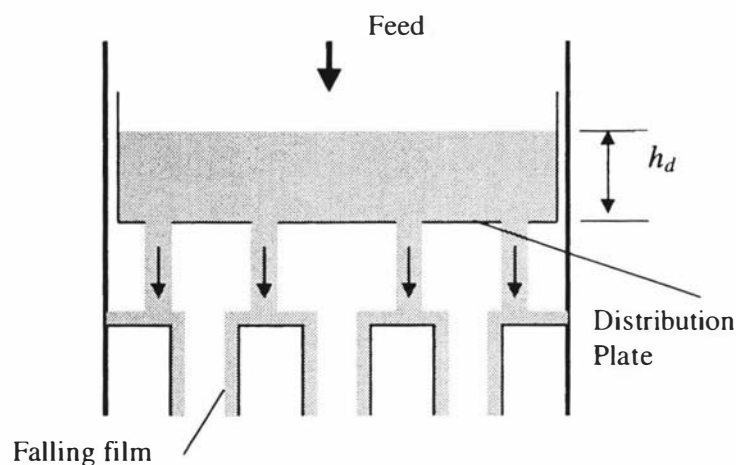
Figure 4.1 – Distribution plate arrangement in the whey evaporator at Fonterra, Whareroa

Where,

h_d - Height of the liquid above the distribution plate (m)

C_d - Discharge coefficient (-)

The literature contains many reports of studies on the coefficient of discharge for large orifices and large liquid heads (Mohanty, 1986; Vennard & Street, 1982; Daugherty, 1965) and a few reports of studies with small orifices and large liquid heads (Trinh et al., 1996; Chee et al., 1988). Vennard & Street (1982) and Daugherty (1965) concluded that the discharge coefficient is strongly influenced by the orifice shape and the liquid head (Chapter 2). Chee et al. (1988) claimed that the orifice size (range 4 mm to 8 mm) had no effect on the discharge coefficient. Mackereth (1993) and Winchester (2000) have suggested that a discharge coefficient of 0.6 can be used for flow calculations in the distribution plate regardless of the type of product. Vennard & Street (1982) and Daugherty (1965) stated that the effect of surface tension on the discharge coefficient becomes significant with small orifices and small liquid heads, but did not specify the orifice size and the liquid height below which the surface tension force becomes significant. In all the above studies, the thickness of the orifice was neglected as this was assumed to be small compared to the liquid head; this is also one of the assumptions in the discharge flow model derivation. The assumption is justified with large liquid heads but with small heads the orifice height becomes significant. For example, the orifice thickness in the whey evaporator (5 mm) is significant compared to the liquid height above the distribution plate (10 to 20 mm). The following shortcomings were identified with regard to existing data on discharge coefficients.

- The significance of hydraulic diameter and the orifice shape on the coefficient of discharge is not known

- The operating Reynolds numbers are different for water and whey products (all the literature studies were based on water)

- Predictions of liquid height above the distribution plate using a discharge coefficient of 0.6 (as suggested by Mackereth, 1993 and Winchester, 2000) were unsatisfactory.

An investigation was therefore carried out to determine the effect of hydraulic diameter and orifice shape on discharge coefficients for whey products. Laboratory experiments were conducted at Fonterra, Whareroa. Data were also collected from the whey evaporator at Fonterra Whareroa.

4.2 Methodology

Figure 4.2 shows the apparatus used for the discharge coefficient measurements. The liquid flow into the apparatus was adjusted to achieve the required liquid head (pre-set using the adjustable overflow pipe). Once the liquid head was steady, the liquid flow rate through the orifice was determined by using a stopwatch to measure the time taken to fill a container of known volume. Three repeated measurements were performed at each liquid head. The Reynolds number range for the measurements was 1000 to 12000 for water and 100 to 1000 for whey products. The reason for selecting this range of Reynolds numbers for water and whey products was to keep the measurements close to the actual operating conditions in the evaporator and thereby obtain a representative value for the discharge coefficient.

Three series of experiments were carried out.
1. Testing the influence of hydraulic diameter on the discharge coefficient.
2. Testing the effect of orifice shape on the discharge coefficient.
3. Measuring discharge coefficients for whey products.

The experiments 1 & 2 were carried out with water. The results of these experiments were used to select a suitable orifice for the measurements with whey products.

Firstly, the influence of the hydraulic diameter, the pitch length of the holes, in the distribution plate was investigated. For this, an identical orifice size (7.5 mm diameter) was made for two different sized tubes (65 mm and 150 mm diameter). The thickness of the orifice in both cases was 1.5 mm.
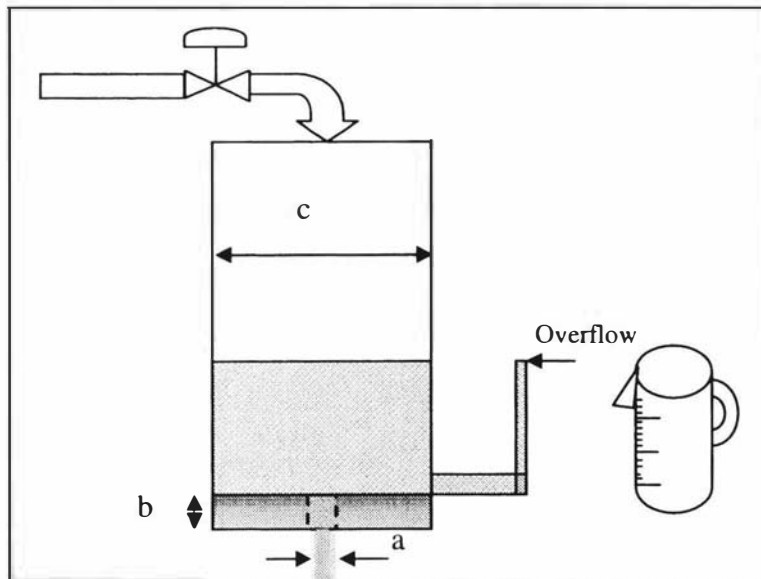
Figure 4.2: Apparatus for discharge coefficient measurements
a- orifice diameter, b- orifice thickness, c- vessel diameter (= hydraulic diameter)

Secondly, the influence of the shape of the orifice was investigated. Holes of the same diameter were made in three different plates, and the top edge of each hole was rounded to a different degree. One hole was left without a rounded edge (i.e. flat edge), the second with a slightly rounded edge and the third with a more rounded edge. Discharge coefficients for each hole were measured with water. The thickness of the orifices was 5 mm this is same as the size of the orifices in the evaporator. To select the exact type of orifice with those in the real plant, the data on the liquid height in the distribution plate were taken from the whey evaporator when running on water.

Finally, discharge coefficients for whey products (WPC-3 and WPI) were measured using the correct orifice shape identified in the experiments with water. The effect of surface tension on the discharge coefficient was calculated using the following force balance (Mohanty, 1986):

$$P \cdot \pi r^2 = 2\pi r \cdot \sigma \quad \text{And} \quad P = h_l \rho g \tag{4.1}$$

Where,

P - Excess pressure over atmosphere at equilibrium (N m^{-2})

σ - Surface tension force per unit length (N m^{-1})

r - Radius of the orifice (m)

h_l - Liquid height needed to overcome the surface tension force (m)

ρ - Density of product (kg m^{-3})

g - Acceleration due to gravity (m s^{-2})

The measurement error in the discharge coefficient was estimated using the following equation:

$$C_d = \frac{Q_d \left(1 - \left(\frac{A_o}{A_h}\right)^2\right)}{n\sqrt{2g\left(h_d + t_p\right)}} \times \frac{1}{A_o} \tag{4.2}$$

$$dC_d = \left.\frac{\partial C_d}{\partial Q_d}\right|_0 dQ_d + \left.\frac{\partial C_d}{\partial A_0}\right|_0 dA_0 + \left.\frac{\partial C_d}{\partial A_h}\right|_0 dA_h + \left.\frac{\partial C_d}{\partial h_d}\right|_0 dh_d + \left.\frac{\partial C_d}{\partial t_p}\right|_0 dt_p \tag{4.3}$$

Where,

Q_d - Volumetric flow rate through the orifice (m^3 s^{-1}).

A_o - Area of the orifice (m^2).

A_h - Area of the vessel (m^2).

t_p - Thickness of the plate (m).

4.3 Results and discussion

Figure 4.3 shows the effect of hydraulic diameter and liquid height on the discharge coefficient for water. The difference in the discharge coefficients was within 0.05 and the measurement error was approximately 0.06. Figure 4.3 shows that there was little difference in the discharge coefficients regardless of liquid height. Therefore, the rest of the experiments were conducted for a hydraulic diameter the same as that of the real evaporator (whey products, Fonterra Whareroa).
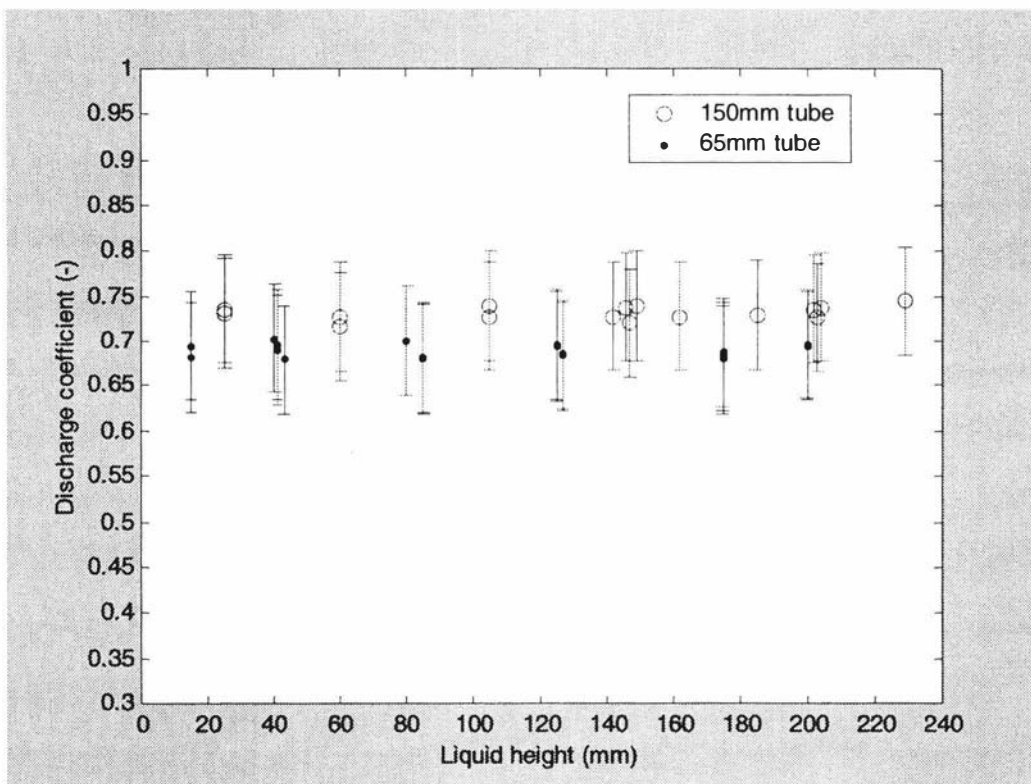
**Figure 4.3: The effect of liquid height on the coefficient of discharge as a
function of tube diameter**

Figure 4.4 shows the influence of different hole shapes— highly rounded edge, little rounded edge and flat edge— on the discharge coefficient for water. It is clear that the shape of the orifice top edge does influence the coefficient of discharge.

Whey evaporator model predictions of the liquid height above the distribution plate were made using these discharge coefficients. The data (approximate measurements) collected from the whey evaporator plant were then compared to the predictions for different orifice shapes to select the best fit orifice shape. The discharge coefficient for the flat edged orifice gave a good fit between predicted and measured liquid heights for the whey evaporator and thus used in the experiments with whey products.
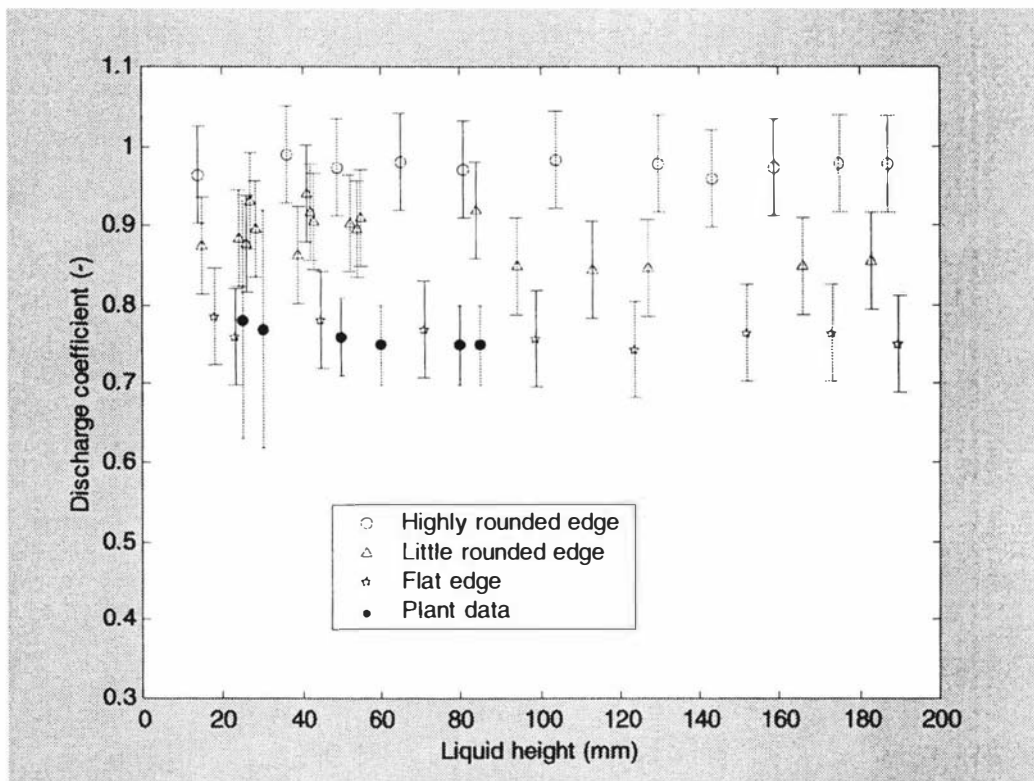
Figure 4.4: The effect liquid height on coefficient of discharge with water as a function of the hole top edge shape

Figure 4.5 shows the discharge coefficients measured for whey products, WPI and WPC-3, compared with the value recommended by Mackereth (1993) and Winchester (2000). The orifice edge shape in both cases (Figure 4.3 and 4.4) was flat, but the orifice thickness was 1.5 mm and 5 mm respectively. This difference justified the relaxation of the assumption (orifice thickness is negligible compared to the liquid height) in the model derivation (Chapter 6). The reason for this increase in discharge coefficient with the orifice thickness is the increase in coefficient of contraction (cross sectional area of the liquid jet exiting the orifice to the orifice cross sectional area). These results agree with the literature results of Vennard & Street, (1982).
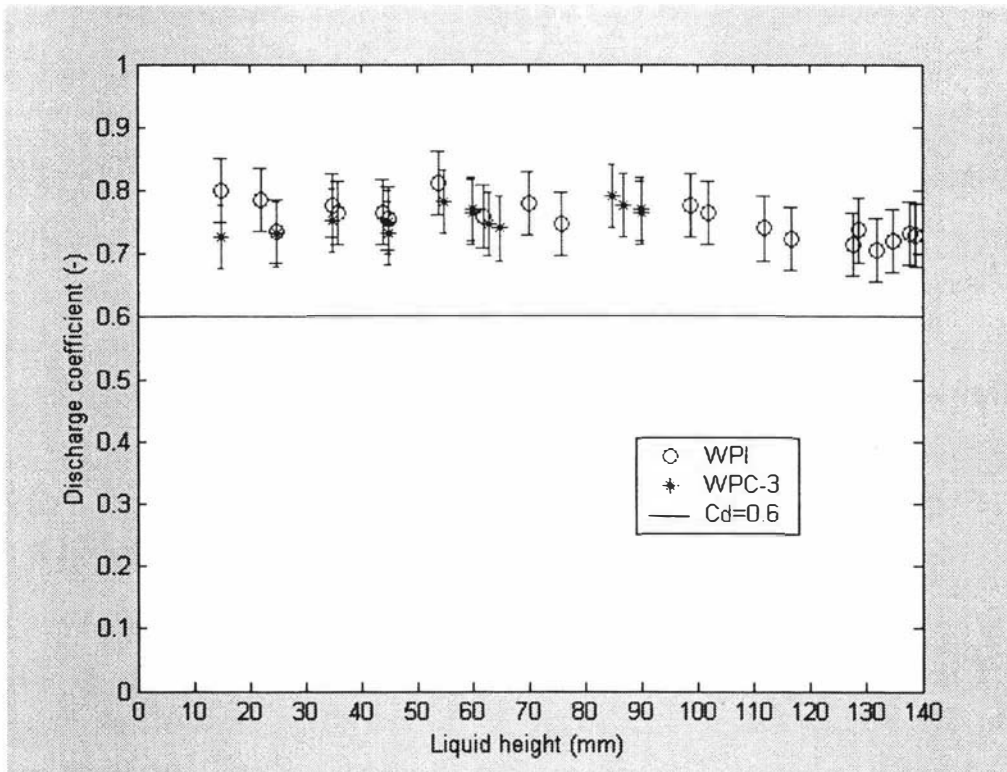
Figure 4.5: Coefficient of discharge for WPC and WPI

Trinh et al. (1996) has stated that the effect of surface tension on the discharge coefficient is negligible. To verify this, the surface tension force was estimated using equation (4.1) and converted to equivalent head. The estimated liquid head to overcome the surface tension force with water was approximately 0.4 mm. This head is negligible compared to the liquid head above the distribution plate. The resistance due to surface tension was therefore neglected in the discharge coefficient calculations.

4.4 Conclusions

The shape of the distribution hole has significant influence on the discharge coefficient for flow from the evaporator distribution plate. Hydraulic diameter and product properties had no significant influence on the discharge coefficient. A value of 0.6 is reported in the literature whereas a value of 0.75 was measured in the current study. The reason for this is that discharge measurements reported in the literature involve large liquid heads and ignore the plate thickness (If the plate thickness is included a 22% change is observed in the discharge coefficient at 10 mm liquid head and a 2.7% change with 150 mm liquid head).

PART 2

Modelling of a falling-film evaporator

5. Modelling overview

In this section the method used in the evaporator modelling is discussed. Then the key model parameters for falling-film evaporator process at Fonterra Ingredients-Whareroa are described.

5.1 Model structure

The systems approach (as adopted by Quaak et. al, 1990; Winchester, 2000) was used to model the evaporator. The evaporator was divided into four main *sub-systems* (Figure 5.1); the *Preheat/Vacuum* condenser section, the *Distribution* plate section, the *Evaporation* section and the *Thermal Vapour Recompression* (TVR) section. The distribution plate and evaporation sub-systems will be identical in each effect of the evaporator, while the vacuum condenser and the TVR section are included for the total evaporator system. Each sub-system was modelled and analysed separately.
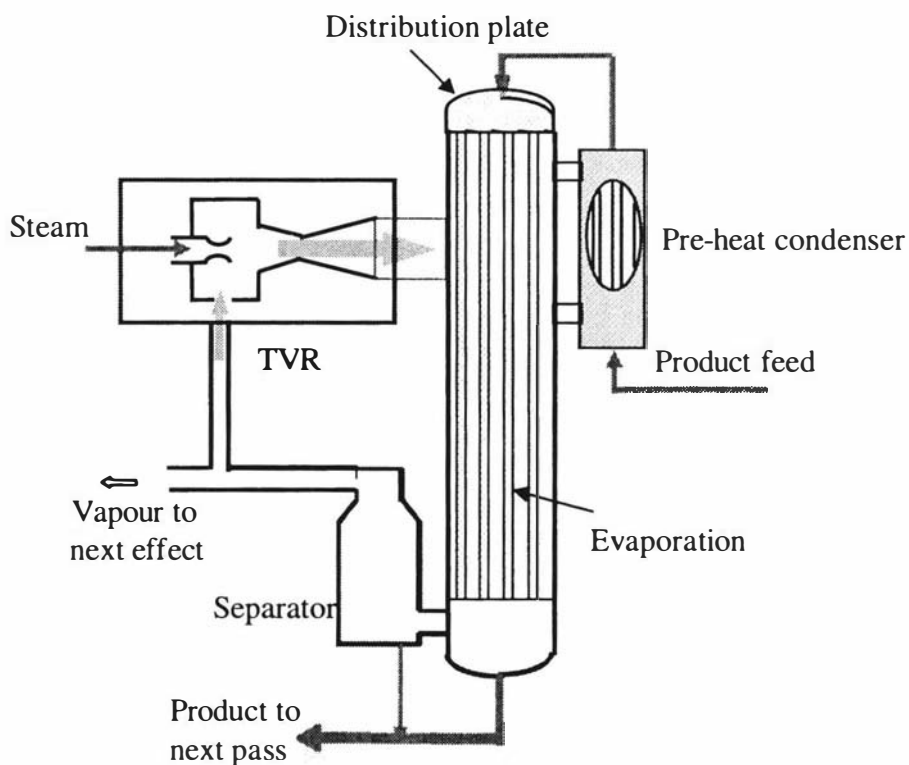
Figure 5.1: First effect of a two-effect falling-film evaporator

A dynamic model, a steady state model and a linear dynamic model were developed for each sub-system. The dynamic model derivations were based on the conservation laws of mass and energy. The steady state models were derived from the dynamic models by making the variables time independent. Finally, the linear dynamic models were developed from the dynamic models by linearising the non-linear terms.

5.2 Whey evaporator parameters

Figure 5.2 shows a schematic of the whey TVR evaporator section of the whey evaporator plant. This is a two-effect system with TVR. The whey evaporation process is discussed in Chapter 2 and is reviewed in this section to introduce the modelling parameters.

Feed whey first enters the *preheat condensers* attached to the first and second effects to bring the temperature to just above that of the 1st effect. The feed is characterised by its mass flow (M_f), temperature (T_f) and total solids concentration (w_f). The product leaves the preheat condensers at a temperature T_{phc3} and passes to the *distribution plate* of the first pass of the first effect, which distributes the product evenly to all evaporating tubes. Steam or vapour on the outside of the tubes heats the product that flows down the tubes. From the bottom of the separator the product is pumped to the distribution plate of the second pass of the first effect. After two passes in the first effect the product is pumped to the second effect. After passing through the second effect the whey leaves the evaporator with a concentrated mass flow M_{p3}, temperature T_{e2} and solids content w_{p3}. Part of the separated vapour from the 1st effect is compressed by high pressure steam (pressure P_s and mass flow rate m_{steam}) injected through a nozzle in the *TVR compressor*, and is then recycled to the shell side of the 1st effect. The rest of the vapour from the first effect goes to the 2nd effect and acts as the heating medium for this effect. Cooling water is used in the vacuum condenser tubes, with a mass flow of M_{cw} and a temperature of T_{cwin}.
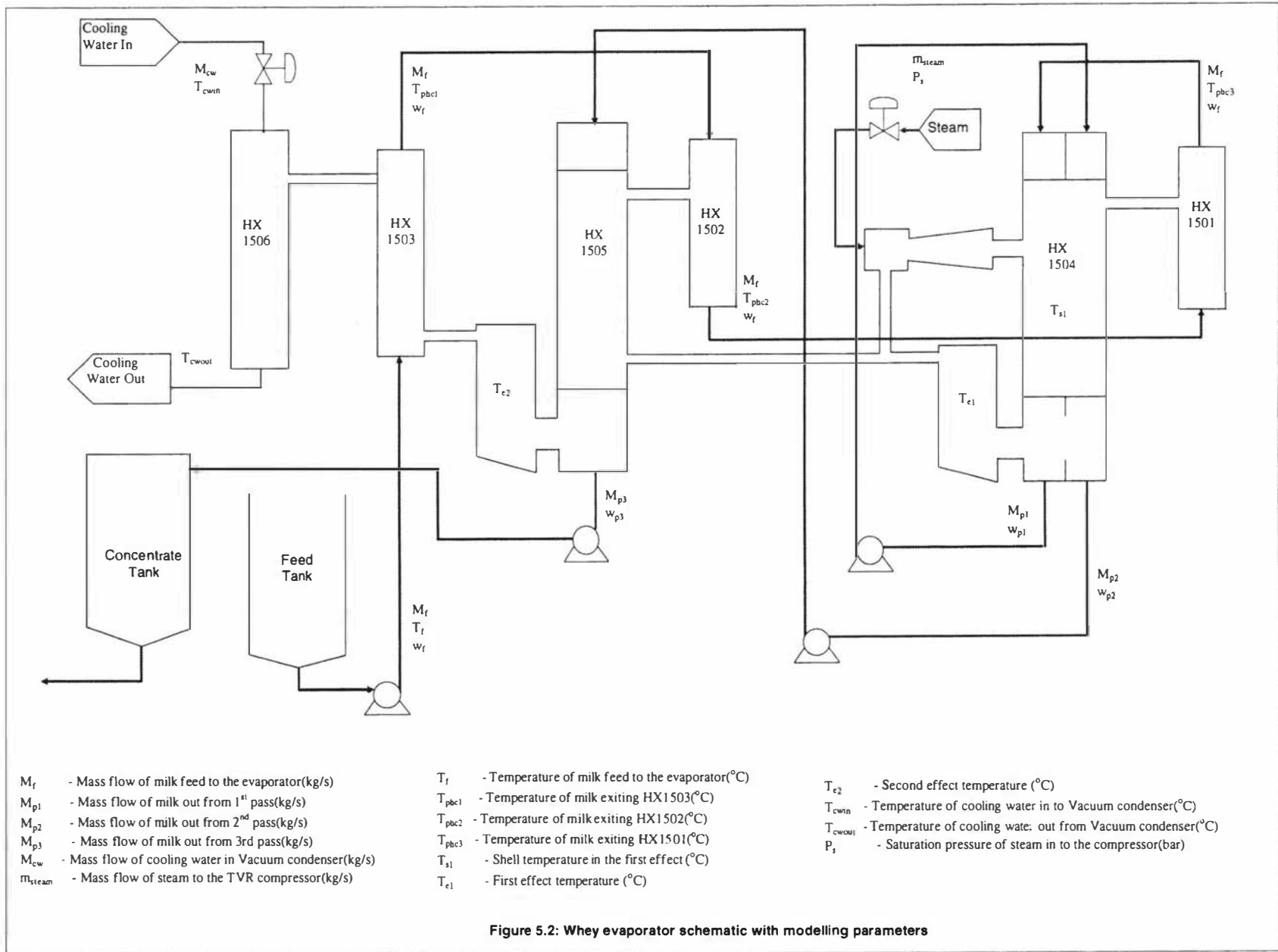
Figure 5.2: Whey evaporator schematic with modelling parameters

M_f — Mass flow of milk feed to the evaporator(kg/s)

M_{p1} — Mass flow of milk out from 1st pass(kg/s)

M_{p2} — Mass flow of milk out from 2nd pass(kg/s)

M_{p3} — Mass flow of milk out from 3rd pass(kg/s)

M_{cw} — Mass flow of cooling water in Vacuum condenser(kg/s)

m_{steam} — Mass flow of steam to the TVR compressor(kg/s)

T_f — Temperature of milk feed to the evaporator($^{\circ}$C)

T_{pbc1} — Temperature of milk exiting HX1503($^{\circ}$C)

T_{pbc2} — Temperature of milk exiting HX1502($^{\circ}$C)

T_{pbc3} — Temperature of milk exiting HX1501($^{\circ}$C)

T_{s1} — Shell temperature in the first effect ($^{\circ}$C)

T_{e1} — First effect temperature ($^{\circ}$C)

T_{e2} — Second effect temperature ($^{\circ}$C)

T_{cwin} — Temperature of cooling water in to Vacuum condenser($^{\circ}$C)

T_{cwout} — Temperature of cooling water out from Vacuum condenser($^{\circ}$C)

P_s — Saturation pressure of steam in to the compressor(bar)

6. Dynamic Model derivation

In this section the dynamic models for the evaporator sub-systems (distribution plate, condenser, evaporator and TVR compressor) are derived. The important steps in the derivations are shown here and the detailed derivation is given in Appendix B.

6.1 Distribution plate

The major key to successful operation of falling-film evaporators is maintaining uniform distribution of the product over the heating surface. The liquid height above the distribution plate is also important to filter high frequency feed disturbances. The distribution plate (Figure 6.1) is assumed to be an ideally mixed vessel with variable level. The product accumulates several millimetres above the perforated plate and flows off through the holes under gravity. The temperature of the feed whey that enters the 1st pass in each effect is normally higher than the effect temperature and this causes part of the water in the feed whey to evaporate. Therefore, the flow and the total solids concentration of the whey product exiting the distribution plate are changed slightly.
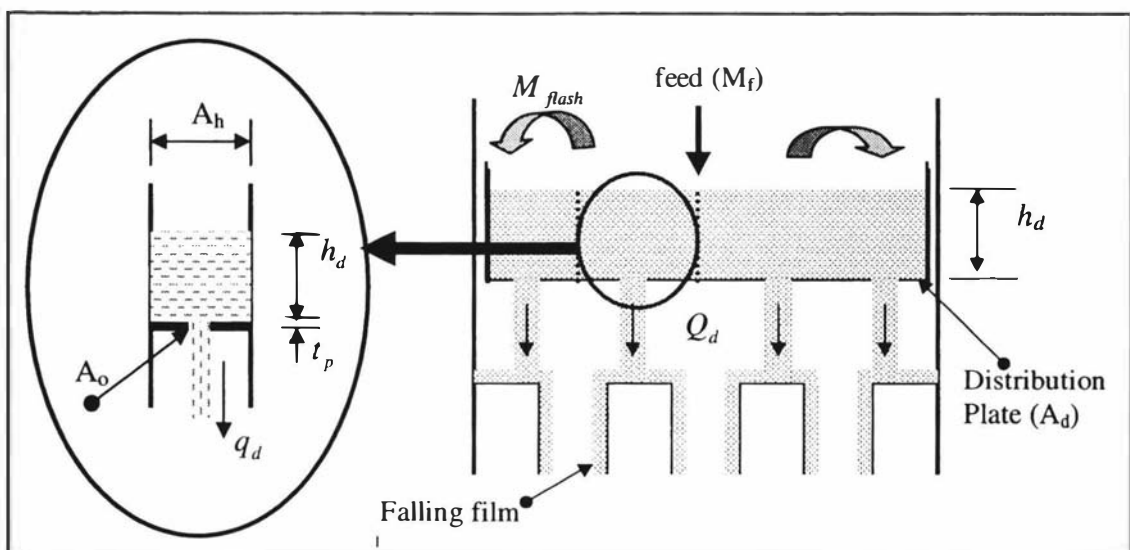
Figure 6.1: Distribution plate sub-system

Overall balance

The whey evaporator has three passes and therefore three distribution plate systems. The configuration of all these three distribution plates is identical. The general differential equations for the flow and the solid content of the whey product exiting the distribution plate were derived from overall volume, mass and solids balances across the distribution plate (the rate of accumulation of volume, mass or solids = the total volume, mass or solids in flow - the total volume, mass or solids out flow in the liquid phase – the total volume, mass or solids out flow in the vapour phase).

By mass balance, $\dfrac{d\left(h_d(t)A_d\rho_d\right)}{dt} = M_f(t) - M_{flash}(t) - M_d(t)$ (6.1)

By solids balance, $\dfrac{d\left(h_d(t)A_d\rho_d w_d(t)\right)}{dt} = M_f(t)w_f(t) - M_d(t)w_d(t)$ (6.2)

Where,

$$M_{flash}(t) = \frac{M_f(t)Cp_f\left[T_f(t) - T_e(t)\right]}{\lambda} \qquad\qquad M_d(t) = Q_d(t)\rho_d$$

Equation (6.1) can be rewritten in terms of mass and density to derive the differential equation for the whey level in the distribution plate:

$$\frac{d\left(h_d(t)\right)}{dt} = \left(\frac{1}{A_d\rho_d}\right)\left(M_f(t) - M_{flash}(t) - M_d(t)\right) \qquad\qquad (6.3)$$

Expanding equation (6.3) substituting equation (6.1) and then substituting for mass of flash vapour, produces the following differential equation for the total solids concentration of the whey on the distribution plate.

$$\frac{d\left(w_d(t)\right)}{dt} = \left(\frac{1}{h_d(t)A_d\rho_d}\right)\left\{M_f(t)\cdot\left[w_f(t) - w_d(t)\right] + M_{flash}(t)\cdot w_d(t)\right\} \qquad (6.4)$$

A_d - Area of distribution plate (m^2)

M_{flash} - Mass of water evaporated due to flash on the distribution plate (kg s^{-1})

w_f - Solids concentration of the feed whey (kg kg^{-1})

w_d - Solids concentration of the whey leaving the distribution plate (kg kg^{-1})

M_d - Mass of whey leaving the distribution plate (kg s^{-1})

T_f - Temperature of feed whey to distribution plate ($^{\circ}$C)

T_e - Temperature of the evaporator effect ($^{\circ}$C)

λ - Latent heat of vaporisation (J kg^{-1})

Cp_f - Specific heat capacity of whey (J kg^{-1} K^{-1})

ρ_d - Density of whey leaving the distribution plate (kg m^{-3})

ρ_{water} - Density of water (kg m^{-3})

Flow through orifice

The whey level in the distribution plate depends upon the volume flow out from the distribution plate Q_d and the volume flow in Q_f. The standard orifice flow equation used in most of fluid mechanics applications is:

$$Q_d = \frac{nC_d A_o}{\left[1-\left(\dfrac{A_o}{A_h}\right)^2\right]}\sqrt{2h_d g} \tag{6.5}$$

Equation (6.6) was derived from Bernoulli's equation (Graebel, 2001; Mohanty, 1986) and is true when,

- the dimensions of the orifice are small compared to the liquid head
- both the feed and exit side pressures are the same

This equation is commonly used without any modifications in evaporator applications to calculate the flow through the distribution plates (Trinh et al, 1996; Winchester, 2000). However, it was shown in Chapter 4 that for the whey evaporator the thickness of the distribution plate is significant compared to the liquid head. The plate thickness should therefore be included in Equation (6.5).

The modified orifice equation for evaporator applications is given by equation (6.6). The derivation is given in appendix B.

$$Q_d = \frac{nC_d A_o}{\left[1 - \left(\frac{A_o}{A_h}\right)^2\right]}\sqrt{2(h_d + t_p)g} \qquad (6.6)$$

Where,

g - Acceleration due to gravity (m s^{-2})

A_o - Cross sectional area of the orifice (m^2)

A_h - Cross sectional area of the virtual diameter of the pipe ahead of orifice (m^2)

C_d - Coefficient of discharge (-)

Q_d - Discharge flow from the distribution plate (m^3/s)

h_d - Height of the liquid above the orifice (m)

n - Number of distribution holes (-)

t_p - Thickness of the plate (m)

6.2 Preheat condensers / Vacuum condenser

Preheat or vacuum condensers used in the dairy industry are vertical shell and tube type heat exchangers. Saturated steam condenses on the shell side of the tube walls, supplying heat to the product that passes through the tubes. The whey evaporator has four shell and tube condensers, three to preheat the incoming whey to the temperature

of the first evaporator effect and one to maintain the vacuum within the evaporator. The first preheat condenser (HX1503) is attached to the 2nd effect, the second preheat condenser (HX1502) is attached to the shell of the 2nd effect, the third (HX1501) is attached to the shell of the 1st effect and the vacuum condenser (HX1506) is attached to the 2nd effect as shown in Figure 5.2. Figure 6.2 shows a generic diagram of the condensers used in the whey evaporator. A small element of the condenser liquid was considered for the condenser temperature and heat flow derivation.
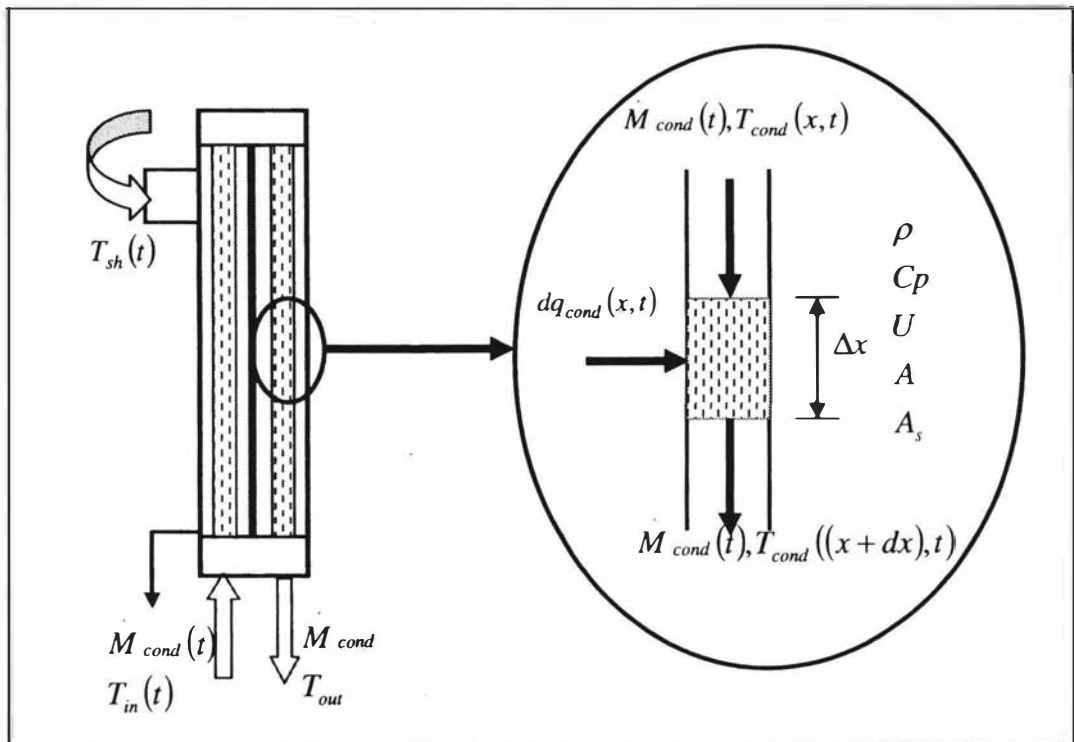
Figure 6.2: Condenser sub-system

The condenser model is developed from the energy balance around an infinitesimal cross section of the condenser tube. The temperature of the liquid varies along the tubes and with time. The assumptions made in the derivations are,

- Constant heat capacity (Cp)

- Constant density (ρ)

The energy balance (rate of heat of accumulation = net heat flow in- net heat flow out + heat gained) across the condenser tube element (figure 6.2) is given by the equation (6.7).

$$\frac{\partial\left[\rho A C_p \cdot T_{cond}(x,t)dx\right]}{\partial t} = M_{cond}(t)\cdot C_p \cdot T_{cond}(x,t) + dq(x,t) - M_{cond}(t)\cdot C_p \cdot T_{cond}((x+dx),t) \tag{6.7}$$

Substituting $\rho\cdot A = \dfrac{M_{cond}(t)}{v_{cond}(t)}$ in equation (6.7) and dividing by $M_{cond}(t)\cdot Cp\cdot dx$ gives:

$$\frac{\partial T_{cond}(x,t)}{\partial t} + v_{cond}(t)\cdot\frac{\partial T_{cond}(x,t)}{\partial x} = \left(\frac{v_{cond}(t)}{M_{cond}(t)\cdot Cp\cdot dx}\right)dq(x,t) \tag{6.8}$$

Substituting back $\dfrac{M_{cond}(t)}{v_{cond}(t)} = \rho\cdot A$, $dq(x,t) = U(x,t)\cdot A_s\cdot\left[T_{sh}(x,t) - T_{cond}(x,t)\right]$ and $A\cdot dx = V_{cond}$ into (6.8) produces the partial differential equation (6.9) for the liquid temperature in the tubes of the condenser.

$$\frac{\partial T_{cond}(x,t)}{\partial t} + v_{cond}(t)\frac{\partial T_{cond}(x,t)}{\partial x} = \frac{U(x,t)\cdot A_s}{\rho\cdot Cp\cdot V_{cond}}\left[T_{sh}(x,t) - T_{cond}(x,t)\right] \tag{6.9}$$

To simplify the models, Winchester (2000) and Newman (2001) solved equation (6.9) assuming a constant heat transfer coefficient (U) and a tube wall temperature equal to the shell side temperature ($T_w = T_{sh}$). These models are shown in (6.10) to (6.13). The detailed derivations are given in Appendix B.

$$T_{out}(t) = T_{dum}(t) + e^{\frac{\tau_{RT}}{\tau_{TC}}}T_{in}(t - \tau_{RT}) - \frac{\tau_{RT}\left(T_{sh}^0 - T_{in}^0\right)e^{\frac{\tau_{RT}}{\tau_{TC}}}}{M_{cond}^0\tau_{TC}}\cdot M_{dum}(t) \tag{6.10}$$

$$\tau_{TC}\frac{dT_{dum}(t)}{dt} = -T_{dum}(t) + T_{sh}(t) - e^{\frac{\tau_{RT}}{\tau_{TC}}}T_{sh}(t - \tau_{RT}) \tag{6.11}$$

$$\tau_{RT}\frac{dM_{dum}(t)}{dt} = M_{cond}(t) - M_{cond}(t - \tau_{RT}) \tag{6.12}$$

$$\frac{dq_{cond}}{dt} = UA\frac{dT_{sh}}{dt} - \frac{1}{\tau_{TC}}q_{cond} + \frac{UA}{\tau_{RT}}\left[T_{out} - T_{in}\right] \tag{6.13}$$

Where, $\tau_{TC} = \dfrac{\rho Cp V_{cond}}{UA}$, $\tau_{RT} = \dfrac{\rho V_{cond}}{M_{cond}}$

T_{sh} - Temperature in the shell of the condenser (^{o}C)

T_{in} - Feed temperature of condenser liquid (^{o}C)

T_{out} - Outlet temperature from the condenser (^{o}C)

T_{cond} - Temperature of liquid in the condenser (^{o}C)

T_{s}^{0} - Steady state temperature in the shell of the condenser (^{o}C)

T_{f}^{0} - Steady state temperature of the feed (^{o}C)

M_{cond} - Feed flow to the condenser (kg s^{-1})

M_{cond}^{0} - Steady state feed flow to the condenser (kg s^{-1})

M_{dum} - Dummy variable used in the condenser model (kg)

T_{dum} - Dummy variable used in the condenser model (^{o}C)

A_{s} - Heat transfer surface area (m^{2})

V_{cond} - Volume of liquid in the condenser tubes (m^{3})

ρ - Density of condenser liquid (kg m^{-3})

Cp - Heat capacity of condenser liquid (J kg^{-1} K^{-1})

U - Heat transfer coefficient in the condenser (W m^{-2} K^{-1})

A - Tube cross sectional area (m^{2})

6.3 Evaporation

The heart of every evaporator is the evaporation sub-system. The evaporation sub-system can be divided into three different sections. These are the falling-film, the effect and the shell of the evaporator. The evaporation sub-system is where the liquid is actually being concentrated. It resembles a vertical calandria heat exchanger with heating tubes, tube sheets, shell and flanged joints. The dynamic models of the process in each section of this sub-system are derived as follows.

6.3.1 Falling-film

The cross section of the tube illustrating the heat transfer in a falling-film is shown in Figure 6.3. The steam condenses on the outside of the tube and releases its latent heat,

85

which is supplied to the falling-film on the tube side (effect) for evaporation. The flow rate of the condensed water on the shell side will increase from top to bottom of the tube while the volume of liquid in the tube will decrease due to evaporation. There are three evaporation passes present in the whey evaporator (two in HX1504 and one in HX1505). The product enters the tube from the distribution plate with a mass flow and total solids content of $M_d(t)$ and $w_d(t)$ while the product leaving the tube has a flow of $M_e(t)$ and a solids content of $w_e(t)$. Differential equations for mass flow and concentration were developed from energy and mass balances across the finite element shown in Figure (6.3).
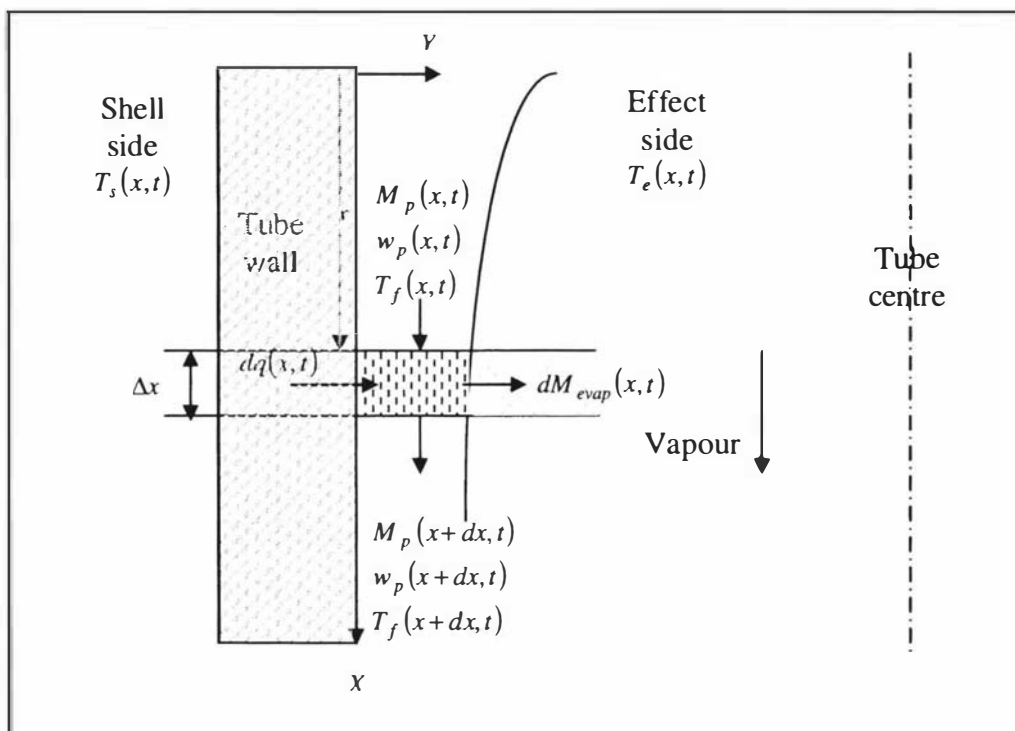
Figure 6.3: Falling-film in an evaporator tube

A mass flow balance (rate of mass of accumulation = total mass flow in − total mass flow out − mass rate of evaporation) across the element gives equation (6.14).

$$\frac{\partial[\rho(x,t)\cdot A(x,t)\cdot \Delta x]}{\partial t} = M(x,t) - M(x+dx,t) - dM_{evap}(x,t) \tag{6.14}$$

A solids content balance (rate of accumulation of solids = total solids with flow in – total solids with flow out) gives equation (6.15).

$$\frac{\partial[\rho(x,t)\cdot A(x,t)\cdot \Delta x\cdot w(x,t)]}{\partial t} = M(x,t)\cdot w(x,t) - M(x+dx,t)\cdot w(x+dx,t) \tag{6.15}$$

An energy balance (rate of accumulation of energy = total energy flow in with product + total heat transferred through the tube wall – total energy flow out with product – total energy flow out with the evaporation) gives equation (6.16).

$$\frac{\partial[\rho(x,t)\cdot A(x,t)\cdot Cp(w(x,t))\cdot T_f(x,t)\Delta x]}{\partial t} = M(x,t)\cdot Cp(w(x,t))\cdot T_f(x,t) + dq(x,t)$$

$$- M(x+dx,t)\cdot Cp(w(x+dx,t))\cdot T_f(x+dx,t) - [\lambda + Cp_w \cdot T_f(x,t)]dM_{evap}(x,t) \tag{6.16}$$

Equation (6.17) can be derived from equations (6.14), (6.15) and (6.16). The detailed derivation of equation 6.17 is given in Appendix B. Following the example of other researchers (Quaak et. al, 1994; Winchester, 2000), the following simplifying assumptions were made in this derivation

- Constant falling-film velocity;
- Uniform heat transfer along the tube wall;
- Negligible thermal inertia

$$\frac{1}{v}\cdot\frac{\partial M(x,t)}{\partial t} + \frac{\partial M(x,t)}{\partial x} + \frac{1}{\lambda\cdot L}q_{shell}(t) = 0 \tag{6.17}$$

Where $q_{shell}(t) = \int_0^L U(x,t)\cdot A(x,t)\cdot [T_s(x,t) - T_e(x,t)]dx$

Converting equation (6.17) into the Laplace domain, integrating and converting back to time domain produces equation (6.18) for the mass flow of product exiting the tube.

$$M_e(t) = M_d(t-\tau_e) - M_{tubes}(t) \tag{6.18}$$

Where $\dfrac{dM_{tubes}(t)}{dt} = \dfrac{1}{\lambda \cdot \tau_e}\left[q_{shell}(t) - q_{shell}(t - \tau_e)\right]$ and $\tau_e = \dfrac{L}{v}$

Using equations (6.15) and (6.18) we can simplify, integrate and rearrange to get equation (6.19) for the solids content of the product leaving the tube:

$$w_e(t) = \dfrac{M_d(t - \tau_e) \cdot w_d(t - \tau_e)}{\left[M_d(t - \tau_e) - M_{tubes}(t)\right]} \tag{6.19}$$

Where,

M_d - Mass flow rate of the feed to the tube (kg s^{-1})

M_e - Mass flow rate at the exit of the tube (kg s^{-1})

w_d - Total solids content of the feed (kg kg^{-1})

w_e - Total solids content at the exit (kg kg^{-1})

v - Velocity of the falling-film (m s^{-1})

λ - Latent heat of vaporisation (J kg^{-1})

L - Length of the tube (m)

T_s - Temperature of the shell (^{o}C)

T_e - Temperature of the effect (^{o}C)

τ_e - Falling-film residence time in the effect (s)

M_{tubes} - Mass of evaporation (kg s^{-1})

T_f - Temperature of the product feed to the evaporator (^{o}C)

q_{shell} - Heat transfer through the tubes (J)

6.3.2 Evaporator effect

The whey evaporator has two effects. The differential equations for effect temperatures were derived from energy balances across control volumes in each effect. A single effect temperature was assumed for the distribution plate, falling film, metal, whey product and the vapour in each evaporator effect.

First effect

An energy balance was derived around a control volume in the first effect. The whey feed and the vapour condensing in the shell, provide the energy flow into this control volume

while energy flows out with product, the condensing water, the evaporated vapour and via heat losses from the surfaces. Equation (6.20) was derived from the fundamental energy balance (rate of energy accumulation = net energy flow in − net energy flow out).

$$\frac{d[K_{e1} \cdot T_{e1}]}{dt} = M_f \cdot Cp_f \cdot T_{phc3} + q_{shell-e1} - M_{p2} \cdot Cp_{p2} \cdot T_{e1} - q_{shell-e2} - q_{phc2}$$

$$- M_{comp}\left(Cp_{water} \cdot T_{e1} + \lambda\right) - M_{cond-e1} \cdot Cp_{water} \cdot T_{e1} - q_{loss-E1} \qquad (6.20)$$

Where,

$$K_{e1} = M_{met-e1} \cdot Cp_{met} + M_{whey-e1} \cdot Cp_{whey} + M_{vapour-e1} \cdot Cp_{vapour}$$

$$q_{loss-E1} = q_{loss-e1} + q_{loss-s2} + q_{loss-phc2} \qquad\qquad M_{cond-e1} = \left(M_{cond-phc2} + M_{cond-s2}\right)$$

Substituting $q_{feed1} = M_f \cdot Cp_f \cdot w_f \left(T_{phc3} - T_{e1}\right)$, $Cp_f = Cp_{water} - Cp_{TS} \cdot w_f$,

$Cp_{p2} = Cp_{water} - Cp_{TS} \cdot w_{p2}$, $q_{comp} = \lambda \cdot m_{comp}$, $M_{p2} = M_f - m_{comp} - M_{cond-e1}$ and

$M_{p2} \cdot w_{p2} = M_f \cdot w_f$ into equation (6.20) and rearranging produces differential equation (6.21) for the 1st effect temperature.

$$K_{e1} \cdot \frac{dT_{e1}}{dt} = q_{feed1} + q_{shell-e1} - q_{comp} - q_{shell-e2} - q_{phc2} - q_{loss-e1} \qquad (6.21)$$

The heat losses for the above energy balances arise from three different parts: the first effect, the shell of HX1502 and the shell of HX1505. It was assumed that the main losses are due to convection and are thereby given by equation (6.22).

$$q_{loss-E1} = \left[\left(U_{l-e1} \cdot A_{l-e1}\right) + \left(U_{l-s2} \cdot A_{l-s2}\right) + \left(U_{l-phc2} \cdot A_{l-phc2}\right)\right] \cdot \left(T_{e1} - T_a\right) \qquad (6.22)$$

Where,

T_{phc3} - HX 1501 exit temperature (°C)

M_{met-e1} - Mass of metal in the 1st effect (kg)

Cp_{met-e1} - Heat capacity of metal (J kg^{-1} °C^{-1})

M_{p2} - Mass flow rate of whey exiting the 1st effect (kg s^{-1})

m_{comp} - Mass flow rate of vapour compressed by the TVR (kg s^{-1})

Cp_{water} - Heat capacity of water (J kg^{-1} °C^{-1})

q_{feed1} - Net energy flow rate with the feed whey to the 1st effect (W)

$q_{shell-e1}$ - Heat flow rate passing through HX1504 (W)

$q_{shell-e2}$ - Heat flow rate passing through HX1505 (W)

q_{phc2} - Heat flow rate passing through HX 1502 (W)

$q_{loss-E1}$ - Loss heat flow rate from the 1st effect (W)

U_i - Overal losses heat transfer coefficient (W m^{-2} °C^{-1})

A_i - Surface area for heat loss (m^2)

T_a - Ambient temperature (°C)

Second effect

Differential equation (6.23) was derived for the second effect temperature in the same manner as for the first effect temperature:

$$\frac{d[K_{e2} \cdot T_{e2}]}{dt} = M_{p2} \cdot Cp_{p2} \cdot T_{e1} + q_{shell-e2} - M_{p3} \cdot Cp_{p3} \cdot T_{e2} - q_{vacc} - q_{phc1}$$

$$- M_{cond-e2} \cdot Cp_{water} \cdot T_{e2} - q_{loss-E2} \qquad (6.23)$$

Where,

$$K_{e2} = M_{met-e2} \cdot Cp_{met} + M_{whey-e2} \cdot Cp_{whey} + M_{vapour-e2} \cdot Cp_{vapour}$$

$$q_{loss-E2} = q_{loss-e2} + q_{loss-vacc} + q_{loss-phc1} \qquad\qquad M_{cond-e2} = \left(M_{cond-phc1} + M_{cond-vacc} \right)$$

Substituting $q_{feed2} = M_{p2} \cdot Cp_{p2} \cdot w_{p2}(T_{e1} - T_{e2})$, $Cp_{p2} = Cp_{water} - Cp_{TS} \cdot w_{p2}$,

$Cp_{p3} = Cp_{water} - Cp_{TS} \cdot w_{p3}$, $M_{p3} = M_{p2} - M_{cond-e2}$ and $M_{p2} \cdot w_{p2} = M_{p3} \cdot w_{p3}$ into equation (6.23) and rearranging produce differential equation (6.24) for the 2nd effect temperature.

$$K_{e2} \cdot \frac{dT_{e2}}{dt} = q_{feed2} + q_{shell-e2} - q_{vacc} - q_{phc1} - q_{loss-e2} \qquad (6.24)$$

The heat losses occur from three different parts: the second effect, the shell of HX1503 and the shell of HX1506. Equation (6.25) describes the total heat losses from the effect.

$$q_{loss-E2} = \left[\left(U_{l-e2} \cdot A_{l-e2} \right) + \left(U_{l-vacc} \cdot A_{l-vacc} \right) + \left(U_{l-phc1} \cdot A_{l-phc1} \right) \right] \cdot \left(T_{e2} - T_a \right) \tag{6.25}$$

Where,

T_{e2} - Temperature of the 2nd effect (^{o}C)

M_{p3} - Mass flow rate of whey exiting the 2nd effect (kg/s)

q_{phc1} - Heat flow rate to HX1503 tubes (W)

q_{feed2} - Net energy flow rate with the feed whey to the 2nd effect (W)

6.3.3 Evaporator shell

The whey evaporator has two shells, one in each effect. Since the shell of the second effect is the same as the first effect, the differential equations for the shells of both effect. A differential equation for shell temperature was derived from energy balances across a control volume in the shell. This equation applies to the metal and the vapour in the evaporator shell. The differential equation describing the shell temperature is given by equation (6.26). The TVR compressor supplies energy while condensing water and surface losses remove energy.

$$\frac{d[K_s \cdot T_s]}{dt} = M_{comp} [Cp_{water} \cdot T_{e1} + \lambda] + m_{steam} \cdot h_{steam} - q_{shell-e1} - q_{phc3}$$

$$- M_{cond-s} \cdot Cp_{water} \cdot T_s - q_{loss-s} \tag{6.26}$$

Where,

$$K_s = M_{met-s} \cdot Cp_{met} + M_{vapour-s} \cdot Cp_{vapour}$$

$$q_{loss-s} = q_{loss-se1} + q_{loss-phc3} \qquad M_{cond-s} = \left(M_{cond-se1} + M_{cond-phc3} \right)$$

Substituting $q_{comp} = M_{comp} Cp_{water} \left(T_{e1} - T_{s1} \right) + M_{comp} \lambda$, $W_{comp} = \left(h_{steam} - Cp_{water} T_{s1} \right) m_{steam}$ and $M_{cond} = M_{comp} + m_{steam}$ into equation (6.26) and rearranging produces equation (6.27).

$$K_s \cdot \frac{dT_s}{dt} = q_{comp} + W_{comp} - q_{shell-el} - q_{phc3} - q_{loss-s} \tag{6.27}$$

Heat losses occur from the shell of HX1504 and the shell of HX1501. Equation (6.28) describes the total heat losses.

$$q_{loss-s} = \left[\left(U_{l-sel} \cdot A_{l-sel} \right) + \left(U_{l-phc3} \cdot A_{l-phc3} \right) \right] \cdot \left(T_s - T_a \right) \tag{6.28}$$

Where,

m_{steam} - Mass flow rate of steam to the TVR compressor (kg/s)

h_{steam} - Enthalpy of steam supplied to the TVR compressor (J/kg)

6.4 Thermal Vapour Recompression

TVR (Thermal Vapour Recompression) is the process of using high-pressure steam to recompress low-pressure steam (Figure 6.4). Steam jets accomplish compression through momentum transfer. A steam jet ejector consists of three parts: a motive steam nozzle, a mixing chamber and a diffuser..

High-pressure steam is accelerated to high velocity in the steam nozzle as it expands through the converging and diverging section of the steam nozzle where potential energy in the form of pressure is converted into kinetic energy in the form of velocity. This high-velocity jet of steam enters the mixing chamber where vapour from the suction line is entrained in the steam flow. The mixture of motive and suction vapour at a lower velocity enters the diffuser in which the kinetic energy of the mixture in the form of velocity is converted back to potential energy in the form of pressure. The mixture is discharged at an intermediate pressure with a value somewhere between that of the motive steam and the suction vapour pressure.

In the whey evaporator plant, a TVR unit compresses some of the vapour from effect-1 back into shell-1. The remainder of the vapour from effect-1 is used in shell-2. The TVR compressor in the whey evaporator was designed to

entrain 1 kg of vapour for each kg of high-pressure steam used. Thus, for every 2 kg vapour leaving effect-1, 1 kg is recycled to shell-1 and the remaining 1 kg passes to shell-2. The net result is that each kg of high-pressure steam results in overall evaporation of approximately 3 kg of water. Various authors have presented models to estimate the steam and the entrainment ratio of a thermal vapour re-compressor (van Wylen, 1994; Kessler, 1981; Mooney & Dotterweich, 1955; Winchester, 2000; Minton, 1986).
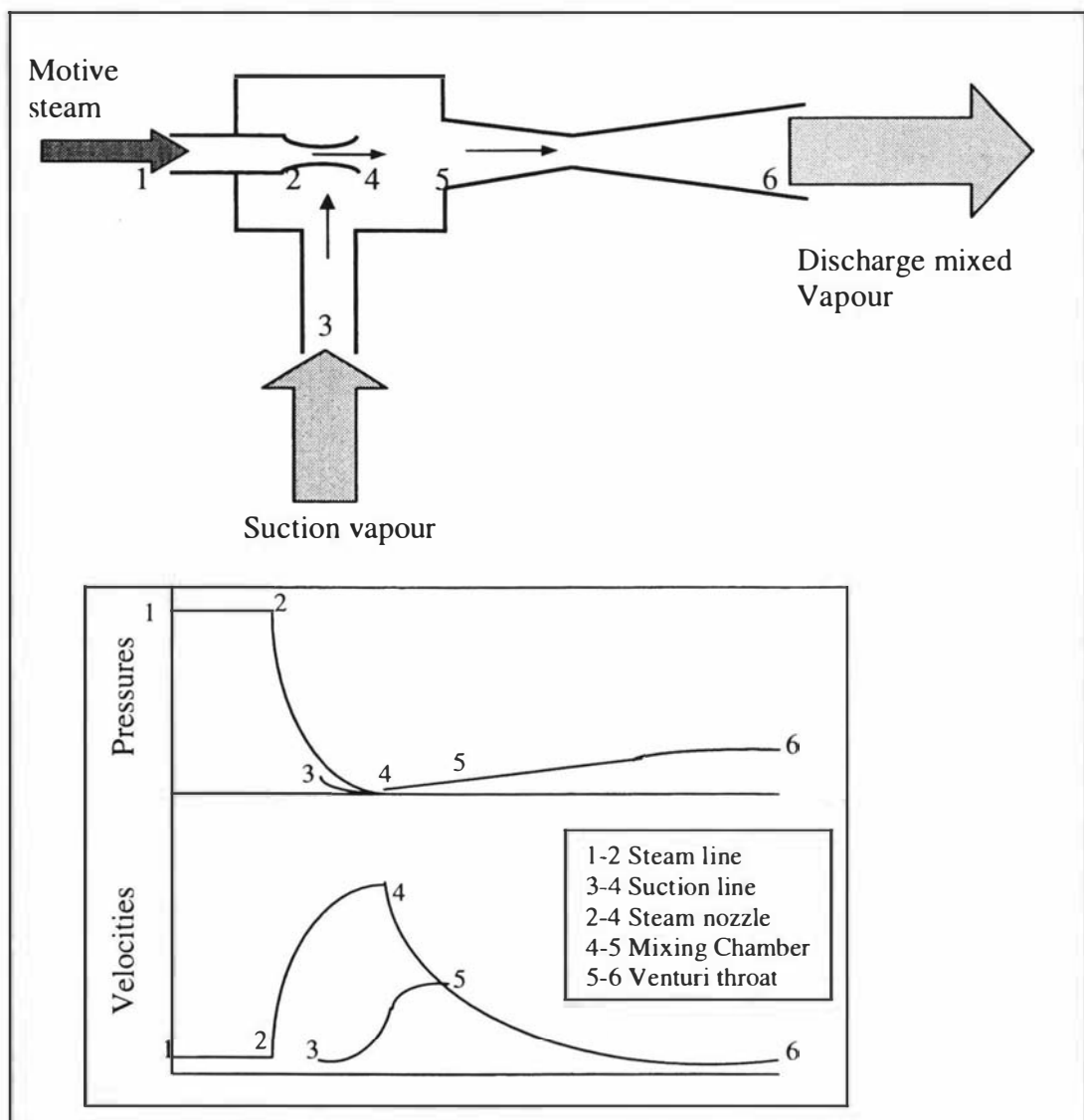
Figure 6.4: Thermal Vapour Recompression system

Winchester (2000) reviewed the literature models (Kessler, 1981; Mooney & Dotterweich, 1955) but concluded that these models did not give reliable results. Winchester (2000) then developed an empirical equation (6.30) for the mass of recycled vapour flow and used the model of van Wylen (1994) equation (6.31) for the estimation of the mass flow of motive steam. Minton (1986) developed models that were not reviewed compared by Winchester. The models of Minton (1986) are given by equations (6.20) to (6.34).

$$m_{comp} = \frac{A_{TVR} \cdot B_{TVR} \cdot P_{e1} \cdot P_s}{P_{steam}^{C_{TVR}}} \tag{6.29}$$

$$m_{steam} = A_{throat} \sqrt{\frac{2}{RT} \left(\frac{2}{\gamma+1}\right)^{\left(\frac{\gamma+1}{\gamma-1}\right)}} \cdot P_s = A_{TVR} \cdot P_s \tag{6.30}$$

Equation (6.32) and (6.33) give the mass flow rate of steam and recycled vapour flows.

$$m_{steam} = K_{TVR} \cdot d^2 \cdot P_{steam}^{0.96} \tag{6.31}$$

$$\frac{m_{steam}}{m_{comp}} = K_{HTC} \cdot \exp\left(4.6 \frac{\ln\left(\frac{P_s(t)}{P_{e1}(t)}\right)}{\ln\left(\frac{P_{steam}(t)}{P_{e1}(t)}\right)}\right) \tag{6.32}$$

The energy flows with the motive steam are given by equations (6.33) and (6.34).

$$W_{comp} = (H_{steam} - Cp_{water} \cdot T_s) \cdot m_{steam} \tag{6.33}$$

$$Q_{comp} = W_{comp} \cdot m_{comp} \tag{6.34}$$

Where,

m_{steam} - Mass flow of motive steam to the TVR compressor (kg/s)

A_{TVR} - TVR compressor parameter (m.s)

B_{TVR} - TVR compressor parameter ($m^{0.03} \cdot s^{0.06}/kg^{0.03}$)

C_{TVR} - TVR compressor parameter (-)

K_{TVR} - TVR compressor parameter (s/m)

d - Diameter of the TVR nozzle (m)

K_{HTC} - TVR compressor parameter (-)

P_{e1} - Pressure in the 1st effect (Nm^{-2})

P_s - Pressure in the shell of the 1st effect (Nm^{-2})

P_{steam} - Pressure of the motive steam (Nm^{-2})

R - Universal gas constant (kJ/kg. K)

T - Temperature of motive steam (K)

γ - Ratio of constant pressure and volume heat capacities (-)

A_{throat} - Cross sectional area of TVR compressor nozzle throat (m^2)

The above models were tested against experimental data from the Fonterra, Whareroa whey evaporator. The model (equation 6.30) of Van Wylen (1994) underestimates the motive steam flow whereas the model (equation 6.29) of Winchester (2000) overestimates the flow of recycled vapour (Figure 6.5 and 6.6). The models (equation 6.31 and 6.32) of Minton (1986) were found to give good predictions of both the motive steam flow and the flow of recycled vapour.
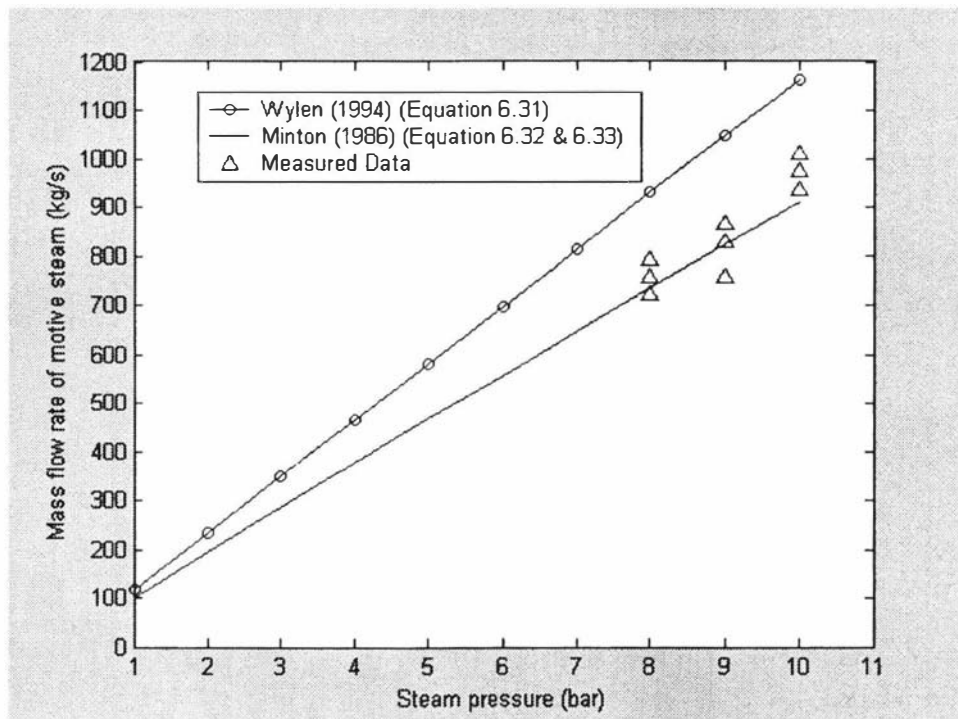
Figure 6.5: TVR models compared for motive steam flow with experimental data
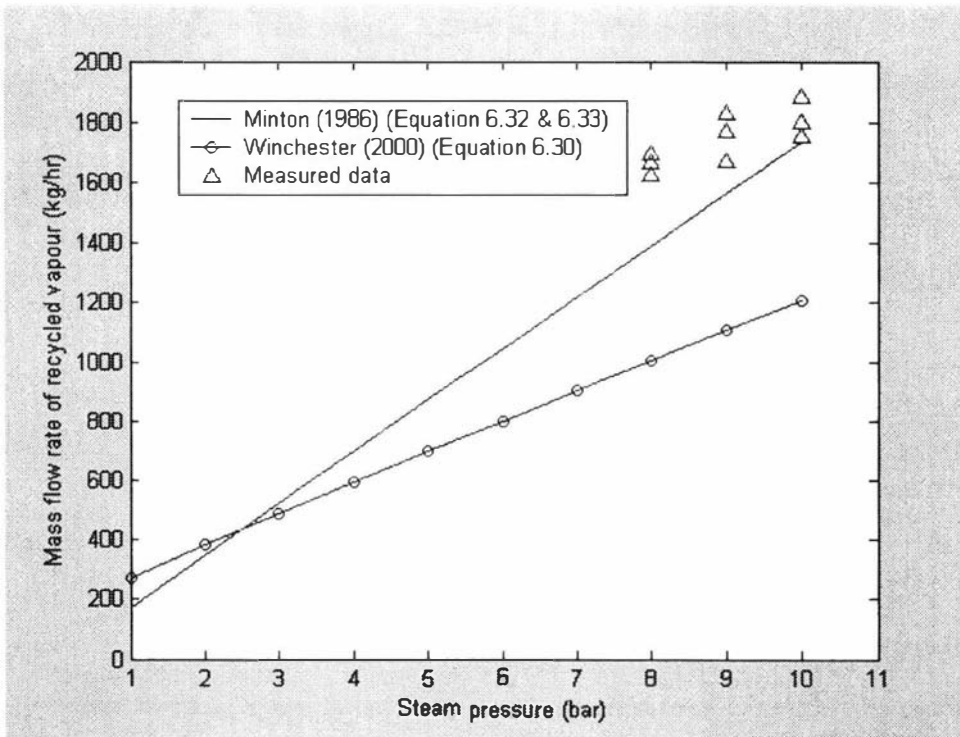
Figure 6.6: TVR models for recycled vapour flow compared with experimental data

6.5 Conclusions

The distribution plate models reported in the literature have assumed that plate thickness is negligible compared to the liquid height. In this study plate thickness (5mm) was significant compared to the liquid head in the evaporator (10 – 40 mm). This is of significance with respect to the applicability of literature reports of discharge coefficients to the whey evaporator application.

The preheat condenser models reported in the literature assume constant product density and heat capacity. These properties are very sensitive to the total solids concentration, but as there is no variation in solids concentration in the preheat condensers, these assumptions are justified.

The evaporation sub-system was divided into effect, shell and falling-film sections and models for each were derived separately. The derivation of the falling-film model was complicated by the variable properties of the falling film along the tube. It was found from the falling-film model simulation that the falling-film residence time and the heat transfer coefficient have a significant impact on model predictions.

The thermal vapour compressor models involved two parts, one the mass of motive steam flow and the second the mass of recycled vapour flow (the compression ratio). This study has identified the key parameters that affect the compressor performance. The models developed in this work can be applied to any evaporators that use a thermal vapour recompression unit.

7. Steady State Models and Model Parameters

In this section steady state methods were derived from the dynamic model developed in the previous chapter. The physical constants in the steady sate model were determined and data collected in a commercial evaporator (Fonterra) were used to validate the models.

Steady state models

Dynamic models for the whey evaporator were developed in Chapter 6. Steady state models for each sub-system were developed from the dynamic models by making the derivative terms with respect to time equal to zero.

7.1 Distribution plate

The dynamic models for the distribution plate are given by equations (6.3) and (6.4). There are three distribution plates in the whey evaporator, with significant flash on the 1st and the 3rd distribution plates and no flash on the 2nd distribution plate. The generic steady state equations for the distribution plate are given by equations (7.1) to (7.3), where Q_d is the volumetric flow rate from the distribution plate (m^3 s^{-1}), h_d is the liquid level in the distribution plate (m) and w_d is the total solids content in the product flow from the distribution plate (w/w). Equation 6.6 is rearranged to get equation 7.2.

$$Q_d = \frac{M_d}{\rho_d} = \frac{\left(M_f - M_{flash}\right)}{\rho_d} \tag{7.1}$$

$$h_d = \frac{1}{2g}\left\{\frac{Q_d}{nC_dA_o}\times\left[1-\left(\frac{A_o}{A_h}\right)^2\right]\right\}^{\frac{1}{2}} - \frac{1}{2gt_p} \tag{7.2}$$

$$w_d = \frac{M_f \cdot w_f}{\left(M_f - M_{flash}\right)} \tag{7.3}$$

7.2 Preheat condensers / Vacuum condenser

The dynamic models of the condensers are given by equations (6.10) to (6.13). There are three preheat condensers and one vacuum condenser in the whey evaporator. All these are of shell and tube type. The generic steady state models for the condenser are given by equations (7.4) and (7.5), where T_{out} is the temperature of the product exiting the preheat condenser (°C), q_{cond} is the total heat flow rate through walls of the preheat condenser tubes (W), τ_{TC} is the time constant of the condenser (s) and τ_{RT} is the total residence time of the product in the preheat condenser (s).

$$T_{out} = T_{sh} - (T_{sh} - T_{in})e^{-\frac{\tau_{RT}}{\tau_{TC}}} \tag{7.4}$$

$$q_{cond} = U_{cond}A_{cond}\frac{[T_{out}-T_{in}]}{\ln\left(\dfrac{T_{sh}-T_{in}}{T_{sh}-T_{out}}\right)} \tag{7.5}$$

Where, $\tau_{TC} = \dfrac{\rho_m.C_p.V_{phehc}}{U_{prehc}.A_{prehc}}$, $\tau_{RT} = \dfrac{\rho_m.V_{prehc}}{M_f}$

7.3 Evaporation

Dynamic models for the evaporation sub-system were developed separately for the falling-film, the effect and the shell. The steady state equations for the evaporator sub-system can be categorised into mass balances and energy balances. The energy balances cover the effect, the shell and the TVR systems, while the mass balances cover the falling-film.

7.3.1 Energy balance

There are two effects and one shell in the whey evaporator. The dynamic models derived for these are given by equations (6.21) to (6.32). The steady state equations are given by equations (7.6) to (7.10), where q is energy flow (W), W_{comp} is the energy supplied by the motive steam (W), m_{steam} is the motive steam flow (kg s^{-1}) and m_{comp} is the flow of recycled vapour in the TVR compressor (kg s^{-1}).

$$q_{feed1} + q_{shell-e1} - q_{comp} - q_{shell-e2} - q_{phc2} - q_{loss-e1} = 0 \tag{7.6}$$

$$q_{feed2} + q_{shell-e2} - q_{vacc} - q_{phc1} - q_{loss-e2} = 0 \tag{7.7}$$

$$q_{comp} + W_{comp} - q_{shell-e1} - q_{phc3} - q_{loss-s} = 0 \tag{7.8}$$

$$m_{steam} = K_{TVR} \cdot d^2 \cdot P_{steam}^{0.96} \tag{7.9}$$

$$\frac{m_{steam}(t)}{m_{comp}(t)} = K_{HTC} \cdot \exp\left(4.6 \frac{\ln\left(\dfrac{P_s(t)}{P_{e1}(t)}\right)}{\ln\left(\dfrac{P_{steam}(t)}{P_{e1}(t)}\right)} \right) \tag{7.10}$$

7.3.2 Falling-film model

The falling film model can be solved in two ways, one with the assumption of constant physical properties along the tube and the second with variable physical properties. A number of researchers (Quaal et. al, 1994; Bouman et. al, 1993; Choudhary and Shaukat, 1996; Angeletti and Moresi, 1983; Mackereth, 1993) adopted the variable property in their models while a number (Winchester et. al, 1999; Jebson and Iyer, 1991; Murthy and Sarma, 1977; Unterberg and Edwards, 1965; Kroll and McCutchan, 1968; Seban and Chun, 1972) assumed constant properties. The reasons for assuming constant falling-film properties are for the following reasons:

1. The variation of physical properties along the tube length is considered negligible. The validity of this assumption depends on the liquid. For example water has a negligible change in physical properties along the tube.

2. A variable property model requires that the physical property characteristics be known or modelled.

Both constant and variable property models are discussed here.

Variable property model

A differential equation (7.11) was derived as shown in Appendix B, (B.27). This relaxed the assumptions (uniform heat transfer along the tube wall) that were made during the derivations of the simple models shown in equations (6.17) to (6.19). The whey evaporator has three passes and the equations are similar in each pass. M_d and M_p are the product mass flow rates from the distribution plate and from the end of the pass (kg s^{-1}).

$$\frac{1}{v} \cdot \frac{\partial M(x,t)}{\partial t} + \frac{\partial M(x,t)}{\partial x} = \frac{U(w(x,t)) \cdot \pi \cdot d \cdot n \cdot [T_s(x,t) - T_e(x,t)]}{\lambda} \tag{7.11}$$

The steady state simplification of equation (7.11) is given by equation (7.12).

$$\frac{dM(x)}{dx} = \frac{U(x) \cdot \pi \cdot d \cdot n \cdot [T_s(x) - T_e(x)]}{\lambda} \tag{7.12}$$

Integrating both sides of equation (7.12) with respect to x will produces equation (7.13).

$$M_d - M_p = M_{tubes} = \left(\frac{\pi \cdot d \cdot n}{\lambda} \right) \cdot \int_0^L U(x) \cdot [T_s(x) - T_e(x)] \cdot dx \tag{7.13}$$

Equation (7.13) gives a deeper understanding of the behaviour of the falling-film along the tubes, whereas the constant property model gives the steady state values into and out of the tubes. The integration of equation (7.13) requires models for heat transfer coefficients, temperatures and the physical properties of the evaporating liquid and condensing water. Heat transfer coefficients, boiling point elevation, pressure drop and vapour drag are discussed in Appendix C. The physical properties of the evaporating and condensing liquids have been discussed in Chapter 3.

Constant property model

This model assumes constant properties along the falling-film. This approach simplifies the falling film model and has been adopted by many researchers (Quaak et. al, 1994; Winchester, 2000). The steady state equations for these simple models are given by equations (7.14) to (7.16), where M_{tubes} is the mass of evaporated vapour in the pass (kg s^{-1}), M_p is the product mass flow rate from the pass (kg s^{-1}) and w_p is the solids content in the product flow from the pass (w/w).

$$M_{tubes} = \frac{U(w) \cdot \pi \cdot d \cdot L \cdot n \cdot [T_s - T_e]}{\lambda} \qquad (7.14)$$

$$M_p = M_d - M_{tubes} \qquad (7.15)$$

$$w_p = \frac{M_d \cdot w_d}{[M_d - M_{tubes}]} \qquad (7.16)$$

Model Parameters

The models developed in chapters 5 and 6 contain unknown physical constants that need to be identified in order to use those models. The process parameters were estimated by minimising the model deviations from historical data. This is a standard technique of calculating the sum of squared errors in the model deviations and minimising this by varying the process parameters. The model validity was investigated after identifying the process parameters. This was done by testing the model predictions against historical or measured data.

7.4 Model parameters

Table 7.1 lists the parameters to be determined for the whey evaporator model.

Table 7.1: Process constants in the evaporation process

	Description	Units
U_{phc}	Preheat condenser overall heat transfer coefficient	W m^{-2} K^{-}
U_l	Surface losses overall heat transfer coefficient	W m^{-2} K^{-1}
U_o	Falling-film overall heat transfer coefficient	W m^{-2} K^{-1}
h_{fi}, h_{fo}	Falling-film fouling coefficient	W m^{-2} K^{-1}
τ_{RT}	Falling-film residence time	s
K_{TVR}	TVR model constant	kg h^{-1}cm^{-2} bar$^{-.96}$
K_{HTC}	TVR model constant	-

7.4.1 Preheat condenser overall heat transfer coefficient

Substituting the expressions for the time constants into equation (7.4) and rearranging gives the equation (7.17). In this equation the temperatures, mass flow rate, surface area and heat capacity are known but not the heat transfer coefficient.

$$U_{phc} = -\left(\frac{M_f \times C_{pm}}{A_{phc}}\right) \times \ln\frac{(T_{sh} - T_{out})}{(T_{sh} - T_{in})} \tag{7.17}$$

The inlet and outlet temperatures were measured using a surface temperature probe and all other values obtained from the historical data. Values of U_{phc} for different products were calculated and plotted against mass flow rate (Figure 7.1) and liquid viscosity (Figure 7.2). The viscosity of the feed products was measured at the feed temperatures into the 1st preheat condenser attached to the 2nd effect. The measurement data are given in Appendix A. The lower set of heat transfer values with WPI are for the 1st preheat condenser and the higher values for the 2nd and 3rd preheat condensers.
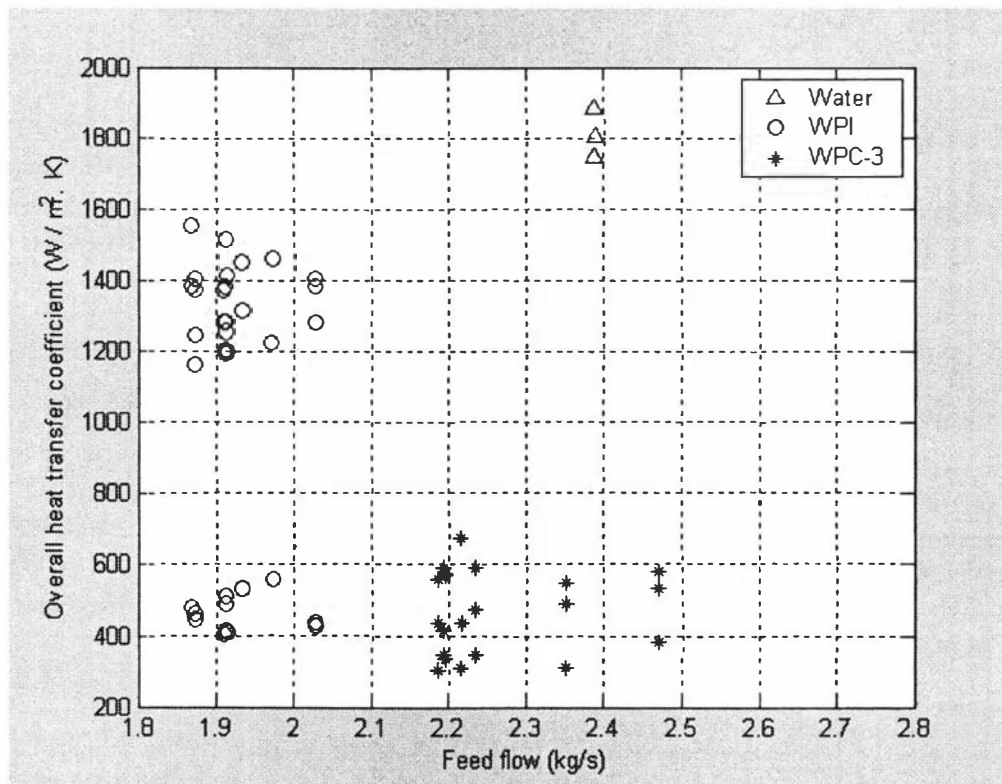
Figure 7.1: Preheat condenser overall heat transfer coefficient as a function of the feed mass flow rate.

The heat transfer coefficient related to the mass flow rate only is valid if the product viscosities are not significantly different (Winchester, 2000; Coulson and Richardson, 1991; Perry and Green, 1984). However, the viscosity of different whey products differs significantly. It is clear from Figures 7.1 and 7.2 that the preheat condenser overall heat transfer coefficient is strongly dependent on product viscosity. The data for WPI in the 1st preheat condenser are plotted in Figure 7.2, but were excluded from the regression.

Figure 7.2: Preheat condenser overall heat transfer coefficient as a function of the feed viscosity.

As the viscosity of WPI is lower than that of WPC-3, one would expect a higher overall heat transfer coefficient for WPI. However, the 1st preheat condenser overall heat transfer coefficient of WPI was low compared to that of water and WPC-3. This was due to the presence of non-condensable gases in the heating side of the 1st preheat condenser (discussed further and proved in chapter 9 (section 9.3.1)).

The heat transfer coefficient was found to vary linearly with the log of product feed viscosity (Figure 7.2). Linear regression was performed to quantify the relationship between U_{phc} and $\ln\mu$. The regression equation is given by shown in equation (7.18) and can be used to estimate the heat transfer coefficient knowing the product feed viscosity to the preheat condenser. The viscosity of the feed products can be estimated using the viscosity model developed in Chapter 3.

$$U_{phc} = 1808.1 - 525.37 \times \ln\mu \qquad (7.18)$$

Where,

U_{phc} - Preheat condenser overall heat transfer coefficient (W m^{-2} K^{-1})

μ - Viscosity of feed product to the condenser (cP)

To validate the condenser model, temperature predictions for a different product (WPC-2) were compared with historical data, and literature heat transfer coefficients for water and milk products were compared with those predicted by equation (7.18). Figure 7.3 shows the comparison of predicted temperatures against the historical data for WPC-2. The temperatures were predicted with an error of less than 5%. Continuous line in figure 7.3 represents the data with zero error.

Winchester (2000) performed condenser heat transfer calculations with water and Sophie-Lo (low protein whole milk). The feed temperature to the condenser was 60°C and the viscosities of water and Sophie-Lo at this temperature were 0.48 cP and 0.65 cP respectively. The overall heat transfer coefficients estimated using equation (7.18) are 2194 W m^{-2} K^{-1} for water and 2034 W m^{-2} K^{-1} with Sophie-Lo. These predicted values are very close to those determined by Winchester (2000) from experimental data: 2300 ± 150 W m^{-2} K^{-1} for water and 2075 ± 100 W m^{-2} K^{-1} for Sophie-Lo.
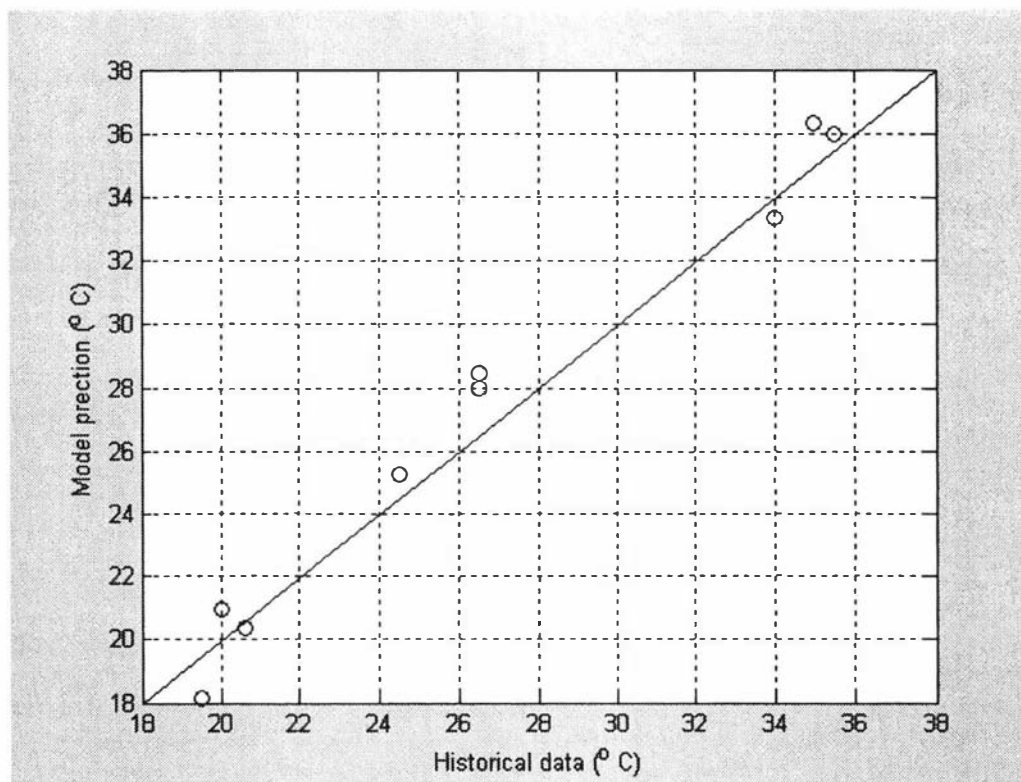
Figure 7.3: Preheat condenser outlet temperature predictions versus historical data for WPC-2

7.4.2 Surface energy losses overall heat transfer coefficient

The energy losses from the evaporator surfaces occur by convection (a combination of heat conduction between the fluid particles and the energy transport due to the fluid motion itself) and radiation. The heat losses from the evaporator occur from both evaporator effects, from the shells of the evaporator effects and from the shell of the preheat condensers. The evaporator shells are insulated (outer surface temperature is approximately the same as the room temperature) but not the preheat condensers. Therefore, it was assumed that there are negligible or no energy losses from the evaporator shells and that losses occur only from the effects and the shell of the preheat condensers.

The energy losses from the effects and the preheat condensers were calculated using equations 6.22 and 6.28. These equations were combined and rearranged to derive the steady state equation 7.19. All the terms in this equation could be estimated from historical data except the energy losses from the surface (q_{loss}).

The surface energy losses can also estimated from equation 7.20, from which the overall losses heat transfer coefficient (U_{loss}) can be identified.

$$Q_{feed1} + W_{comp} - q_{phc2} - q_{phc3} - q_{loss} - q_{condensate} = 0 \qquad (7.19)$$

$$q_{loss} = U_{loss} A_{loss} (T_s - T_a) \qquad (7.20)$$

The losses heat transfer coefficient was identified by minimising the error between the model (7.20) and the total heat losses calculated from the historical data. Figure 7.4 shows the model deviations from the historical data, with an optimum value for U_{loss} of 10 ± 2 Wm^{-2} K^{-1}. This is higher than the value estimated from literature models (2.24, 4.3 and 3.6 W m^{-2} K^{-1}, Appendix C) but close to the value of 12 W m^{-2} K^{-1}, determined by Winchester (2000) for a milk evaporator.
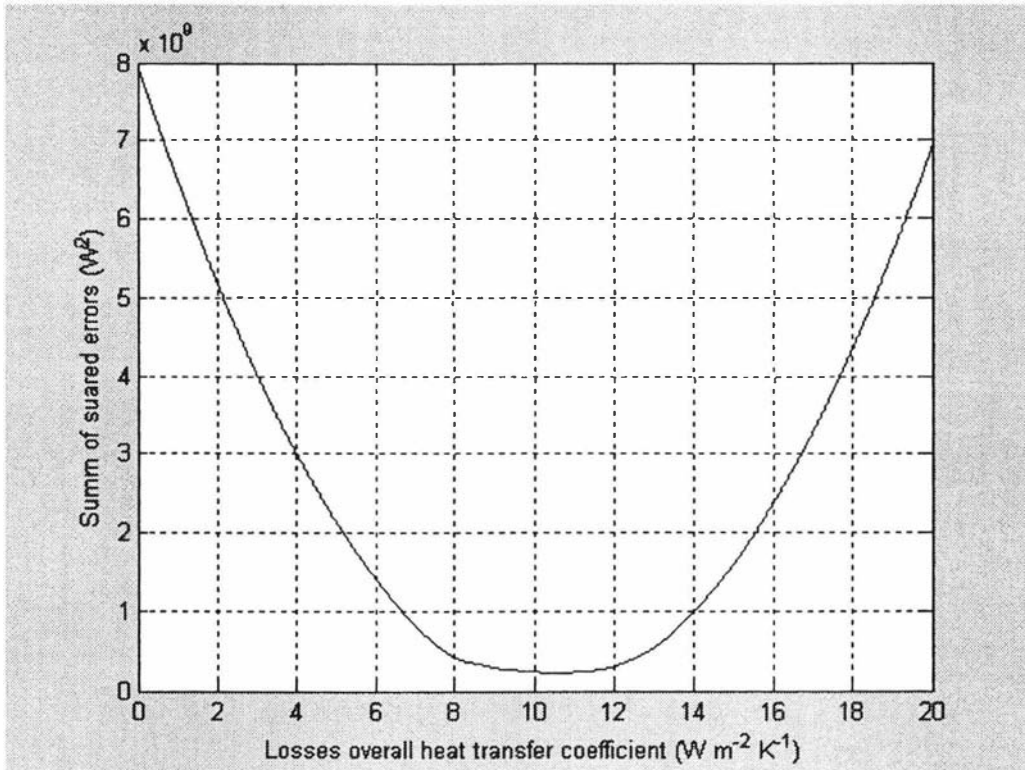
Figure 7.4: Overall energy balance sum of squared error as a function of U_{loss}

7.4.3 Falling-film overall heat transfer coefficient

The constant property and variable property steady state falling-film model developed in section 7.3.2 (equations 7.13 to 7.16) were used as a basis for deriving a model to predict the overall evaporation heat transfer coefficient for any product. The average overall evaporation heat transfer coefficients for both water and whey products were calculated from historical data and total solids measurements around the evaporator.

Constant property model

The average overall evaporation heat transfer coefficient calculation based on the assumption of constant physical properties and a constant temperature profile along the evaporator tubes.

Water

The overall heat transfer coefficient for water was estimated using equations 7.21 and 7.22, derived from the overall energy and mass balances for the effects (Equation 7.14 to 7.16) to eliminate the unknown flows in between passes. M_{evap1} and M_{evap1} (kg s^{-1}) are the masses of evaporated vapour in the 1st and 2nd effect respectively.

$$M_{evape1} = M_{phc3} - M_{p2} = M_{flash1} + M_{tubes} = \frac{M_{phc3}C_p}{\lambda}\left(T_{phc3} - T_{e1}\right) + \frac{U_o A_{se1}\left(T_s - T_{e1}\right)}{\lambda} \quad (7.21)$$

$$M_{evape2} = M_{p2} - M_{p3} = M_{flash2} + M_{tubese2} = \frac{M_{p2}C_p}{\lambda}\left(T_{e1} - T_{e2}\right) + \frac{U_o A_{se2}\left(T_{e1} - T_{e2}\right)}{\lambda} \quad (7.22)$$

All the terms in these equations are known except the overall heat transfer coefficient, U_o. The overall heat transfer coefficients were identified for the 1st and the 2nd effect by minimising the sum of squared errors as shown in Figure 7.5. The optimum overall heat transfer coefficients were 2250±100 W m^{-2} K^{-1} and 2450±100 W m^{-2} K^{-1} for the 1st and 2nd effect respectively.

The higher heat transfer coefficient in the 2nd effect could be due to a smaller falling-film thickness. This is because there were more tubes in the 2nd effect than in the 1st effect and there is consequently less flow per tube in the 2nd effect.
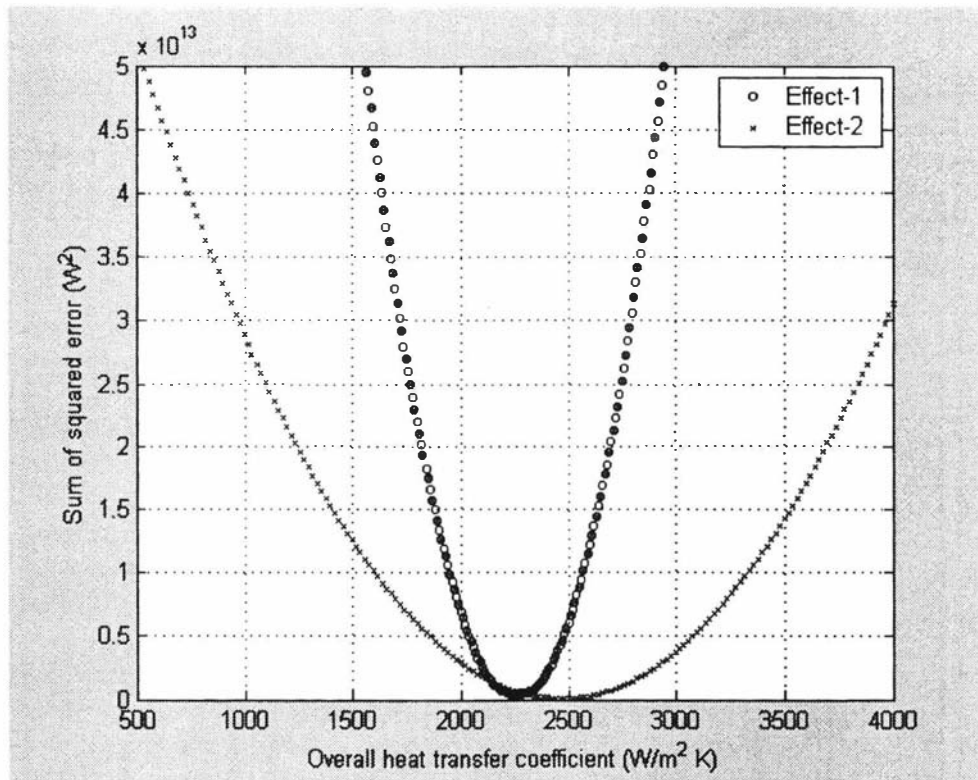
Figure 7.5: Deviation between equations 7.21/7.22 and historical data as a function of overall evaporation heat transfer coefficient for water

Whey products

The overall heat transfer coefficient for whey products was estimated using equation 7.23, derived from equations 7.14 to 7.16. The total solids from each pass were measured as discussed in Chapter 3, and all other terms (except the heat transfer coefficient) were taken from historical data.

$$U_o = \frac{M_d \left(1 - \dfrac{w_d}{w_p}\right)\lambda}{A_s\left(T_s - T_e\right)} \tag{7.23}$$

Figures 7.6 and 7.7 show the overall evaporation heat transfer coefficients estimated for WPC-3 and WPI respectively. The Figures also show the regression lines fitted to the estimated data.
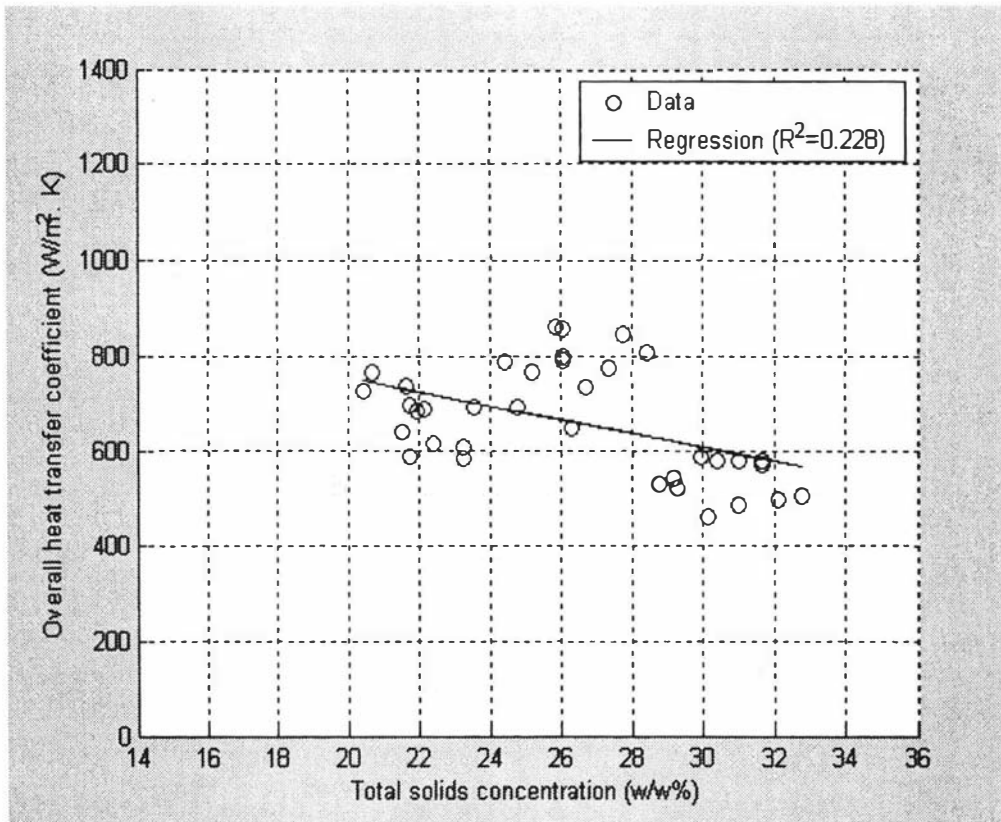
Figure 7.6: Overall evaporation heat transfer coefficient for WPC-3 as a function of total solids concentration

Mass flow rate, evaporating temperature and total solids concentration have a weak influence on the overall heat transfer coefficient. The temperature profile in the evaporator is the same with all whey products except with WPI (up to 5°C). The feed flow rate to the evaporator is approximately same with all whey products except with WPI (18% lower). This is discussed in Chapter 9. A significant factor affecting the overall heat transfer coefficient for a given product is the product total solids concentration (proportional to the product viscosity).

It is clear from Figures 7.6 and 7.7 that is not possible to get a good fit for the overall heat transfer coefficient as a function of total solids content. This is due to the fact that, besides viscosity, the air content in the product and the product type (discussed in Chapter 9) also influence the overall heat transfer coefficient. Therefore, more accurate estimates of the overall evaporating heat transfer coefficient were sought using the variable property model. This was feasible through application of the physical property models developed in Chapter 3.

112
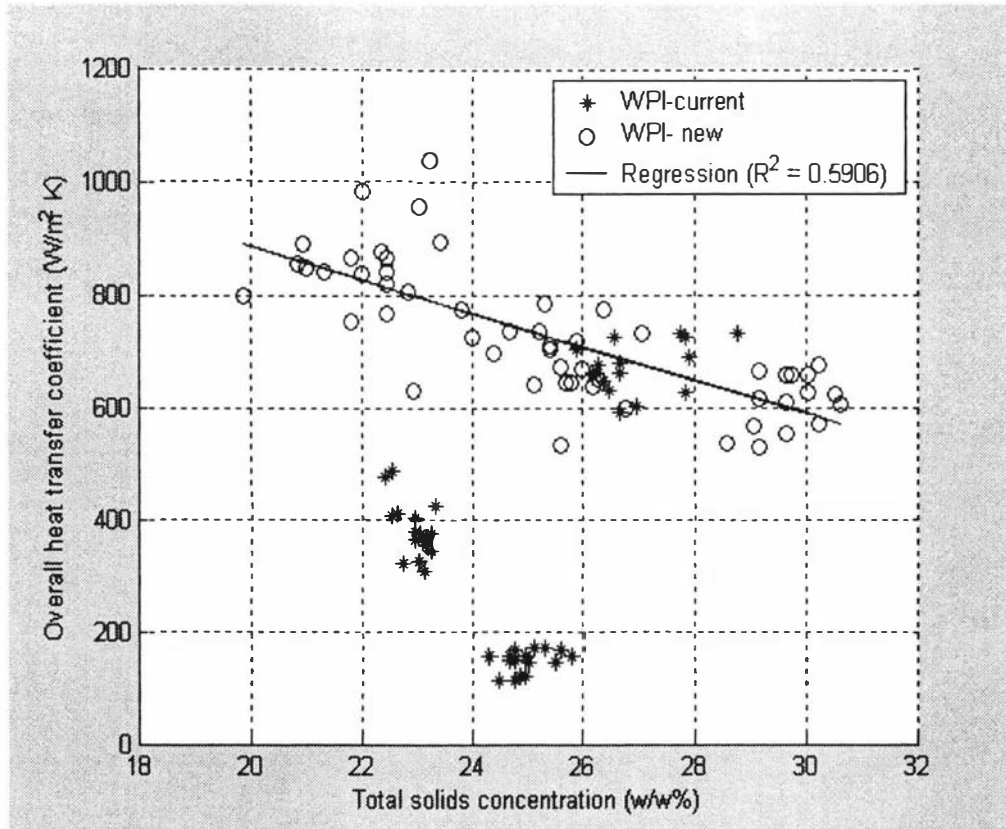
Figure 7.7: Overall evaporation heat transfer coefficient of WPI as a function of total solids concentration

Variable property model

The variable property falling-film model was derived in section 7.3.2 (equation 7.13). All the variables (overall heat transfer coefficient, shell and effect temperatures) vary along the evaporator tubes. The temperature variation is due to boiling point elevation and the pressure drop is due to co-current vapour flow in the tube. The variation of the local heat transfer coefficient of the falling-film on the product side is due to the variation in flow rate and physical properties. The flow variation is the only cause for changes in the local heat transfer coefficient of the falling-film on the heating (steam) side. The wavy falling-film model of Chun and Seban (1971), (equation 7.24), was chosen for calculating the falling-film heat transfer coefficient for the following reasons,

1. The equation is derived to suit wavy falling films.

2. The operating regime in the whey evaporator is wavy laminar (Reynolds numbers from 500 to 1400 for water and from 30 to 150 for whey products.

113

3. The model has been widely applied by other researchers for a range of applications (Mackereth, 1993; Chen, 1997; Mills, 1995; Chen and Jebson, 1997; Angeletti and Moresi, 1983; Fujita and Udea, 1978; Hirshburg and Florschuetz, 1982; Murthy and Sarma, 1977; Berntsson and Asblad, 1991; Stuhltrager, 1995). Literature falling-film models are discussed in Appendix C.

$$Nu = 0.822\,\mathrm{Re}^{-0.22} \qquad\qquad (7.24)$$

Where, $Nu = \dfrac{h\left(\mu^2 / g \cdot \rho^2\right)^{1/3}}{k}$, $\mathrm{Re} = \dfrac{4\Gamma}{\mu}$

The overall evaporation heat transfer coefficient was calculated from the model of Richardson and Coulson (1991):

$$\frac{1}{U_o} = \frac{1}{h_o} + \frac{\dfrac{d_o}{d_i}}{h_i} + \frac{\dfrac{d_o}{2} \cdot \ln\left(\dfrac{d_o}{d_i}\right)}{k_w} + \frac{1}{h_f} \qquad\qquad (7.25)$$

Where,

Nu - Nusselt number (-)

Re   - Reynolds number (-)

U_o - Overall evaporation heat transfer coefficient (W m^{-2} K^{-1})

μ - Viscosity of the fluid (Pa. s)

k_w - Thermal Conductivity of the tube material (W m^{-1} K^{-1})

g - Acceleration due to gravity (m s^{-2})

d_o - Tube outside diameter (m)

d_i - Tube inside diameter (m)

h_i - Inside fluid fi!m coefficient (W m^{-2} K^{-1})

h_o - Outside fluid film coefficient (W m^{-2} K^{-1})

h_f - Fouling coefficient (W m^{-2} K^{-1})

All the terms in equations 7.24 and 7.25 are known except the fouling coefficient and the overall heat transfer coefficient. The average overall heat transfer coefficients calculated from the total solids measurements (discussed in constant property model)

for whey products were used to identify the fouling coefficients by minimising the deviation between predicted and measured mass of evaporation.
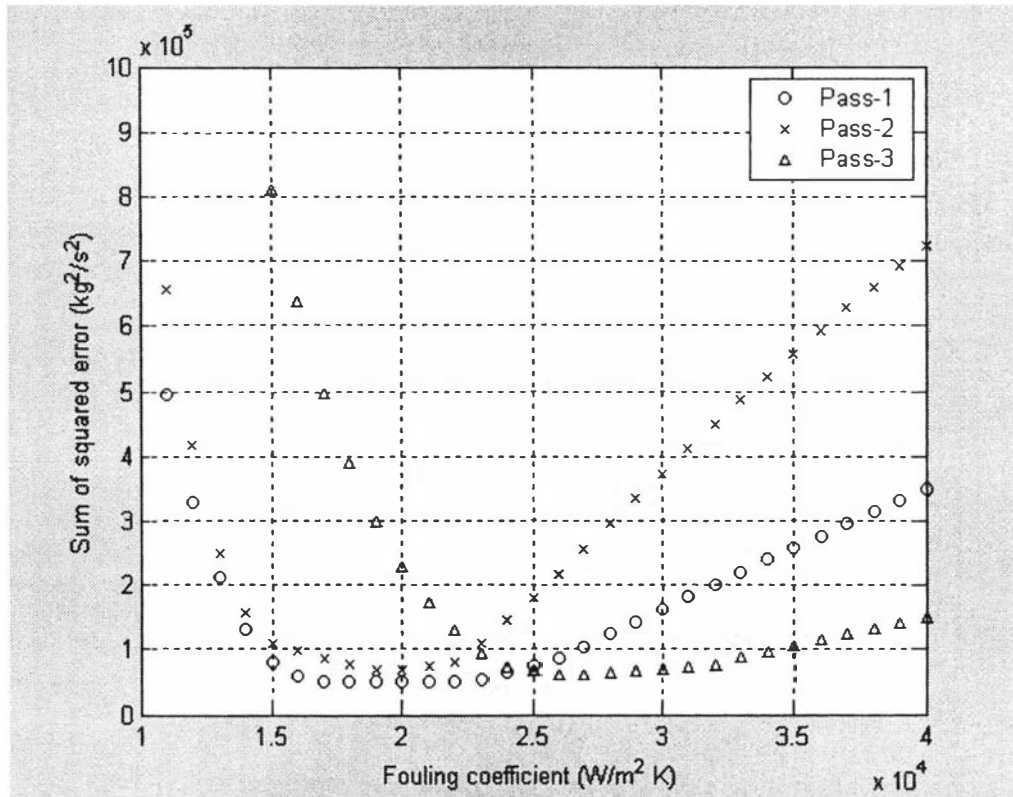
Figure 7.8: Fouling coefficient for water
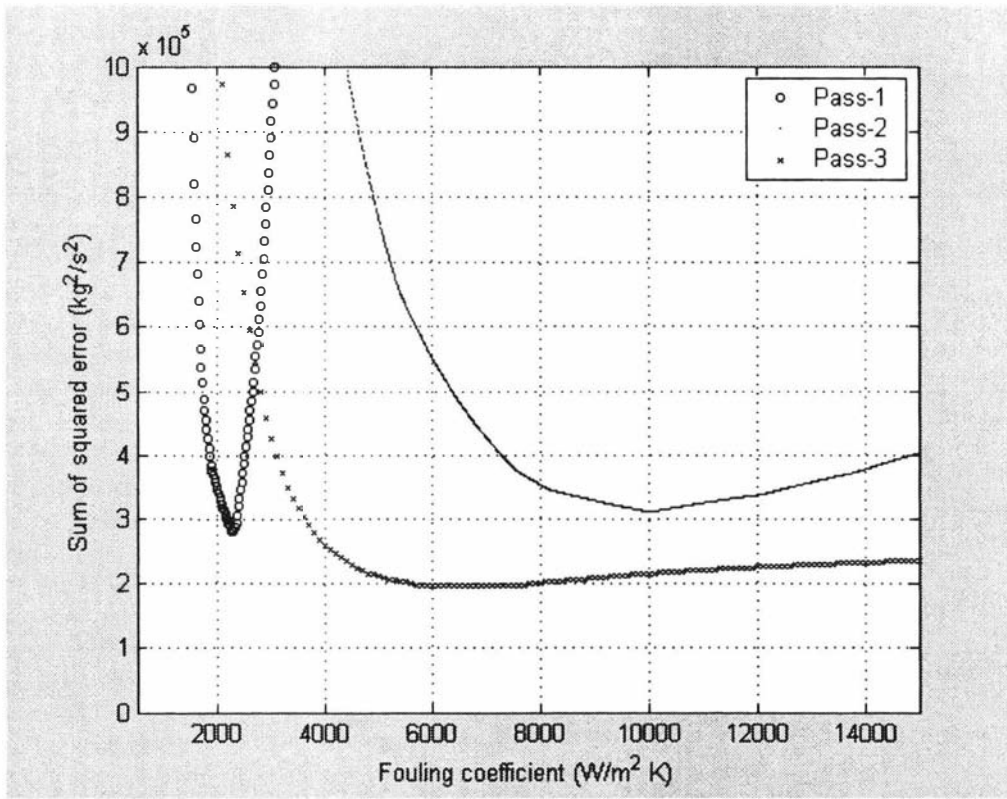
Figure 7.9: Fouling coefficient for WPC-3
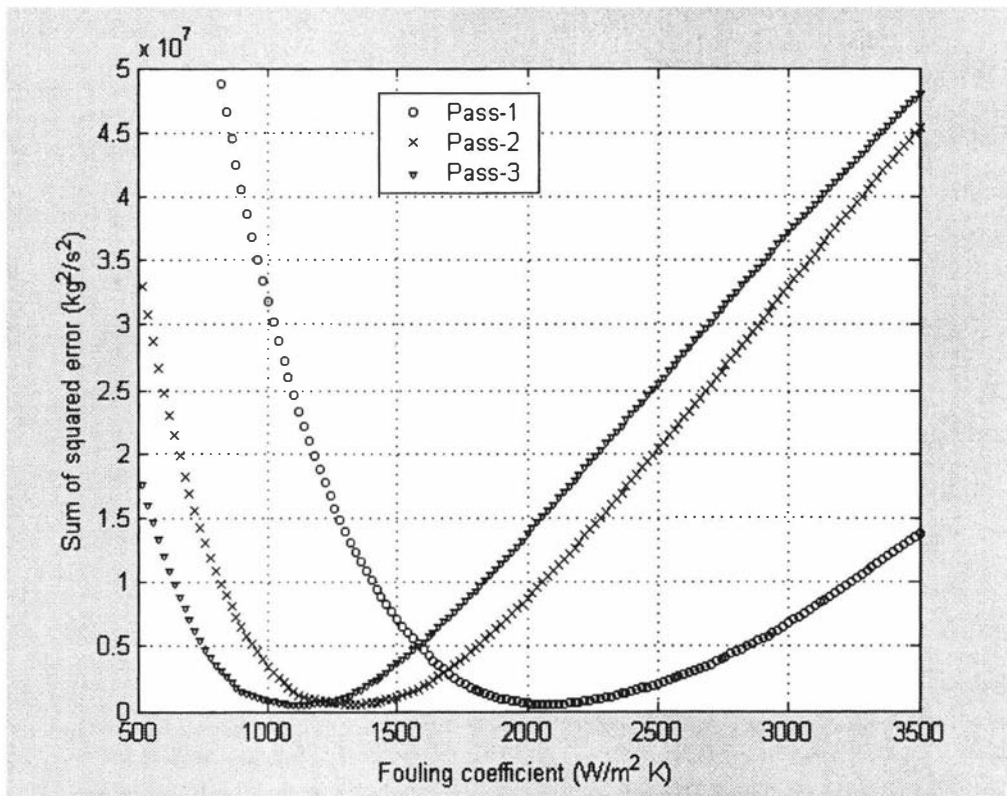
Figure 7.10: Fouling coefficient for WPI- new (optimum operating conditions)

116
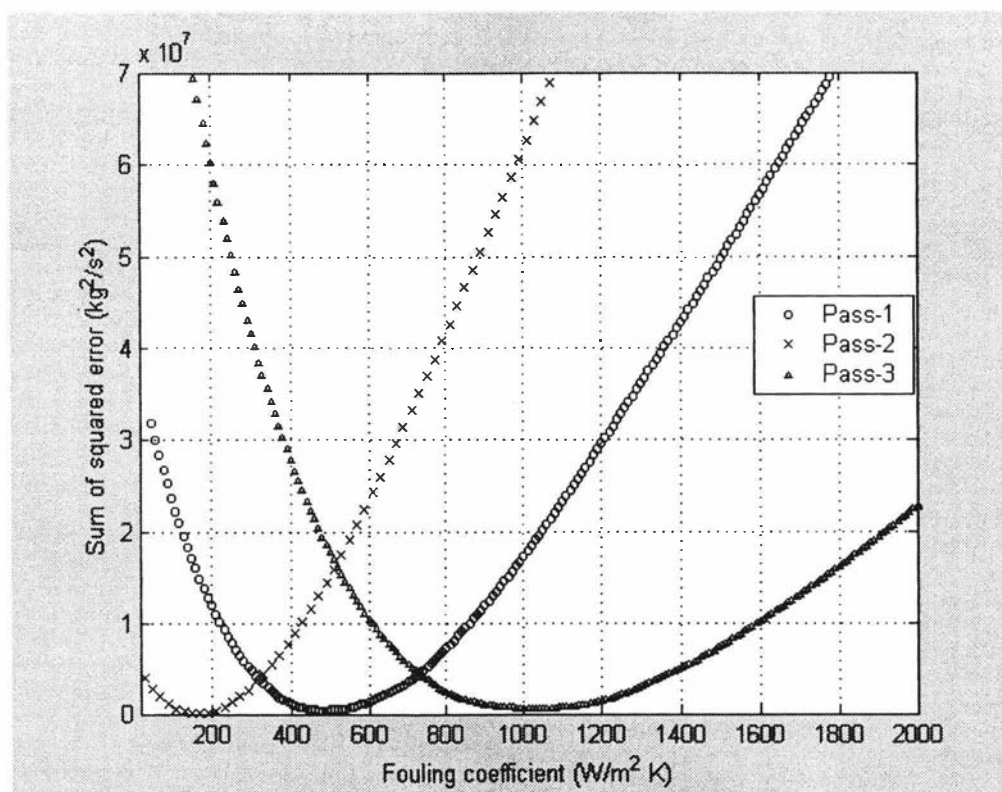
Figure 7. 11: Fouling coefficient for WPI- current (current operating conditions)

Figures 7.8 to 7.11 show the fouling coefficients estimated from the calculated overall heat transfer coefficients. The fouling coefficients for different products are tabulated in Table 7.2. The effects of boiling point elevation and pressure drop on effect temperature are discussed in Appendix C.

Table 7.2: Fouling coefficients

Products	Pass	Fouling coefficients (W m^{-2} K^{-1})
Water	1 /2 /3	20000 / 20000 / 27000
WPC-3	1 /2 /3	2400 / 10000 / 6000
WPI-current	1 /2 /3	500 / 190 / 1000
WPI-new	1 /2 /3	2100 / 1300 / 1100
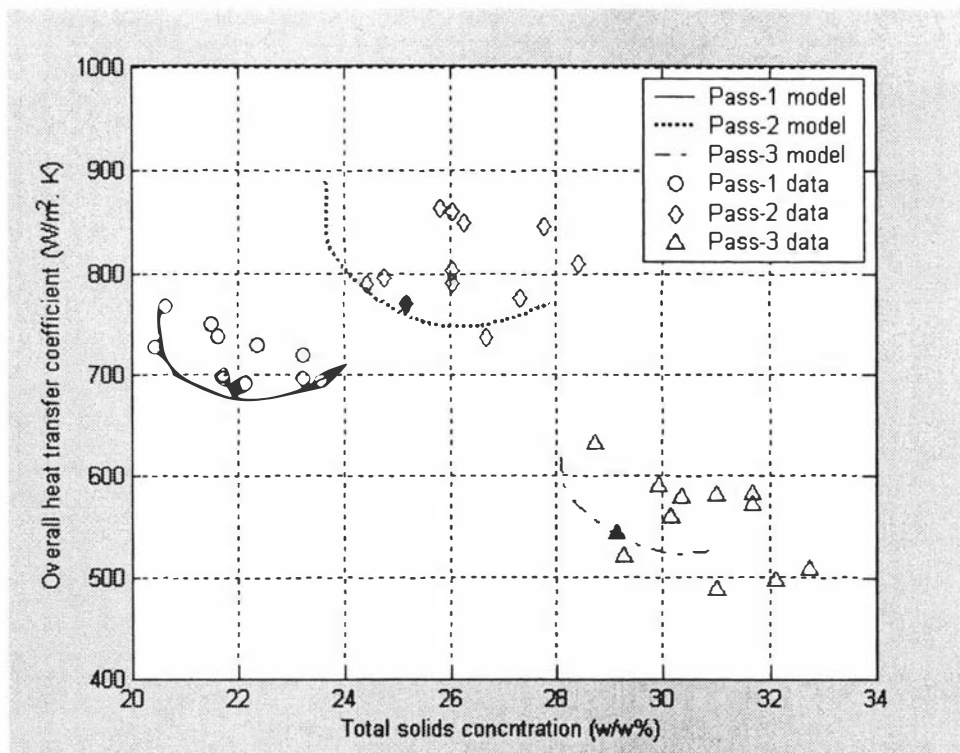
Figure 7.12: Comparison of predicted heat transfer coefficients with values calculated from experimental data for WPC-3

The model validity was tested by comparing the heat transfer coefficients predicted by equation 7.24 with the calculated average heat transfer coefficients (Figures 7.12 to 7.14). The solids profile predicted for a new product (WPC-2) using the variable property model was then compared with the measured data (Figure 7.15).
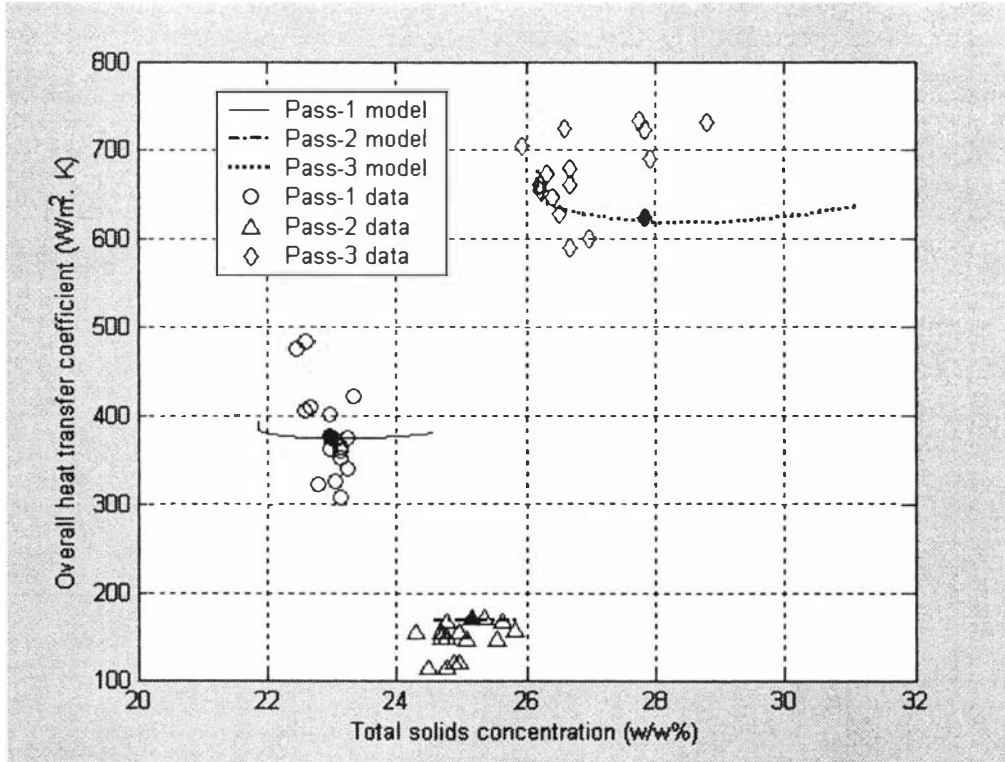
Figure 7.13: Model testing for WPI-current (current operating conditions)
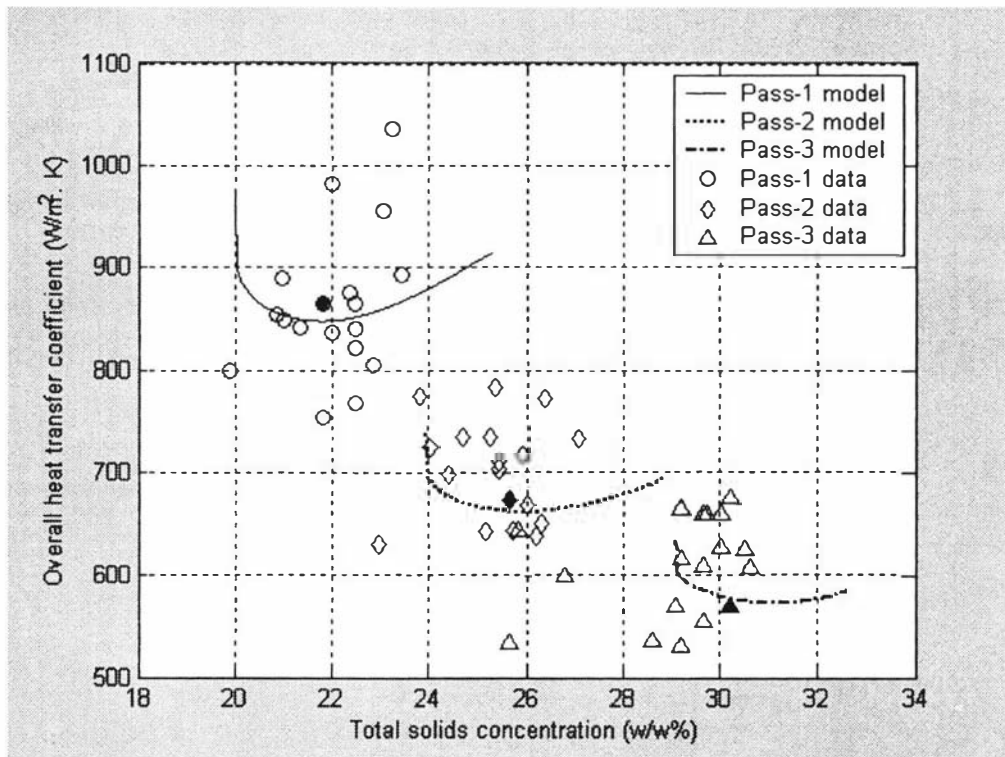
Figure 7.14: Model testing for WPI-new (optimum operating conditions)

The model predictions shown in Figures 7.12 to 7.14 with selected operating conditions (highlighted data in figures) whereas the calculated data included different operating conditions (temperatures feed solids and flow rates). The model predicted the calculated heat transfer coefficients with less than 5% error, and the solids profile with less than 1.5% error (this is equivalent to 0.5% w/w). Figure 7.15 shows the predicted concentrate solids against measured data for WPC-2. These results further validate that the solids profile can be predicted using the variable property model with an error of less than 1.5%.
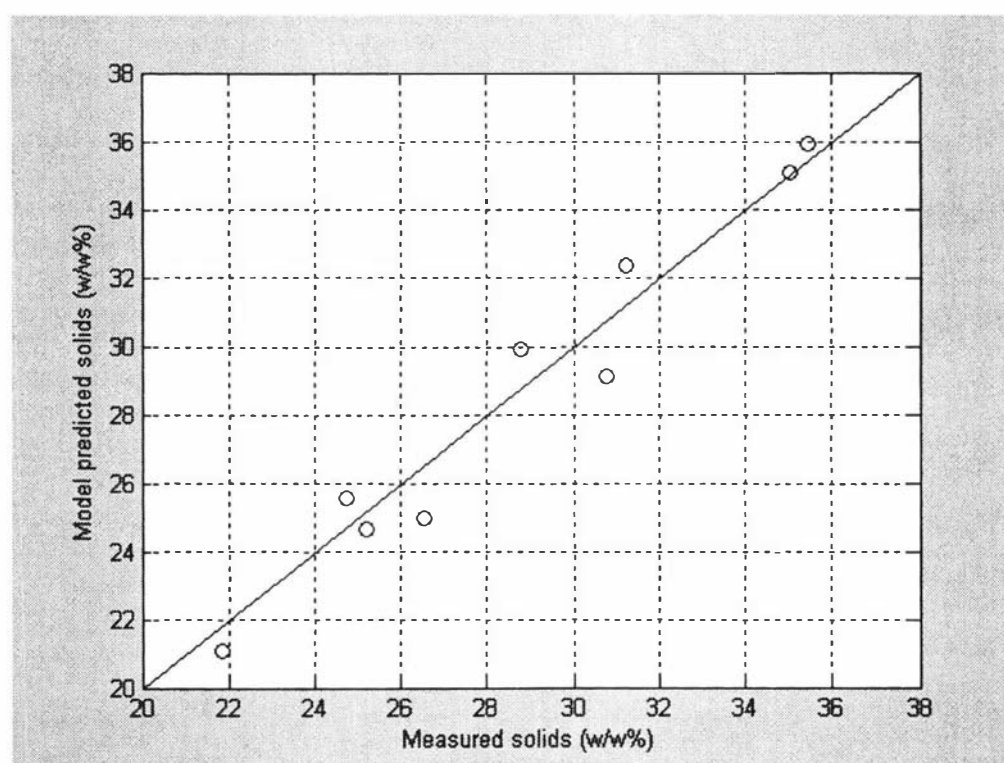
Figure 7.15: Model testing with WPC-2

The advantages of the variable property models compared to the constant property models are,

1. The solids and mass profile for a new product can be estimated reasonably accurately without wasting the product.
2. The operating conditions for new products can be determined with minimal downtime and resources.
3. Rapid and simplified troubleshooting and optimisation for existing products

7.4.4 Evaporator falling-film residence time

The residence time in the evaporator is influenced by the product physical properties. Winchester (2000) and Mackereth (1993) suggest that 50 s is the average falling film residence time for milk and that the liquid loading has no influence on the residence time. However, there is no experimental work has been reported that confirms this for milk products or whey products. Therefore, laboratory scale measurements were conducted to determine falling-film residence times for water and milk concentrates.

To measure residence times, liquid was forced to flow like a falling film along a flat vertical surface and the flow was filmed continuously. The surface metal along which the liquid flowed was of the same material and polish as the evaporator tubes. A food dye was used to produce a colour spot in the falling liquid film so that the flow path was visible on the recorded video. Water and whole milk at 10% and 20% total solids concentrations were used in this experiment with three replicates for each liquid. The viscosities of these liquids were 1, 1.45 and 2.9 cp respectively (Chapter 3). The time taken for the food colouring to pass through a known distance was noted from the video by playing it frame by frame. Each frame in the video was 1/25 s. The residence times measured for water and milk concentrates are shown in Table 7.3.

Table 7.3: Residence time measurements

Product	Viscosity (cp)	Wetting flow rate (kg m^{-1} s^{-1})	Re	Residence time (s / m length)
Water	1	0.946	4018	0.72
Whole milk (10%)	1.45	0.826	2270	0.72
Whole milk (20%)	2.9	0.787	1083	0.76

The residence time of the falling-film in the whey evaporator can potentially be determined from equation (7.26). However, this was not possible in the current work as there is no solids measurement in the feed to the evaporator.

$$\frac{w_{p3}(s)}{w_f(s)} = \frac{M_{p3}^0}{M_f^0} e^{-\tau_T s}, \quad w_{p3}(t) = \frac{M_f^0}{M_{p3}^0} w_f(t-\tau_T) \qquad (7.26)$$

Where, τ_T is the total plant residence time, M_f and w_f are the evaporator feed flow and the solids and M_{p3} and w_{p3} are the flow and solids exiting from the evaporator.

The total residence time of whey products in the evaporator was recorded physically in the plant (time for the product to exit through the last pass since the start of feeding from the balance tank). This total time can also be estimated from historical data (concentrate density data). The total residence time in the evaporator includes the pumping delays, residence time in the preheat condensers and the falling-film residence time. The pumping delays and the preheat condenser residence times were estimated from the known evaporator geometry and the feed flow rate (Appendix C). The flow regime of the all the products was wavy laminar. Therefore, the wavy falling-film models (Alhusseini et. al, 1998; Chun and Seban, 1972) in the literature (Appendix C) were used to predict the falling-film residence time. The results are plotted in Figure (7.16).

The residence time results with water and WPC-3 suggest that the wavy laminar model-2 predicts the falling film residence time well. It was not possible to measure the total plant residence time for WPI due to high foamability. Since, the experimental with water was conducted with no evaporation and WPC-3 data were calculated from the plant total residence time, the residence time in each pass was the same.

7.4.5 TVR model coefficients

The TVR steam mass flow and the recycled vapour flow are given by equations 7.27 and 7.28 respectively. The constant in equation 7.27, K_{TVR}, depends on the TVR nozzle geometry, whereas the constant in equation 7.28, K_{HTC}, depends on the mass of evaporation in the 1st effect (i.e depends on the heat transfer coefficient, Chapter 5 & 6). All the variables in equation 7.27 are known except the nozzle constant, K_{TVR}. The value of this constant for the whey evaporator was estimated by minimising the deviation

between equation 7.27 and historical data for the mass flow rate of steam. The constant, K_{HTC} in equation 7.28 was estimated similarly.
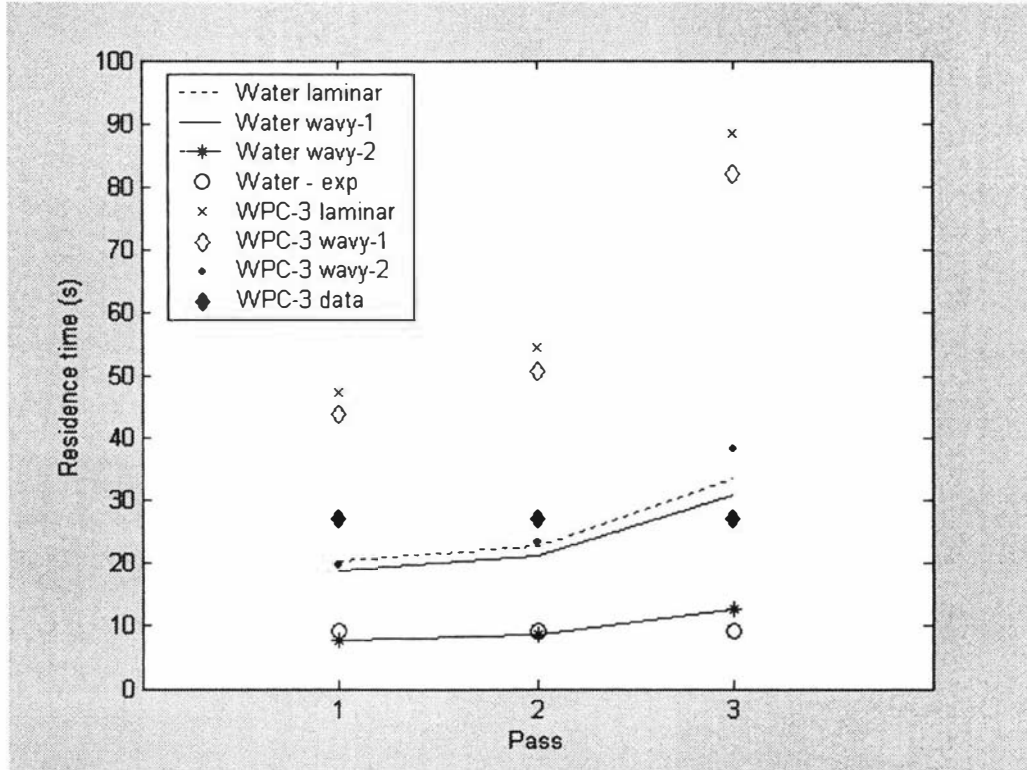
Figure 7.16: Residence time predictions compared with experimental data

$$m_{steam} = K_{TVR} \times d^2 \times P_{steam}^{0.96} \tag{7.27}$$

$$\frac{K_{tvr} \times d^2 \times P_{steam}^{0.96}}{m_{comp}} = K_{HTC} \cdot \exp\left(4.6 \frac{\ln\left(\dfrac{P_s(t)}{P_{el}(t)}\right)}{\ln\left(\dfrac{P_{steam}(t)}{P_{el}(t)}\right)}\right) \tag{7.28}$$

Figures 7.17 and 7.18 show the TVR constants estimated from historical data for water, WPC-3 and WPI. The optimal value for the steam mass flow constant (K_{TVR}) was 45.87±1 and this was independent of the product. The optimal values for the recycled vapour constant (K_{HTC}) were 1.7±0.2, 0.43±0.02, 0.4±0.02 and 0.37±0.02 for WPI-current, WPI-new, WPC-3 and water respectively.
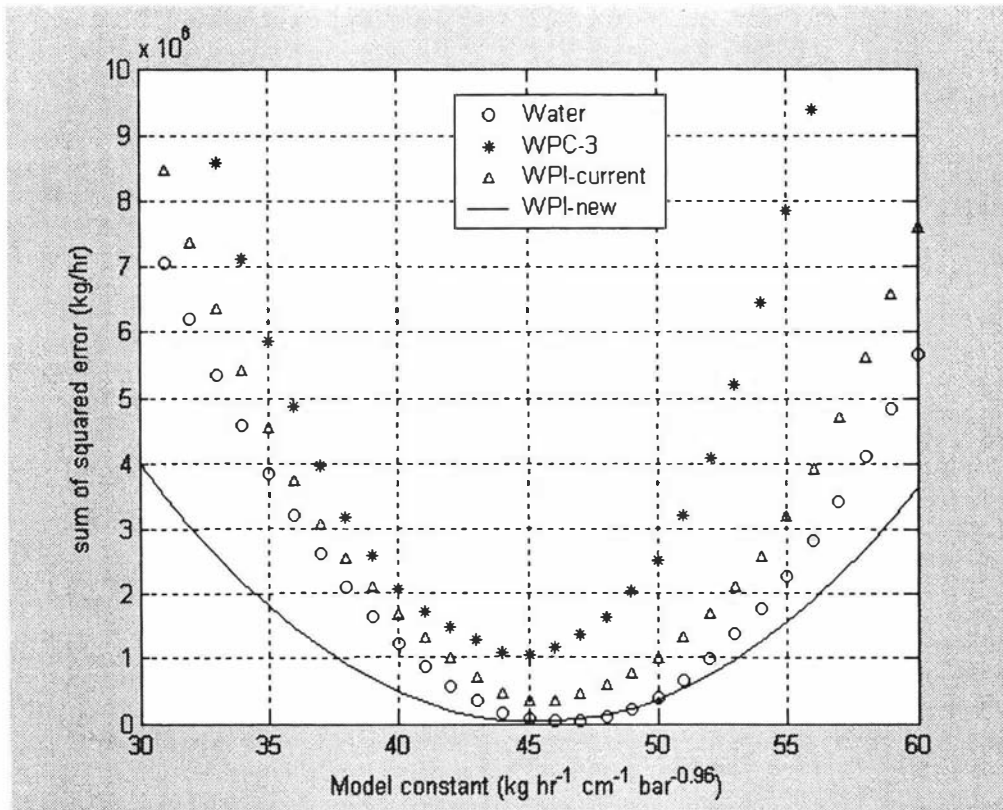
Figure 7.17: Optimum values of TVR steam model constant, K_{TVR}
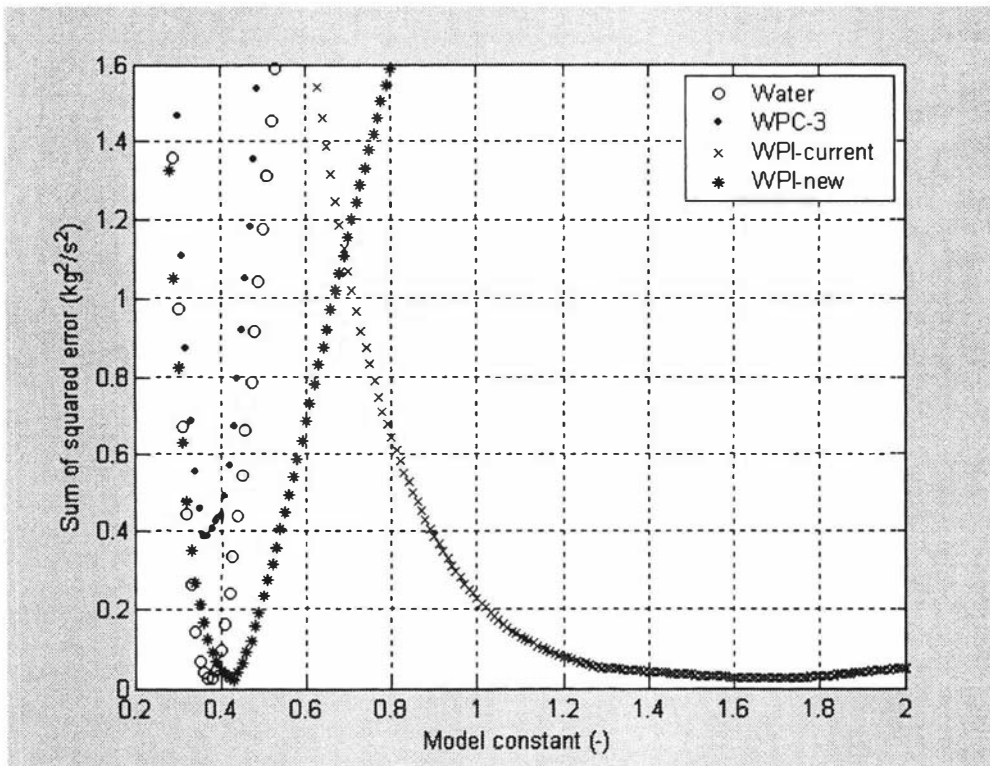
Figure 7.18: Optimum values of TVR vapour flow constant, K_{HTC}

To validate the TVR model, the model predictions were compared with historical data at different operating conditions for all products. Figure 7.19 shows the mass of recycled vapour plotted against the TVR discharge pressure for ranges of motive steam pressure and effect temperature for which the model was validated.
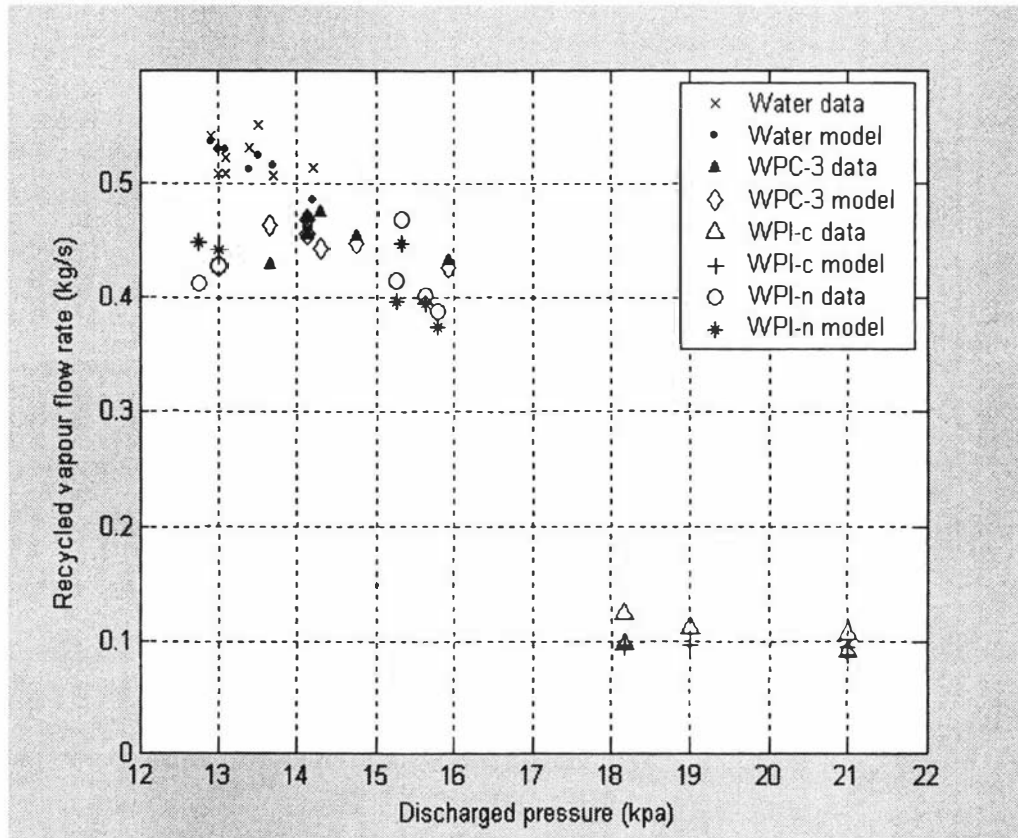
Figure 7.19: TVR model predictions against the plant data

The model predictions match the plant data with reasonable accuracy (less than 10% error). The mass of recycled vapour flow varies with the discharge pressure and the motive steam pressure. These results agree with the TVR theory presented in the literature (Hansen, 1985).

7.5 Conclusions

The preheat condenser heat transfer coefficients were strongly influenced by product viscosity. The viscosities of water, WPI and WPC-3 are significantly different and had a greater influence on the condenser heat transfer coefficients than on the product flow rate. A regression equation was developed for the preheat condenser to relate the product viscosities to the condenser heat transfer coefficients. The regression model predictions were tested for other whey products and for milk products. The heat transfer coefficient predictions were very close (difference is less than 5%) to values reported in the literature for water and milk products.

The surface loss heat transfer coefficient was identified from historical data. The value obtained was higher (10 $Wm^{-2}K^{-1}$) than values from theoretical models ($2-4$ $Wm^{-2}K^{-1}$). The heat transfer coefficient reported in the literature (12 $Wm^{-2}K^{-1}$) agreed with the value identified in this work.

The falling film heat transfer coefficients were identified using the constant property model. It was difficult to relate the heat transfer coefficients to any of the parameters in the evaporator. The resistance to evaporation was proportional to the product viscosity and therefore to the total solids concentration. There was a linear relationship between heat transfer coefficient and total solids for low viscosity products (water and WPI), but a non-linear relationship was observed for high viscosity products (WPC-3). The fouling coefficient in the variable property model was identified and the behaviour of the falling film is well explained by the falling film sub-model. The falling film model was tested with WPC-1 and the total solids predictions were made with less than 0.5% (w/w) error.

The residence time of the falling-film affects the linear dynamic model predictions. The total residence time was estimated from historical data and from physical observations in the plant. Knowing the pipe and preheat condenser dimensions, the total falling-film residence time was estimated. A laboratory scale experiment was conducted with water and whole milk to measure the residence time. The experimental residence times were

compared with the falling-film model predictions. Average residence time of 35 s was observed in the plant and between 30 and 70 s with the model predictions. Since the wavy model predicts the residence time for water well, it was assumed that this model was also applicable for whey products. A residence time of 50 s was used in the literature for the evaporator of 16 m long tubes (Winchester, 2000). This residence time was used in the whey evaporator control studies but no plant experimental work was done to compare the results.

8. Linear Dynamic Models

This section first introduces the linearisation and delay term approximation process. Then the non-linear models of the evaporator are linearised and a complete linear dynamic model is developed for the whey evaporator. Finally, the Padé approximations of the delay terms in the evaporator models are derived.

8.1 Linearisation

The approximation of non-linear models to linear ones is widely used in the study of process dynamics and design of control systems for the following reasons:

- Analytical solutions exist for linear systems and thus a complete and general picture of a process's behaviour can be gained independently of the particular values of the parameters and input variables.
- The complexity, maintenance difficulties and the high cost associated with non-linear control systems.

A linear system should satisfy the principle of superposition and the property of homogeneity. To satisfy both of these requirements, non-linear models are linearised around the operating conditions. The variables used are deviation variables from the steady state operating values. A Taylor series expansion (e.g. Skogestad and Postlewaite, 1996) is used to linearise the non-linear equations and the Padé approximation is used to approximate the pure delay terms.

The linear approximation of the non-linear equation, $\dfrac{dx}{dt} = f(x,u)$, using the Taylor series expansion is given by, $\dfrac{dx}{dt} = \dfrac{\partial f}{\partial x}\bigg|_0 \Delta x + \dfrac{\partial f}{\partial u}\bigg|_0 \Delta u$ where, $\Delta x, \Delta u$ are the deviation variables from the operating conditions $\left(x^0, u^0\right)$ and are given by $\Delta x = \left(x - x^0\right)$,

$\Delta u = \left(u - u^0\right)$. The nth order Pade approximation to the Laplace transform of the pure

dead time, t_d, is $\dfrac{\left(1 - \dfrac{t_d}{2n} s\right)^n}{\left(1 + \dfrac{t_d}{2n} s\right)^n}$. All the variables in the linear equations are the deviation

variables.

8.2 Development of linear dynamic models

The non-linear dynamic models for the evaporator set in Fonterra, Whareroa's Whey Products were developed in Chapter 6. The evaporator is a two-effect three-pass falling film evaporator. The evaporator non-linear models were linearised using the Taylor series to derive the linear dynamic models. The models were developed for each sub-system (TVR compressor, distribution plate, evaporation system, condensers and the transport system) separately and finally combined to form the complete linear dynamic model for the evaporator set. The variables used in this section are the same as those defined in Chapter 6 unless otherwise defined within this section. A superscript of the symbol 'o' is used to denote the values of variables at the steady state operating condition.

8.2.1 TVR compressor

The TVR compressor equations (8.1) and (8.2) were developed from equations (6.32) to (6.35) in Chapter 6.

$$W_{comp}(t) = (H_{steam} - Cp_w \cdot T_s(t)) \times K_{TVR} \times d^2 \times P_{steam}^{0.96}(t) \tag{8.1}$$

$$Q_{comp}(t) = \left(\frac{K_{TVR} \cdot d^2}{K_{HTC}}\right) \times \frac{P_{steam}^{0.96}(t)}{\exp\left(4.6 \frac{\ln\left(\frac{P_s(t)}{P_{e1}(t)}\right)}{\ln\left(\frac{P_{steam}(t)}{P_{e1}(t)}\right)}\right)} \times [H_{steam} - Cp_w(T_s(t) - T_{e1}(t))] \tag{8.2}$$

130

Equation (8.1) is non-linear with respect to P_{steam} and T_s. These terms were linearised to produce equation (8.3).

$$W_{comp}(t) = \alpha_1 \cdot P_{steam}(t) + \alpha_2 \cdot T_s(t) \tag{8.3}$$

Where,

$$\alpha_1 = 0.96 \times K_{TVR} \times d^2 \times \left(H_{steam} - Cp_w \cdot T_s^0\right) \text{ and}$$

$$\alpha_2 = -K_{TVR} \times d^2 \times Cp_w \times P_{steam}^{0.96\,0}$$

The relationship between saturation pressure and temperature shown in equation 8.4 (Winchester, 2000) was substituted for the pressure terms in equation (8.2) to produce a non-linear equation with respect to P_{steam}, T_s and T_{e1}. This non-linear equation was then linearised to produce equation (8.5).

$$\ln(P_{sat}) = A_w - \frac{B_w}{T_{sat} + 273.15 - C_w} \tag{8.4}$$

$$Q_{comp}(t) = \beta_1 \cdot P_{steam}(t) + \beta_2 \cdot T_s(t) + \beta_3 \cdot T_{e1}(t) \tag{8.5}$$

Where,

P_{sat} - Saturated pressure (Pa)

T_{sat} - Saturated temperature ($^\circ$C)

A_w - Constant (10.59)

B_w - Constant (3680.11 $^\circ$K)

C_w - Constant (41.69 $^\circ$K)

$$\beta_1 = K_0 K_1 \cdot \left[0.96 + \frac{4.6 \times B_w \left(T_s^0 - T_{e1}^0\right)\left(T_{e1}^0 + 273.15 - C_w\right)}{\left(T_s^0 + 273.15 - C_w\right)\left[\left(T_{e1}^0 + 273.15 - C_w\right)\ln\left(P_{steam}^0\right) - A_w\left(T_{e1}^0 + 273.15 - C_w\right) + B_w\right]} \right]$$

$$K_0 = \left(\frac{K_{TVR} \times d^2}{K_{HTC}} \right) \left[H_{steam} - Cp_w \left(T_s^0 - T_{e1}^0 \right) \right] \cdot \left(P_{steam}^{-0.04} \right)^0$$

$$K_1 = \exp \left[\frac{-4.6 \cdot B_w \left(T_s^0 - T_{e1}^0 \right)}{\left(T_s^0 + 276.15 - C_w \right) \cdot \left[\left(T_{e1}^0 + 273.15 - C_w \right) \cdot \ln \left(P_{steam}^0 \right) - A_w \cdot \left(T_{e1}^0 + 273.15 - C_w \right) + B_w \right]} \right]$$

$$\beta_2 = K_1 K_2 \cdot \left[-CP_w - \left(\frac{\left[H_{steam} - Cp_w \left(T_s^0 - T_{e1}^0 \right) \right] 4.6 \times B_w \left[\left(T_s^\circ + 273.15 - C_w \right) - \left(T_s^0 - T_{e1}^0 \right) \right]}{\left[\left(T_{e1}^0 + 273.15 - C_w \right) \ln \left(P_{steam}^0 \right) - A_w \left(T_{e1}^\bullet + 273.15 - C_w \right) + B_w \right] \left(T_s^0 + 273.15 - C_w \right)^2} \right) \right]$$

$$K_2 = \left(\frac{K_{TVR} \times d^2}{K_{HTC}} \right) \left(P_{steam}^{0.96} \right)^0$$

$$\beta_3 = K_1 K_2 \left\{ CP_w + \left[H_{steam} - Cp_w \left(T_s^0 - T_{e1}^0 \right) \right] \left[\frac{4.6 \times B_w \times K_3}{\left(T_s^0 + 273.15 - C_w \right)} \right] \right\}$$

$$K_3 = \left[\frac{\left(T_s^0 - T_{e1}^0 \right) \left(\ln P_{steam}^0 - A_w \right) + \left[\left(T_{e1}^0 + 273.15 - C_w \right) \ln P_{steam}^0 - A_w \left(T_{e1}^0 + 273.15 - C_w \right) + B_w \right]}{\left[\left(T_{e1}^0 + 273.15 - C_w \right) \ln P_{steam}^0 - A_w \left(T_{e1}^0 + 273.15 - C_w \right) + B_w \right]^2} \right]$$

8.2.2 Distribution plates

The whey evaporator has two passes in the 1st effect and one pass in the second effect. Each distribution plate was considered separately, yielding three linear models. The general differential equations (6.4) and (6.5) for the distribution plate dynamics with flash were derived in Chapter 6 and are shown in (8.6) and (8.7).

$$\frac{d(h_d(t))}{dt} = \left(\frac{1}{A_d} \right) \left(\frac{M_f(t)}{\rho_f} - \frac{M_{flash}(t)}{\rho_{water}} - \frac{M_d(t)}{\rho_d} \right) \tag{8.6}$$

$$\frac{d(w_d(t))}{dt} = \left(\frac{1}{h_d(t) A_d \rho_d} \right) \left\{ M_f(t) \cdot \left[w_f(t) - w_d(t) \right] + M_{flash}(t) \cdot w_d(t) \right\} \tag{8.7}$$

First distribution plate

There is significant flash on the first distribution plate. Equation (8.6) and (8.7) were modified for the first distribution plate as shown in (8.8) and (8.9).

$$\frac{dh_{d1}(t)}{dt} = \frac{1}{A_{d1}\rho_{d1}}\left(M_f\left(t-\tau_{fd}\right)-M_{flash1}(t)-M_{d1}(t)\right) \tag{8.8}$$

$$\frac{d\left(h_{d1}(t)w_{d1}(t)\right)}{dt} = \frac{1}{A_{d1}\rho_{d1}}\left(M_f\left(t-\tau_{fd}\right)w_f\left(t-\tau_{fd}\right)-M_{d1}(t)w_{d1}(t)\right) \tag{8.9}$$

Where,

$$M_{d1}(t) = C_d A_{h1}\rho_{d1}\sqrt{2g\left(h_{d1}+t_p\right)(t)}$$

$$M_{flash1}(t) = \frac{M_f\left(t-\tau_{fd}\right)Cp_f\left(T_{phc3}(t)-T_{e1}(t)\right)}{\lambda_1}$$

The terms for mass of flash (M_{flash}) and mass flow through the plate (M_{d1}) in equation (8.8) are non-linear. These terms were linearised with respect to M_f, T_{phc3}, T_{e1} and h_{d1} to give equation (8.10). Equation (8.9) is non-linear and was linearised with respect to $M_f, w_{d1}, T_{phc3}, T_{e1}$ and w_f to give equation (8.11).

$$\frac{dh_{d1}(t)}{dt} = \left(\frac{1}{A_{d1}\rho_{d1}}\right)\left[\frac{\lambda_1 - Cp_f\left(T_{phc3}^o - T_{e1}^o\right)}{\lambda_1}\right]\cdot M_f\left(t-\tau_{fd}\right)-\left(\frac{Cp_f\cdot M_f^o}{\lambda_1 A_{d1}\rho_{d1}}\right)\cdot T_{phc3}(t)$$

$$+\left(\frac{Cp_f\cdot M_f^o}{\lambda_1 A_{d1}\rho_{d1}}\right)\cdot T_{e1}(t)-\left(\frac{1}{\tau_{hd1}}\right)\cdot h_{d1}(t) \tag{8.10}$$

$$\frac{dw_{d1}(t)}{dt} = \left[\frac{w_f^o - w_{d1}^o + \frac{Cp_f w_{d1}^o \left(T_{phc3}^o - T_{e1}^o\right)}{\lambda_1}}{M_f^o \cdot \tau_{wd1}} \right] \cdot M_f \left(t - \tau_{fd}\right) - \left[\frac{1 - \frac{Cp_f \left(T_{phc3}^o - T_{e1}^o\right)}{\lambda_1}}{\tau_{wd1}} \right] \cdot w_{d1}(t)$$

$$+ \left(\frac{Cp_f w_{d1}^o}{\lambda_1 \cdot \tau_{wd1}}\right) \cdot T_{phc3}(t) - \left(\frac{Cp_f w_{d1}^o}{\lambda_1 \cdot \tau_{wd1}}\right) \cdot T_{e1}(t) + \left(\frac{1}{\tau_{wd1}}\right) \cdot w_f \left(t - \tau_{fd}\right) \qquad (8.11)$$

Where,

$$\tau_{hd1} = \frac{M_{d1}^0 \cdot A_{d1}}{\left(C_d \cdot A_{h1}\right)^2 \cdot g \cdot \rho_{d1}} \quad \text{And} \quad \tau_{wd1} = \frac{M_f^0 \cdot A_{d1}}{\left(C_d \cdot A_{h1}\right)^2 \cdot 2g \cdot \rho_{d1}}$$

τ_{fd} - Delay time between the feed and the 1st distribution plate (s)

h_{d1} - Liquid height above the distribution plate in the 1st pass (m)

w_{d1} - Total solids concentration of the product on the 1st distribution plate (w/w)

T_{phc3} - Temperature of the product entering the 1st distribution plate (^{o}C)

λ_1 - Latent heat of vaporisation in the 1st effect (J kg^{-1} K^{-1})

M_{d1} - Mass flow rate of product through the 1st distribution plate (kg s^{-1})

Second distribution plate

There is no flash on the 2nd distribution plate and therefore no term for flash in the dynamic equations. The dynamic equations were modified for the 2nd distribution plate as shown in (8.12) and (8.13).

$$\frac{dh_{d2}(t)}{dt} = \frac{1}{A_{d2}\rho_{d1}} \left(M_{p1}\left(t - \tau_{p1p2}\right) - M_{d2}(t)\right) \qquad (8.12)$$

$$\frac{d\left(h_{d2}(t)w_{d2}(t)\right)}{dt} = \frac{1}{A_{d2}\rho_{d2}} \left(M_{p1}\left(t - \tau_{p1p2}\right)w_{p1}\left(t - \tau_{p1p2}\right) - M_{d2}(t)w_{d2}(t)\right) \qquad (8.13)$$

Equation (8.12) is already linear with respect to M_{p1}, M_{d2} and this linear equation is given in (8.14). Equation (8.13) is non-linear and was linearised with respect to w_{p1} and w_{d2} to give equation (8.15).

$$\frac{dh_{d2}(t)}{dt} = \left(\frac{1}{A_{d2}\rho_{d1}}\right) \cdot M_{p1}\left(t - \tau_{p1p2}\right) - \left(\frac{1}{A_{d2}\rho_{d1}}\right) \cdot M_{d2}(t) \tag{8.14}$$

$$\frac{dw_{d2}(t)}{dt} = \left(\frac{1}{\tau_{wd2}}\right)w_{p1}\left(t - \tau_{p1p2}\right) - \left(\frac{1}{\tau_{wd2}}\right)w_{d2}(t) \tag{8.15}$$

Where,

$$\tau_{wd2} = \frac{M_{p1}^0 \cdot A_{d2}}{\left(C_d \cdot A_{h2}\right)^2 \cdot 2g \cdot \rho_{d2}}$$

τ_{p1p2} -Delay between the 1st pass and the 2nd distribution plate (s)

w_{d2} - Total solids concentration of the product on the 2nd distribution plate (w/w)

M_{d2} - Mass flow rate of product through the 2nd distribution plate (kg s^{-1})

h_{d2} - Liquid height above the distribution plate in the 2nd pass (m)

Third distribution plate

There is significant flash on the third distribution plate. The dynamic equations for the third distribution plate are shown in (8.16) and (8.17).

$$\frac{dh_{d3}(t)}{dt} = \frac{1}{A_{d3}\rho_{d3}}\left(M_{p2}\left(t - \tau_{p2p3}\right) - M_{flash2}(t) - M_{d3}(t)\right) \tag{8.16}$$

$$\frac{d(h_{d3}(t)w_{d3}(t))}{dt} = \frac{1}{A_{d3}\rho_{d3}}\left(M_{p2}\left(t - \tau_{p2p3}\right)w_{p2}\left(t - \tau_{p2p3}\right) - M_{d3}(t)w_{d3}(t)\right) \tag{8.17}$$

Where,

$$M_{flash2}(t) = \frac{M_{p2}(t - \tau_{p2p3})Cp_{p3}(T_{e1}(t) - T_{e2}(t))}{\lambda_2}$$

The terms for mass of flash (M_{flash}) in equation (8.16) is non-linear though the other terms are linear with respect to M_{p2} and M_{d3}. The non-linear term was linearised with respect to M_{p2}, T_{e2} and T_{e1} to give equation (8.18). Equation (8.17) is non-linear and was linearised with respect to $M_{p2}, w_{d3}, T_{e2}, T_{e1}$ and w_{p2} to give equation (8.19).

$$\frac{dh_{d3}(t)}{dt} = \left(\frac{1}{A_{d3}\rho_{d3}}\right)\left[\frac{\lambda_2 - Cp_{p3}(T_{e1}^o - T_{e2}^o)}{\lambda_2}\right] \cdot M_{p2}(t - \tau_{p2p3}) - \left(\frac{Cp_{p3} \cdot M_{p2}^o}{\lambda_2 A_{d3}\rho_{d3}}\right) \cdot T_{e1}(t)$$

$$+ \left(\frac{Cp_{p3} \cdot M_{p2}^o}{\lambda_2 A_{d3}\rho_{d3}}\right) \cdot T_{e2}(t) - \left(\frac{1}{\tau_{hd3}}\right) \cdot h_{d3}(t) \qquad (8.18)$$

$$\frac{dw_{d3}(t)}{dt} = \left[\frac{w_{p2}^o - w_{d3}^o + \dfrac{Cp_{p3}w_{d3}^o(T_{e1}^o - T_{e2}^o)}{\lambda_2}}{M_{p2}^o \cdot \tau_{wd3}}\right] \cdot M_{p2}(t - \tau_{p2p3}) - \left[\frac{1 - \dfrac{Cp_{p3}(T_{e1}^o - T_{e2}^o)}{\lambda_2}}{\tau_{wd3}}\right] \cdot w_{d3}(t)$$

$$+ \left(\frac{Cp_{p3}w_{d3}^o}{\lambda_2 \cdot \tau_{wd3}}\right) \cdot T_{e1}(t) - \left(\frac{Cp_{p3}w_{d3}^o}{\lambda_2 \cdot \tau_{wd3}}\right) \cdot T_{e2}(t) + \left(\frac{1}{\tau_{wd3}}\right) \cdot w_{p2}(t - \tau_{p2p3}) \qquad (8.19)$$

Where, $\tau_{hd3} = \dfrac{M_{d3}^0 \cdot A_{d3}}{(C_d \cdot A_{h3})^2 \cdot g \cdot \rho_{d3}}$ And $\tau_{wd3} = \dfrac{M_{p2}^0 \cdot A_{d3}}{(C_d \cdot A_{h3})^2 \cdot 2g \cdot \rho_{d3}}$

τ_{p2p3} - Delay between 2nd pass and the 3rd distribution plate (s)

h_{d3} - Liquid height above the distribution plate in the 3rd pass (m)

w_{d3} - Total solids concentration of the product on the 3rd distribution plate (w/w)

λ_2 - Latent heat of vaporisation in the 2nd effect (J kg^{-1} K^{-1})

M_{d3} - Mass flow rate of product through the 3rd distribution plate (kg s^{-1})

8.2.3 Evaporation system

The evaporation sub-system consists of three different sections as discussed in Chapter 6. These are the shell, the effect and the falling film. Each section was linearised separately. The delay approximations are discussed in section 8.4.

Evaporator shell

The differential equation for the shell temperature was derived in Chapter 6 (equation 6.28) and is shown here as equation (8.20).

$$K_s \cdot \frac{dT_s}{dt} = q_{comp} + W_{comp} - q_{shell-el} - q_{phc3} - q_{loss-s} \tag{8.20}$$

The heat flow through the tubes in the 1st effect is given by equation (8.22), assuming constant heat transfer coefficients. The heat losses from the surface are given by equation (8.21).

$$q_{loss-s} = U_{ls} \cdot A_{ls} \cdot (T_s(t) - T_a(t)) \tag{8.21}$$

$$Q_{shellel}(t) = (U_1 A_{s1} + U_2 A_{s2}) \cdot (T_s(t) - T_{el}(t)) \tag{8.22}$$

In equation (8.20), terms q_{comp} and W_{comp} are non-linear while all other terms are linear. The terms W_{comp} and q_{comp} have already been linearised and are shown in equations (8.3) and (8.5). Equations (8.5), (8.3), (8.21) and (8.22) were substituted into equation (8.20) to produce a linear equation (8.23) for shell temperature.

$$\frac{dT_s(t)}{dt} = \left(\frac{1}{\tau_{TS}}\right) T_s(t) + a_1 P_{steam}(t) + a_2 T_{el}(t) + a_3 q_{phc3}(t) + a_4 T_a(t) \tag{8.23}$$

Where,

$$\tau_{TS} = \frac{K_s}{[\beta_2 + \alpha_2 - (U_1 A_{s1} + U_2 A_{s2}) - U_{ls} \cdot A_{ls}]}, \qquad a_1 = \frac{\beta_1 + \alpha_1}{K_s},$$

137

$$a_2 = \frac{(\beta_3 + U_1 A_{s1} + U_2 A_{s2})}{K_s}, \qquad a_3 = \left(\frac{-1}{K_s}\right), \qquad a_4 = \left(\frac{U_{ls} \cdot A_{ls}}{K_s}\right)$$

τ_{TS} -Time constant of the shell temperature (s)

U_1 -Overall heat transfer coefficient in the 1st pass (W m^{-2} K^{-1})

U_2 -Overall heat transfer coefficient in the 2nd pass (W m^{-2} K^{-1})

A_{s1} -Surface area for evaporation in the 1st pass (m^2)

A_{s2} -Surface area for evaporation in the 2nd pass (m^2)

1st evaporator effect

The differential equation for the 1st effect temperature was derived in Chapter 6 (equation 6.22) and shown here as equation (8.24).

$$K_{e1} \cdot \frac{dT_{e1}}{dt} = q_{feed1} + q_{shell-e1} - q_{comp} - q_{shell-e2} - q_{phc2} - q_{loss-e1} \qquad (8.24)$$

The heat flow through the tubes in the 2nd effect is given by equation (8.25), assuming a constant heat transfer coefficient. The heat losses from the surface and the heat flow with the feed are given by equations (8.26) and (8.27).

$$Q_{shelle2}(t) = U_3 A_{s3} \cdot (T_{e1}(t) - T_{e2}(t)) \qquad (8.25)$$

$$q_{loss-e1} = U_{le1} \cdot A_{le1} \cdot (T_{e1}(t) - T_a(t)) \qquad (8.26)$$

$$q_{feed1} = M_f(t) \cdot Cp_f \cdot w_f(t)(T_{phc3}(t) - T_{e1}(t)) \qquad (8.27)$$

Equations (8.5), (8.22), (8.25), (8.26) and (8.27) were substituted into equation (8.24) to produce linear equation (8.28).

$$\frac{dT_{e1}(t)}{dt} = \left(\frac{-1}{\tau_{Te1}}\right)T_{e1}(t) + b_1 M_f\left(t - \tau_{fd}\right) + b_2 T_s(t) + b_3 P_{steam}(t) + b_4 T_{phc3}(t)$$

$$+ b_5 q_{phc2}(t) + b_6 T_{e2}(t) + b_7 T_a(t) \tag{8.28}$$

Where,

$$\tau_{Te1} = \frac{K_{e1}}{\left(Cp_f M_f^0 + (U_1 A_{s1} + U_2 A_{s2} + U_3 A_{s3}) + \beta_3 + U_{le1} \cdot A_{le1}\right)}, \quad b_1 = \frac{Cp_f\left(T_{phc3}^0 - T_{e1}^0\right)}{K_{e1}},$$

$$b_2 = \frac{(U_1 A_{s1} + U_2 A_{s2} - \beta_2)}{K_{e1}}, \qquad b_3 = \left(\frac{-\beta_1}{K_{e1}}\right), \qquad b_4 = \frac{Cp_f \cdot M_f^0}{K_{e1}}, \qquad b_5 = \left(\frac{-1}{K_{e1}}\right),$$

$$b_6 = \frac{U_3 A_{s3}}{K_{e1}}, \qquad\qquad b_7 = \frac{U_{le1} \cdot A_{le1}}{K_{e1}}$$

τ_{Te1} -Time constant for 1st effect temperature (s)

U_3 -Overall heat transfer coefficient in the 3rd pass (W m^{-2} K^{-1})

A_{s3} -Surface area for heat transfer in the 3rd pass (m^2)

2nd evaporator effect

The differential equation for the 2nd effect temperature was derived in Chapter 6 (equation 6.25) and shown here as equation (8.29).

$$K_{e2} \cdot \frac{dT_{e2}}{dt} = q_{feed2} + q_{shell-e2} - q_{vacc} - q_{phc1} - q_{loss-e2} \tag{8.29}$$

The heat losses from the surface and the heat flows in with the feed are given by equations (8.30) and (8.31).

$$q_{loss-e2} = U_{le2} \cdot A_{le2} \cdot (T_{e2}(t) - T_a(t)) \tag{8.30}$$

$$q_{feed2} = M_{p2}(t) \cdot Cp_{p2} \cdot w_{p2}(t)(T_{e1}(t) - T_{e2}(t)) \tag{8.31}$$

Equations (8.31), (8.30) and (8.25) were substituted into equation (8.29) to produce the linear equation (8.32) for the 2nd effect temperature.

$$\frac{dT_{e2}(t)}{dt} = \left(\frac{-1}{\tau_{Te2}}\right)T_{e2}(t) + c_1 M_{p2}(t - \tau_{p2p3}) + c_2 T_{e1}(t) + c_3 q_{vc}(t)$$

$$+ c_4 q_{phc1}(t) + c_5 T_a(t) \tag{8.32}$$

Where,

$$\tau_{Te2} = \frac{K_{e2}}{\left(Cp_{p2}M_{p2}^0 + U_3 A_{s3} + U_{le2} \cdot A_{le2}\right)}, \qquad c_1 = \frac{Cp_{p2}\left(T_{e1}^0 - T_{e2}^0\right)}{K_{e2}},$$

$$c_2 = \frac{\left(Cp_{p2} \cdot M_{p2}^0 + U_3 A_{s3}\right)}{K_{e2}}, \quad c_3 = \left(\frac{-1}{K_{e2}}\right), \quad c_4 = \left(\frac{-1}{K_{e2}}\right), \quad c_5 = \frac{U_{le2} \cdot A_{le2}}{K_{e2}}$$

τ_{Te2} -Time constant for the 2nd effect temperature (s)

8.2.4 Preheat and vacuum condensers

The condenser dynamic models derived in Chapter 6 are shown here as equations (8.34) to (8.37).

$$T_{out}(t) = T_{dum}(t) + e^{\frac{\tau_{RT}}{\tau_{TC}}} T_{in}(t - \tau_{RT}) - \frac{\tau_{RT}\left(T_{sh}^0 - T_{in}^0\right)e^{\frac{\tau_{RT}}{\tau_{TC}}}}{M_{cond}^0 \tau_{TC}} M_{dum}(t) \tag{8.34}$$

$$\tau_{TC}\frac{dT_{dum}(t)}{dt} = -T_{dum}(t) + T_{sh}(t) - e^{\frac{\tau_{RT}}{\tau_{TC}}} T_{sh}(t - \tau_{RT}) \tag{8.35}$$

$$\tau_{RT}\frac{dM_{dum}(t)}{dt} = M_{cond}(t) - M_{cond}(t - \tau_{RT}) \tag{8.36}$$

$$\frac{dq_{cond}}{dt} = UA\frac{dT_{sh}}{dt} - \frac{1}{\tau_{TC}}q_{cond} + \frac{UA}{\tau_{RT}}\left[T_{out} - T_{in}\right] \tag{8.37}$$

The temperature equation (8.34) is non-linear. A linear model was derived by Winchester (2000) and simplified as shown in equation (8.38). The inverse Laplace Transform of equation (8.38) was taken and simplified to produce the linear equation (8.39) for temperature in the time domain.

$$(\tau_{TCO}s+1) \cdot T_{out}(s) = T_{sh}(s) - e^{\frac{-\tau_{RT}}{\tau_{TCO}}} \cdot e^{-\tau_{RT}s} \cdot T_{sh}(s) + (\tau_{TCO}s+1) \cdot e^{\frac{-\tau_{RT}}{\tau_{TCO}}} \cdot e^{-\tau_{RT}s} \cdot T_{in}(s)$$

$$- (\tau_{TCO}s+1) \left[\frac{(T_{sh}^o - T_{in}^o) \cdot e^{\frac{-\tau_{RT}}{\tau_{TCO}}}}{\tau_{TCO} \cdot M_{cond}^o} \right] \left[\frac{1 - e^{-\tau_{RT}s}}{s} \right] M_{cond}(s) \tag{8.38}$$

$$\tau_{TC} \cdot \frac{dT_{out}(t)}{dt} = -T_{out}(t) + T_{sh}(t) - e^{\frac{-\tau_{RT}}{\tau_{TC}}} \cdot T_{sh}(t-\tau_{RT}) + e^{\frac{-\tau_{RT}}{\tau_{TC}}} \cdot T_{in}(t-\tau_{RT})$$

$$- \left[\frac{(T_{sh}^o - T_{in}^o) \cdot e^{\frac{-\tau_{RT}}{\tau_{TC}}}}{\cdot M_{cond}^o} \right] M_{cond}(t) \tag{8.39}$$

Equation (8.37) for the condenser heat flow is already linear with the equation for shell temperature linearised (equation 8.23). There are three preheat condensers and a vacuum condenser in the whey evaporator set. Linear models for each condenser were derived separately as they are located at different places in the whey evaporator set.

1st preheat condenser (HX1503)

This preheat condenser is attached to the second effect of the evaporator. The linear equation for the temperature exiting the condenser is shown in equation (8.40).

$$\tau_{TPC1}\frac{dT_{phc1}(t)}{dt} = -T_{ph}(t) + T_{e2}(t) - e^{\left(\frac{-\tau_{PC1}}{\tau_{TPC1}}\right)}T_{e2}(t - \tau_{PC1}) + e^{\left(\frac{-\tau_{PC1}}{\tau_{TPC1}}\right)}T_f(t - \tau_{PC1})$$

$$-\left[\frac{\left(T_{e2}^o - T_f^o\right) \cdot e^{\left(\frac{-\tau_{PC1}}{\tau_{TPC1}}\right)}}{M_f^o}\right]M_f(t) \qquad (8.40)$$

Where,

$$\tau_{PC1} = \frac{V_{phc1} \cdot \rho_{phc1}}{M_f}, \quad \tau_{TPC1} = \frac{\rho_{phc1} \cdot Cp_{phc1} \cdot V_{phc1}}{U_{phc1} A_{phc1}}$$

The heat flow in the first condenser is given by equation (8.41).

$$\frac{dq_{phc1}(t)}{dt} = U_{phc1}A_{phc1}\frac{dT_{e2}}{dt} - \frac{q_{phc1}(t)}{\tau_{TPC1}} + \frac{U_{phc1}A_{phc1}\left(T_{phc1}(t) - T_f(t - \tau_{PC1})\right)}{\tau_{PC1}} \qquad (8.41)$$

Equation (8.32) was substituted into equation (8.40) and the result rearranged to produce the linear equation (8.43) for the heat flow in the 1st condenser.

$$\frac{dq_{phc1}(t)}{dt} = U_{phc1}A_{phc1}\left[\frac{-T_{e2}(t)}{\tau_{Te2}} + c_1 M_{p2}(t - \tau_{p2p3}) + c_2 T_{e1}(t) + c_3 q_{vc}(t) + c_4 q_{phc1}(t) + c_5 T_a(t)\right]$$

$$- \frac{q_{phc1}(t)}{\tau_{TPC1}} + \frac{U_{phc1}A_{phc1}\left(T_{phc1}(t) - T_f(t - \tau_{PC1})\right)}{\tau_{PC1}} \qquad (8.42)$$

$$\frac{dq_{phc1}(t)}{dt} = \left(\frac{-U_{phc1}A_{phc1}}{\tau_{Te2}}\right) \cdot T_{e2}(t) + \left(U_{phc1}A_{phc1}c_1\right) \cdot M_{p2}\left(t - \tau_{p2p3}\right) + \left(U_{phc1}A_{phc1}c_2\right) \cdot T_{e1}(t)$$

$$+ \left(U_{phc1}A_{phc1}c_3\right) \cdot q_{vc}(t) + \left(U_{phc1}A_{phc1}c_4 - \frac{1}{\tau_{TPC1}}\right) \cdot q_{phc1}(t) + \left(\frac{U_{phc1}A_{phc1}}{\tau_{PC1}}\right) \cdot T_{phc1}(t)$$

$$+ \left(\frac{-U_{phc1}A_{phc1}}{\tau_{PC1}}\right) \cdot T_f\left(t - \tau_{PC1}\right) + \left(U_{phc1}A_{phc1}c_5\right) \cdot T_a(t) \tag{8.43}$$

T_{phc1} - Temperature of the product exiting the 1st preheat condenser (^{o}C)

q_{phc1} - Heat flow in the 1st condenser (J)

U_{phc1} - Overall heat transfer coefficient in the 1st condenser (W m^{-2} K^{-1})

A_{phc1} - Surface area of heat transfer in the 1st condenser (m^2)

V_{phc1} - Volume of the tubes in the 1st condenser (m^3)

2nd preheat condenser (HX 1502)

This preheat condenser is attached to the first effect of the evaporator. The linear equation for the temperature exiting the condenser is shown in equation (8.44).

$$\tau_{TPC2}\frac{dT_{phc2}(t)}{dt} = -T_{phc2}(t) + T_{e1}(t) - e^{\left(\frac{-\tau_{PC2}}{\tau_{TPC2}}\right)}T_{e1}\left(t - \tau_{PC2}\right) + e^{\left(\frac{-\tau_{PC2}}{\tau_{TPC2}}\right)}T_{phc1}\left(t - \tau_{PC2}\right)$$

$$- \left[\frac{\left(T_{e1}^{o} - T_{phc1}^{o}\right) \cdot e^{\left(\frac{-\tau_{PC2}}{\tau_{TPC2}}\right)}}{M_{phc1}^{o}}\right]M_{phc1}(t) \tag{8.44}$$

Where,

$$\tau_{PC2} = \frac{V_{phc2}\rho_{phc2}}{M_{phc1}}, \quad \tau_{TPC2} = \frac{Cp_{phc2}\rho_{phc2}V_{phc2}}{U_{phc2}A_{phc2}}$$

143

The heat flow through the 2nd condenser is given by equation (8.45).

$$\frac{dq_{phc2}(t)}{dt} = U_{phc2}A_{phc2} \cdot \frac{dT_{e1}(t)}{dt} - \frac{q_{phc2}(t)}{\tau_{TPC2}} + \frac{U_{phc2}A_{phc2}\left(T_{phc2}(t) - T_{phc1}(t - \tau_{PC2})\right)}{\tau_{PC2}} \qquad (8.45)$$

Equation (8.28) was substituted into equation (8.45) and the result rearranged to produce the linear equation (8.48) for the heat flow in the 2nd condenser.

$$\frac{dq_{phc2}(t)}{dt} = U_{phc2}A_{phc2}\left[\frac{-T_{e1}(t)}{\tau_{Te1}} + b_1 M_f\left(t - \tau_{fd}\right) + b_2 T_s(t) + b_3 P_{steam}(t) + b_4 T_{phc3}(t)\right]$$

$$+ U_{phc2}A_{phc2}\left[b_5 q_{phc2}(t) + b_6 T_{e2}(t) + b_7 T_a(t)\right] - \frac{q_{phc2}(t)}{\tau_{TPC2}}$$

$$+ \frac{U_{phc2}A_{phc2}\left(T_{phc2}(t) - T_{phc1}(t - \tau_{PC2})\right)}{\tau_{PC2}} \qquad (8.46)$$

$$\frac{dq_{ph2}(t)}{dt} = \left(\frac{-U_{ph2}A_{ph2}}{\tau_{Te1}}\right) \cdot T_{e1}(t) + \left(U_{ph2}A_{ph2}b_1\right) \cdot M_f\left(t - \tau_{fd}\right) + \left(U_{ph2}A_{ph2}b_2\right) \cdot T_s(t)$$

$$+ \left(U_{ph2}A_{ph2}b_3\right) \cdot P_{steam}(t) + \left(U_{ph2}A_{ph2}b_5 - \frac{1}{\tau_{TPC2}}\right) \cdot q_{ph2}(t)$$

$$+ \left(U_{ph2}A_{ph2}b_4\right) \cdot T_{ph3}(t) + \left(U_{ph2}A_{ph2}b_6\right) \cdot T_{e2}(t) + \left(\frac{U_{ph2}A_{ph2}}{\tau_{PC2}}\right) \cdot T_{ph2}(t)$$

$$+ \left(\frac{-U_{ph2}A_{ph2}}{\tau_{PC2}}\right) \cdot T_{ph1}\left(t - \tau_{PC2}\right) + \left(U_{ph2}A_{ph2}b_7\right) \cdot T_a(t) \qquad (8.47)$$

$T_{pl\ 2}$ - Temperature of the product exiting the 2nd preheat condenser (^oC)

q_{phc2} - Heat flow in the 2nd condenser (J)

U_{phc2} - Overall heat transfer coefficient in the 2nd condenser (W m$^-$2 K^{-1})

A_{phc2} - Surface area of heat transfer in the 2nd condenser (m^2)

V_{phc2} - Volume of the tubes in the 2nd condenser (m^3)

M_{phl} -Mass flow of product to second condenser (kg s^{-1})

3rd preheat condenser (HX1501)

The third preheat condenser is attached to the shell of the first effect in the evaporator. The linear equation for the temperature exiting the condenser is:

$$\tau_{TPC3}\frac{dT_{phc3}(t)}{dt} = -T_{phc3}(t) + T_s(t) - e^{\left(\frac{-\tau_{PC3}}{\tau_{TPC3}}\right)}T_s(t - \tau_{PC3}) + e^{\left(\frac{-\tau_{PC3}}{\tau_{TPC3}}\right)}T_{phc2}(t - \tau_{PC3})$$

$$- \left[\frac{(T_s^o - T_{phc2}^o) \cdot e^{\left(\frac{-\tau_{PC3}}{\tau_{TPC3}}\right)}}{M_{phc2}^o}\right]M_{phc2}(t) \qquad (8.48)$$

Where,

$$\tau_{PC3} = \frac{V_{phc3}\rho_{phc3}}{M_{phc2}} \quad , \quad \tau_{TPC3} = \frac{Cp_{phc3}\rho_{phc3}V_{phc3}}{U_{phc3}A_{phc3}}$$

The heat flow through the third condenser is given by equation (8.49).

$$\frac{dq_{phc3}(t)}{dt} = U_{phc3}A_{phc3} \cdot \frac{dT_s(t)}{dt} - \frac{q_{phc3}(t)}{\tau_{TPC3}} + \frac{U_{phc3}A_{phc3}(T_{ph3}(t) - T_{phc2}(t - \tau_{PC3}))}{\tau_{PC3}} \qquad (8.49)$$

Equation (8.23) was substituted into equation (8.49) and the result rearranged to produce the linear equation (8.51) for the heat flow in the 3rd condenser.

$$\frac{dq_{phc3}(t)}{dt} = U_{phc3}A_{ph3}\left[\frac{T_s(t)}{\tau_{TS}} + a_1 P_{steam}(t) + a_2 T_{e1}(t) + a_3 q_{phc3}(t) + a_4 T_a(t)\right] - \frac{q_{phc3}(t)}{\tau_{TPC3}}$$

$$+ \frac{U_{phc3}A_{phc3}(T_{phc3}(t) - T_{phc2}(t - \tau_{PC3}))}{\tau_{PC3}} \qquad (8.50)$$

$$\frac{dq_{ph3}(t)}{dt} = \left(\frac{U_{ph3}A_{ph3}}{\tau_{TS}}\right)\cdot T_s(t) + \left(U_{ph3}A_{ph3}a_1\right)\cdot P_{steam}(t) + \left(U_{ph3}A_{ph3}a_2\right)\cdot T_{e1}(t)$$

$$+\left(U_{ph3}A_{ph3}a_3 - \frac{1}{\tau_{TPC3}}\right)\cdot q_{ph3}(t) + \left(\frac{U_{ph3}A_{ph3}}{\tau_{PC3}}\right)\cdot T_{ph3}(t)$$

$$+\left(\frac{-U_{ph3}A_{ph3}}{\tau_{PC3}}\right)\cdot T_{ph2}\left(t - \tau_{PC3}\right) + \left(U_{ph3}A_{ph3}a_4\right)\cdot T_a(t) \tag{8.51}$$

T_{phc3} - Temperature of the product exiting the 3rd preheat condenser ($^{\circ}$C)

q_{phc3} - Heat flow in the 3rd condenser (J)

U_{phc3} - Overall heat transfer coefficient in the 3rd condenser (W m^{-2} K^{-1})

A_{phc3} - Surface area of heat transfer in the 3rd condenser (m^2)

V_{phc3} - Volume of the tubes in the 3rd condenser (m^3)

M_{ph2} -Mass flow of product to third condenser (kg s^{-1})

Vacuum condenser (HX1506)

The vacuum condenser is attached to the second effect in the evaporator. Equations (8.38) to (8.40) can be applied as given by equations (8.52) and (8.53).

$$(\tau_{Tvc}s+1)\cdot T_{cvout}(s) = T_{e2}(s) - e^{\frac{-\tau_{vc}}{\tau_{Tco}}}\cdot e^{-\tau_{wc}s}\cdot T_{e2}(s) + (\tau_{Tvc}s+1)\cdot e^{\frac{-\tau_{vc}}{\tau_{Tvc}}}\cdot e^{-\tau_{vc}s}\cdot T_{cwin}(s)$$

$$-(\tau_{Tvc}s+1)\left[\frac{\left(T_{cwout}^o - T_{cwin}^o\right)\cdot e^{\frac{-\tau_{vc}}{\tau_{Tvc}}}}{\tau_{Tvc}\cdot M_{cw}^o}\right]\left[\frac{1-e^{-\tau_{vc}s}}{s}\right]M_{cw}(s) \tag{8.52}$$

$$q_{vc}(s) = \frac{\rho_w Cp_w V_{vc}\cdot s}{[\tau_{Tvc}\cdot s+1]}T_{e2}(s) + \frac{Cp_w M_{cw}^0}{[\tau_{Tvc}\cdot s+1]}T_{out}(s) - \frac{Cp_w M_{cw}^0}{[\tau_{Tvc}\cdot s+1]}T_{in}(s)$$

$$+\frac{\left(T_{out}^0 - T_{in}^0\right)}{[\tau_{Tvc}\cdot s+1]}M_{cond}(s) \tag{8.53}$$

The heat flow in the vacuum condenser is shown in equation (8.54) in the time domain.

$$\frac{dq_{vc}(t)}{dt} = U_{vc}A_{vc}\frac{dT_{e2}}{dt} - \frac{q_{vc}(t)}{\tau_{Tvc}} + \frac{U_{vc}A_{vc}\left(T_{cwout}(t) - T_{cwin}(t - \tau_{vc})\right)}{\tau_{vc}}$$

(8.54)

Equation (8.32) was substituted into equation (8.54) and the result rearranged to produce linear equation (8.55) for the heat flow in the vacuum condenser.

$$\frac{dq_{vc}(t)}{dt} = \left(\frac{-U_{vc}A_{vc}}{\tau_{Te2}}\right) \cdot T_{e2}(t) + \left(U_{vc}A_{vc}c_1\right) \cdot M_{p2}\left(t - \tau_{p2p3}\right) + \left(U_{vc}A_{vc}c_2\right) \cdot T_{e1}(t)$$

$$+ \left(U_{vc}A_{vc}c_4\right) \cdot q_{phc1}(t) + \left(U_{vc}A_{vc}c_3 - \frac{1}{\tau_{Tvc}}\right) \cdot q_{vc}(t) + \left(\frac{U_{vc}A_{vc}}{\tau_{vc}}\right) \cdot T_{vc}(t)$$

$$+ \left(\frac{-U_{vc}A_{vc}}{\tau_{vc}}\right) \cdot T_f\left(t - \tau_{vc}\right) + \left(U_{vc}A_{vc}c_5\right) \cdot T_a(t)$$

(8.55)

T_{cwin} -Cooling water inlet temperature (°C)

T_{cwout} -Cooling water exit temperature (°C)

M_{cw} -Mass flow rate of cooling water (kg s^{-1})

q_{vc} -Heat flow in the vacuum condenser (W)

U_{vc} -Overall heat transfer coefficient of vacuum condenser (W m^{-2} K^{-1})

A_{vc} -Surface area of vacuum condenser for heat transfer (m^2)

8.2.5 Falling-film

The falling film models were derived in Chapter 6 and are shown in equations (8.56) to (8.58) with delays. There are three passes, two in the first effect and one in the second effect. The linear models for each pass were derived separately.

$$M_p(t) = M_d\left(t - \tau_d\right) - M_{tubes}(t)$$

(8.56)

$$w_p(t) = \frac{M_d(t - \tau_d).w_d(t - \tau_d)}{[M_d(t - \tau_d) - M_{tubes}(t)]} \tag{8.57}$$

$$\frac{\tau_e.\lambda}{U_s.A_s} \frac{dM_{tubes}(t)}{dt} = [T_s(t) - T_e(t) - T_s(t - \tau_e) + T_e(t - \tau_e)] \tag{8.58}$$

Pass-1

The falling film models for the first pass are shown in equations (8.59) to (8.61).

$$\frac{dM_{tubes1}}{dt} = \left(\frac{U_{s1}A_{s1}}{\tau_{p1}\lambda_1}\right)[(T_s(t) - T_{e1}(t)) - (T_s(t - \tau_{p1}) - T_{e1}(t - \tau_{p1}))] \tag{8.59}$$

$$M_{p1}(t) = M_{d1}(t - \tau_{p1}) - M_{tubes1}(t) \tag{8.60}$$

$$w_{p1}(t) = \frac{M_{d1}(t - \tau_{p1}).w_{d1}(t - \tau_{p1})}{[M_{d1}(t - \tau_{p1}) - M_{tubes1}(t)]} \tag{8.61}$$

Equations (8.59) and (8.60) are already linear but equation (8.61) is non-linear. This equation was linearised to produce the linear equation (8.62).

$$w_{p1}(t) = -k_1 M_{d1}(t - \tau_{p1}) + k_2 w_{d1}(t - \tau_{p1}) + k_3 M_{tubes1}(t) \tag{8.62}$$

Where,

$$K_1 = \frac{w_{d1}^0 \cdot M_{tubes1}^0}{\left(M_{d1}^0 - M_{tubes1}^0\right)^2}, \quad K_2 = \frac{M_{d1}^0}{\left(M_{d1}^0 - M_{tubes1}^0\right)}, \quad K_3 = \frac{M_{d1}^0 \cdot w_{d1}^o}{\left(M_{d1}^0 - M_{tubes1}^0\right)^2}$$

U_{s1} - Overall heat transfer coefficient in the 1st pass (W m^{-2} K^{-1})

A_{s1} - Surface area in the 1st pass (m^2)

τ_{p1} - Residence time in the 1st pass (s)

M_{tubes1} - Mass of evaporation in the 1st pass (kg s^{-1})

Pass-2

The falling film models for the second pass are shown in equations (8.63) to (8.65).

$$\frac{dM_{tubes2}}{dt} = \left(\frac{U_{s2}A_{s2}}{\tau_{p2}\lambda_1}\right)\left[(T_s(t) - T_{e1}(t)) - (T_s(t - \tau_{p2}) - T_{e1}(t - \tau_{p2}))\right] \tag{8.63}$$

$$M_{p2}(t) = M_{d2}(t - \tau_{p2}) - M_{tubes2}(t) \tag{8.64}$$

$$w_{p2}(t) = \frac{M_{d2}(t - \tau_{p2})w_{d2}(t - \tau_{p2})}{\left[M_{d2}(t - \tau_{p2}) - M_{tubes2}(t)\right]} \tag{8.65}$$

Equations (8.63) and (8.64) are already linear but equation (8.65) is non-linear. This equation was linearised to produce the linear equation (8.66).

$$w_{p2}(t) = -k_4 M_{d2}(t - \tau_{p2}) + k_5 w_{d2}(t - \tau_{p2}) + k_6 M_{tubes2}(t) \tag{8.66}$$

Where,

$$K_4 = \frac{w_{d2}^0 \cdot M_{tubes2}^0}{\left(M_{d2}^0 - M_{tubes2}^0\right)^2}, \quad K_5 = \frac{M_{d2}^0}{\left(M_{d2}^0 - M_{tubes2}^0\right)}, \quad K_6 = \frac{M_{d2}^0 \cdot w_{d2}^o}{\left(M_{d2}^0 - M_{tubes2}^0\right)^2}$$

U_{s2} - Overall heat transfer coefficient in the 2nd pass (W/ m^2. K)

A_{s2} - Surface area in the 2nd pass (m^2)

τ_{p2} - Residence time in the 2nd pass (s)

M_{tubes2} - Mass of evaporation in the 2nd pass (kg s^{-1})

Pass-3

The falling film models for the third pass are shown in equations (8.67 to 8.69).

$$\frac{dM_{tubes3}}{dt} = \left(\frac{U_{s3}A_{s3}}{\tau_{p3}\lambda_2}\right)\left[(T_{e1}(t) - T_{e2}(t)) - (T_{e1}(t - \tau_{p3}) - T_{e2}(t - \tau_{p3}))\right] \tag{8.67}$$

$$M_{p3}(t) = M_{d3}(t - \tau_{p3}) - M_{tubes3}(t) \tag{8.68}$$

$$w_{p3}(t) = \frac{M_{d3}(t - \tau_{p3})w_{d3}(t - \tau_{p3})}{[M_{d3}(t - \tau_{p3}) - M_{tubes3}(t)]} \tag{8.69}$$

Equations (8.67) and (8.68) are linear but equation (8.69) is non-linear. This equation was linearised to produce equation (8.70).

$$w_{p3}(t) = -k_7 M_{d3}(t - \tau_{p3}) + k_8 w_{d3}(t - \tau_{p3}) + k_9 M_{tubes3}(t) \tag{8.70}$$

Where,

$$K_7 = \frac{w_{d3}^0 \cdot M_{tubes3}^0}{\left(M_{d3}^0 - M_{tubes3}^0\right)^2} , \quad K_8 = \frac{M_{d3}^0}{\left(M_{d3}^0 - M_{tubes3}^0\right)}, \quad K_9 = \frac{M_{d3}^0 \cdot w_{d3}^o}{\left(M_{d3}^0 - M_{tubes3}^0\right)^2}$$

U_{s3} - Overall heat transfer coefficient in the 3rd pass (W m^{-2} K^{-1})

A_{s3} - Surface area in the 3rd pass (m^2)

τ_{p3} - Residence time in the 3rd pass (s)

M_{tubes3} - Mass of evaporation in the 3rd pass (kg s^{-1})

8.3 Complete linear evaporator model

The linear models developed for the 1st effect and the 2nd effect were combined with the falling film delay terms to form the complete linear model of the evaporator. The falling-film model (equation 8.58) has the delay term that cannot be approximated with 1st order Pade approximations and therefore needs to be considered separately. The delay approximation for the falling-film is discussed in section 8.4.

The first effect linear model excluding the falling film model is given by:

$$
\begin{bmatrix} h_{d1} \\ w_{d1} \\ T_s \\ T_{e1} \end{bmatrix} =
\begin{bmatrix}
\dfrac{-1}{\tau_{hd1}} & 0 & 0 & \left(\dfrac{Cp_f M_f^o}{\lambda_1 A_{d1}\rho_{d1}} \right) \\
0 & \dfrac{-\left(\lambda_1 - Cp_f\left(T_{phc3}^o - T_{e1}^o\right)\right)}{\tau_{wd1}\lambda_1} & 0 & \dfrac{-Cp_f w_{d1}^o}{\lambda_1 \tau_{wd1}} \\
0 & 0 & \dfrac{1}{\tau_{TS}} & a_2 \\
0 & 0 & b_2 & \dfrac{-1}{\tau_{Te1}}
\end{bmatrix}
\begin{bmatrix} h_{d1} \\ w_{d1} \\ T_s \\ T_{e1} \end{bmatrix} +
$$

$$
\begin{bmatrix}
\dfrac{1}{A_{d1}\rho_{d1}}\left[\dfrac{\lambda_1 - Cp_f\left(T_{phc3}^o - T_{e1}^o\right)}{\lambda_1}\right] & 0 & 0 & 0 & 0 & \left(\dfrac{-Cp_f M_f^o}{\lambda_1 A_{d1}\rho_{d1}}\right) & 0 & 0 \\
\dfrac{\lambda_1\left(w_f^o - w_{d1}^o\right)+Cp_f w_{d1}^o\left(T_{phc3}^o - T_{e1}^o\right)}{M_f^o \lambda_1 \tau_{wd1}} & \dfrac{1}{\tau_{wd1}} & 0 & 0 & 0 & \dfrac{Cp_f w_{d1}^o}{\lambda_1 \tau_{wd1}} & 0 & 0 \\
0 & 0 & a_1 & a_3 & a_4 & 0 & 0 & 0 \\
b_1 & 0 & b_3 & 0 & b_7 & b_4 & b_5 & b_6
\end{bmatrix}
\begin{bmatrix} M_f \\ w_f \\ P_{steam} \\ q_{phc3} \\ T_a \\ T_{phc3} \\ q_{phc2} \\ T_{e2} \end{bmatrix}
$$

The second effect linear model excluding the falling film model is given by:

$$
\begin{bmatrix} h_{d3} \\ w_{d3} \\ T_{e2} \end{bmatrix} = \begin{bmatrix} \dfrac{-1}{\tau_{hd3}} & 0 & \dfrac{Cp_{p2}M^{o}_{p2}}{\lambda_2 A_{d3}\rho_{d3}} \\ 0 & \dfrac{-\left(\lambda_2 - Cp_{p2}\left(T^{o}_{e1} - T^{o}_{e2}\right)\right)}{\lambda_2 \tau_{wd3}} & \dfrac{-Cp_{p2}w^{o}_{d3}}{\lambda_1 \tau_{wd3}} \\ 0 & 0 & \dfrac{-1}{\tau_{Te2}} \end{bmatrix} \begin{bmatrix} h_{d3} \\ w_{d3} \\ T_{e2} \end{bmatrix} +
$$

$$
\begin{bmatrix} \dfrac{1}{A_{d2}\rho_{d2}}\left[\dfrac{\lambda_2 - Cp_{p2}\left(T^{o}_{e1} - T^{o}_{e2}\right)}{\lambda_2}\right] & 0 & \dfrac{-Cp_{p2}M^{o}_{p2}}{\lambda_2 A_{d3}\rho_{d3}} & 0 & 0 & 0 \\ \dfrac{\lambda_2\left(w^{o}_{p2} - w^{o}_{d3}\right) + Cp_{p2}w^{o}_{d3}\left(T^{o}_{e1} - T^{o}_{e2}\right)}{M^{o}_{p2}\lambda_2\tau_{wd3}} & \dfrac{1}{\tau_{wd2}} & 0 & \dfrac{Cp_{p2}w^{o}_{d3}}{\lambda_1\tau_{wd3}} & 0 & 0 \\ c_1 & 0 & c_2 & c_3 & c_4 & c_5 \end{bmatrix} \begin{bmatrix} M_{p2} \\ w_{p2} \\ T_{e1} \\ q_{vc} \\ q_{phcl} \\ T_a \end{bmatrix}
$$

Figure 8.1 shows the model interconnections for the complete whey evaporator set. The evaporator linear connections including the falling-film model are discussed in Chapter 10.

8.4 Delay terms approximation

The delay terms in the linear models were approximated using Padé approximations. There are two types of delay in the falling-film evaporator, pumping delay and falling-film delay. The magnitude of the delay depends upon the product operating conditions and the geometry of the evaporator. The selection of a suitable order of Padé approximations was investigated first and then the approximations of the delay terms in the linear models were carried out.

8.4.1 Selection of appropriate order for Pade approximation

Pumping delay

The pumping delays in the evaporator are from the balance tank to the first pass, from one preheat condenser to the next and from pass to pass. The shortest delay of 1.5 s is between the preheat condensers and the longest delay of 75 s is from the balance tank to the first pass of the evaporator.
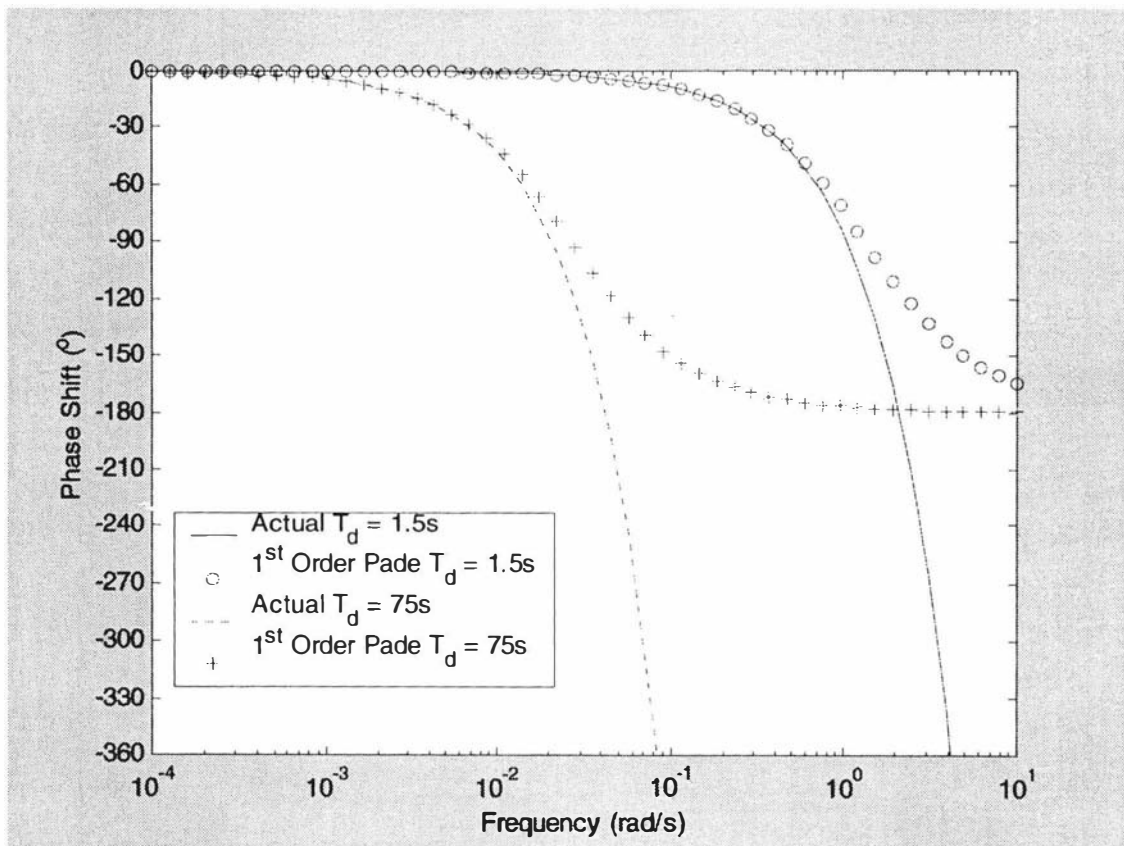
Figure 8.2: First order Pade approximations compared with actual responses for short and long pumping delays

With a PI controller (Proportional and Integral controller) the integrator will give a phase shift of 90°. Therefore, the Pade approximation responses can be considered satisfactory if they match the actual responses up to a phase shift of 90°. First order Pade approximations of both the shortest and longest pumping delays were found to match the actual pumping delays well up to a phase shift of 90° (Figure 8.2). Therefore, a 1st order Pade approximation was carried out for all pumping delay terms.

Falling film delay

The whey evaporator has three passes, in which the product flows down long tubes as a falling film while evaporation takes place. The linearised falling film models are given in equations (8.54) to (8.56). The mass of evaporation related to the temperature difference across the tube walls is shown by equation (8.71).

$$\frac{\tau_d.\lambda}{U_s.A_s}\frac{dM_{tubes}(t)}{dt}=\left[T_s(t)-T_e(t)-T_s(t-\tau_d)+T_e(t-\tau_d)\right] \tag{8.71}$$

Taking the Laplace transform of the above equation and rearranging produces the following equation.

$$\frac{M_{tubest}(s)}{\left[T_{s1}(s)-T_{e1}(s)\right]}=\frac{U_s.A_s}{\lambda}\frac{\left[1-e^{-\tau_{et}.s}\right]}{\tau_{et}.s} \tag{8.72}$$

The right hand side term with the falling film delay has to be approximated as it affects the behaviour of the system. For this purpose, a Laplace variable, $G_{tubes}(s)$, was defined as: $G_{tubes}(s)=\dfrac{\left[1-e^{-\tau_{et}.s}\right]}{\tau_{et}.s}$. The actual and the approximated terms were compared as for the pumping delays to select the appropriate order. To plot the actual Bode magnitude and phase shift of $G_{tubes}(s)$, the Laplace variable was substituted with the complex term jw as shown in (8.73).

$$G_{tubes}(jw)=\frac{\left[1-e^{-j\tau_{et}.w}\right]}{j\cdot\tau_{et}\cdot w}=\frac{\sin(\tau_{et}\cdot w)}{\tau_{et}\cdot w}-j\frac{\left[1-\cos(\tau_{et}\cdot w)\right]}{\tau_{et}\cdot w} \tag{8.73}$$

The complex magnitude and phase shift equations derived from equation (8.73) are shown in (8.74) and (8.75) respectively.

$$\left| G_{tubes}(jw) \right| = \sqrt{\frac{\sin^2(\tau_{et} \cdot w)}{\tau_{et}^2 \cdot w^2} + \frac{[1 - \cos(\tau_{et} \cdot w)]^2}{\tau_{et}^2 \cdot w^2}} = \frac{2}{\tau_{et} \cdot w} \sin\left(\frac{\tau_{et} \cdot w}{2}\right) \tag{8.74}$$

$$\angle G_{tubes}(jw) = \arctan\left[-\frac{(1 - \cos(\tau_{et} \cdot w))}{\sin(\tau_{et} \cdot w)} \right] = -\frac{\tau_{et} \cdot w}{2} \tag{8.75}$$

As can be seen from Figure (8.3), a 5th order Pade approximation gave a close approach to the falling film delay system response up to a phase shift of $90°$.

Where τ_{et} is the falling-film residence time (s)
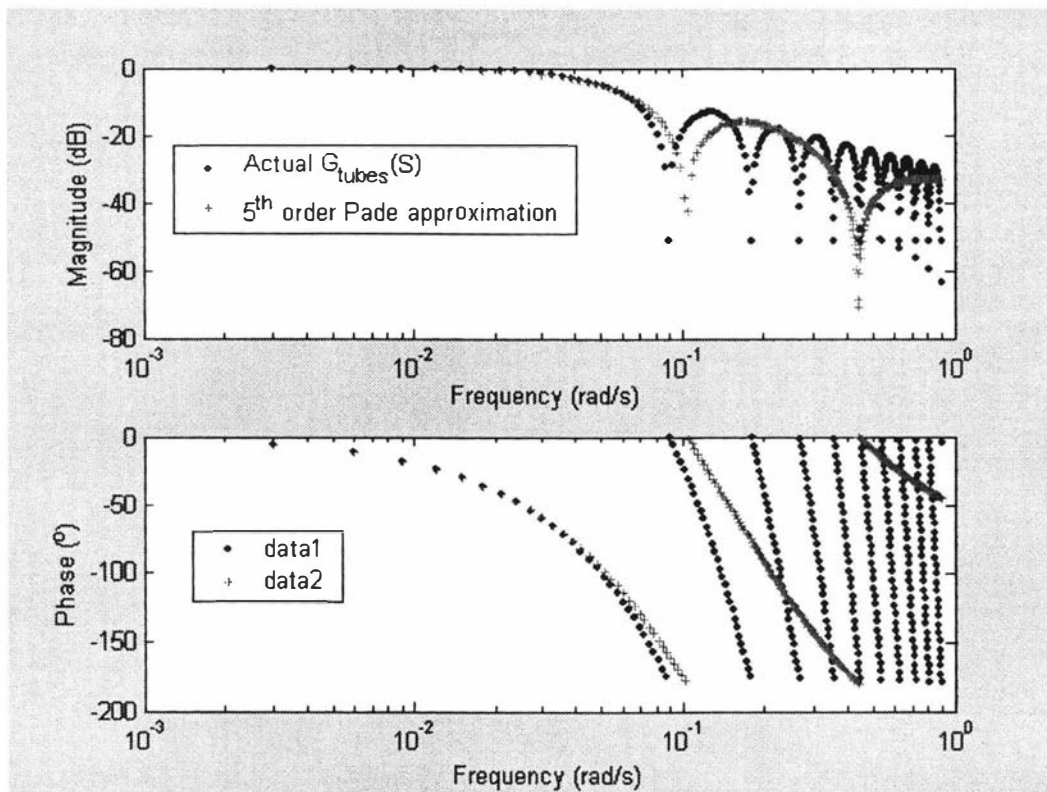
Figure 8.3: Bode plot comparing the fifth order Pade approximation with actual response for falling-film delay

8.4.2 Delay term approximations in the linear model

The pumping delays in the developed linear models were approximated using 1st order Pade approximations. The delays in each sub-system were considered separately. The derivation of the approximated delay equation is shown below for the mass flow rate in the feed.

The linear equation and Laplace transform for the mass flow rate of feed with a delay term are shown in (8.76).

$$M_{fd}(t) = M_f(t - \tau_d) \quad , \quad M_{fd}(s) = e^{-\tau_d s} M_f(s) \tag{8.76}$$

The Laplace Transform of the 1st order Pade approximation to the pumping delay is shown in equation (8.77).

$$e^{-\tau_d s} = \frac{\left(1 - \dfrac{t_d}{2} s\right)}{\left(1 + \dfrac{t_d}{2} s\right)} \tag{8.77}$$

Substituting equation (8.76) into (8.77) and rearranging gives equation (8.78).

$$\frac{\tau_d s}{2} \cdot M_{fd}(s) + M_{fd}(s) = M_f(s) - \frac{\tau_d s}{2} \cdot M_f(s) \tag{8.78}$$

Converting equation (8.78) into the time domain produces equation (8.79), and substituting equation (8.76) into (8.79) will produce (8.80).

$$\frac{\tau_d}{2} \cdot \frac{d(M_{fd}(t))}{dt} + M_{fd}(t) = M_f(t) - \frac{\tau_d}{2} \cdot \frac{d(M_f(t))}{dt} \tag{8.79}$$

$$\frac{\tau_d}{2} \cdot \frac{d(M_f(t-\tau_d))}{dt} + M_f(t-\tau_d) = M_f(t) - \frac{\tau_d}{2} \cdot \frac{d(M_f(t))}{dt} \tag{8.80}$$

A similar approach was used to derive equations for the rest of the delay terms in the linear evaporator models. The approximated delay equations for the linear condenser models are shown below:

1st preheat condenser

$$T_{e2}(t-\tau_{PC1}) = T_{e21d}$$

$$\frac{dT_{e21d}(t)}{dt} = \left(\frac{-2}{\tau_{PC1}}\right)T_{e21d}(t) + \left(\frac{2}{\tau_{PC1}} + \frac{1}{\tau_{Te2}}\right)T_{e2}(t) - c_1 M_{p2}(t-\tau_{p2p3}) - c_2 T_{e1}(t)$$
$$- c_3 q_{vcond}(t) - c_4 q_{ph1}(t) - c_5 T_a(t) \tag{8.81}$$

$$T_f(t-\tau_{PC1}) = T_{fp1} \quad , \qquad\qquad M_f(t-\tau_{PC1}) = M_{fp1} \tag{8.82}$$

2nd preheat condenser

$$T_{e1}(t-\tau_{PC2}) = T_{e1d}$$

$$\frac{dT_{e1d}(t)}{dt} = \frac{-2T_{e1d}(t)}{\tau_{PC2}} + \left(\frac{2}{\tau_{PC2}} + \frac{1}{\tau_{Te1}}\right)T_{e1}(t) - b_1 M_f(t-\tau_{fd}) - b_2 T_s(t) - b_3 P_{steam}(t)$$
$$- b_4 T_{ph3}(t) - b_5 q_{ph2}(t) - b_6 T_{e2}(t) - b_7 T_a(t) \tag{8.83}$$

$$T_{ph1}(t - \tau_{PC2}) = T_{ph1d}$$

$$\frac{dT_{ph1d}(t)}{dt} = \left(\frac{-2}{\tau_{PC2}}\right) T_{ph1d}(t) + \left(\frac{2}{\tau_{PC2}} + \frac{1}{\tau_{TPC1}}\right) T_{ph1}(t) - \frac{T_{e2}(t)}{\tau_{TPC1}}$$

$$+ \frac{e^{\frac{-\tau_{PC1}}{\tau_{TPC1}}}}{\tau_{TPC1}} T_{e21d}(t) - \frac{e^{\frac{-\tau_{PC1}}{\tau_{TPC1}}}}{\tau_{TPC1}} T_{fp1} + \left[\frac{(T_{e2}^o - T_f^o) \cdot e^{\left(\frac{-\tau_{PC1}}{\tau_{TPC1}}\right)}}{M_f^o \cdot \tau_{TPC1}}\right] \cdot \left\{M_f(t) - M_{fp1}(t)\right\} \qquad (8.84)$$

$$M_{ph1}(t) = M_{fp1}(t) \quad , \qquad\qquad M_{ph1}(t - \tau_{PC2}) = M_{fp1p2}(t) \qquad (8.85)$$

3rd preheat condenser

$$T_s(t - \tau_{PC3}) = T_{sd}$$

$$\frac{dT_{sd}(t)}{dt} = \frac{-2T_{sd}(t)}{\tau_{PC3}} + \left(\frac{2}{\tau_{PC3}} - \frac{1}{\tau_{TS}}\right) T_s(t) - a_1 P_{steam}(t) - a_2 T_{e1}(t) - a_3 q_{ph3}(t) - a_4 T_a(t) \qquad (8.86)$$

$$T_{ph2}(t - \tau_{PC3}) = T_{ph2d}$$

$$\frac{dT_{ph2d}(t)}{dt} = \left(\frac{-2}{\tau_{PC3}}\right) T_{ph2d}(t) + \left(\frac{2}{\tau_{PC3}} + \frac{1}{\tau_{TPC2}}\right) T_{ph2}(t) - \frac{T_{e1}(t)}{\tau_{TPC2}} + \frac{e^{\frac{-\tau_{PC2}}{\tau_{TPC2}}}}{\tau_{TPC2}} T_{e1d}(t)$$

$$- \frac{e^{\frac{-\tau_{PC2}}{\tau_{TPC2}}}}{\tau_{TPC2}} T_{ph1d}(t) + \left[\frac{(T_{e1}^o - T_{ph1}^o) \cdot e^{\left(\frac{-\tau_{PC2}}{\tau_{TPC2}}\right)}}{M_f^o \cdot \tau_{TPC2}}\right] \cdot \left\{M_{fp1}(t) - M_{fp1p21}(t)\right\} \qquad (8.87)$$

$$M_{ph2}(t) = M_{fp1p2}(t) \quad , \qquad\qquad M_{ph2}(t - \tau_{PC3}) = M_{fd}(t) \qquad (8.88)$$

Vacuum condenser

$$T_{e2}(t - \tau_{VC}) = T_{e22d}$$

$$\frac{dT_{e22d}(t)}{dt} = \left(\frac{-2}{\tau_{vc}}\right) T_{e22d}(t) + \left(\frac{2}{\tau_{vc}} + \frac{1}{\tau_{Te2}}\right) T_{e2}(t) - c_1 M_{p2}(t - \tau_{p2p3}) - c_2 T_{e1}(t)$$

$$- c_3 q_{vcond}(t) - c_4 q_{ph1}(t) - c_5 T_a(t) \qquad (8.89)$$

PART 3

Model applications

9. Process Improvements

In this section the falling-film evaporator optimisation objectives and the constraints to the whey powder production process are discussed. The performance of the evaporator for different products is compared and investigated. Finally, the trials and the optimum operating conditions for each product are discussed.

9.1 Process optimisation

The desire to achieve the best (increase the profit) in a given situation is the motive force behind optimization. Rapidly changing market conditions, increasingly stringent environmental regulations and advances in competitive technology are continuously challenging the profitability of existing production processes. Optimisation aims to find out the best set of operating conditions in order to minimize operational cost and thereby improve the efficiency of the system.

Optimisation requires that the system under consideration be characterized mathematically, that is, its behaviour is described by a set of mathematical equations called a 'model'. Depending upon the nature of the model, the resulting set of optimised operating conditions can be final or serve as a guide and criterion by which different alternatives can be compared. The cost minimisation technique is widely used in optimising industrial processes, as the cost of production plays a key role in enterprise growth.

The optimisation of the whey products evaporator at NZMP, Whareroa, Fonterra Co-operative Ltd is a challenging process as the evaporator used to concentrate a variety of products. These products are of different compositions and thus show different performance in the evaporator. Evaporator process constraints for different products were therefore investigated first to determine the active constraints. The active constraints were then investigated further to optimise the process.

9.2 Constraints in the evaporation process

Constraints in the evaporation process are the evaporator capacity, the dryer capacity, the evaporator operating temperature, the concentrate total solids and the film break-down. In this section, these constraints are discussed in detail for the evaporator in whey products at Fonterra Ingredients, Whareroa, Fonterra Co-operative Ltd.

9.2.1 Evaporator capacity

The amount of water that can be evaporated in a TVR evaporator depends mainly on the ratio of the mass of recycled vapour to the mass of motive steam (see Chapter 7). The mass of recycled vapour depends on the motive steam pressure. The maximum motive steam pressure available for evaporation at the site is 10 bar. Figure 9.1 shows the average mass of evaporation for different whey products at a motive steam pressure 10 bar (data collected from Fonterra, Whareroa whey evaporator).
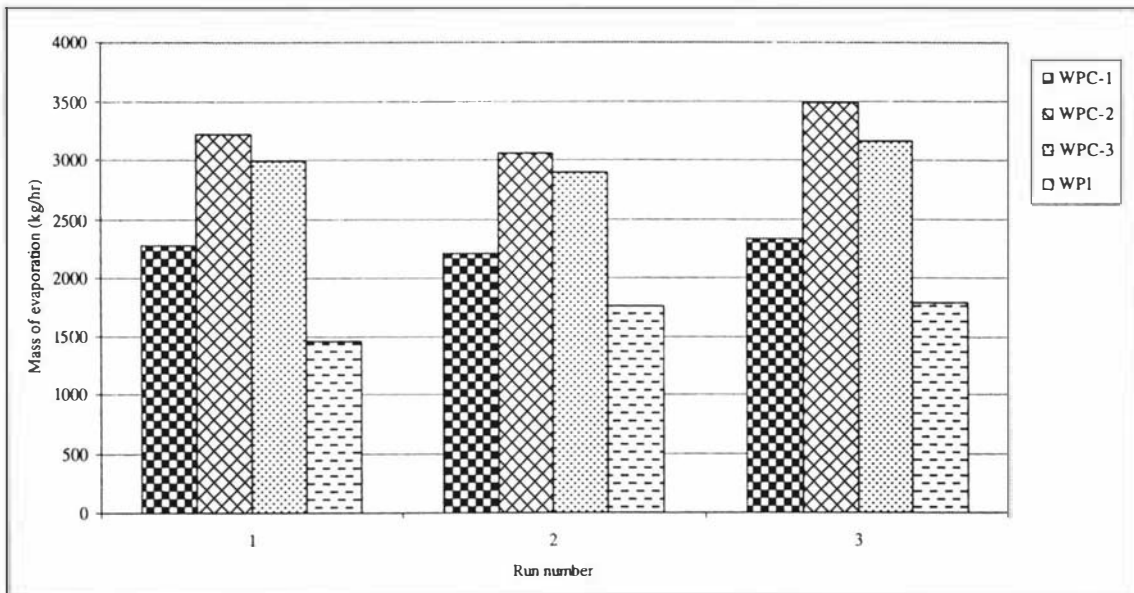
Figure 9.1: Comparison of mass of evaporation in the evaporator for different whey products

There is greatest evaporation for WPC-2 and least evaporation for WPI. All other products lie between these two. This is because of the different heat transfer coefficients for the different products, which was discussed in Chapter 7.

It is clear from Figure 9.1 that the evaporation capacity of the evaporator is limited by both the motive steam pressure and the overall heat transfer coefficient, which is dependent on product composition.

9.2.2 Dryer capacity

The maximum evaporation in the dryer depends on the air flow rates and the air inlet and outlet temperatures. The dryer always runs with maximum air flow, whereas the inlet and outlet temperatures differ with the type of product. Figure 9.2 shows the average amount of water evaporated in the dryer for different products, while Figure 9.3 shows the average powder production rate for different products.
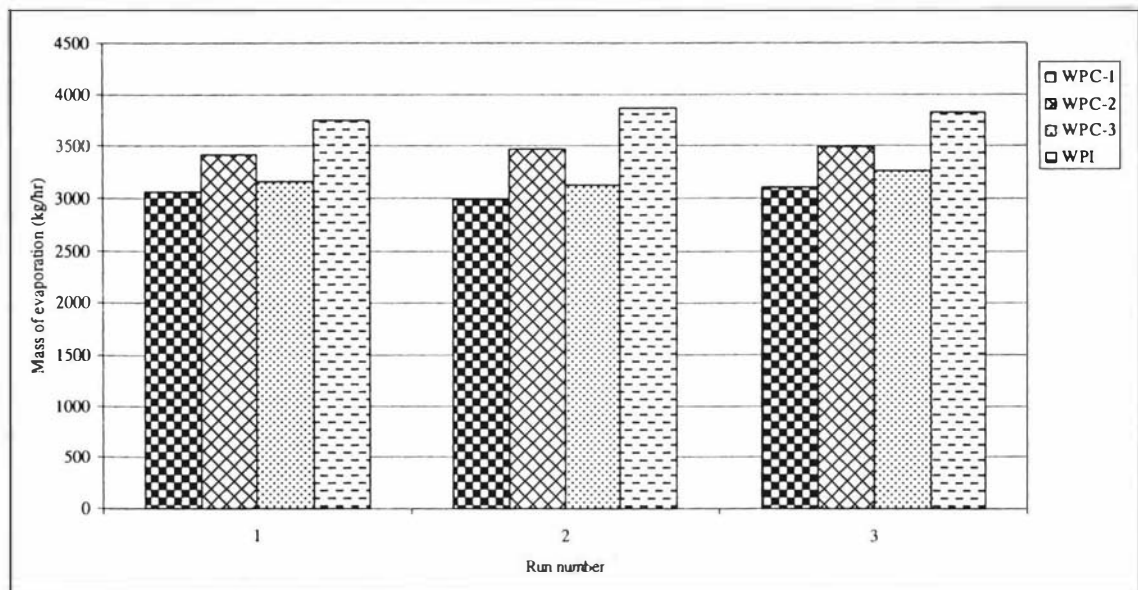
Figure 9.2: Comparison of mass of evaporation in the spray dryer for different whey products

It can be seen from Figures 9.2 that there is a high mass of water evaporation for WPI compared to other products. The dryer temperature difference when running on WPC-1, WPC-2, WPC-3 and WPI are 140, 140, 131 and 132 respectively. This suggests that the reason for this difference in the evaporation in dryer is due to the concentrate viscosity resulting from the different product compositions (see Chapter 3). Thus, the evaporation capacity of the dryer is not only affected by the air flows and the temperatures but also by the product composition in the evaporator.
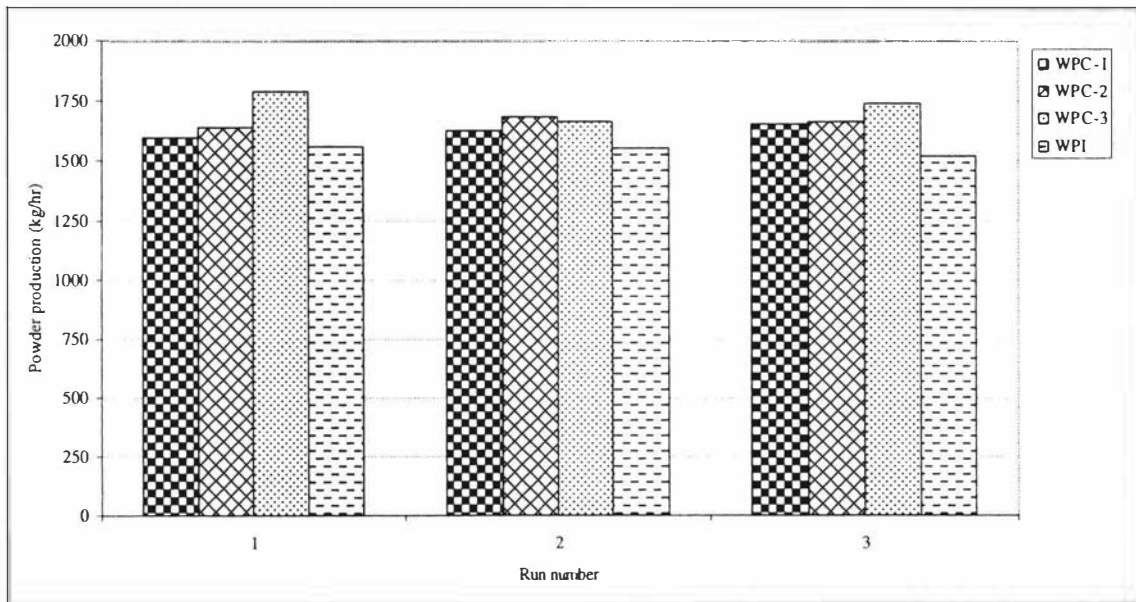
Figure 9.3: Comparison of powder production rate for different whey products

9.2.3 Evaporating temperature

The evaporating temperature is critical for whey products as they contain more than 70% whey protein and these are very sensitive to temperature (see Chapter 2). The evaporating temperature should be selected such that there is minimum whey protein denaturation as the extent of denaturation influences the final product quality. However, the higher the temperature the better the evaporation. The choice of evaporation temperature must therefore be a compromise between the mass of evaporation and the product quality.

Figure 9.4 shows the current operating temperatures for different whey products. The maximum evaporating temperature for all the products is the same except for WPI. This is due to the low evaporation heat transfer coefficient. The viscosity of each product as a function of temperature was measured to determine the maximum permissible operating temperature. Viscosity decreases until a critical temperature known as the denaturation temperature is reached, above which viscosity increases. Figures 9.5 and 9.6 show viscosity as a function of temperature for WPC-3 and WPI respectively. The products show an increase in viscosity at temperatures between 55°C and 60°C; a maximum of 55°C is therefore recommended for evaporation. This maximum evaporation temperature is an active constraint to the whey powder production.
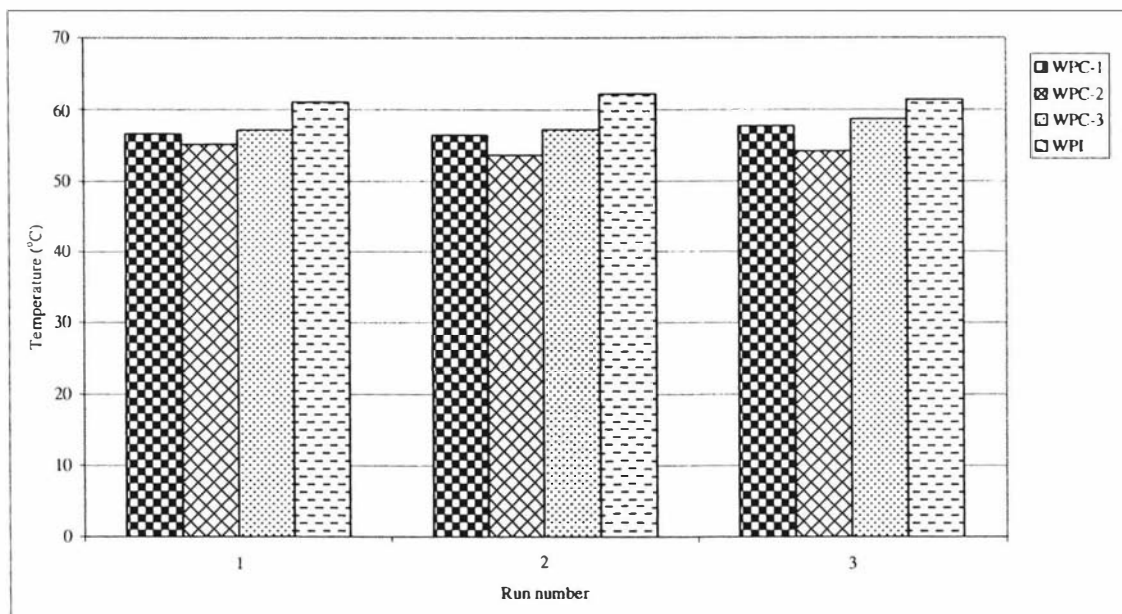
Figure 9.4: Maximum operating temperature for different whey products
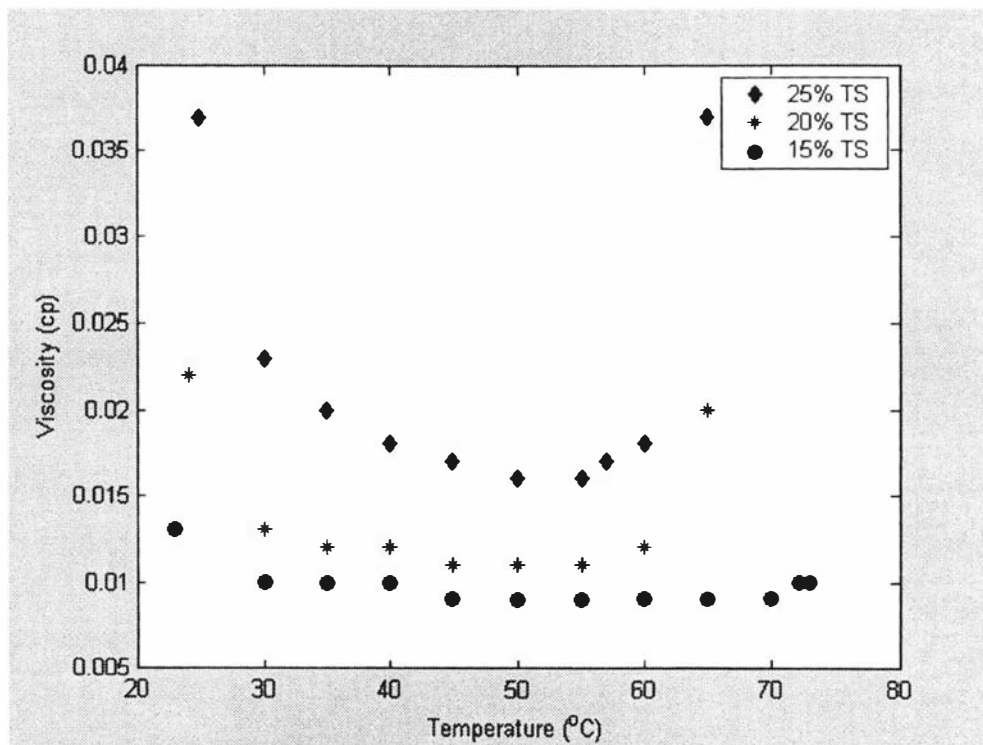
Figure 9.5: Viscosity of WPC-3 as a function of temperature for different total solids concentrations
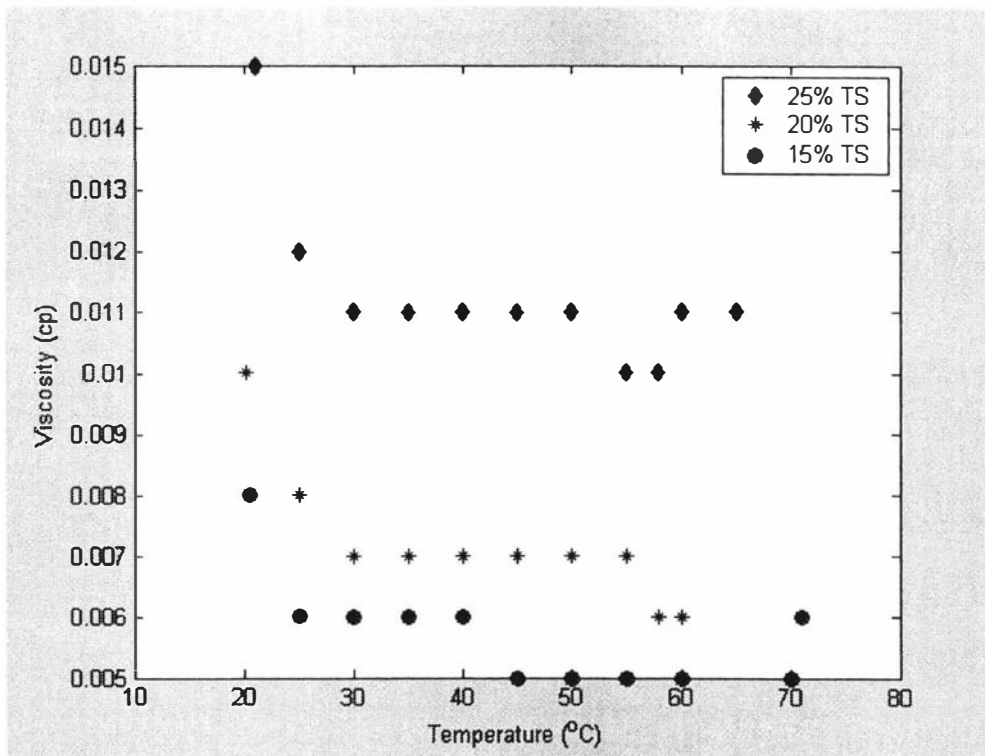
Figure 9.6: Viscosity of WPI as a function of temperature for different total solids concentrations

9.2.4 Product total solids concentration

The physical properties of whey products change with total solids concentration. One of the properties that influence the amount of water evaporation is product viscosity. Viscosity increases with total solids and therefore the evaporation rate reduces with total solids. Figures 9.7 to 9.10 show concentrate viscosity as a function of total solids concentration for WPC-2, WPC-3, WPI and WPC-1 respectively. The figures shows both low shear (100 s^{-1}) and high shear (1200 s^{-1}) viscosities predicted from the models developed in Chapter 3. The current concentration range exiting the evaporator is also shown on the figures.

The current operating solids concentrations for both WPC-2 and WPC-3 are the optimum solids that can be achieved from the evaporator. Any further increase in the solids for these products would result in serious consequences (block concentrate lines, poor product quality and production loss due to down time) due to the high viscosity. It should be noted that viscosity can increase as a result of both high total solids and lower temperature.

166
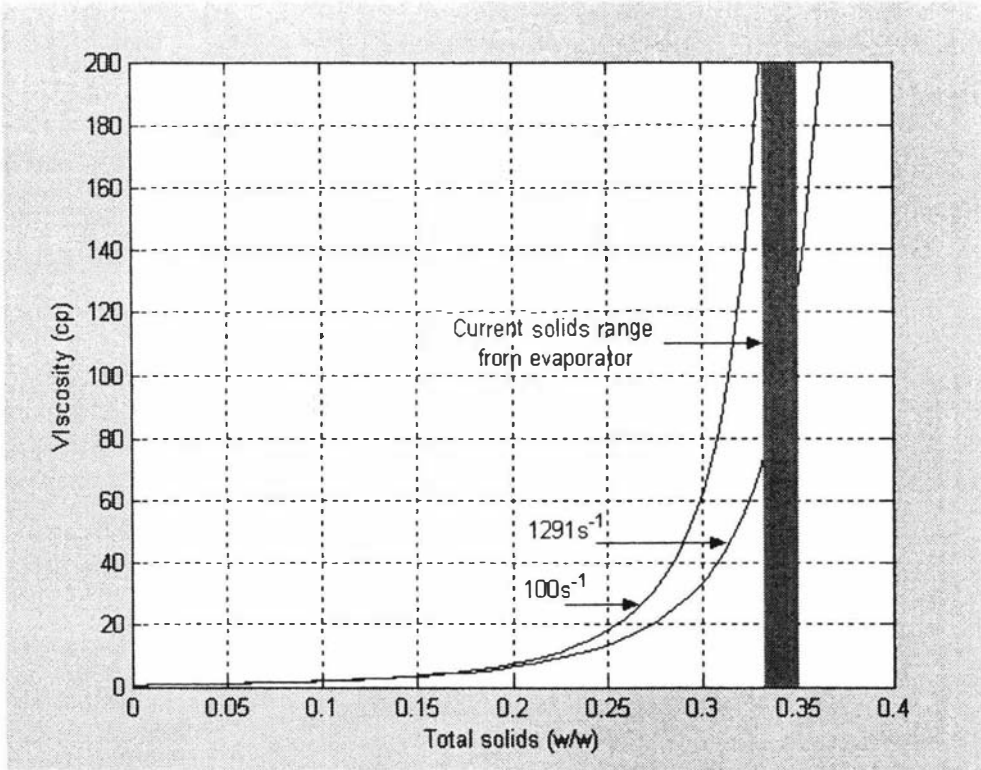
Figure 9.7: Current operating concentration range for WPC-2
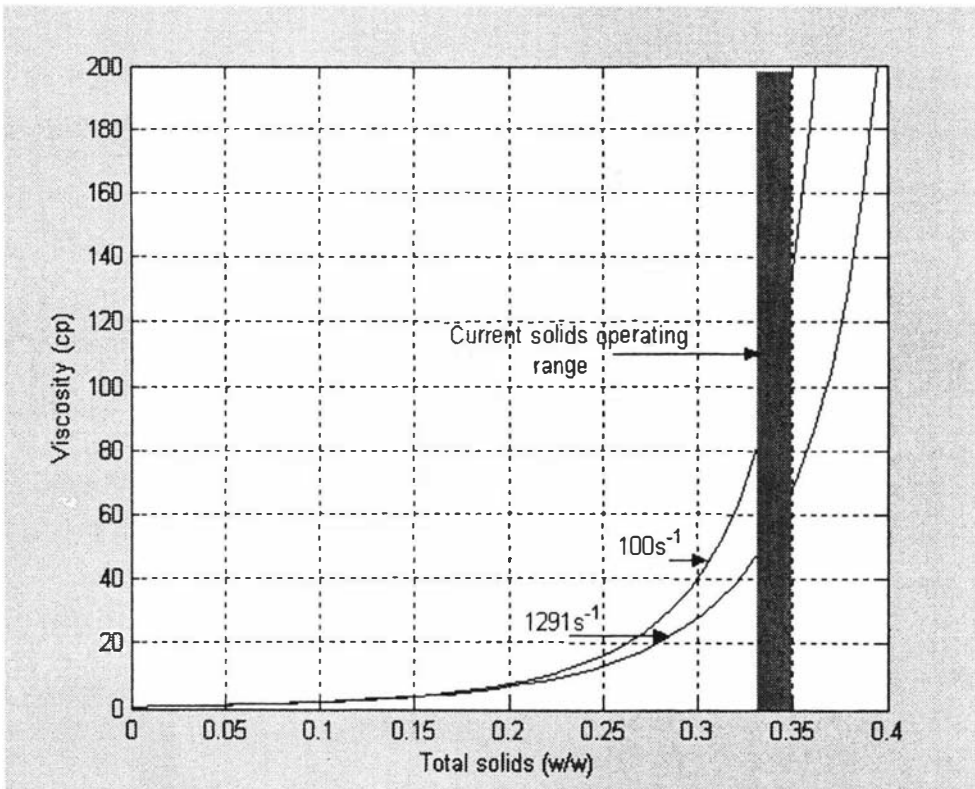
Figure 9.8: Current operating concentration range for WPC-3
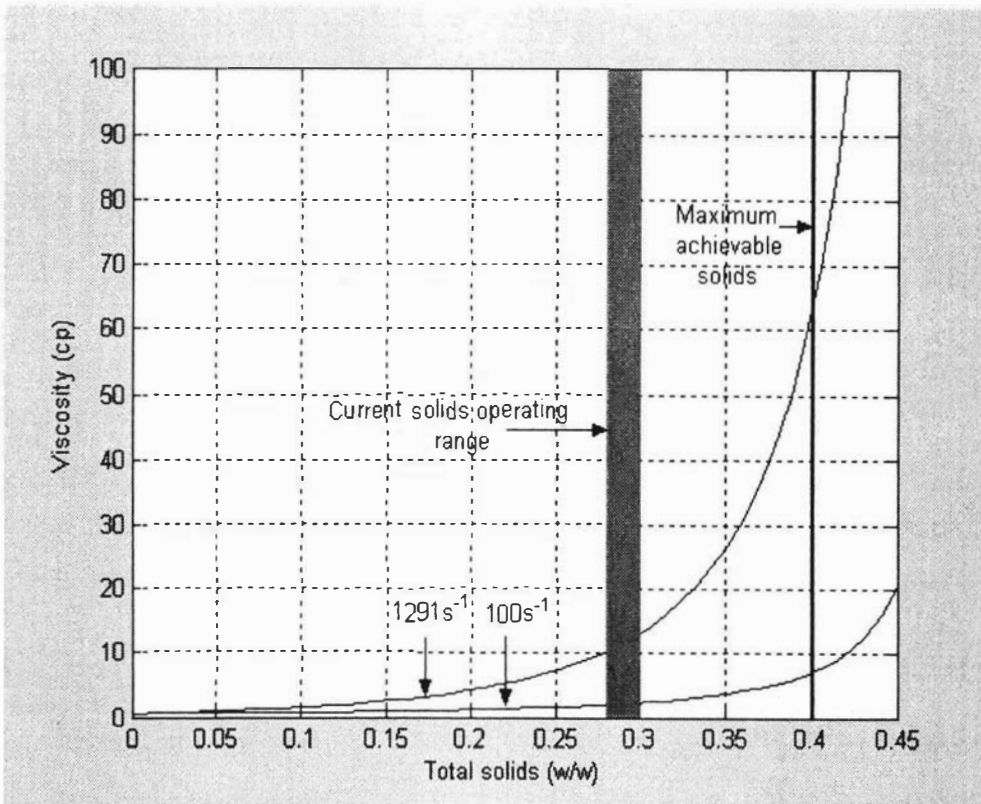
Figure 9.9: Current operating concentration range and maximum achievable solids concentration for WPI
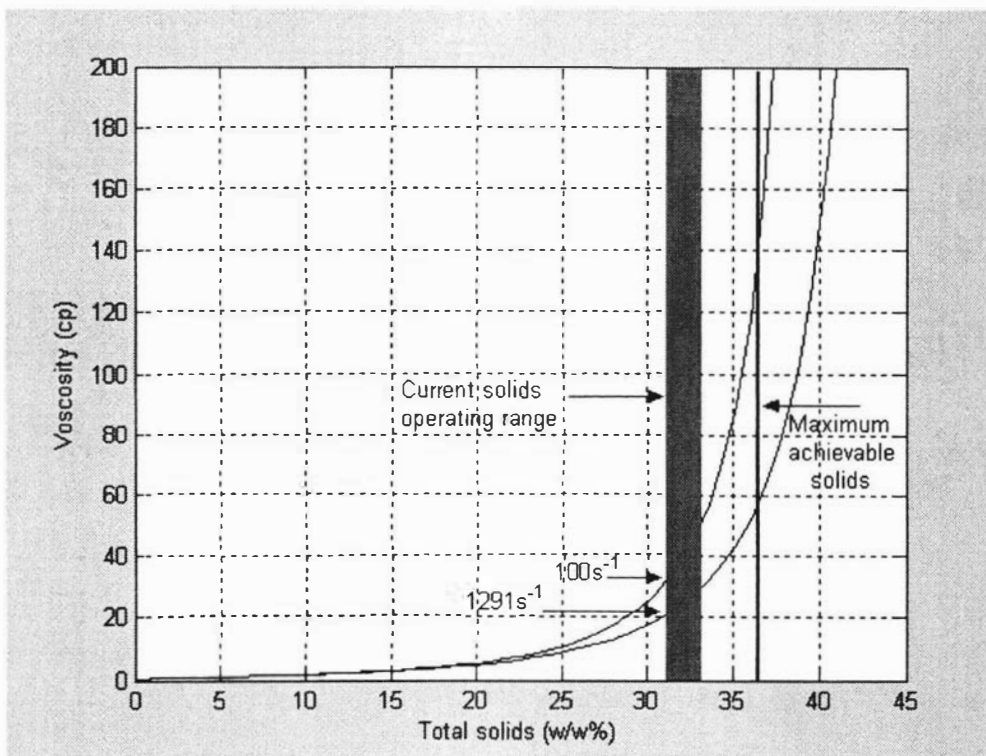
Figure 9.10: Current operating concentration range and maximum achievable solids concentration for WPC-1

The current operating solids concentrations for both WPC-1 and WPI are well below the maximum achievable solids. The maximum achievable solids for WPI and WPC-1 are different because they differ in protein content and the viscosity correlations.

It can be seen from the figures that the maximum concentration that can be achieved from the evaporator is limited by the concentrate viscosity which is product dependent. To avoid the problems that are associated with high viscosity, the total solids concentration exiting the evaporator should not exceed this limit. Therefore, the concentrate viscosity is an active constraint for WPC-2 and WPC-3 but not for WPI and WPC-1.

9.2.5 Film break-down

Insufficient flow within the evaporator tubes cause the film to break and form dry patches. This formation of dry patches on the tube wall may lead to fouling. The behaviour of a dry patch formed on the surface can fall into one of three categories:

1. The dry patch will be stable and remain indefinitely.
2. The dry patch will be slowly rewetted, taking time for the film to completely reform.
3. The dry patch will be quickly rewetted and the film reformed.

If the dry patch behaviour were in either category 1 or 2 then fouling would be likely to occur. To avoid this fouling, the peripheral flow in a falling-film evaporator should exceed the threshold at which stable dry patches can occur. This threshold can be predicted from the force criterion proposed by Hartley and Murgatroyd (1964) and Hoke and Chen (1992). These models are discussed in Appendix C.

The current operating flows and the minimum flows are shown in Figures 9.11 to 9.13 for water, WPI and WPC-3 respectively. The product feed to the evaporator varies in the range 6.5 m^3/hr to 8.5m^3/hr. The water feed flow rate to the evaporator depends on the product type. The plots are shown only for WPI and WPC-3, since WPI has the lowest evaporator feed flow (6.5m^3/hr) and WPC-3 has the highest (8.5m^3/hr).

The product operating flows are above the advancing minimum flow and therefore the product flow rate is sufficient to rewet any dry patch formed while the evaporator is running on product. The operating flows for water are in between the advancing and retreating minimum flows, and below the retreating minimum flow when the feed flow is $6.5m^3$/hr. However, since the product flows are above the advancing minimum flow, the dry patches formed while running on water would be rewetted once the evaporator is fed with product. Therefore, the wetting flow is not a constraint to the evaporation process for any of the whey products.
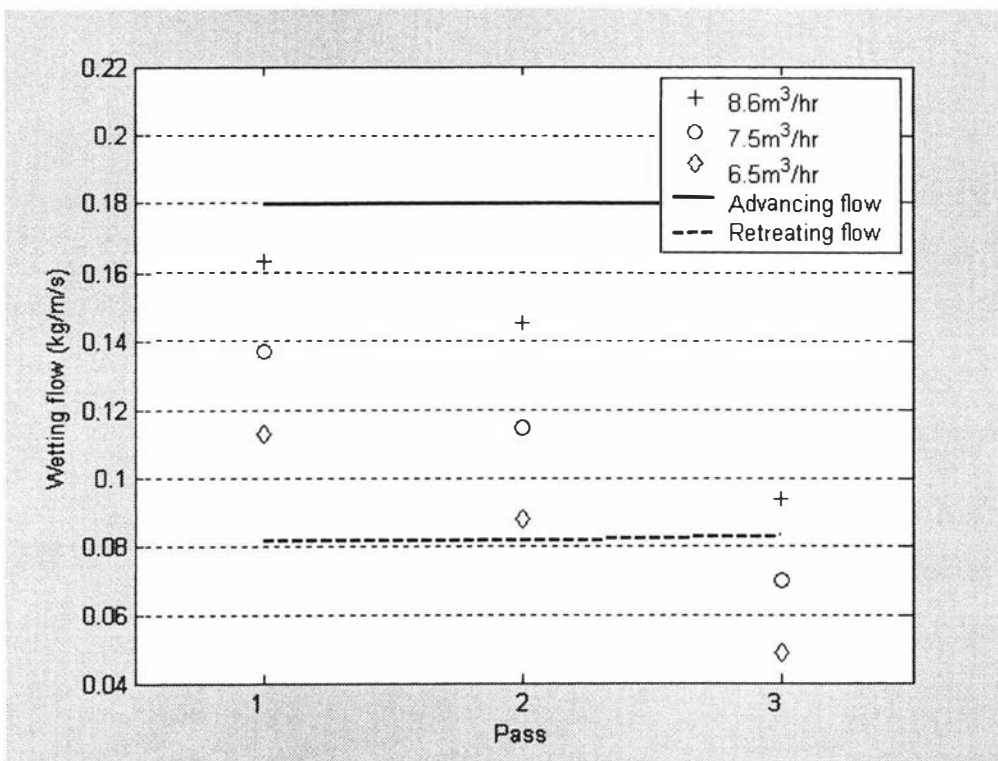
Figure 9.11: Current operating flows and the wetting flow rates for water
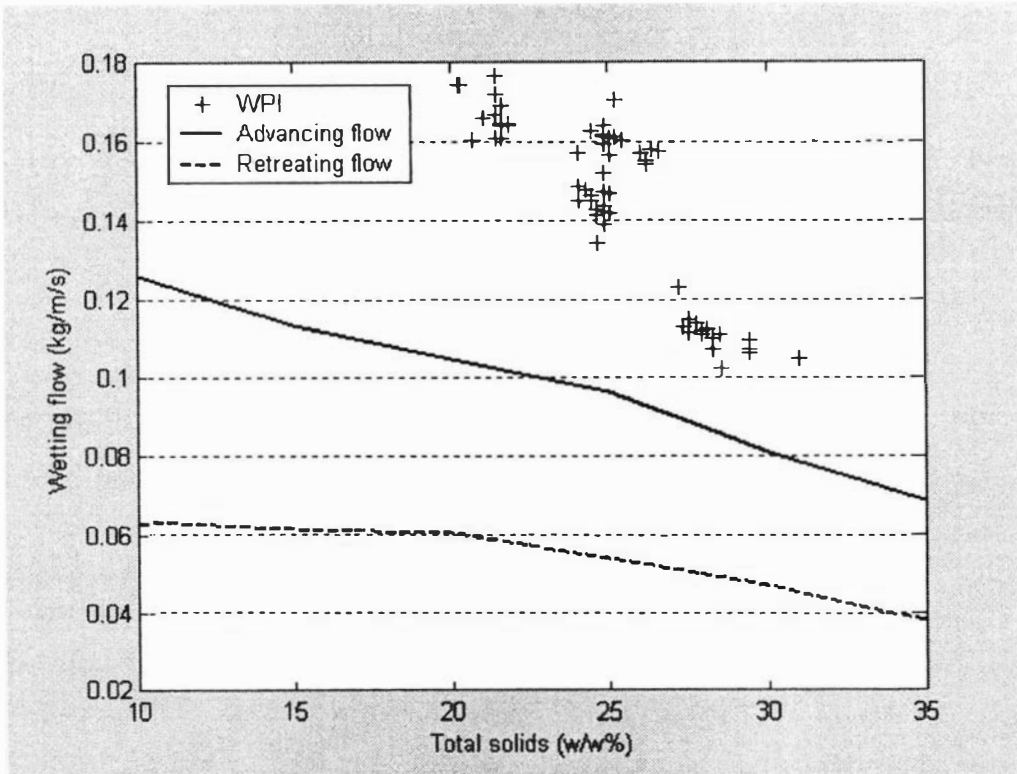
Figure 9.12: Current operating flows and wetting flows for WPI
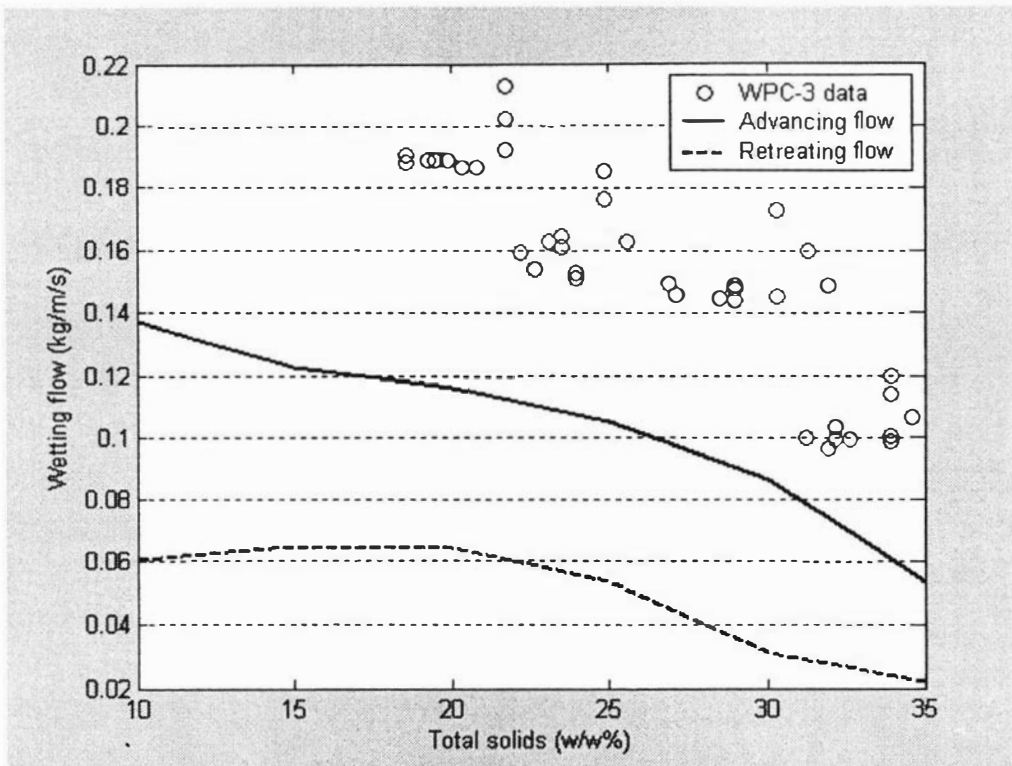
Figure 9.13: Current operating flows and wetting flows for WPC-3

9.3 Whey products evaporator optimisation

The purpose of using the evaporator to concentrate products before they are spray dried to powder is to reduce the production cost. The cost of evaporation in the spray drier is 7 times the cost of evaporation in a TVR evaporator (Winchester, 2000). The primary aim of the whey products evaporator optimisation is to increase the amount of evaporation in the evaporator and thereby to reduce production cost and increase throughput.

The possibilities for increasing evaporator performance were discussed in the previous section and are tabulated in Table 9.1. The active constraint to WPC-2 and WPC-3 production is the concentrate viscosity whereas evaporation capacity constrains both WPI and WPC-1 production. Therefore it is vital to control the solids concentration for both WPC-2 and WPC-3 and to improve the evaporation capacity for both WPI and WPC-1. Any improvement in density control and evaporation capacity would significantly increase process profitability through

1. Increasing throughput.
2. Reducing operating costs.
3. Producing more consistent powder quality.
4. Reducing maintenance costs.
5. Reducing product losses.

Table 9.1: Summary of process constraints for whey products

Constraint	WPC-1	WPC-2	WPC-3	WPI
Evaporator capacity	Active	Not active	Not active	Active
Dryer capacity	Not active	Not active	Not active	Not active
Evaporating temperature	Active	Active	Active	Active
Product total solids	Not active	Active	Active	Not active
Film break-down	Not active	Not active	Not active	Not active

The evaporator performance (i.e. mass of evaporation) observed for both WPC-1 and WPI was poor. Table 9.1 identifies the opportunities for potential improvements. Since WPI was the primary product being processed during the project, the optimisation investigation focused mainly on WPI. The preheating and evaporation systems were investigated, as these are the systems that affect the amount of evaporation.

9.3.1 Preheating

The preheat condensers in the evaporator are of shell and tube design. Preheat condensers are used to heat the incoming product to the evaporation temperature. There are three preheat condensers in the whey evaporator, attached to the 2nd effect, 1st effect and shell of the 1st effect respectively. The calculated overall heat transfer coefficient was used as a measure to compare the performance of the three condensers as shown in Figure 9.14.
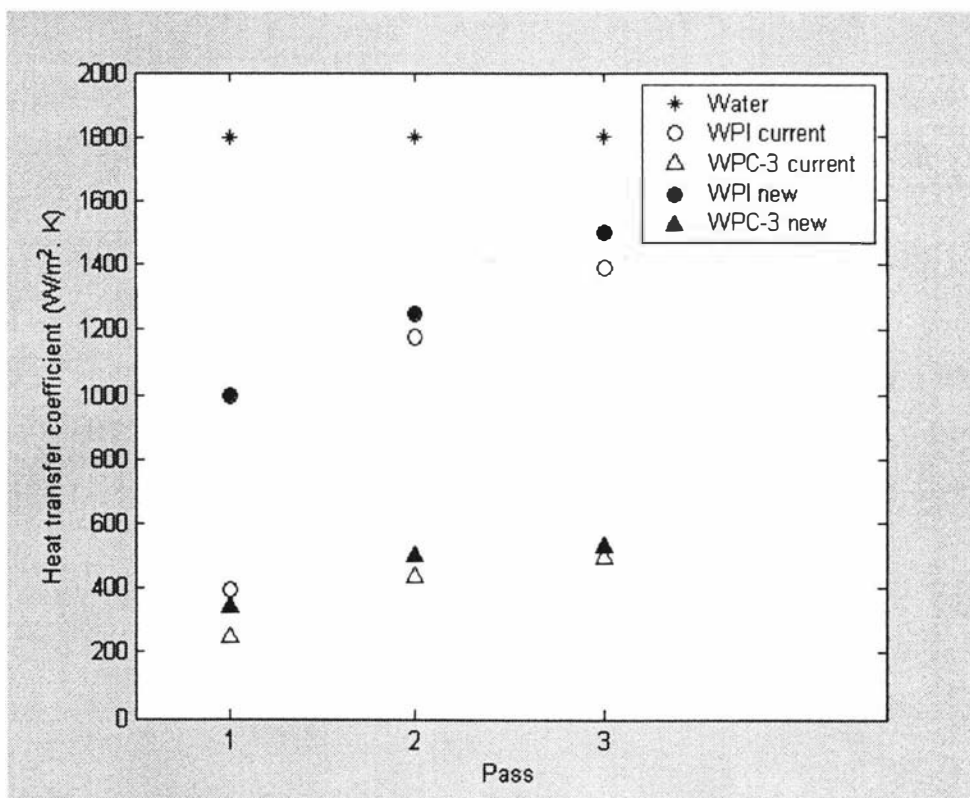
Figure 9.14: Comparison of preheat condenser heat transfer coefficients for water, WPC-3 and WPI

The low operating heat transfer coefficients in the 1st preheat condenser running with WPC-3 and WPI, as shown in Figure 9.14, are due to the presence of air (non-condensable gases) in the shell of the 2nd effect. This occurs because the de-aeration lines from the shells of the effects and from the condensers pass through the shell of the 1st preheat condenser and not directly to the vacuum condenser. It is common practice to direct the de-aeration lines to the vaccum condenser.

To improve the preheat performance, the de-aeration lines were diverted to the vacuum condenser instead of passing through the shell of the 1st preheat condenser. The new heat transfer coefficient values for WPI and WPC-3 are also shown in Figure 9.14. The improvement in the heat transfer coefficient for WPI was significant (150% increase) compared to the improvement observed for WPC-3 (14% increase). This is due to the effect of product viscosity on the heat transfer coefficient ($\mu_w = 1cp$, $\mu_{WPI} = 2cp$, $\mu_{WPC-3} = 20cp$).

9.3.2 Evaporation

The evaporation process removes water from the feed whey so that the whey can be spray dried to powder in a spray drier. The operating cost for removing water in the dryer is more expensive than that of removing the water in the evaporator. Therefore, it is always cost effective to remove as much water as possible in the evaporator. The evaporator in Whey Products has three passes for evaporation. The total mass of water evaporated is product dependent (Figure 9.2). To investigate and improve the evaporation, the overall evaporation heat transfer coefficients for different products were calculated from the historical data and compared. Figure 9.15 shows the overall heat transfer coefficient for water, WPC3 and WPI.

The evaporation of WPC-3 is constrained by the product viscosity, but this is not the case for WPI. The cause of the poor evaporation of WPI was not obvious as the product has a very low viscosity. The following section describes the investigation carried to increase the evaporation of WPI.
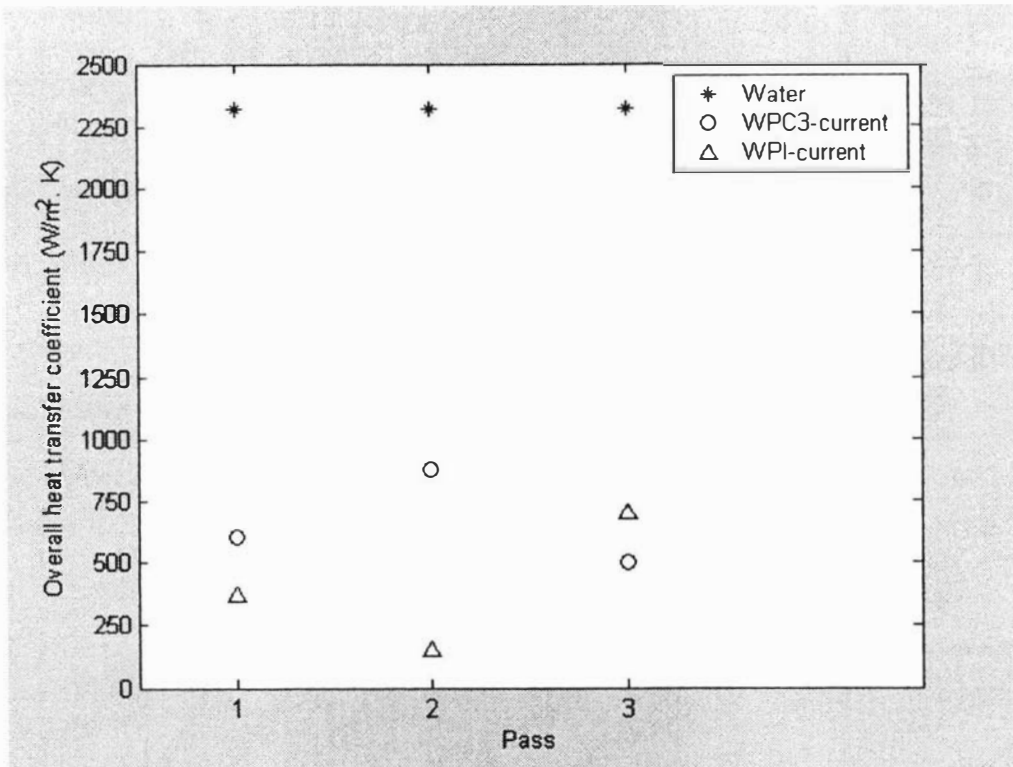
Figure 9.15: Comparison overall evaporation heat transfer coefficient for water, WPC-3 and WPI

9.3.3 Investigation of poor evaporation/ heat transfer coefficient for WPI

The total mass of evaporation for WPI was very poor compared to the evaporation for other products. The suspected causes, based on visual inspection and total solids measurements in the evaporator, are listed below.

1. Product mixing between the two passes on the distribution plate of the 1st effect.
2. High protein content.
3. Large quantity of stable foam.

The suspected causes listed above were investigated in detail as discussed in the following sections.

Product mixing on the distribution plate of the 1st effect

The whey evaporator has two passes in the 1st effect, with a dividing plate separating the 1st pass section from the 2nd pass. It was observed through the sight glasses on the lid of the 1st effect that a large quantity of foam was flowing over the dividing plate from 1st pass section to the 2nd pass section. This carry over of an unknown quantity of product would cause dilution of the concentrate exiting from the 1st pass. The heat transfer coefficient estimated from the solids concentration after each pass would be different if a significant quantity of product was mixing in the distribution plate. It was observed (from comparing the run with that for WPC-3) that the flash on the entry to the evaporator caused the product mixing. To improve performance and to estimate the true heat transfer coefficients for WPI, a trial was conducted to avoid flash on entry to the evaporator. This was achieved by bypassing the 3rd preheat condenser as shown in Figure 9.16.
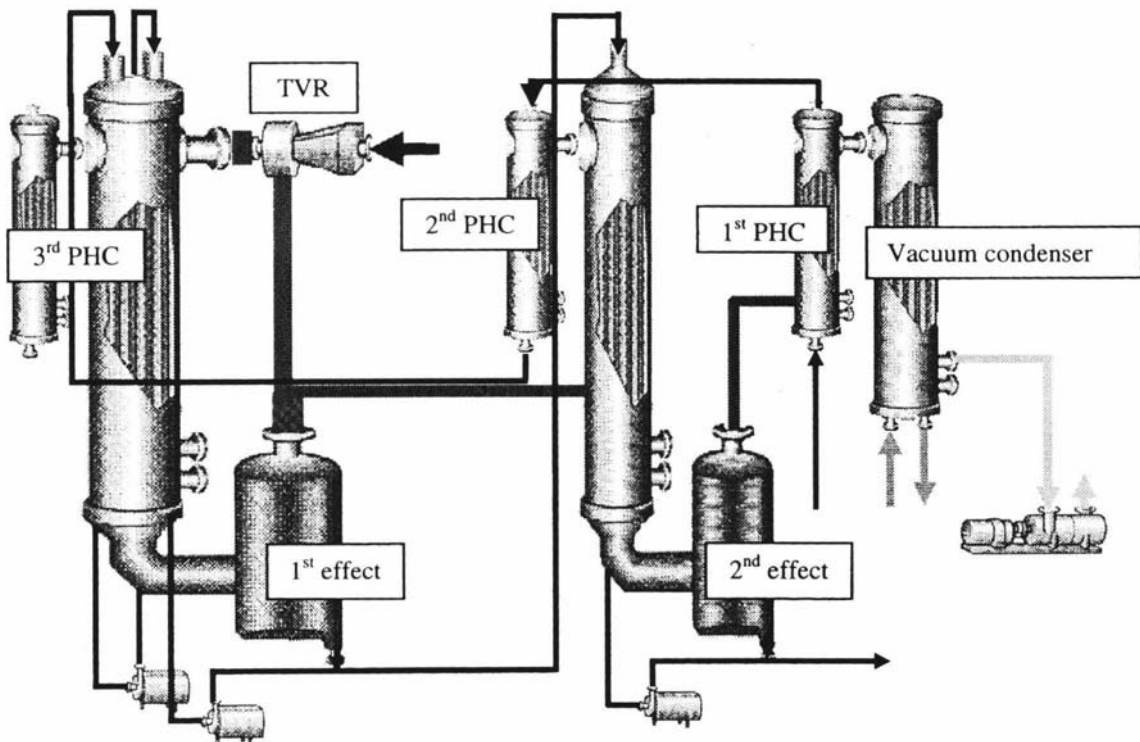
Figure 9.16: Evaporator arrangement for bypassing the 3rd preheat condenser

The 2nd and 3rd preheat condensers are attached to the 1st effect and the shell of the 1st effect respectively. The temperature of the heating medium in the 3rd preheat condenser is higher than the 1st effect temperature, while the temperature of the heating medium in the 2nd preheat condenser is same as the 1st effect temperature. Therefore, the product outlet temperature from the 2nd preheat condenser will always be below the 1st effect temperature, while the product outlet temperature from the 3rd preheat condenser will always be above the 1st effect temperature.

By bypassing the 3rd preheat condenser, flash and therefore product carry over was avoided. Accurate heat transfer coefficients could therefore be estimated from the total solids from each pass. These are shown in Figure 9.17. There was a small improvement in the 2nd pass heat transfer coefficient, but a drop in the 1st pass heat transfer coefficient. This was because the flow of foam to the 2nd pass was stopped by avoiding the flash, leaving the foam causing problems in the 1st pass instead.
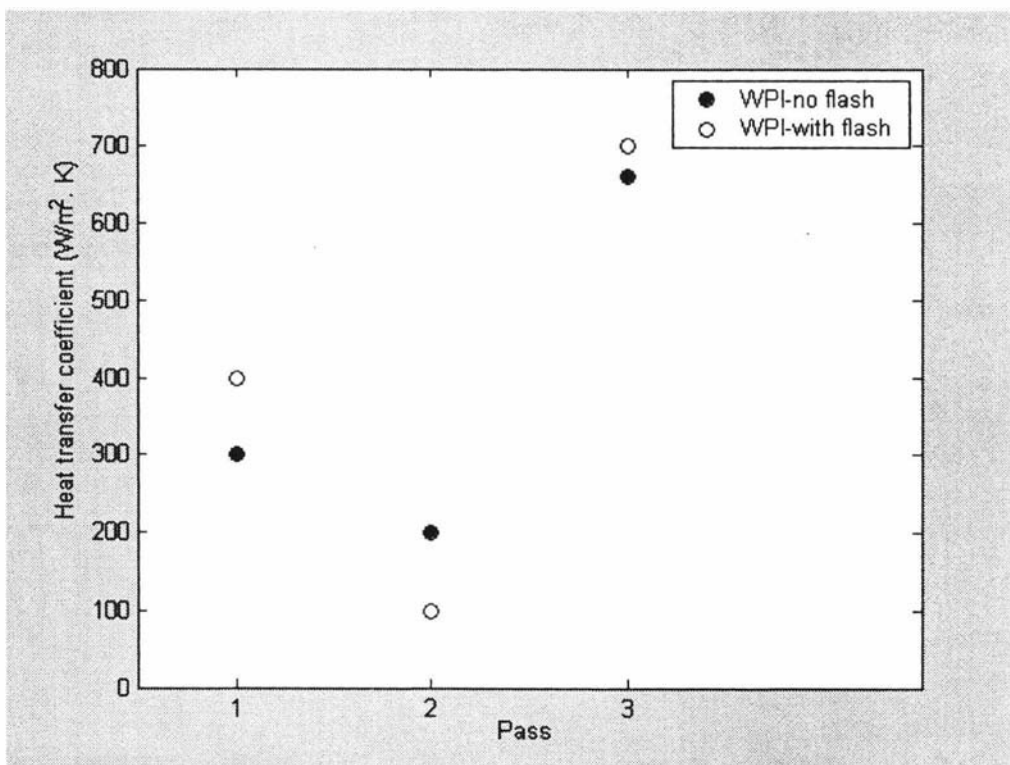
Figure 9.17: Comparison of overall evaporation heat transfer coefficients for WPI with and without flash at entry to the 1st effect

High protein content

WPI has the highest protein content of all the whey products (Chapter 2). To investigate the effect of protein content on the heat transfer coefficient, the performance of two different types of WPI (total protein content is the same but different types of whey protein due to different process steps involved) were compared as shown in Figure 9.18. The details of the whey proteins in these products are commercially sensitive and cannot be discussed in this section.
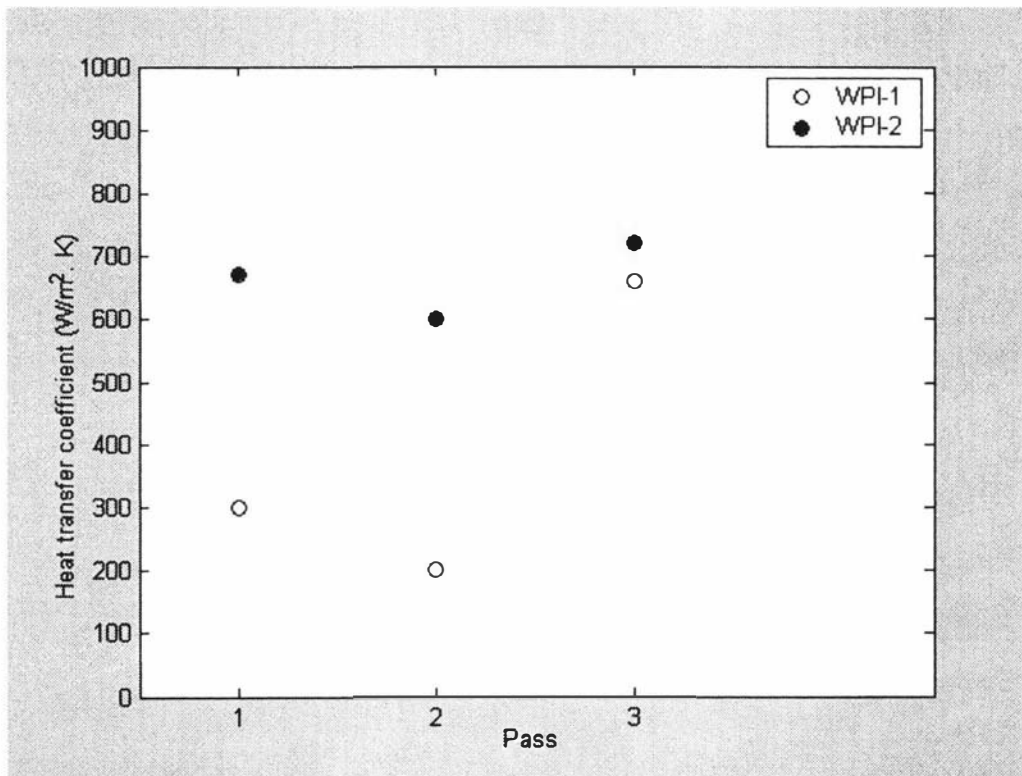
Figure 9.18: Comparison of overall evaporation heat transfer coefficients for different WPI specifications

The above comparison revealed that the protein content has no effect on the heat transfer coefficient. Therefore, the quantity of air present and the protein type of these WPI products have a strong influence in the evaporation. However, the types of whey protein and the manufacturing process are fixed for each WPI specification and cannot be altered. The protein-protein interactions and their state in the concentrate influence the foaming ability (Bickerstaff, 2002) and thus the heat transfer coefficient.

Large quantity of stable foam

The factors that affect the quantity and stability of the foam, and their relevance to whey products are discussed below.

1. Protein-protein interaction and type of protein: - The stability of foam increases with strong protein-protein interactions and with increasing protein concentration. The different whey products concentrated in the evaporator not only differ in the quantity of each component (protein, lactose, fat and minerals) but also the whey protein types in each product. This is due to the manufacturing requirements and the process steps. It is suspected that the presence of glycomacropeptide (GMP) in both WPC-1 and WPI enhance the foaming. The influence of glycomacropeptide on the heat transfer coefficient was not investigated as this was outside the scope of this project. Furthermore, there can be no adjustment to whey protein levels.

2. Air content: - Increasing air content in the product increases the foam volume and reduces the heat transfer coefficient, the later due to the low conductivity of air. It is generally expected that the air in the product will be released as it passes through the evaporator. However, due to the stable foam layers, complete removal of air is not possible. There was no method available for measuring the air content in the feed product, but visual and comparison tests were conducted. The density comparisons (model Vs measurements) in Chapter 3 and the 1st preheat condenser trials (in improving the performance of the 1st preheat condenser performance) further verified the presence of air content in the feed product. Pritchard (1997) conducted trials at Fonterra Marketing and Innovation to remove air from the feed WPI by means of a de-aeration system. The conclusions from Pritchard's experiments (1997) were,

   - It is possible to increase the solids concentration of WPI up to 42° Brix and maintain sufficient heat transfer without de-aeration.
   - There is a significant amount of air present and stable foam formed in the evaporation of WPI.
   - The nature of the product (WPI) and the cost of a de-aeration system present difficulties in removing air from the feed.

179

The experimental work of Pritchard (1997), and the preheat performance for WPI confirms that the poor evaporator performance for WPI is due to the air content in the feed product. The de-aeration option was not considered in this study due to the complexity and cost of the de-aeration system.

3. Operating conditions (pH and temperature): The operating parameters that influence foaming are temperature and pH. High temperature denatures the whey proteins and increases the low surface tension molecules at the air/ product interface. This, in turn, increases the formation of stable foam and thus reduces the evaporation heat transfer coefficient. The pH alters the net charge (pH at which the molecule has no net charge) of the whey proteins. Fox (1992) found that the quantity of foam is highest close to the isoelectric point of the whey products. The isoelectric point of WPI proteins is around 5.5 (Fox, 1992), and the operating pH in the range in the evaporator between 5.5 and 6. This is a processing requirement to ensure a high foaming property in the final product. Therefore, the only variable that can be adjusted is the operating temperature.

9.3.4 Trials at different temperatures to improve the HTC for WPI

Altering the operating temperature was found to be the most feasible means of solving the evaporation problems for WPI. The temperature profiles through the evaporation process for different whey products are given in Table 9.2.

Table 9.2: Current evaporator temperature profiles for different whey products

Product	Prehat Temperature (°C)	1st Effect Temperature (°C)	2nd Effect Temperature (°C)	1st Shell Temperature (°C)	Total Residence time (s)
WPC-1	-	46	40	55	67
WPC-2	32	44	40	53	63
WPC-3	34	44.5	40	53	63
WPI-1	60	50	40	63	77
WPI-2	52	44.5	40	53	67

There is no direct control over the effect temperatures, but the temperature of the product entering the 1st pass could be altered with modifications around the preheat condensers. No reports on the influence of temperature on the evaporation heat transfer coefficient were found in the open literature. Therefore, trials were conducted to correlate the feed temperature and the heat transfer coefficient. The trials that were planned are discussed below.

- Trial-1: The aim of this trial was to completely prevent flash on entry to the 1st effect without preheating prior to the evaporator. This was achieved by installing a plate heat exchanger to cool the product just before the product enters the 1st pass of the evaporator.
- Trial-2: The aim of this trial was to feed the product at 40°C without the preheating prior to the evaporator. This was achieved by bypassing the 3rd preheat condenser with a flexi hose.
- Trial-3: The aim of this trial was to feed the product at 16°C without preheating prior to the evaporator. This was achieved by bypassing both the 2nd and 3rd preheat condensers and part of the 1st preheat condenser.
- Trial-4: The aim of this trial was to feed the product at 25°C with preheating prior to the evaporator. This was achieved with the cooling plate heat exchanger installed just before the 1st pass.

The trials were conducted in the order listed above, and the results are shown in Figures 9.19 and 9.20. Figure 9.19 shows the evaporation heat transfer coefficients for all trial runs while Figure 9.20 shows the feed density against the solids concentration. Results of two different trials that showed completely different performance are shown in figure 9.19. The performance of the Thermal Vapour Re-compressor during normal operation and the trials is shown in Figure 9.21. The temperature profiles through the evaporator for each trial are tabulated in Table 9.3.
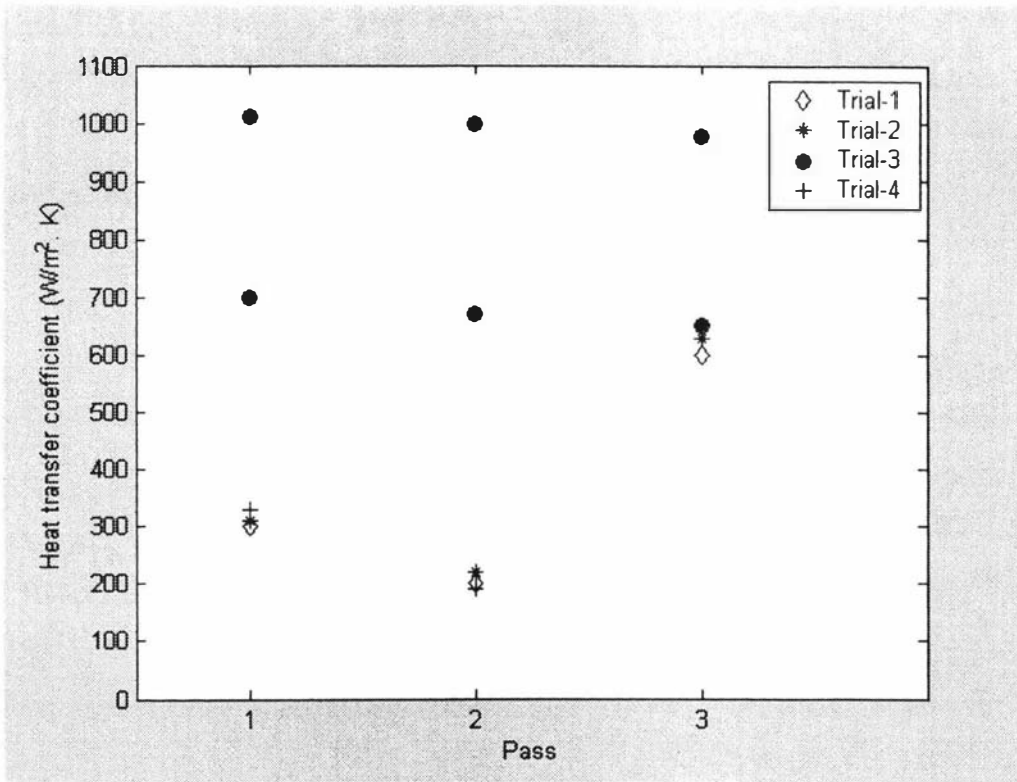
Figure 9.19: Comparison of overall heat transfer coefficients for different feed temperatures
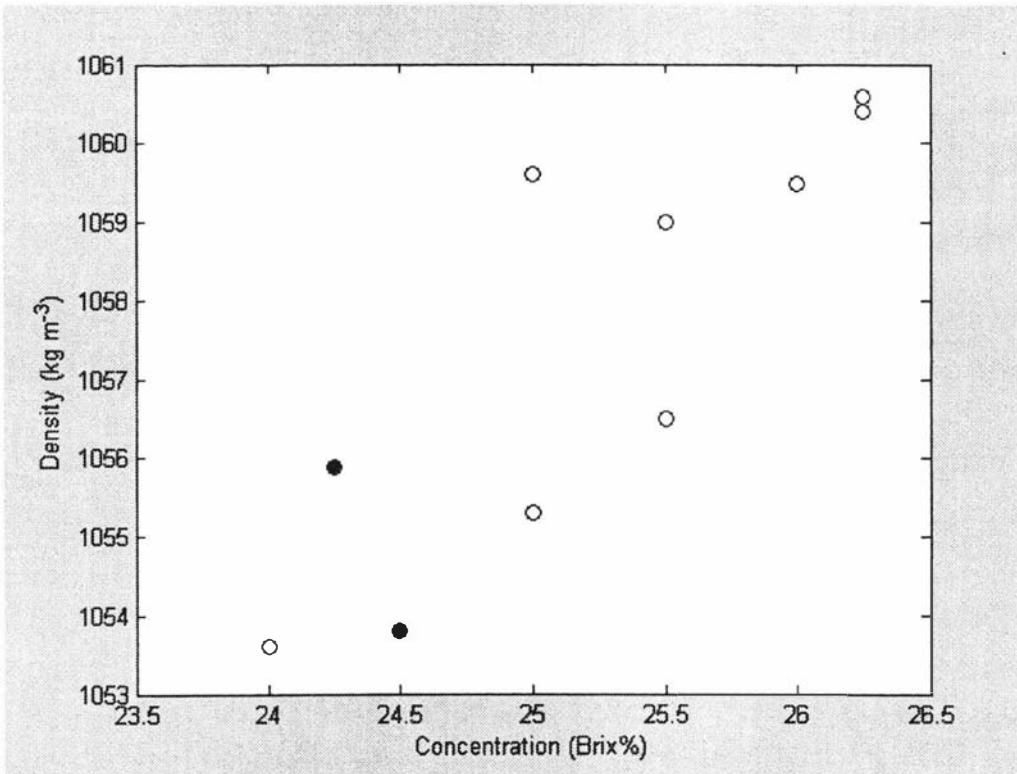
Figure 9.20: Comparison of feed solids and the density with the trial products

The trial heat transfer coefficient results shown in Figure 9.19 suggest that the resistance to evaporation is low at very low feed temperature (Trial-3). The difference in heat transfer coefficients for separate runs during trial-3 was due to different air contents in the feed product. This can be clearly seen from Figure 9.20 (highlighted data points). The different states of whey protein at low and high temperatures influence foaming due to lower surface tension at high temperatures. Therefore, the temperature of the product entering the evaporator and the air content in the feed whey influence the mass of evaporation significantly.

Table 9.3: Evaporator temperature profiles for the trial runs

Product	Feed Temperature (°C)	1st Effect Temperature (°C)	2nd Effect Temperature (°C)	1st Shell Temperature (°C)	Residence time (s)
Trial-1	40	50	40	60	77
Trial-2	40	48.5	40	59	72
Trial-3	16	44.5	40	53	27
Trial-4	25	48	40	60	77

The improvement in heat transfer coefficients during trial-3 not only increased the mass of evaporation but also reduced the product temperature profile in the evaporator. This is an advantage as whey protein is prone to denaturation at elevated temperatures. The disadvantage of low feed temperature is that the first part of the evaporating tubes is used to heat up the feed product to its boiling temperature. From the energy balances (sensible heat = heat transfer through unknown surface area of the tubes) it was estimated that 10% of the surface area in the first pass was used up in heating the feed during trial-3. Trial-4 was conducted at a higher temperature (25°C) to increase the surface area for evaporation. This suggests that the whey protein undergo a irreversible reaction on heat treatment.

The improvement in evaporator performance for WPI at low feed temperature increased the thermal efficiency of the TVR as can be seen in Figure 9.21. The TVR compression ratio for WPI is compared with all whey products. The discharged vapour pressure dropped with the increased heat transfer coefficient in the 1st effect.

183
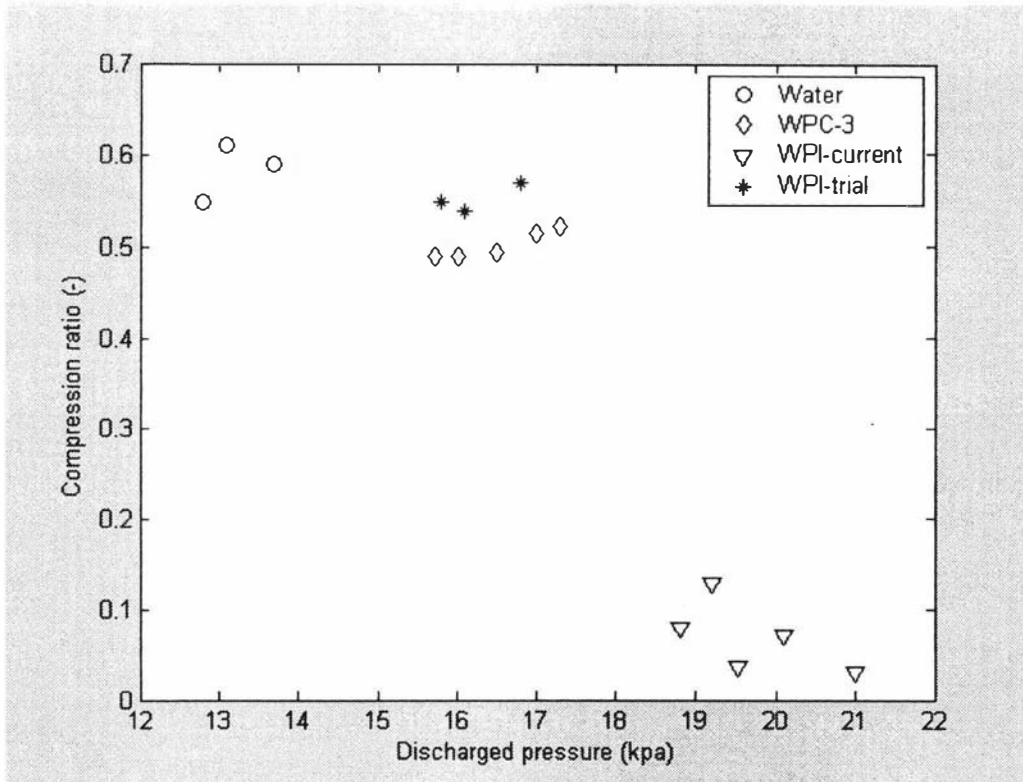
Figure 9.21: Comparison of TVR compression ratio for different products at current and trial operating conditions

9.4 Optimum operating regime

The evaporator has to operate close to the optimum operating conditions in order to maximise the throughput and reduce the operating cost. From the investigation of the evaporator constraints together with the trials discussed in the previous section, the optimum operating conditions for each whey product were chosen. These values are tabulated in Table 9.4.

Table 9.4: Optimum evaporator operating conditions for different products

Product	Maximum Concentration (%)	Feed Temperature (°C)	2nd effect Temperature (°C)	Feed flow (m³/hr)	Preheat condensers	Steam valve (%)
Water	-	-	-	8.5	-	30
WPC-1	36	< 40	44	-	1st full/ Partial	100
WPC-2	35	40	44	-	1st	100
WPC-3	35	40	44	-	1st	100
WPI	40	16	44	-	1st Partial	100

The key advantages of setting the evaporator parameters according to the table are,

1. Increased throughput and reduced operating cost.
2. Reduced energy cost.

9.4.1 Increased throughput and reduced operating cost

Increased throughput in the WPI powder process is achieved through feeding the common WPI specification product at a lower temperature. This can be achieved by bypassing the 2nd and 3rd preheat condensers attached to the evaporator. With this modification, the feed flow was increased from 6.5m³/hr to 7.5m³/hr and the powder throughput increased from 1436kg/hr to 1663kg/hr. This is approximately a 15% increase in the current powder production. For example, for the concentrate solids increased from 28% to 32% with a feed flow of 6840 kg/hr at 21.5% solids, there will be a 656.5 kg/hr increase in the evaporation in the evaporator. This reduces the evaporation load in the dryer and therefore the energy used for spray drying.

The estimated saving from the increased evaporator performance for WPI is NZ$32,000/season (19.695/hr, based on 100 days/season, 5hr/run, $30/t of water evaporation in the dryer, Winchester (2000)). This saving was estimated only from the energy savings from the dryer. The increase in throughput was not taken into account. The evaporator performance for WPC-1 is similar to that of WPI, and this could also be improved by operating at low feed temperature. However, trials with WPC-1 were not carried out as this was not a common product at the time of the project.

9.4.2 Reduced energy cost

Energy savings in the evaporator can be achieved through using the condensate to heat the feed to the required temperature and by controlling the steam pressure effectively to reduce unnecessary evaporation during the water run and during CIP.

The temperature and volume of condensate from the shell of the evaporator is sufficient to lift the cold feed product temperature to the same as that currently exiting the 3rd preheat condenser. This can be achieved by installing a heat exchanger after the 1st preheat condenser. The total estimated savings from this are NZ$19,440/season (200 days/season, 5hr/run, $24/t of steam).

The evaporator must be cleaned (CIP) after each run to clear all the milk deposits in the line. To achieve this there should be less evaporation during this cleaning to ensure more liquid flow through the tubes and pipes. The operating conditions during the water and CIP runs are currently the same as the conditions during production. This energy is wasted and does not enhance effective cleaning. The estimated savings if the motive steam operated at 5bar during the water run and 7 bar during the CIP run (compared to 10 bar currently) is NZ$18,532/season (650 runs/season, 3hr/CIP & water, $24/t of steam). In addition to this energy saving, the lower steam pressure will help ensure sufficient liquid flows for effective cleaning. The relationship between motive steam pressure and control valve position for the Whareroa whey evaporator is shown in Figure 9.22.
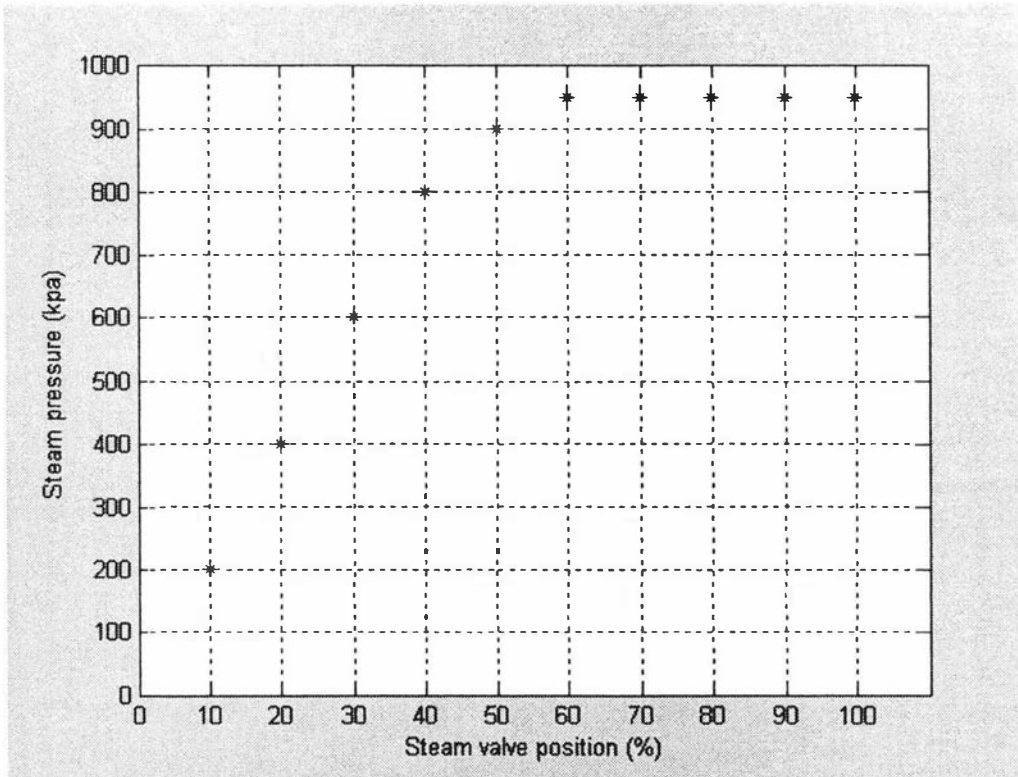
Figure 9.22: Motive steam pressure supplied to the evaporator as a function of control valve position

9.5 Conclusions

Low heat transfer coefficients

Low heat transfer coefficients for WPC-1 and WPI were found to be due to high viscosity and foaming in the evaporator rather than film-breakdown. The heat transfer coefficients predicted for WPC-3 suggest that the viscosity strongly influenced the heat transfer. WPC-3 is the most viscous solution of the three investigated in this study. Therefore, no further research was carried out with WPC-3. The viscosity of WPI is significantly lower compared to that of WPC-3, but the heat transfer coefficients for WPI were nevertheless significantly lower than those for WPC-3. This suggests a significant influence of foaming and protein composition on heat transfer coefficients for WPI. The heat transfer coefficients predicted by the falling-film model further validate this. Further investigation was conducted to improve the heat transfer coefficients without affecting product quality.

A plant trial was conducted where the temperature of the feed was kept below 20°C before entering the evaporator. This prevented flash as well as reducing protein denaturation and thus the quantity of foam. During this trial, less foam was observed through the sight glass on the distribution plate, and the heat transfer coefficients were significantly improved. Maintaining the temperature below 20°C therefore improves the heat transfer but slightly reduces evaporator capacity due to the need for sensible heating to bring the feed to boiling temperature. An alternative way to avoid foaming would be to de-aerate the feed. However, Mike (1995) found difficulties associated with de-aerating WPI. The large carry-over and requirement for additional plant were the main problems with de-aeration.

2.1   TVR compressor

The TVR performance depends on the heat transfer coefficient and on the motive steam pressure. Compressor performance was compared for operation with WPC-3, WPI and water. The discharge pressures, and thus the compression ratios, are markedly different between these products. The low compression ratio and high discharge pressures observed for WPI were due to the low heat transfer coefficients in the 1st effect. The

improvements in the heat transfer coefficient led to a significant improvement in the TVR performance. It was shown that the recycle vapour flow is strongly dependent on the discharge pressure and thus on the 1st effect heat transfer coefficients.

Preheat condenser performance

The preheat condenser showed differing performance with different products due to the difference in viscosities and the air content in the feed. This was confirmed by re-routing the de-aeration line to the vacuum line instead of the 1st preheat condenser thereby reducing the air in the heating media. The performance of the preheat condenser was significantly improved for WPI, but was unchanged for WPC-3.

Film breakdown

Evaporator flow measurements and theoretical minimum flow predictions suggest that there is little risk of film breakdown during product runs, but that film breakdown may occur while running water. This is because whey products have very low surface tension compared to water. Film breakdown while running water is very likely in the 2nd effect, as most of the water evaporation takes place in the 1st effect. Therefore, higher water flows are required to avoid fouling due to film breakdown in the 2nd effect. It was also shown that the water flow rate prior to the product run is not sufficient to wet the tube surface and that film breakdown is unavoidable. Higher water flows are required during start up and should be reduced after start up on a timer or product density basis.

Optimum operating regime

The optimisation studies have identified the optimum operating conditions for whey products and water. The studies and experiments in the commercial plant have shown a significant increase in throughput (15). Whey products are rich in whey proteins which are sensitive to temperature. Under new operating conditions, evaporation is improved significantly without increasing the evaporator temperature profile. The new settings give a lower temperature profile which improves product quality and functionality through reduced denaturation of the whey proteins.

189

10. Controllability Studies

In this section the falling-film evaporator control objectives and the control variables are discussed. The control loops are then investigated separately for the ability to reject the disturbances in the process. Finally, the design and application of a cascade controller to control the product concentration is discussed

10.1 Process control

Process control is the methodology for keeping a process within boundaries or minimizing the variation of a process. A process must satisfy several requirements (safety, production specifications, environmental regulations, operational constraints and economy) imposed by its designers and the general technical, economic and social conditions in the presence of ever-changing external influences (disturbances). These requirements dictate the need for continuous process monitoring and external intervention (control) to guarantee the satisfaction of the operational objectives. Therefore, the process control system is vital to:

- Suppress the influence of external disturbances.
- Ensure the stability of the process.
- Optimise the performance of the process.

10.2 Control in a falling-film evaporator

Three types of variables must be considered in any control system, process variable, manipulated variable and disturbance variables (independent variables). A process variable is the measured parameter that is held at a target value in a control loop by changing the manipulated variable. A manipulated variable is a process stream that is adjusted by some control algorithm to hold the process variable at a target value. Disturbance variables are inputs to the process that are not controlled by the specific control system under investigation.

191

The variables that are relevant to falling-film evaporator control are listed in Table 10.1. Figure 10.1 shows these variables diagrammatically.

Table 10.1: Control variables in the TVR falling-film evaporator

Process Variables	Manipulated Variables	Disturbance Variables
Product concentration(w_{p3})	Steam pressure (P_{steam})	Feed concentration (w_f)
2nd effect temperature (T_{e2})	Cooling water flow (M_{cw})	Feed temperature (T_f)
Product flow rate (M_{p3})	Feed flow rate (M_f)	Cooling water temperature (T_{cwin})
		Steam supply(P_{steam})

Product density (rather than concentration) is the fundamental process variable in the falling-film evaporator. However, the model developed in Part-1 can be used to predict density from the product total solids concentration with less than 1% error. Therefore, product concentration was used as the process variable in the control studies instead of density.
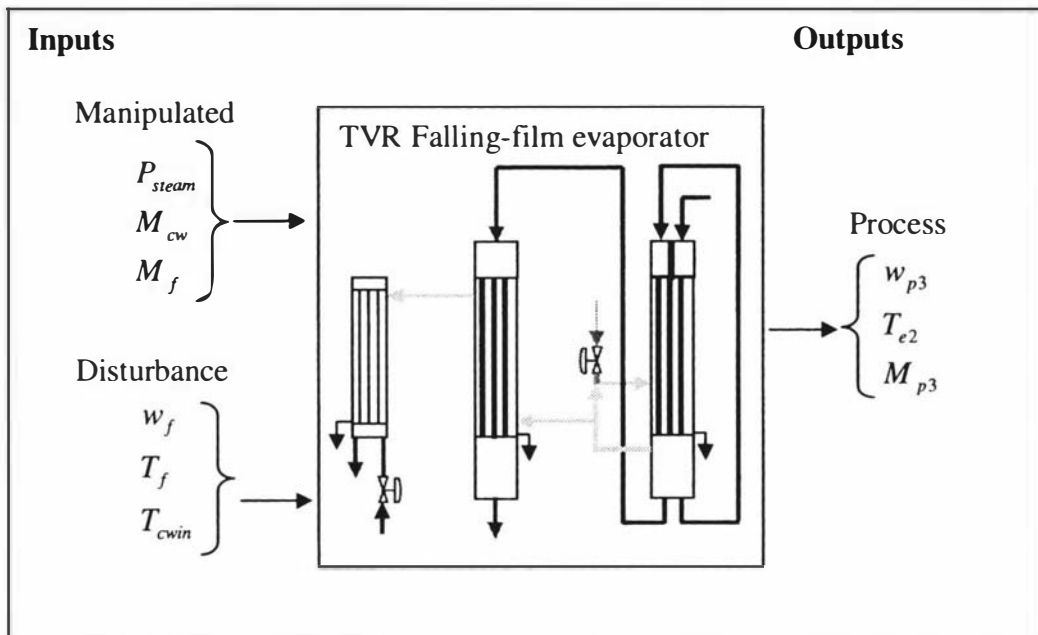
Figure 10.1: Control variables in the TVR falling-film evaporator

10.3 Evaporator controllability analysis

The TVR falling-film evaporator at Fonterra Ingredients-Whareroa, Fonterra Co-op Group Ltd is used to concentrate a variety of products (Chapter 2). The control ability of the evaporator was studied with WPC-3 for the following reasons.

- Product concentration for both WPC-1 and WPI is always below the target concentration due to poor evaporator performance (Chapter 9).
- WPC-1 and WPC-2 were not common products during this project.
- WPC-3 has a long falling film residence time compared to WPI.

Scaling and Relative gain array

Scaling is very important in practical applications as it makes model transfer function analysis meaningful. It requires a judgement at the start of the design process about the required performance of the system. To do this, decisions are made on the expected magnitudes of disturbances and reference changes, on the allowed magnitude of each input signal, and on the allowed deviation of each output. The scaling parameters for the evaporator are listed in Table 10.2 and the scaled steady state gains are shown in Table 10.3.

Table 10.2: Scaling parameters for controllability analysis

Variables	Scaling value	Units
w_{p3}	0.01	(kg/kg)
w_f	0.01	(kg/kg)
T_{e2}	1	°C
T_f	3	°C
T_{cwin}	3	°C
M_f	0.5	kg/s
M_{cw}	1	kg/s
P_{steam}	2	bar

Table 10.3: Scaled static process gains for the evaporator with WPC-3

Manipulated variables → Steady state values → Process variables ↓	P_{sp} = 9.5 bar	M_f = 1.92 kg/s	T_f = 11 °C	w_f = 0.205 kg/kg	M_{cw} = 6.8 kg/s	T_{cw} = 17 °C
T_{e2} = 39.53 °C	4.1060	-1.5527	0.7668	0.0309	-0.7348	1.9569
w_{p3} = 0.342 kg/kg	4.1600	-3.4000	0.1500	1.6700	0.0008	-0.2400
M_{p3} = 1.151 kg/s	-0.2668	1.0406	-0.0108	-0.0008	-0.0054	0.0150

The relative gain array method was used to pair the control loop variables in the falling film evaporator. The relative-gain array (RGA) has been widely used as a measure of process interactions and as a tool for control structure selection for decentralised (multi-loop) control systems. Many fundamental closed-loop system properties, such as stability and decentralised integral controllability have been developed based on the open-loop RGA. Furthermore, because plants with large RGA elements are very sensitive to modelling errors, the RGA can be used as a sensitivity measure with respect to model uncertainty.

There are three process variables (w_{p3}, T_{e2}, M_{p3}) that need to be controlled in the TVR falling-film evaporator by three manipulated variables (P_{steam}, M_{cw}, M_f). The static relative gain array was calculated from the evaporator scaled state gains and is shown in equation (10.2).

$$
RGA = \begin{matrix} w_{p3} & T_{e2} & M_{p3} \\ \begin{bmatrix} 1.2983 & -0.0291 & -0.2692 \\ 0.0012 & 1.0151 & -0.0164 \\ -0.2995 & 0.0139 & 1.2856 \end{bmatrix} & \begin{matrix} P_{steam} \\ M_{cw} \\ M_f \end{matrix} \end{matrix}
\tag{10.2}
$$

The static relative gain array shows that all of the diagonal elements are positive and therefore that the correct control loop pairings have been chosen for the evaporator ($w_{p3}/P_{steam}, T_{e2}/M_{cw}$ and M_{p3}/M_f). There will be interaction between the product concentration and product flow loops and this is inevitable. The high frequency

variability in product flow rate can be tolerated (concentrate balance tank) and so the focus is on minimising variation in product concentration. Therefore, the product flow rate control is ignored and only product concentration and 2nd effect temperature loops were considered.

10.4 Control loops performance

The whey product evaporator has two key control loops, product concentration and 2nd effect temperature control, as shown in Figure 10.2. The first control loop, total solids concentration exiting the evaporator, is an important control loop in the evaporation operation as it affects the spray dryer performance (where the concentrate is converted into powder). The dryer should be supplied with consistent concentrate total solids to achieve consistent powder quality. Any disturbance that occurs in the evaporation process should therefore be rejected before it significantly affects the concentrate total solids.

The second key control loop in the evaporation process, regulation of the second effect temperature, is also important as it affects the evaporator temperature profile. This control should be fast enough to reduce interactions with the concentration control.

The motive steam flow and the cooling water flow are the manipulated variables in controlling the product concentration and the 2nd effect temperature respectively. The complete evaporator linear model connections are shown in Figure 10.3 with delay terms.

195
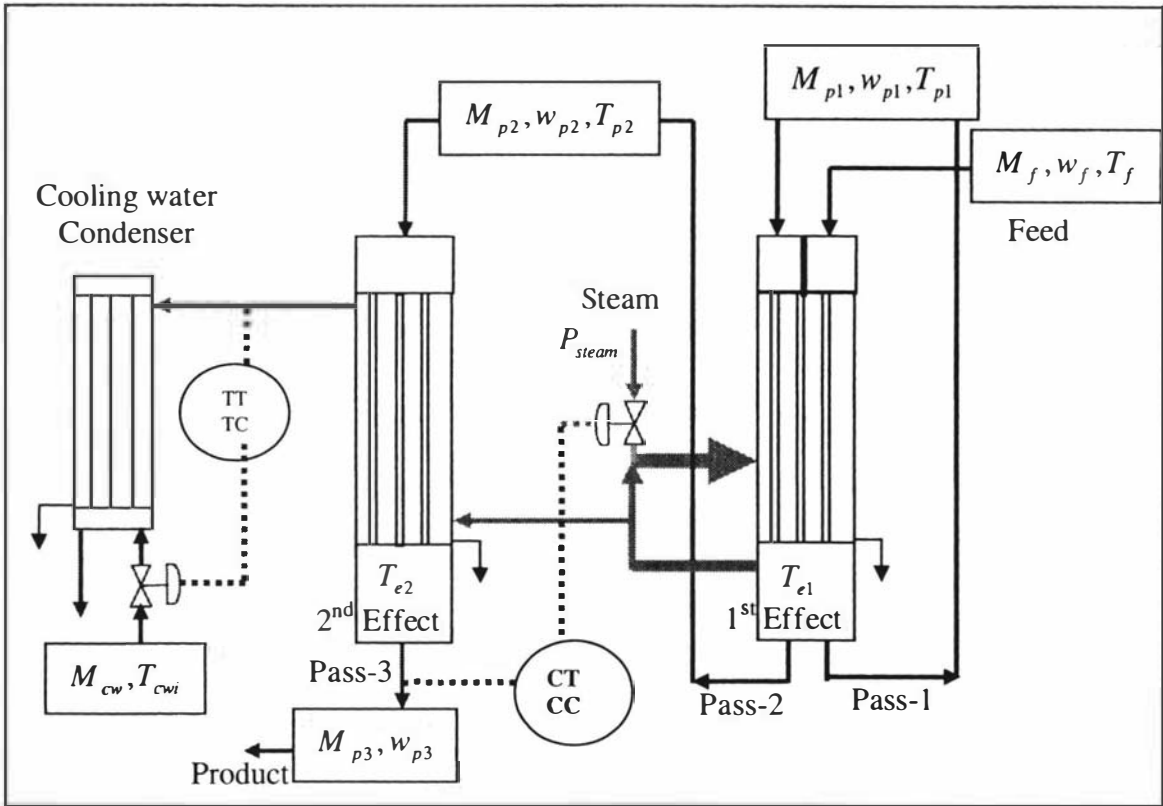
Figure 10.2: Falling-film evaporator control loops

10.4.1 Disturbances in the evaporator

The disturbances to the evaporation process are the feed total solids concentration, the feed temperature, the cooling water inlet temperature and the main steam pressure. The steam pressure entering the evaporator is controlled and the response is quick (Winchester, 2000) so that the steam pressure can be assumed equal to the set point $\left(P_{steam} = P_{steam}^{sp}\right)$. The effects of other disturbances $\left(w_f, T_f, T_{cwi}\right)$ on the controlled variables were investigated. It is clear from the scaled static gains that the feed total solids concentration $\left(w_f\right)$ has a significant effect on the product concentration $\left(w_{p3}\right)$ while the other disturbances $\left(T_f, T_{cwi}\right)$ are insignificant. Similarly, the effect of cooling water feed temperature $\left(T_{cwi}\right)$ has a significant effect on the 2nd effect temperature $\left(T_{e2}\right)$ compared to the other disturbances $\left(T_f, w_f\right)$.
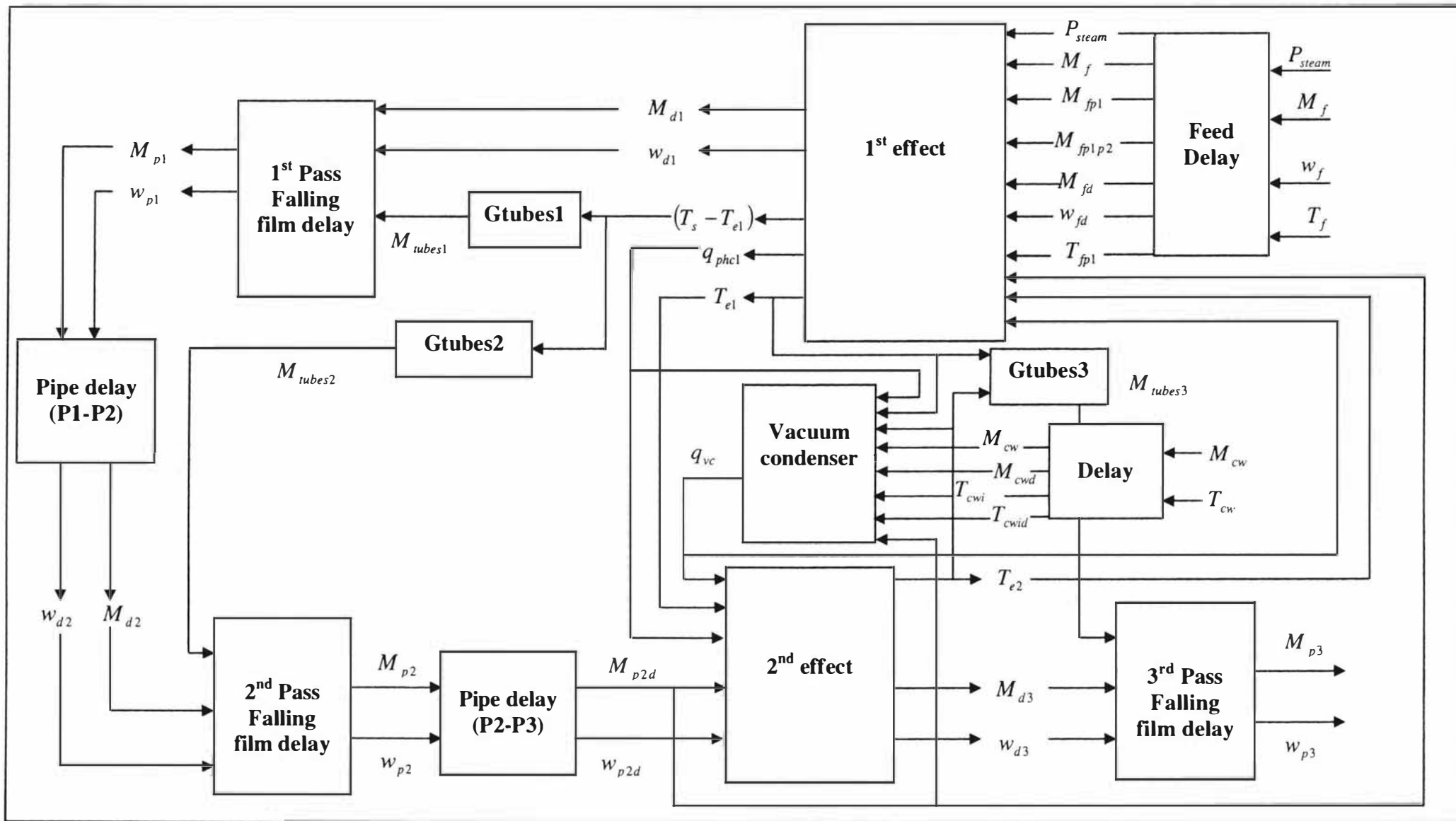
Figure 10.3: Three-pass evaporator linear models interconnections

Figure 10.4 shows the effect of feed flow to the distribution plate on the discharge flow from the distribution plate $\left(\dfrac{M_d(s)}{M_f(s)} = \dfrac{1}{(\tau_{hd} s + 1)} \right)$ .It can be seen from the Figure 10.4 that the distribution plates filter out some of the high frequency disturbances, depending upon the liquid height. This would increase the disturbance rejection bandwidth that one expected to achieve with the controller. The ability to reject the disturbances and the improvements in disturbance rejection bandwidth of those control loops are discussed in the following sections. A similar case can be observed for the effect of feed solids to the distribution plate on the discharge solids from the distribution plate $\left(\dfrac{w_d(s)}{w_f(s)} = \dfrac{1}{(\tau_{wd} s + 1)} \right)$.
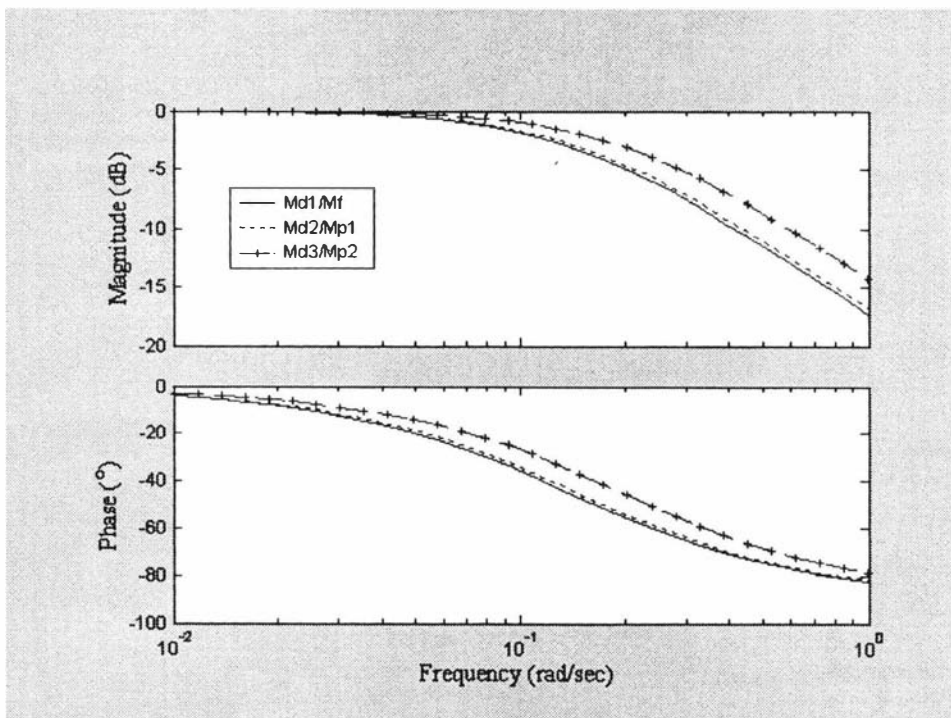
Figure 10.4: Bode plot of disturbance transfer functions (effect of feed flow on the exit flow from the distribution plate)

197

10.4.2 2nd effect temperature control

Figure 10.5 shows the effect of disturbances on the 2nd effect temperature. The process

and disturbance transfer functions are $\left(\dfrac{T_{e2}(s)}{M_{cw}(s)}\right)$ and $\left(\dfrac{T_{e2}(s)}{T_{cwi}(s)}\right)$ respectively. Since the

phase crossover frequency of the process transfer function is much greater than the gain

crossover frequencies of the disturbance transfer function, the controller will be able to

reject disturbances. There will be no saturation problem as the gain of the disturbance

transfer function is less than the process transfer function.
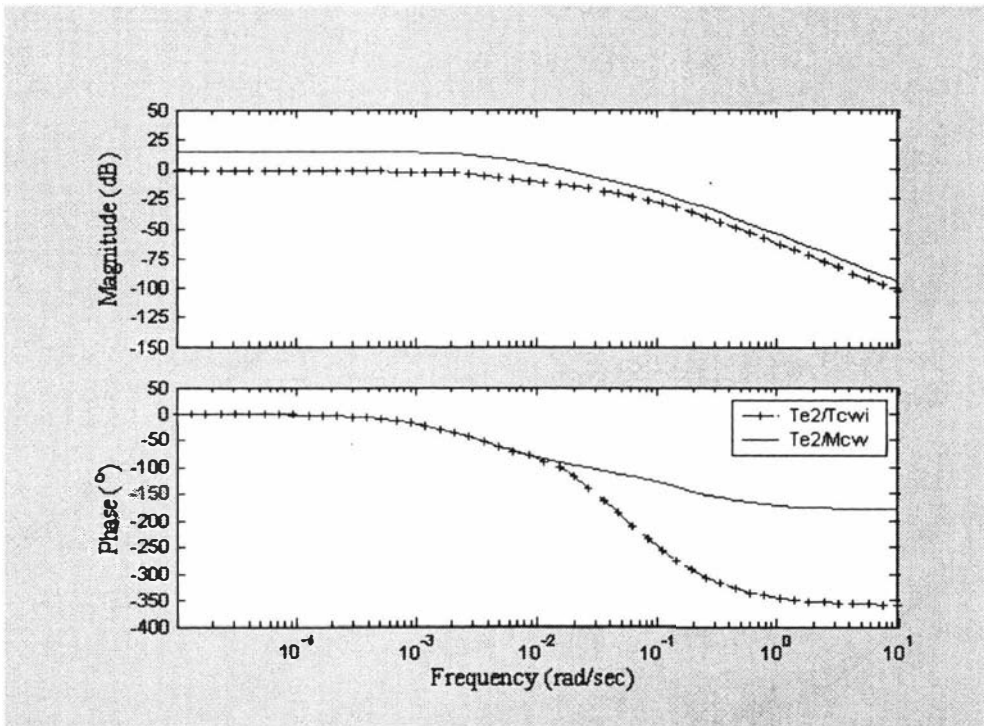
**Figure 10.5: Bode plot of transfer functions (effect of disturbances
and the manipulation on the 2nd effect temperature)**

The PI controller parameters were chosen $\left(T_i = 67s, K_c = 20\right)$ using the technique set

out by Skogestad and Postlethwaite (1996) for SISO systems. The closed loop gain of

the disturbance transfer function is reduced throughout the entire frequency range as can

be seen from the Figure 10.6. This confirms the ability of the 2nd effect temperature

control loop to better reject cooling water inlet temperature disturbances. The response

of this control action is very quick so that the assumption of constant 2nd effect temperature in the concentration control analysis in the following section is justified.
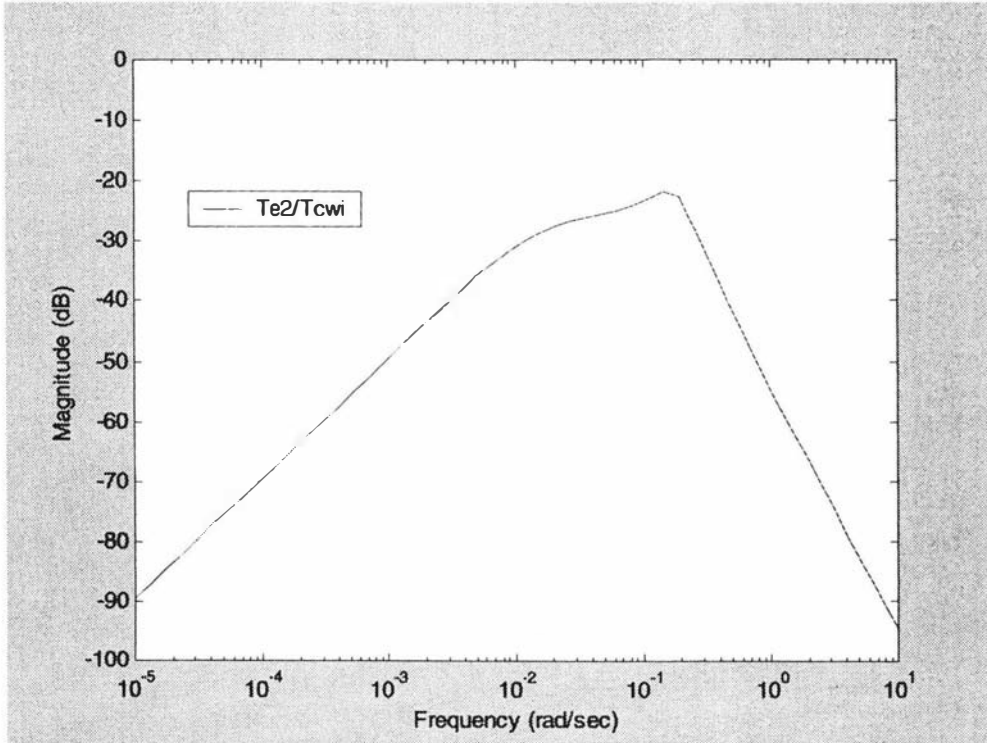
Figure 10.6: Magnitude bode plot of closed loop disturbance transfer function

10.4.3 Product concentration control

It has already been shown in section (10.3.1) that the significant disturbance to the product concentration is the feed solids concentration. Figure 10.7 shows the effect of steam pressure (P_{steam}^{sp}) and the feed solids concentration (w_f) on the concentrate total solids concentration (w_{p3}). The model transfer functions for the process and disturbance are $\left(\dfrac{w_{p3}(s)}{P_{steam}^{sp}(s)} \right)$ and $\left(\dfrac{w_{p3}(s)}{w_f(s)} \right)$ respectively.

199

The phase crossover frequency of the transfer function $\left(\dfrac{w_{p3}(s)}{P_{steam}^{sp}(s)} \right)$ is less than the gain

cross over frequency of the $\left(\dfrac{w_{p3}(s)}{w_f(s)} \right)$ transfer function. Therefore, the product

concentration control loop has disturbance rejection problems. This is due to the large

time delay in the falling film evaporator.
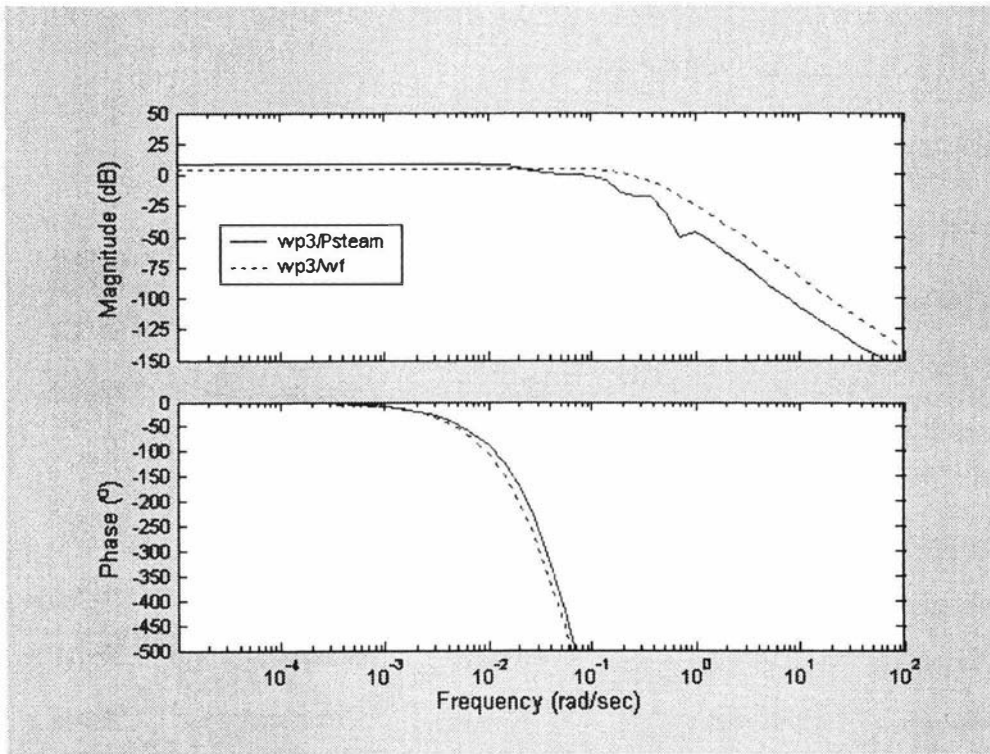
**Figure 10.7: Bode plot of transfer functions (effect of disturbances
and the manipulation on the product concentration)**

Since the gain of the process transfer function is greater than the disturbance transfer

function at low frequencies, there will not be any saturation problems. However the

ability of the concentration control loop used in the falling film evaporator (Figure

10.8), to reject disturbances was investigated.
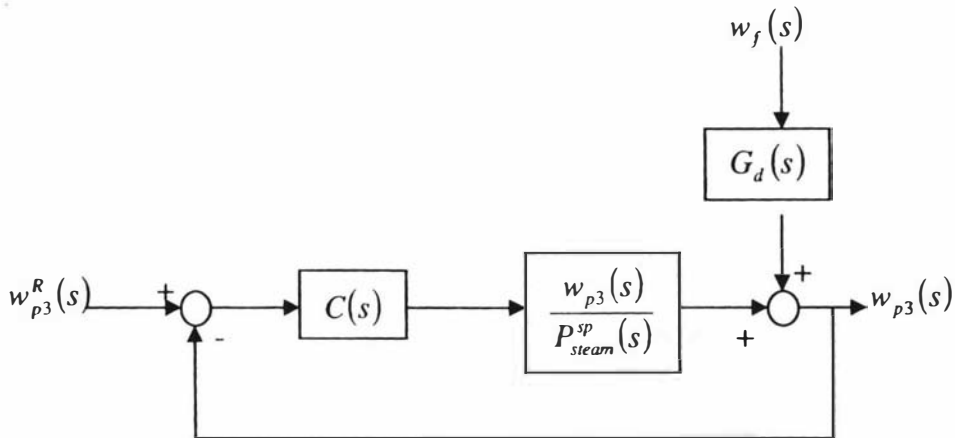
Figure 10.8: Single loop feedback control of product solids concentration
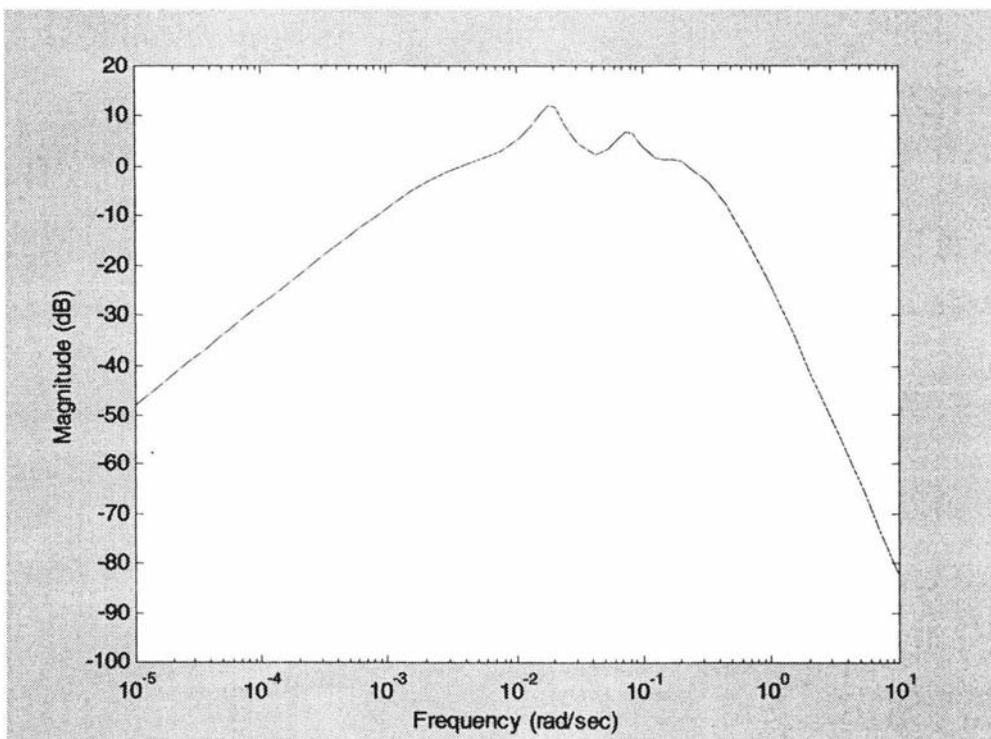
Figure 10.9: Magnitude bode plot of closed loop disturbance transfer function

The PI controller parameters $(T_i = 200s, K_c = 30)$ for the concentration control loop were chosen using the technique set out by Skogestad and Postlethwaite (1996) for SISO systems. The bode plot of the closed loop disturbance transfer function is shown in Figure 10.9. The disturbance gain is not low enough close to the crossover frequencies and thus the rejection bandwidth is low (0.006 rad/sec).

The concentration control loop will therefore have disturbance rejection problems. This prompted further study on the application of alternative control strategies to control product concentration. Since the surrogate process variable (solids dry matter exiting the 1st pass) can be measured, the impact of the disturbance is observable and where it can be substantially rejected (there is less phase lag), the applicability of cascade control was investigated in the first instance. The design of a cascade controller and the improvements in the disturbance rejection bandwidth are discussed in the following section.

10.5 Cascade controller application to control product concentration

A study on the applicability of cascade control to control the product concentration in falling-film evaporators was conducted. The linear dynamic models for this system were developed in Chapter 8. The interconnections for the linear models of all three passes of the evaporator are shown in Figure 10.10. The necessary transfer functions for the analyses were drawn from this model.

10.5.1 Cascade controller design

The primary process variables in the whey evaporator are the product total solids concentration (w_{p3}) and the 2nd effect temperature (T_{e2}). It was shown in the previous section that the 2nd effect temperature control loop can reject the cooling water temperature disturbances quickly enough so that the 2nd effect temperature can be assumed to be constant in this study.

The process variable of interest is therefore the product concentration exiting Pass-3 (w_{p3}) and the manipulated variable is the steam pressure (P_{steam}^{sp}). It has been shown (section 10.3.1) that the principle disturbances arise due to variation in the feed concentration (w_f). For the purpose of this study, ideal control was assumed in the second effect temperature loop, i.e. the second effect temperature is held constant. The disturbances in the feed concentration have a significant effect on the primary process
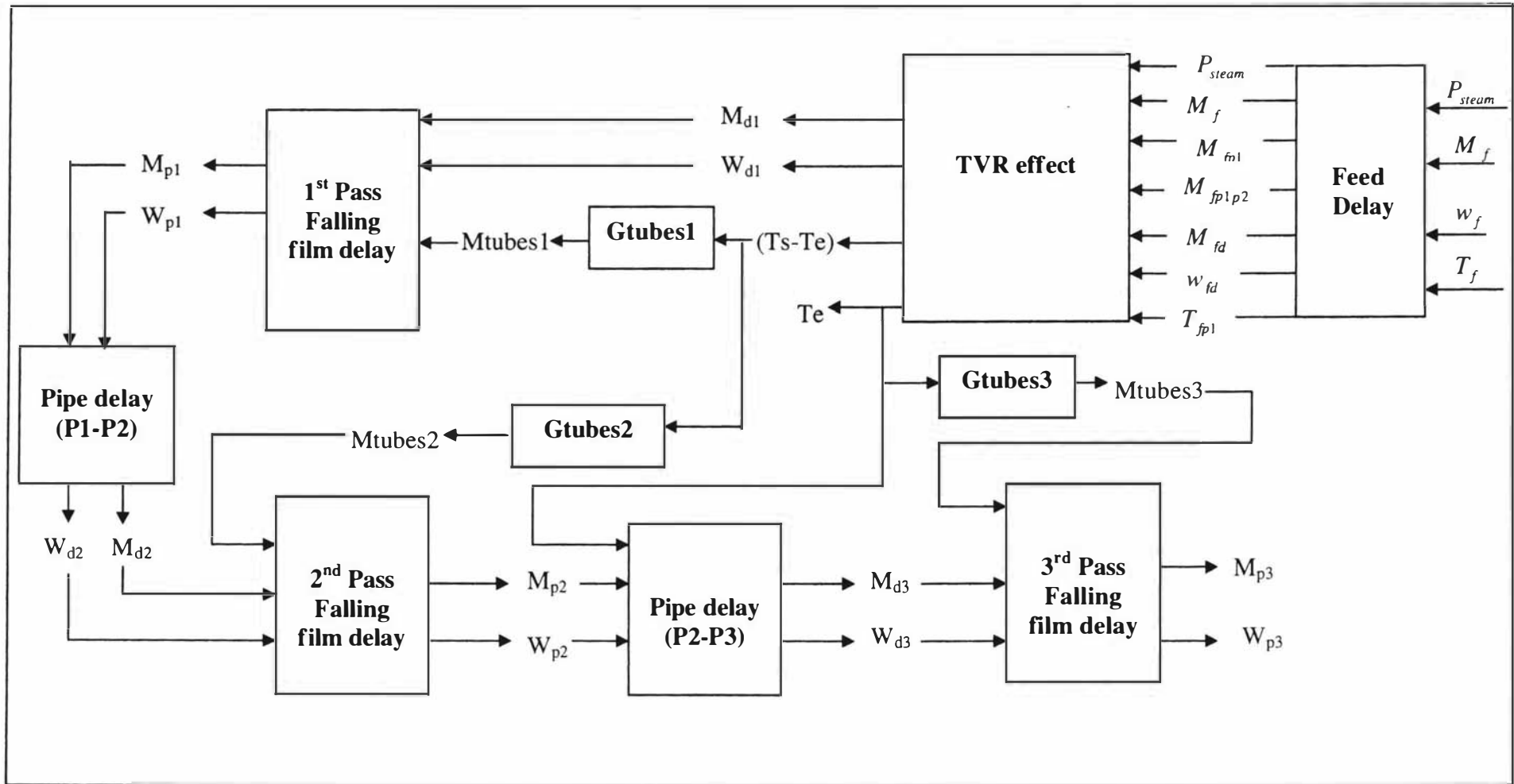
Figure 10.10: Three-pass evaporator linear models interconnections $\left(T_{e2} = T_{e2}^{sp}\right)$

variable up to a high frequency (0.5 rad/sec) since there is little natural attenuation of the disturbance. Thus, a controller with a high disturbance rejection bandwidth is needed. The disturbance rejection bandwidth of the controller is constrained by the phase crossover frequency of the plant, which is low due to the large delays, and thus it is not possible to achieve the bandwidth sought. This problem can be partially ameliorated by measuring the concentration exiting Pass-1 and using it as a surrogate process variable in a cascade control approach (Figure 10.11).
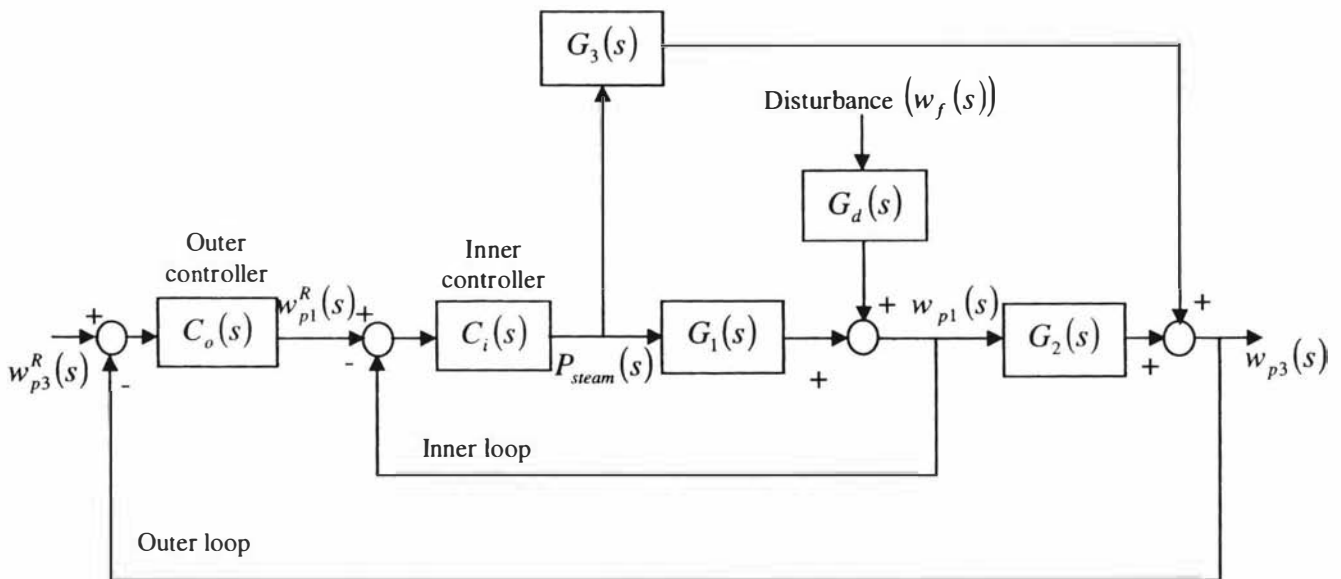
Figure 10.11: Block diagram of the modified cascade control loop for product concentration control

There is one key difference between the cascade problem here and the conventional cascade control architecture, as shown in Figure 10.12. In this case (Figure 10.12) only part of the effect of the manipulated variable, P_{steam}, is observable through the surrogate process variable, w_{p1}. The manipulated variable has a direct effect on the primary process variable as described by the transfer function $G_3(s)$ in Figure 10.11. Physically: manipulating the motive steam supply pressure will affect the temperature difference across the whole first effect, (that is Pass-1 and Pass-2), and it will also affect the temperature difference across Pass-3 or the second effect. Transfer Function $G_1(s)$ captures the effects of the changes in temperature difference for the first pass and $G_3(s)$ the effects of temperature difference for Pass-2 and Pass-3.

The implication of this is that the usual tuning technique for cascade control (tune the inner loop first and then tune the outer loop with the inner loop fixed) can not be adopted, verbatim, in this case.
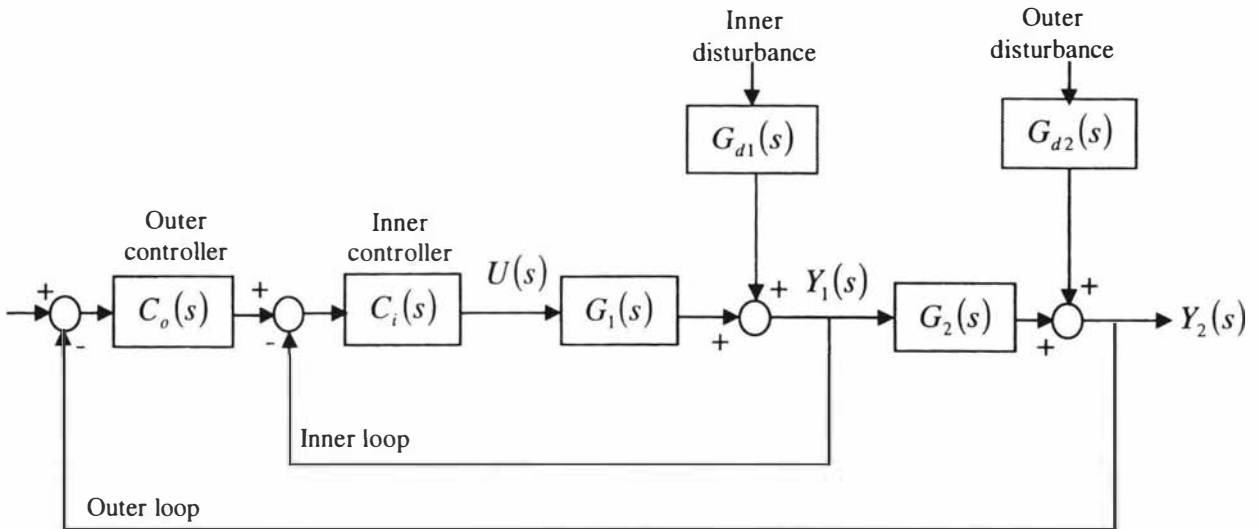
Figure 10.12: Block diagram of a conventional cascade control loop

10.5.2 Block simplification and analysis

Control analysis by the block reduction method has the advantage of affording a better understanding of the contribution of each component than is possible by the manipulation of equations. Figure 10.11 shows the block diagram for the cascade closed-loop control of product concentration in the falling-film evaporator shown in Figure 10.2. This was reduced to the block diagram shown in Figure 10.13 in order to get the transfer function relating its output to its inputs.
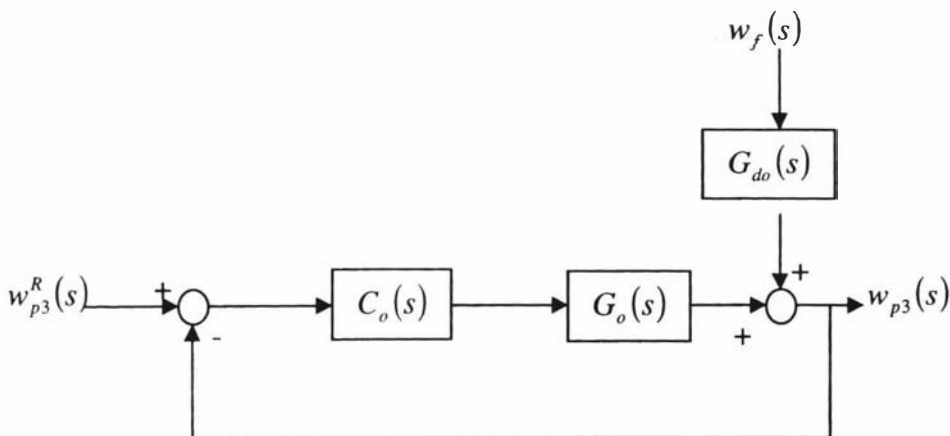
Figure 10.13: Simplified cascade feedback loop for product concentration control

Where,

$$G_o(s) = T_i(s) \cdot G_2(s) + C_i(s) \cdot S_i(s) \cdot G_3(s),$$

$$G_{do}(s) = G_d(s) \cdot S_i(s) \cdot G_2(s) - G_d(s) \cdot C_i(s) \cdot S_i(s) \cdot G_3(s)$$

$$S_i = (1 + C_i \cdot G_1)^{-1}, \ T_i = C_i \cdot G_1(1 + C_i \cdot G_1)^{-1}$$

S_i and T_i are the inner loop sensitivity and complementary sensitivity transfer functions respectively. The equation relating the output, $w_{p3}(s)$, to the inputs, $w_f(s)$ and w_{p3}^R thus follows as:

$$w_{p3}(s) = \left(\frac{C_o(s) \cdot G_o(s)}{1 + C_o(s) \cdot G_o(s)} \right) \cdot w_{p3}^R(s) + \left(\frac{G_{do}(s)}{1 + C_o(s) \cdot G_o(s)} \right) \cdot w_f(s)$$

To minimise the effects of $w_f(s)$ on $w_{p3}(s)$ it is necessary to minimise the gain of $G_{do}(s)$ over as wide a range of frequencies as possible and to maximise the phase crossover frequency of $G_o(s)$. It can be shown that the inner loop controller has negligible impact on the phase crossover frequency of $G_o(s)$ and hence the inner loop design focused on minimising the gain of $G_{do}(s)$.

10.5.3 Tuning

Considering $G_{do}(s)$, it should first be noted that for single loop (no cascade) control, $G_{do}(s) = G_d(s) \cdot G_2(s)$. The cascade controller should improve upon this. For high inner loop gains (tuned to maximise the rejection of disturbances on w_{p1}) the magnitude of the $G_d(s) \cdot S_i(s) \cdot G_2(s)$ term will be small as $S_i(s)$ will be small for a large range of frequencies. However, the $G_d(s) \cdot C_i(s) \cdot S_i(s) \cdot G_3(s)$ term will be large and dominate. Conversely, for very low inner loop gains $S_i(s)$ will be not be small and hence the $G_d(s) \cdot S_i(s) \cdot G_2(s)$ will not be suppressed and will dominate. Thus, a compromise is needed in choosing the inner loop gain. Figure 10.14 shows the Bode magnitude plot of $G_{do}(s)$ for a range of inner loop controller settings.

It can be seen that for a very low proportional gain of 10, there is little improvement on the single loop scenario. At a gain of 400 (which maximises the rejection of disturbances on w_{p1}), the $G_d(s) \cdot C_i(s) \cdot S_i(s) \cdot G_3(s)$ term can be seen to make a significant contribution, particularly the undesirable resonant peak at approx. 0.2 rad/s. A good compromise is achieved with a gain of 85, with a general improvement on the single loop controller at most frequencies and just a small degradation around 0.15 rad/s. The latter is an unavoidable consequence of the '$G_3(s)$' mechanism. It can be seen in Figure 10.14 that there is no significant benefit (no difference in the disturbace rejection frequencies) from adding integral action to the inner loop controller.
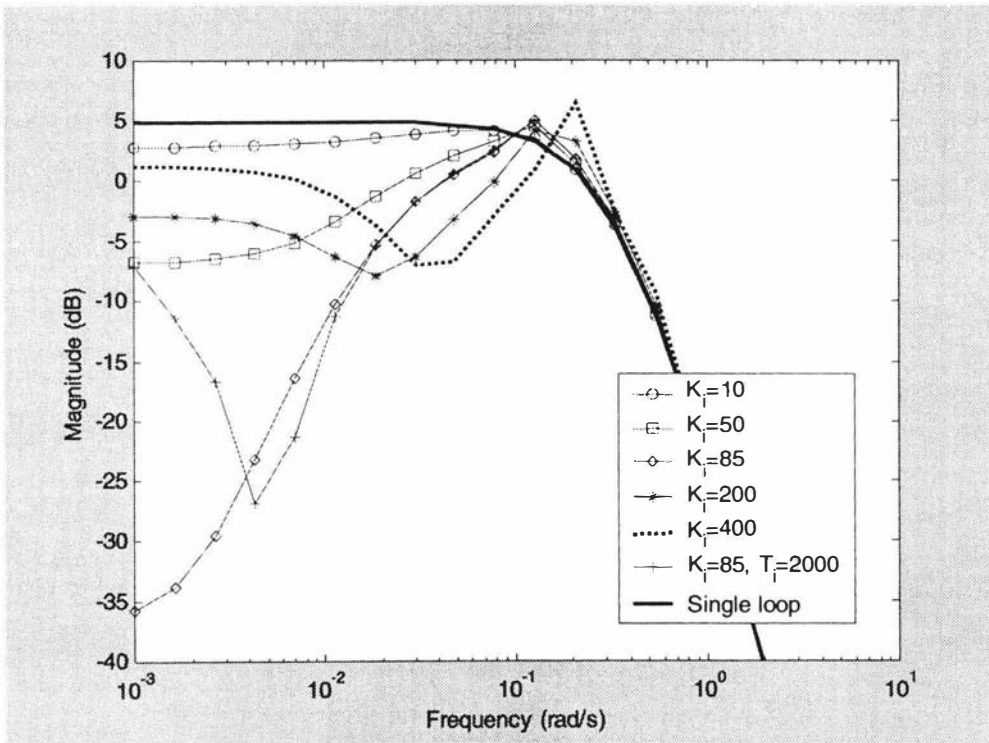
Figure 10.14: Bode magnitude plot of G_{do} for different inner loop controller settings

With the inner loop controller tuned, the outer loop can be tuned using the usual criteria to give good disturbance rejection and tracking performance. A PI controller is needed to achieve both of these tasks.

The integral time, T_I, was chosen to have phase lead before the phase cross over frequency, and the proportional constant was selected to achieve the best compromise between the disturbance rejection and noise suppression bandwidths. The selected controller settings for the outer controller were $K_c = 0.3$ and $T_I = 73$.

10.5.4 Results and discussion

Figure 10.15 compares the effect of feed disturbances on the concentrate total solids (magnitude of the transfer function from w_f to w_{p3}) for single loop control (discussed in the previous section) and the cascade controller. The disturbance rejection bandwidth with cascade control is 0.06 rad/s where it is 0.006 rad/s with single feedback control. Therefore, the improvement afforded by the cascade controller is evident.
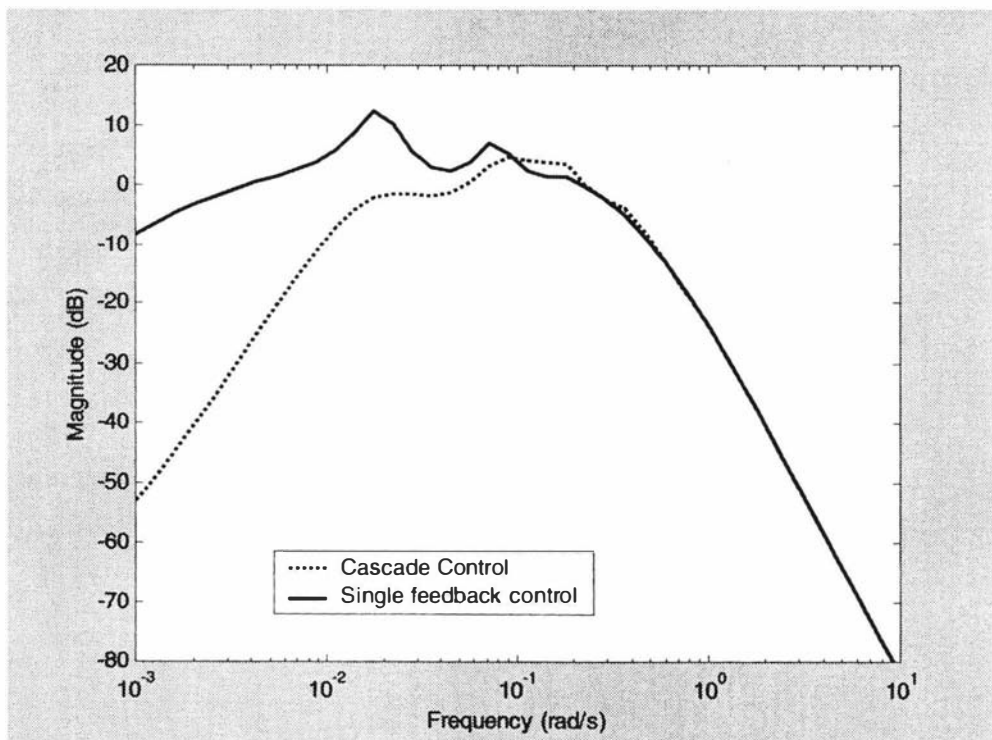
**Figure 10.15: Bode Magnitude plots of transfer function $w_{p3}(s)/w_f(s)$
for single loop and cascade control**
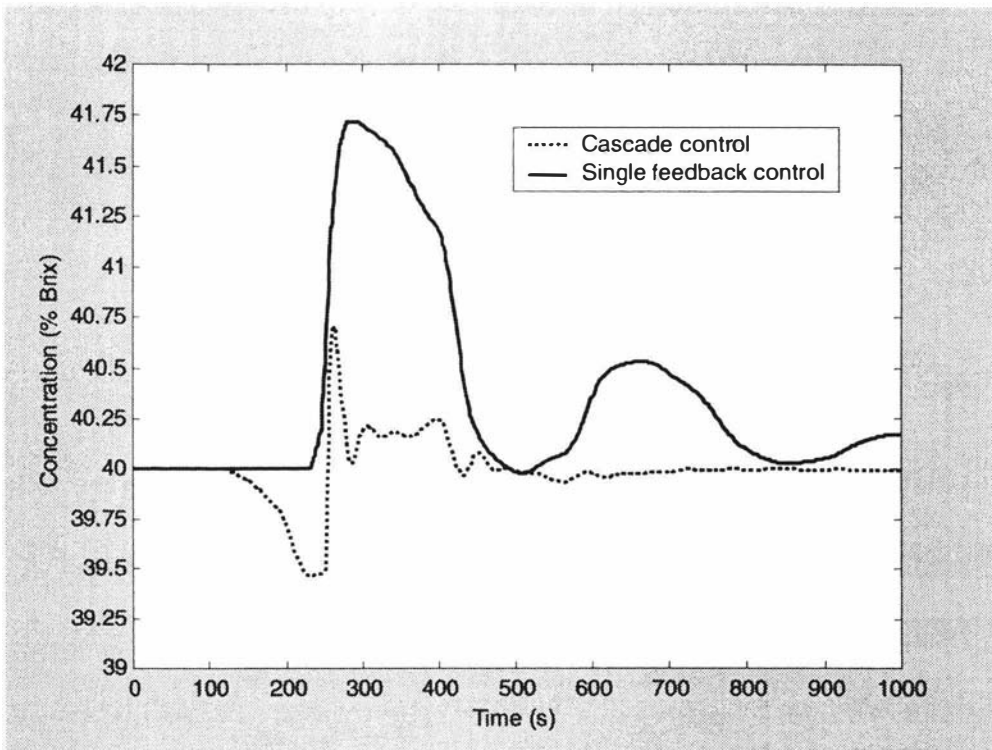
Figure 10.16: Product concentration in response to a disturbance in the feed concentration
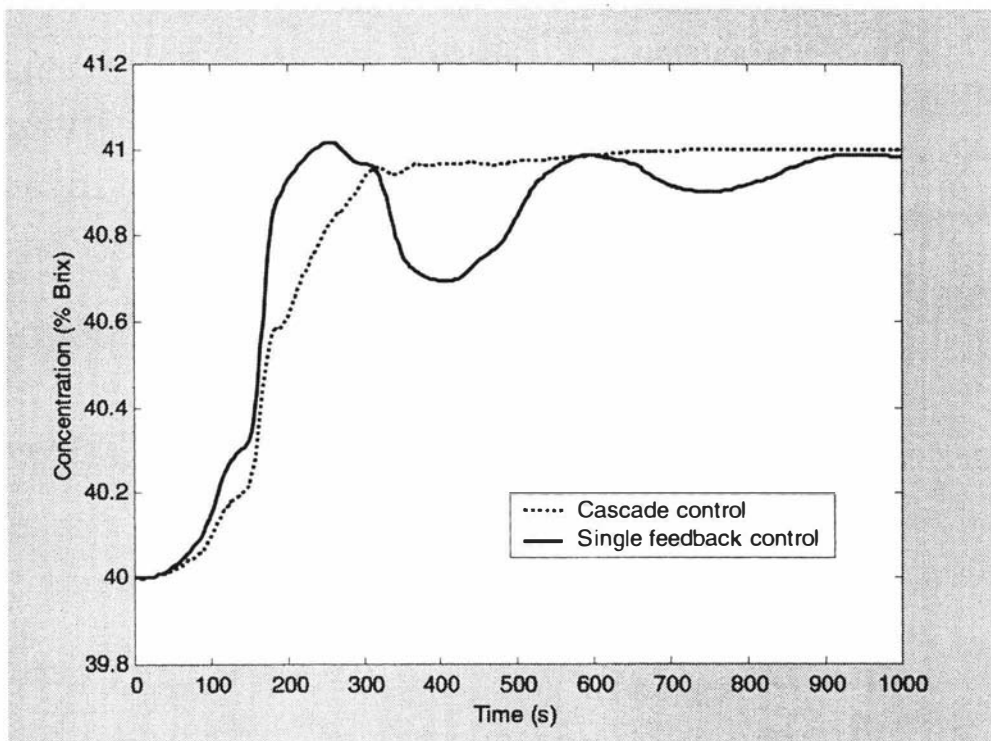
Figure 10.17: Product concentration in response to a step change in set point

Figure 10.16 demonstrates the superior action of the cascade controller by comparing the time-domain responses of w_{p3} to a step disturbance in w_f. To complete the analysis, a set-point change simulation was compared for the two controllers (Figure 10.17). Even though this was not the focus of the design for the cascade controller, the cascade controller can be seen to out perform the single loop controller for this test also. It can be seen from figures 10.16 and 10.17 that the evaporator with a single feedback control would need 15 minutes to settle after a disturbance or a set point change. This would be less than 5 minutes with the cascade control.

10.6 Conclusions

The control of the 2nd effect temperature and the product concentration was investigated. It was found that disturbances on the 2nd effect temperature were well rejected but that there was poor disturbance rejection of the disturbances on the concentrate density. This is due to the large falling film delay in the evaporator. The product density control loop was further investigated to improve the disturbance rejection.

It was demonstrated that the control of concentrate total solids exiting a multi-pass, multi-effect falling film evaporator can be enhanced by the use of cascade control architecture. In addition to measuring the primary process variable (the final concentrate total solids), a surrogate process variable (the total solids after the first pass) was measured and used in the cascade strategy. For tuning the inner loop controller it is important to note that only part of the effect of the inner loop manipulations is observed by the surrogate process variable and thus tuning the inner loop to maximise the rejection of disturbances on the surrogate process variable is not appropriate. Rather, a compromise gain needs to be chosen which provides some rejection of disturbances on the surrogate process variable but does not contribute excessively to the disturbance of the primary process variable. The simulation results show that the disturbance rejection can be improved significantly with cascade control in the whey evaporator.

Chapter 11 : Overall Conclusions

The aim of this study is to improve the evaporation process and the steps involved are,

- Derive steady state and linear dynamic models and identify the model constants.

- Measure and model the physical properties of whey products.

- Troubleshoot and optimise the evaporator operation using the steady sate models.

- Improve the control ability of key controls around the whey evaporator.

Regression models developed for density, viscosity, advancing contact angle and surface tension are applicable for concentrates up to 35%w/w and temperatures between 20 and 60°C with error less than 5% error. Semi-empirical models were also developed for density and viscosity to extend the limited application range of the regression models with less than 10% error. The accuracy of the semi-empirical models is good enough for troubleshooting and process improvements. There were no measurements conducted on the thermal conductivity and specific heat capacity. However, predictions of semi-empirical models for thermal conductivity and specific heat capacity were tested for milk concentrates and assumed to predict with same accuracy for whey concentrates. Discharge coefficient measurements suggest that the discharge coefficient used in the literature (0.6) not applicable to milk evaporators and the value is dependant on the orifice shape and the thickness of the plate. The value found for the whey evaporator was 0.75. The physical property models developed in this work are recommended as useful for,

- Estimating product properties at different operating conditions.

- Determining the product density control set point.

- Optimising evaporator solids concentration.

- Determining evaporator wetting flows

- Determining the liquid height in the distribution plates

There is significant work in the literature on the evaporator modelling but few areas left unfinished. The equation to estimate the flow through the distribution plate orifice was improved relaxing the assumption that the orifice thickness is negligible compared to the liquid head. Derivation of Thermal Vapour Recompression evaporator used in whey products. The model constants were identified using the historical data and experimental data to improve the accuracy of the model predictions. Preheat condenser, Thermal Vapour Recompression and the falling-film models can predict the plant data with less than 5% error. It was proven that the physical property of whey products has strong influence on the model predictions.

The aim of the optimisation study was to improve the performance of the whey products evaporator set. The system was investigated for low heat transfer coefficients, film breakdown and poor TVR performance. Investigation on the WPI performance suggests that any preheat above 20°C destabilises the whey protein which enhances the foamability. Increased in high heat transfer coefficients and plant throughput were observed during the trials with low preheat temperatures (less than 20°C). The performance of the preheat condensers found to have strong influence on the amount of non-condensable gas and on the product viscosity. Reduced steam pressure (5bar) during the water run gave better wetting rates in the evaporator. The energy savings of about NZ$70,000/season was achieved due to the increased evaporation in the evaporator and the resulting reduced steam requirements in the spray dryer.

Product concentration and the second effect temperature controls are the key control loops in the whey evaporator. The second effect temperature control found to have no disturbance rejection problems due to short residence time in the vacuum condenser. The concentrate control found to have severe problems with the disturbance rejection due to the long falling-film delay. It was proved that the disturbance rejection bandwidth of the concentration control was increased from   by applying cascade control instead of the single feedback control.

Chapter 12 : Recommendations and Future Work

12.1 Recommendations

- The mass of evaporation in the whey evaporator is limited by the concentrate viscosity for WPC-2 and WPC-3. Use the property models to determine the optimum concentrate solids for those products to avoid the problems and downtime resulting from too high a viscosity.

- There must be sufficient liquid height above the distribution plate to ensure uniform distribution and to reject high frequency disturbances. Use the modified distribution plate equation to determine the liquid height above the distribution plate and the discharge coefficient for future calculations.

- The presence of non-condensable gas in the shell of the condensers will increase the resistance to heat transfer. Therefore, always direct the non-condensable gas line from the calendria to a location close to the vacuum pump in the falling-film evaporator.

- The overall evaporation heat transfer coefficient for water is much higher than that for whey products. The evaporator should therefore be supplied with less steam when running water than it is when running whey products. Due to the non-linearity of the steam control valve, the steam flow is maximised once the valve is at 70% open. This steam valve set point should be reduced to 45% during the water run. This not only maintains sufficient flow in the tubes, but also reduces energy consumption.

213

- Whey products are rich in whey proteins that are sensitive to high temperatures. Currently the evaporator feed product is heated to 55 to 65°C. This can denature the whey protein and enhance foaming. To improve evaporator performance, avoid heat treatment of whey products after ultra-filtration and prior to the evaporator to improve the evaporator performance.

- The trials from this study clearly show improvements in evaporator performance at low product feed temperatures (below 20°C). There is a small reduction in evaporator capacity with a low temperature feed, but a significant gain in the overall mass of evaporation.

- Due to high heat transfer coefficients for water, high water flows are needed to maintain full wetting of evaporator tubes. This is most critical when the evaporator is about to switch to product as the settings are similar to the product run. Therefore, a higher flow is needed at the start up followed by a gradual drop in flow.

- An in-line viscosity measurement is vital with whey products as the concentrate viscosity increases exponentially at a lower solids concentration than for milk products. Therefore, the evaporator exit solids concentration should be determined from the product viscosity.

12.2 Future work

Properties

Information on the physical properties of whey products is essential in analysing the evaporation and drying process. Viscosity and thermal conductivity of whey products are not fully understood, nor are sufficient data available to validate the model. Viscosity determines the optimum concentrate total solids in the evaporator, while thermal conductivity explains the falling-film heat transfer coefficient. The viscosity measurements for different whey products showed the influence of composition on viscosity. It was difficult to correlate viscosity to composition due to insufficient information (ability to change the product components individually). There is a need for further investigation and more measurements to understand why viscosity is markedly different between products and how molecular interactions and shear rate influence viscosity.

There were no thermal conductivity measurements carried out for whey and it was assumed that the semi-empirical model predictions are accurate. This may not be true due to the presence of air in the whey products. The model needs to be validated against thermal conductivity measurements for different whey products.

Model development and identification

The model constants were identified from historical and measured data. The heat transfer coefficients and the falling-film residence time significantly influence the evaporation process and the dynamic behaviour of the system. Heat transfer coefficients of falling films within the evaporators should be identified accurately for whey products to improve the steady state model predictions. The major problem with the current work is the lack of data on the thermal conductivity of whey products and the air content in the products. There is a need for a model that can predict the falling-film heat transfer coefficient from the product components and the operating conditions. For this a reliable method for estimating the air content in the product is required. This could be an area for future work.

Another parameter that is not well characterised is the falling film residence time. This is again related to the physical properties of the products, evaporator geometry and the operating conditions. There were not enough data available from this work or literature to investigate the influence of each key factor on the falling-film residence time. A better understanding of these influences is needed, as well as a model to estimate the residence time.

Optimisation

The aim of this work was to improve the evaporator performance through increasing the energy efficiency and the product quality. This had to be achieved by changing only the operating conditions without changing the product compositions and functional properties. It has been shown that the evaporator performance with cheese whey protein concentrates is poor compared to performance with whey products from other sources. This could be related to the whey protein types and their behaviour in the evaporator. An in depth study of the protein types and their interactions and behaviour in liquids would be useful to enhance understanding of the whey powder process.

Control

This study demonstrates that the control of concentrate total solids exiting a multi-pass, multi-effect falling-film evaporator can be enhanced by the use of a cascade control architecture. The accuracy of the predictions depends on the accuracy of the falling-film models and the falling-film residence times. The linear dynamic model simulation predictions showed an improvement in the product density control but this has not been tested in a commercial or pilot scale evaporator. Such testing would be worthwhile.

Nomenclature

Here we list many of the variables used in this thesis. The dynamic variables of the whey evaporator plant model have also been listed here. The static variables are denoted with the additional superscript.

A	Cross sectional area of the condenser tubes	(m^2)
A_d	Area of distribution plate	(m^2)
A_{d1}	Area of 1st distribution plate	(m^2)
A_{d2}	Area of 2nd distribution plate	(m^2)
A_{d3}	Area of 3rd distribution plate	(m^2)
A_h	Area of the virtual pipe ahead of orifice	(m^2)
A_{h1}	Area of the virtual pipe ahead of orifice in 1st distribution plate	(m^2)
A_{h2}	Area of the virtual pipe ahead of orifice in 1st distribution plate	(m^2)
A_{h3}	Area of the virtual pipe ahead of orifice in 1st distribution plate	(m^2)
A_i	Surface area for heat loss	(m^2)
a_i	Constant	(kgm^{-3})
A_o	Cross sectional area of the orifice	(m^2)
a_{oc}	Constant	$(^o)$
a_{os}	Constant	(Nm^{-1})
A_{phc}	Area of preheat condenser tubes	(m^2)
A_s	Heat transfer surface area	(m^2)
A_{s1}	Surface area for evaporation in the 1st pass	(m^2)
A_{s2}	Surface area for evaporation in the 2nd pass	(m^2)
A_{s3}	Surface area for heat transfer in the 3rd pass	(m^2)
A_{throat}	Cross sectional area of TVR compressor nozzle throat	(m^2)
A_{TVR}	TVR compressor parameter	$(m.s)$

a_{Tc}	Constant	$(^{\circ}/K)$
a_{Ts}	Constant	(Nm^{-1}/K)
a_{TSc}	Constant	$(^{\circ}/w/w)$
a_{TSs}	Constant	$(Nm^{-1}/w/w)$
A_w	Constant	(10.59)
b_i	Constant	(kgm^{-3}/K)
B_{TVR}	TVR compressor parameter	$(m^{0.03}.s^{0.06}/kg^{0.03})$
B_w	Constant	$(3680.11 \, ^{\circ}K)$
C_d	Coefficient of discharge	$(-)$
c_i	Constant	$(J \, kg^{-1} \, K^{-1})$
Cp	Heat capacity of product	$(J \, kg^{-1} \, K^{-1})$
Cp_f	Heat capacity of feed product	$(J \, kg^{-1} \, K^{-1})$
Cp_{p1}	Heat capacity of 1st pass product	$(J \, kg^{-1} \, K^{-1})$
Cp_{p2}	Heat capacity of 2nd pass product	$(J \, kg^{-1} \, K^{-1})$
Cp_{p3}	Heat capacity of 3rd pass product	$(J \, kg^{-1} \, K^{-1})$
Cp_i	Specific heat capacity of ith component	$(J \, kg^{-1} \, K^{-1})$
Cp_{met-e1}	Heat capacity of metal	$(J \, kg^{-1} \, K^{-1})$
Cp_w	Heat capacity of water	$(J \, kg^{-1} \, K^{-1})$
Cp_{water}	Heat capacity of water	$(J \, kg^{-1} \, K^{-1})$
C_{TVR}	TVR compressor parameter	$(-)$
C_w	Constant	$(41.69 \, ^{\circ}K)$
d	Diameter of the TVR nozzle	(m)
d_i	Tube inside diameter	(m)
d_i	Constant	$(J \, kg^{-1} \, K^{-2})$
d_o	Tube outside diameter	(m)
e	Constant	$(-)$

e_2	Constant	(-)
e_3	Constant	(-)
e_i	Constant	$(J\ kg^{-1}\ K^{-3})$
f_i	Constant	$(W\ m^{-1}\ K^{-1})$
g	Acceleration due to gravity	(ms^{-2})
g_i	Constant	$(W\ m^{-1}\ K^{-2})$
h	Film heat transfer coefficient	$(W/m^2.\ K)$
h_d	Height of the liquid above the orifice	(m)
h_{d1}	Liquid height above the distribution plate in the 1st pass	(m)
h_{d2}	Liquid height above the distribution plate in the 2nd pass	(m)
h_{d3}	Liquid height above the distribution plate in the 3rd pass	(m)
h_f	Fouling coefficient	$(W\ m^{-2}\ K^{-1})$
h_{fi}	Inside fouling coefficient	$(W/m^2.\ K)$
h_{fo}	Outside fouling coefficient	$(W/m^2.\ K)$
h_i	Inside fluid film coefficient	$(W/m^2.\ K)$
h_o	Outside fluid film coefficient	$(W/m^2.\ K)$
h_l	Liquid height needed to overcome the surface tension force	(m)
H_{steam}	Enthalpy of steam supplied to the TVR compressor	(J/kg)
H_{steam}	Enthalpy of steam	(J/kg)
k	Thermal Conductivity of the tube material	$(W\ m^{-1}\ K^{-1})$
Ka	Kapitza number	(-)
K_{e1}	Thermal inertia for 1st effect	(J)
K_{e2}	Thermal inertia for 2nd effect	(J)
k_i	Thermal conductivity of ith component	$(W\ m^{-1}\ K^{-1})$
k_p	Thermal conductivity of product	$(W\ m^{-1}\ K^{-1})$
k_v	Viscosity model constant	(-)

k_w	Thermal conductivity of water	$(\text{W m}^{-1}\text{ K}^{-1})$
K_{TVR}	TVR compressor parameter	(s/m)
K_{HTC}	TVR compressor parameter	(-)
L	Length of the tube	(m)
m	Mass fraction of the components	(-)
m_{comp}	Mass flow rate of vapour compressed by the TVR	(kg/s)
M_{cw}	Mass flow rate of cooling water to vacuum condenser	(kg/s)
M_{cond}	Feed flow rate to the condenser	(kg/s)
M_{cond}^{0}	Steady state feed flow to the condenser	(kg/s)
M_d	Mass of whey leaving the distribution plate	(kg/s)
M_{dum}	Dummy variable used in the condenser model	(kg)
M_{d1}	Mass flow rate of product through the 1st distribution plate	(kg/s)
M_{d2}	Mass flow rate of product through the 2nd distribution plate	(kg/s)
M_{d3}	Mass flow rate of product through the 3rd distribution plate	(kg/s)
M_e	Mass flow rate at the exit of the tube	(kg/s)
M_{evape1}	Mass of evaporation in the 1st effect	(kg/s)
M_{evape2}	Mass of evaporation in the 2nd effect	(kg/s)
M_f	Mass flow rate of product to the evaporator	(kg/s)
M_f°	Steady state mass flow rate to the evaporator	(kg/s)
M_{flash}	Mass of water evaporated due to flash in the distribution plate	(kg/s)
M_{flash1}	Mass of water evaporated due to flash in the 1st distribution plate	(kg/s)
M_{flash2}	Mass of water evaporated due to flash in the 2nd distribution plate	(kg/s)
M_i	Molecular weight	(kg/kmol)
M_{met-e1}	Mass of metal in the 1st effect	(kg)
M_{p1}	Mass flow rate of product from pass 1	(kg/s)

M_{p2}	Mass flow rate of product from pass2	(kg/s)
M_{p3}	Mass flow rate of product from pass3	(kg/s)
M_{p3}°	Steady state mass flow rate of product from pass3	(kg/s)
M_{phc3}	Mass flow rate to 3rd preheat condenser	(kg/s)
m_{steam}	Mass flow of motive steam	(kg/s)
M_{tubes}	Mass of evaporation in the evaporation tubes	(kg/s)
n	Number of distribution holes	(-)
Nu	Nusselt number	(-)
P	Excess pressure over atmosphere at equilibrium	(N m^{-2})
P_{e1}	Pressure in the 1st effect	(Nm^{-2})
Pr	Prandtl number	(-)
P_s	Pressure in the shell of the 1st effect	(Nm^{-2})
P_{steam}	Pressure of the motive steam	(Nm^{-2})
q_{cond}	Heat transfer through condenser tubes	(W)
Q_d	Discharge flow from the distribution plate	(m^3/s)
q_d	Discharge flow through one of the orifices in the distribution plate	(m^3/s)
q_{feed1}	Net energy flow rate with the feed whey	(W)
q_{feed2}	Net energy flow rate with the feed whey to the 2nd effect	(W)
$q_{loss-E1}$	Loss heat flow rate from the 1st effect	(W)
$q_{loss-E2}$	Loss heat flow rate from the 2nd effect	(W)
q_{loss-s}	Loss heat flow rate from the shell of the 1st effect	(W)
q_{phc1}	Heat flow rate to HX1503 tubes	(W)
q_{phc2}	Heat flow rate passing through HX 1502	(W)
q_{phc3}	Heat flow rate passing through HX 1501	(W)
q_{shell}	Heat transfer through the tubes	(J)
$q_{shell-e1}$	Heat flow rate passing through HX1504	(W)

$q_{shell-e2}$	Heat flow rate passing through HX1505	(W)
R	Universal gas constant	(kJ/kg. K)
r	Radius of the orifice	(m)
Re	Reynolds number	(-)
RI	Refractive Index value	(%Brix)
r	Radius of the orifice	(m)
r_i	Constant	(w/w%/ %Brix)
SL	Number of falling film elements in the simulation	(-)
s_i	Constant	(w/w%)
t	time	(s)
T	Temperature of the concentrate	(°C)
T_a	Ambient temperature	(°C)
T_{cwin}	Vacuum condenser cooling water inlet temperature	(°C)
T_{cwout}	Vacuum condenser cooling water exit temperature	(°C)
T_{cond}	Temperature of liquid in the condenser	(°C)
T_{dum}	Dummy variable used in the condenser model	(°C)
T_e	Temperature of the evaporator effect	(°C)
T_{e1}	First effect temperature	(°C)
T_{e2}	Second effect temperature	(°C)
T_{e2}°	Steady state second effect temperature	(°C)
T_{e1}°	Steady state first effect temperature	(°C)
T_f	Feed temperature of the product	(°C)
T_f^0	Steady state temperature of the feed	(°C)
T_{in}	Feed temperature of condenser liquid	(°C)
T_{out}	Outlet temperature from the condenser	(°C)
T_{phc1}	HX1503 exit temperature	(°C)
T_{phc1}°	Steady state HX1503 exit temperature	(°C)
T_{phc2}	HX1502 exit temperature	(°C)

T°_{phc2}	Steady state HX1502 exit temperature	($^{\circ}$C)
T_{phc3}	HX1501 exit temperature	($^{\circ}$C)
T°_{phc3}	Steady state HX1501 exit temperature	($^{\circ}$C)
t_p	Thickness of the distribution plate	(m)
T_{phc3}	Temperature of the product entering the 1st distribution plate	($^{\circ}$C)
T_s	Temperature of the shell	($^{\circ}$C)
T_{s1}	First shell temperature	($^{\circ}$C)
T_{sh}	Temperature in the shell of the condenser	($^{\circ}$C)
T^0_s	Steady state temperature in the shell of the condenser	($^{\circ}$C)
T_{sat}	Saturation temperature of boiling water	($^{\circ}$C)
U	Heat transfer coefficient in the condenser	(W/m^{2}K)
U_i	Overal losses heat transfer coefficient	(W/m^2.$^{\circ}$C)
U_1	Overall heat transfer coefficient in the 1st pass	(W/m^2. K)
U_2	Overall heat transfer coefficient in the 2nd pass	(W/m^2. K)
U_3	Overall heat transfer coefficient in the 3rd pass	(W/m^2. K)
U_o	Overall heat transfer coefficient based on the outside area	(W/m^2. K)
U_{phc}	Overall heat transfer coefficient in the preheat condenser	(W/m^2. K)
v_{cond}	Velocity of the liquid	(m/s)
v_i	Voluminosity of ith component	(m^3 kg^{-1})
V_{cond}	Volume of liquid in the condenser tubes	(m^3)
w	Dry matter	(kg/kg)
w_d	Dry matter of the product leaving the distribution plate	(kg/kg)
w_{d1}	Total solids concentration of the product in the 1st distribution plate	(w/w%)
w_{d2}	Total solids concentration of the product in the 2nd distribution plate	(w/w%)
w_{d3}	Total solids concentration of the product in the 3rd distribution plate	(w/w%)
w°_{d1}	Steady state dry matter of the product leaving 1st distribution plate	(kg/kg)

w_{d2}°	Steady state dry matter of the product leaving 2nd distribution plate	(kg/kg)
w_{d3}°	Steady state dry matter of the product leaving 3rd distribution plate	(kg/kg)
w_e	Total solids content at the exit	(kg/kg)
w_f	Dry matter of the feed product	(kg/kg)
w_i	Weight fraction of ith component	(kg/kg)
w_{ls}	Concentration of the lactose solution if it were the only component	(w/w)
w_{max}	Maximum concentration before gel	(w/w)
w_p	Dry matter of the product	(kg/kg)
w_{p1}	Dry matter of the product from pass1	(kg/kg)
w_{p2}	Dry matter of the product from pass2	(kg/kg)
w_{p3}	Dry matter of the product from pass3	(kg/kg)
w_{p1}°	Steady state dry matter of the product leaving 1st pass	(kg/kg)
w_{p2}°	Steady state dry matter of the product leaving 2nd pass	(kg/kg)
w_{p3}°	Steady state dry matter of the product leaving 3rd pass	(kg/kg)
w_{TS}	Total Solids concentration	(w/w%)
x_l	Dry matter fraction of the lactose in the whey concentrate	(w/w)
x_{cp}	Dry matter fraction of the casein protein in the whey concentrate	(w/w)
x_{wp}	Dry matter fraction of the whey protein in the whey concentrate	(w/w)
x_f	Dry matter fraction of the fat in the whey concentrate	(w/w)
x_{sol}	Molar concentration of dissolved particles	(mol/mol)
x	Distance along x axis	(m)
MVR	Mechanical Vapour Recompression	
TVR	Thermal Vapour Recompression	
WPI	Whey Protein Isolate	
WPC-1	Cheese Whey Protein Concentrate	
WPC-2	High Fat Whey Protein Concentrate	
WPC-3	Casein Whey Protein Concentrate	
TC	Time constant	
RT	Residence time	

λ	Latent heat of vaporisation	(J/kg)
λ_1	Latent heat of vaporisation in the 1st effect	(J/kg. K)
λ_2	Latent heat of vaporisation in the 2nd effect	(J/kg. K)
ρ	Density of condenser liquid/ Product	(kg/m³)
ρ_d	Density of whey leaving the distribution plate	(kg/m³)
ρ_{d1}	Density of whey leaving the 1st distribution plate	(kg/m³)
ρ_{d2}	Density of whey leaving the 2nd distribution plate	(kg/m³)
ρ_{d3}	Density of whey leaving the 3rd distribution plate	(kg/m³)
ρ_f	Density of feed whey	(kg/m³)
ρ_i	Density of ith component	(kg m⁻³)
ρ_{max}	Density of the maximum concentration	(kg/m³)
ρ_p	Density of product	(kg/m³)
ρ_w	Density of water	(kg/m³)
ρ_{water}	Density of water	(kg/m³)
ρ_{wpc-3}	Density of WPC-3	(kg/m³)
ρ_{wpi}	Density of WPI	(kg/m³)
v	Velocity of the falling-film	(m/s)
γ	Ratio of constant pressure and volume heat capacities	(-)
τ_e	Falling-film residence time	(s)
τ_{et}	Falling-film residence time	(s)
τ_{fd}	Delay time between the feed and the 1st distribution plate	(s)
τ_{hd1}	Time constant for liquid in the 1st distribution plate	(s)
τ_{hd2}	Time constant for liquid in the 2nd distribution plate	(s)
τ_{hd3}	Time constant for liquid in the 3rd distribution plate	(s)
τ_{p1p2}	Delay between the 1st pass and the 2nd distribution plate	(s)
τ_{p2p3}	Delay between 2nd pass and the 3rd distribution plate	(s)

τ_{RT}	Residence time	(s)
τ_T	Total plant residence time	(s)
τ_{TC}	Time constant	(s)
τ_{TS}	Time constant of the shell temperature	(s)
τ_{Te1}	Time constant for 1st effect temperature	(s)
τ_{Te2}	Time constant for the 2nd effect temperature	(s)
τ_{wd1}	Time constant for dry matter leaving 1st distribution plate	(s)
τ_{wd2}	Time constant for dry matter leaving 2nd distribution plate	(s)
τ_{wd3}	Time constant for dry matter leaving 3rd distribution plate	(s)
ΔT_{BPE}	Boiling point elevation	(°C)
θ_a	Advancing contact angle	(°)
σ	Surface tension	(Nm^{-1})
v_i	Voluminosity of ith component	(m^3 kg^{-1})
v_{cp}	Voluminosity of casein protein	(m^3 kg^{-1})
v_{wp}	Voluminosity of whey protein	(m^3 kg^{-1})
v_f	Voluminosity of fat	(m^3 kg^{-1})
ϕ_i	Volume fraction of ith component	(-)
ϕ	Volume fraction of a component	(-)
ϕ_t	Total volume fraction	(-)
ϕ_m	Maximum volume fraction	(-)
μ	Viscosity of the fluid	(cp)
μ_s	Viscosity of lactose solution	(cp)
μ_w	Viscosity of water	(cp)
μ_{WPI}	Viscosity of WPI	(cp)
μ_{WPC-3}	Viscosity of WPC-3	(cp)
Γ	Peripheral flow	(kgm^{-1}s^{-1})

References

Adam M, Celba J, Havlicek Z et al. (1994), "Thermophysical and rheological properties of foods", Institute of Agricultural and Food Information, Prague.

Alhusseini A A, Tuzla K and Chen J C (1998), "Falling film evaporation of single component liquids", International Journal of Heat and Mass Transfer, Vol. 41(12), pp. 1623-1632.

Angeletti S and Moresi M (1983), "Modelling of multiple-effect falling-film evaporators", Journal of Food Technology, Vol. 18, pp. 539-563.

Antonio J B (1983), "Surface tension of whole and skim milk between 18 and 135°C", Journal of Dairy Research, Vol. 50, pp. 259-267.

Aris R (1999), "Mathematical Modelling: A Chemical Engineer's Perspective", Academic press, London.

Bender E A (1978), "An Introduction to Mathematical Modelling", John Wiley & Sons, USA.

Berntsson T and Asblad A (1991), "Surface evaporation of turbulent falling films", International Journal of Heat and Mass Transfer, Vol. 34(3), pp. 835-841.

Bickerstaff G, " Foaming properties", Enzyme Technology, Department of Biological sciences, University of Paisley, (Accessed September 2002) www.biol.paisley.ac.uk/courses/enzymes/glossary/foaming

Billet R (1989), "Evaporation Technology- principles, applications and economics", VCH publishers, Germany

Bloore C G and Boag I F (1981), " Some factors affecting the viscosity of concentrated skim milk", New Zealand Journal of Dairy Science and Technology, Vol. 16, pp.143-154.

Bouman S, Waalewijn, John P De and Van Der Linden (1993), "Design of falling-film evaporators in the dairy industry", Journal of the society of dairy Technology, Vol. 46(3), pp. 100-106.

Bui T D and Dhir V K (1985), "Film boiling heat transfer on an isothermal vertical surface", Journal of heat transfer, Vol. 107, pp. 764-771

Buma T J (1980), "Viscosity and density of concentrated lactose solutions and concentrated cheese whey", Netherlands Milk Dairy Journal, Vol. 34, pp. 65-68

Bylund G (1995), "Dairy Processing Handbook", Tetra Pak Processing Systems AB, S-221 86 Lund, Sweden.

Castellan G W (1964), "Physical Chemistry", Addison-Wesley publishing Company, Massachusetts.

Chee L, Franich P and Lawn N (1988), "Determination of background parameters for evaporator distributor design", MP short project report, DIGPT, Fonterra Research Centre, New Zealand.

Chen H (1997), "Factors affecting heat transfer in the falling film evaporator", PhD thesis, Massey University, Palmerston North, New Zealand.

Chen H and Jebson R S (1997), "The performance of falling film evaporators on whole milk and a comparison with performance on skim milk", Journal of dairy research, Vol. 64, pp.57-67.

Choudhary R, Ali S and Das H (1996), "A heat transfer model for performance evaluation of a single effect multistage mechanical vapour recompression evaporator", Journal of Food Science Technology, Vol. 33, No. 4, pp.308-312.

Christopher M A, "Falling-film evaporators in the food industry - heat transfer coefficient", web page, http://www.cheresources.com (accessed April 2001)

Chun K R and Seban R A (1971), "Heat transfer to evaporating liquids film", Journal of Heat Transfer, Transaction of the ASME, Vol. 93(4), pp. 391-396.

Chun K R and Seban R A (1972), "Performance Prediction of Falling-film Evaporators", Journal of Heat Transfer, Transaction of the ASME, pp. 432-436.

Coulson J M and Rechardson J F (1991), "Chemical Engineering: An Introduction to Chemical Engineering Design-Volume 6", Pergamon Press, New York.

Daugherty R L and Franzini J B (1965), "Fluid Mechanics with Engineering Applications", McGraw Hill Book Company, New York.

De Wit J N (1988), "Functional properties of whey proteins", VERSLAG V281, NIZO, Netherland.

De Wit J N (1989), "The use of whey protein products", VERSLAG V295, NIZO, Netherland.

Fernadez-Martin F (1971), "Influence of temperature and composition on some physical properties of milk and milk concentrates", Journal of Dairy Research, Vol. 39, pp. 75-82.

Fox P F (1992), "Advanced dairy Chemistry: Proteins", Elsevier Science publishers Ltd., England.

Fujita T and Udea T (1978), "Heat transfer to falling liquid films and film breakdown", Journal of Heat and Mass transfer, Vol. 21, pp. 109-118.

Gebhard S (1981), "Introduction to Practical Viscometry", HAAKE Viscometers, West Germany.

German J B (1990), "Food Emulsions and Foams: Theory and practice", American Institute of Chemical Engineers Symposium Series, Vol. 86, pp.62-70.

Glasscock D A and Hale J C (1994), "Process simulation: The art and science of modelling, Chemical Engineering, Vol. 101(11), pp. 82-89

Guoxin Luo (1998), "Modelling of evaporators in the production of milk evaporators", Dissertation, Dublin City University, Ireland

G&P engineering software, web page, http://www.cheresources.com (accessed December 2001)

Haggarty N (1995), "The thermal denaturation of whey proteins", New Zealand dairy Research Institute, PT95R03

Hansen R (1985), "Evaporation, Membrane Filtration and Spray Drying in milk powder and cheese production", North European Dairy Journal, Denmark

Hartley D E and Murgatroyd W (1964), "Criteria for the break-up of thin liquid layers flowing isothermally over solid surfaces", International Journal of Heat and Mass Transfer, Vol 7, pp. 1003-1015.

Heldman D R and Singh R P (2001), "Introduction to Food Engineering", Academic press, New Jersey.

Hirshburg R I and Florschuetz L W (1982), "Laminar Wavy- Film Flow: Part1, Hydrodynamic Analysis", Journal of Heat transfer, Vol. 104, pp. 452-458.

Hirshburg R I and Florschuetz L W (1982), "Laminar Wavy- Film Flow: Part2, Condensation and Evaporation", Journal of Heat transfer, Vol. 104, pp. 459-463.

Hoke B C and Chen J C (1992), "Thermocapillary breakdown of subcooled falling liquid films", Industrial Engineering and Chemistry Research, Vol.31, 688-694.

Jebson R S and Iyer M (1991), "The performance of falling film evaporators", Journal of dairy research, Vol. 58, pp.29-38.

Jeffreys G V and Jenson V G (1977), "Mathematical methods in Chemical Engineering", Academic press Inc. (London) Ltd., London.

Jeurnink T J M and Kruif K G De (1993), "Changes in milk on heating: viscosity measurements", Journal of Dairy Research, Vol. 60, pp. 139-150.

Ken K (1987), "The effects of evaporation and spray drying operations on whey protein concentrate gel strength", Dip.Tech report, Massey University, Palmerston North, New Zealand.

Kessler H G (1981), "Food Engineering and dairy Technology", Freising, Germany.

Kroll J E and McCutchan J W (1968), "Heat Transfer in an LTV Falling Film Evaporator: A Theoretical and experimental analysis", Journal of Heat Transfer, pp.201-210.

Lakkis J and Villota R (1990), "A study on the foaming and emulsifying properties of whey protein hydrolysates", American Institute of Chemical Engineers Symposium Series, Vol. 86, pp.87-101.

Lahtinen S T (2001), "Identification of fuzzy controller for use with a falling-film evaporator", Food Control, Vol.12, 179-180.

Lozano J E, Elustondo M P and Romagnoli J A (1984), "Control Studies in an Industrial Apple Juice Evaporator", Journal of food science, Vol.49, 1422-1427.

Mackereth A R (1993), "Thermal and Hydraulic Aspects of Falling Film Evaporator", PhD thesis, University of Canterbury, Christchurch, New Zealand.

Mackereth A R, Trinh K T and Woodhall M C (2003), Milk Powder Technology, New Zealand Dairy Research Institute.

Martin J A, Brian J W and Norman A T (1998), "Seasonal and lactational influences on bovine milk composition in New Zealand", Journal of Dairy Research, Vol. 65, pp. 401-411.

McAdams W H (1983), "Heat Transmission", 3rd Edition. Japan: McGraw-Hill Book Company.

McCabe W L, Smith J C and Harriott P (2001), "Unit operation of Chemical Engineering", 6th Edition. New York: McGraw-Hill Book Company.

Middleton J (1996), "Physical Properties of Dairy Products", MAF Quality Management, Ministry of Agriculture, New Zealand.

Mike W (1995), "De-aeration of whey protein concentrates", Dairy Research Institute, New Zealand, Project report #A59.02

Mills A F (1995), "Heat and Mass Transfer", IRWIN, Chicago, USA.

Minton P E (1986), "Handbook of Evaporation Technology", Noyes Publications, New Jersy, USA.

Mohanty A K (1986), "Fluid Mechanics", Prentice Hall of India Private Limited, India.

Mooney C V and Dotterweich F H (1955), "How to design and operate gas jet compressors", Petroleum refiner, Vol. 34(10), pp. 104-109.

Murakami E G and Okos M R (1989), "Measurement and prediction of thermal properties of foods", Food Properties and Computer-Aided Engineering of Food Processing Systems, Academic Publishers.

Murthy V N and Sarma P K (1977), "Falling-film evaporators- A design equation for heat transfer rates", The Canadian Journal of Chemical Engineering, Vol. 55, pp. 732-735.

Newman A (2001), "Solving a Traditional Shell and Tube Heat exchanger problem", Department of chemical engineering, Dissertation, University of Tennessee, USA

Oldfield D J (1996), "Heat-induced whey protein reactions in milk", PhD thesis, Massey University, Palmerston North, New Zealand.

Ozilgen M (1998), "Food Process Modelling and Control: Chemical Engineering Applications", Gordon and Breach Sciences publishers, The Netherlands.

Paramalingam S (1999), "The wetting constraint in falling-film evaporators", Dip.Tech. Dissertation, Massey University, New Zealand.

Paramalingam S, Huub H C Bakker and Chen H (2001), "Investigation of minimum flow conditions for milk products in falling-film evaporators", World Congress of Chemical Engineering, Melbourne, paper # 1648.

Paramalingam S, Winchester J and Marsh C (1999), "On the fouling of falling-film evaporators due to film break-up", Transaction of the Institute of Chemical Engineers, Vol. 78(C), pp.79-84.

Pascas H (2003), "Jamming of Sheared Concentrated Suspensions – a presentation at Massey University, New Zealand", ESPCI-Paris, France.

Perry R H and Green D W (1984), "Perry's Chemical Engineering Handbook", McGraw-Hill International, 5th Edition

Pritchard M (1997), "De-aeration of WPI retentate", New Zealand Dairy Research Institute, New Zealand.

Quaak P and Gerritsen J B M (1990), "Modelling dynamic behaviour of multi-effect Falling-film evaporators, Computer Applications in Chemical Engineering, Amsterdam: Elsevier, pp. 59-64.

Quaak P, Wijck M P C M and van Haren J J (1994), "Comparison of process identification and physical modelling for falling-film evaporators", Food Control, Vol. 5, No. 2, pp. 73-82.

Robert H P and Don W G (1997), "Perry's Chemical Engineering Handbook", McGraw-Hill International, 7th Edition

Runyon C H, Rumsey T R and McCarthy K L (1991), "Dynamic Simulation of a Non-linear Model of a Double Effect Evaporator", Journal of Food Engineering, Vol. 14, pp.185-201.

Snoeren T H M, Damman A J and Klok H J (1982), "The viscosity of skim milk concentrates", Netherlands Milk Dairy Journal, Vol. 36, pp.305-316.

Snoeren T H M, Damman A J and Klok H J (1983), "The viscosity of whole milk Concentrate and its effect on the properties of the powder", Zuivelzicht, Vol. 75(39), pp.847-849.

Schramm G (1981), "Introduction to Practical Viscometry", HAAKE Viscometers, West Germany.

Shekriladze I G and Gomelauri V I (1966), "Theoretical study of laminar film condensation of flowing vapour", International Journal of Heat and Mass Transfer, Vol. 9, pp.581-591.

Stephanopoulos G (1984), "Chemical process control: An introduction o theory and practice", Prentice hall International series, USA

Skogestad G and Postlethwaite I (1996), "Multivariable feedback control: Analysis and design", John Wiley and Sons, USA

Stuhltrager E (1995), " Flow dynamics and heat transfer of a condensate film on a vertical wall-II", International Journal of Heat and Mass Transfer, Vol. 38(15), pp. 2715-2722.

Tade M O and Le Page G P (1998), "Implementation of a differential geometric nonlinear controller on an industrial evaporator system", Control Engineering Practice, 6, 1309-1319.

Trinh K T, Mackereth A R and Woodhall M C (1996), " Milk powder Technology: Principles and process applications", New Zealand Dairy Research Institute, New Zealand.

Unterberge W and Edwards D K (1965), "Evaporation from Falling Saline Water Films in Laminar Transitional Flow", Journal of American Institute of Chemical Engineers, Vol. 11, pp. 1073-1079.

Van Der Mast V C and Bromley L A (1976), "Journal of American Institute of Chemical Engineers", Vol. 22, pp. 533-538.

Van Wylen G J, Sonntag R E and Borgnakke C (1994), "Fundamentals of classic thermodynamics", John Wiley and sons, Inc.

Velez-Ruiz J F and Barbosa-Canovas G V (1998), "Rheological Properties of Concentrated Milk as a Function of Concentration, Temperature and Storage Time", Journal of Food Engineering, Vol. 35, pp. 177-190.

Vennard J K and Street R L (1982), "Elementary Fluid Dynamics", Sixth edition, John Wiley and sons, New York.

Webb J and Alford (1974), "Fundamentals of Dairy Chemistry", The AVI publishing company, United States.

Winchester J A (2000), "Model based Analysis of the Operation and Control of falling film evaporators", PhD thesis, Massey University, Palmerston North, New Zealand.

Winchester J and Marsh C (1999), "Dynamics and control of falling-film evaporators with mechanical vapour recompression", Transaction of the Institute of Chemical Engineers, Part A, Vol. 77, pp 357-371.

Wong H Y (1977), "Heat transfer for engineers", Longman Group Limited, London.

Zhu H and Damodaran S (1994), "Effects of calcium and magnesium ions on aggregation of whey protein isolate and its effect on foaming properties", Journal of Agricultural food chemistry, Vol. 42, pp.856-862.

Appendix A: Physical property

In this section the principles and calibration method with each property measurements were described. The seasonal variation in the compositions is discussed. Then the measurement data is tabulated and the regression analysis with each property are discussed

A.1 Total solids Refractive Index (RI) Correlations

A.1.1 Principle of measurement

The Refractometer determines the refractive index (RI) of the process solution by measuring the critical angle of refraction. The light from a light source (L) (figure A.1.1) is directed against the interface between a prism (P) and the process solution (S). Two of the prism surfaces (M) are total reflecting mirrors bending the light rays. The light rays meet the interface at different angles. The reflected rays from an image (ACB), where (C) is the position of the critical angle ray. The rays at (A) are totally reflected at the process interface, the rays at (B) are partially reflected and partially refracted into the process solution. In this way the optical image is diverted into a light (A) area and a dark area (B). The position of the borderline (C) between the areas shows the value of the critical angle and thus of the refractive index of the process solution. The refractive index normally increases with increasing concentration.

From this follows that the optical image changes with the process concentration as shown in figure A.1.2. By this method the concentration of the solution is measured. The advantage of this method to measure the concentration is that the colour, gas bubbles, and suspended particles do not interfere with the result.
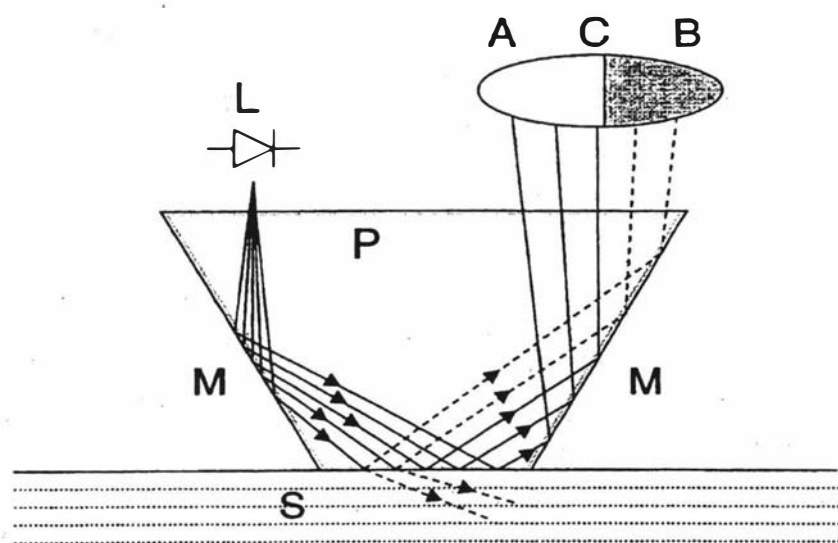
Figure A.1.1: Principles of Refractometer measurements

Low concentration   High concentration

Figure A.1.2: Optical images (*Atago Co. Ltd, Tokyo, Japan*)

A.1.2 Calibration and Temperature corrections

Calibration

The calibration procedure for different range RI meters is different. To calibrate the RI meter of the range 0-32% Brix, the RI reading of distilled water was measured at 20°C. The scale adjustment screw was adjusted to make the boundary coincide with 0%. Saturated sodium chloride solution was used to calibrate the RI meter of the range 28-62% Brix. The standard RI values of the saturated sodium chloride solutions are given in table A.1.1.

Table A.1.1: Refractometer calibration solution

Temperature (^{o}C)	Refractive Index (% Brix)
15	29.9
20	29.6
25	26.2
30	28.7

Temperature corrections

The temperature corrections to the RI values measured at different temperatures are shown in table A.1.2.

Table A.1.2: Refractometer temperature corrections (*Atago Co. Ltd, Tokyo, Japan*)

Temperature (°C)	Brix %																	
	0	5	10	15	20	25	30	35	40	45	50	55	60	65	70	75	80	85
	Subtract from the measured value																	
15	0.29	0.30	0.32	0.33	0.34	0.35	0.36	0.37	0.37	0.38	0.38	0.38	0.38	0.38	0.38	0.38	0.37	0.37
16	0.24	0.25	0.26	0.27	0.28	0.28	0.29	0.30	0.30	0.30	0.31	0.31	0.31	0.31	0.31	0.30	0.30	0.30
17	0.18	0.19	0.20	0.20	0.21	0.21	0.22	0.22	0.23	0.23	0.23	0.23	0.23	0.23	0.23	0.23	0.23	0.22
18	0.12	0.13	0.13	0.14	0.14	0.14	0.15	0.15	0.15	0.15	0.15	0.15	0.15	0.15	0.15	0.15	0.15	0.15
19	0.06	0.06	0.07	0.07	0.07	0.07	0.07	0.08	0.08	0.08	0.08	0.08	0.08	0.08	0.08	0.08	0.08	0.07
	Add to the measured value																	
21	0.06	0.07	0.07	0.07	0.07	0.07	0.08	0.08	0.08	0.08	0.08	0.08	0.08	0.08	0.08	0.08	0.08	0.07
22	0.13	0.14	0.14	0.14	0.15	0.15	0.15	0.15	0.16	0.16	0.16	0.16	0.16	0.16	0.15	0.15	0.15	0.15
23	0.20	0.21	0.21	0.22	0.22	0.23	0.23	0.23	0.23	0.24	0.24	0.24	0.24	0.23	0.23	0.23	0.23	0.22
24	0.27	0.28	0.29	0.29	0.30	0.30	0.31	0.31	0.31	0.32	0.32	0.32	0.32	0.31	0.31	0.31	0.30	0.30
25	0.34	0.35	0.36	0.37	0.38	0.38	0.39	0.39	0.40	0.40	0.40	0.40	0.40	0.39	0.39	0.38	0.38	0.37
26	0.42	0.43	0.44	0.45	0.46	0.46	0.47	0.47	0.48	0.48	0.48	0.48	0.48	0.47	0.47	0.46	0.46	0.45
27	0.50	0.51	0.52	0.53	0.54	0.55	0.55	0.56	0.56	0.56	0.56	0.56	0.56	0.55	0.55	0.54	0.53	0.52
28	0.58	0.59	0.60	0.61	0.62	0.63	0.64	0.64	0.64	0.65	0.65	0.64	0.64	0.63	0.63	0.62	0.61	0.60
29	0.66	0.67	0.68	0.70	0.71	0.71	0.72	0.73	0.73	0.73	0.73	0.73	0.72	0.72	0.71	0.70	0.69	0.67
30	0.74	0.76	0.77	0.78	0.79	0.80	0.81	0.81	0.82	0.82	0.81	0.81	0.80	0.80	0.79	0.78	0.76	0.75
31	0.83	0.84	0.85	0.87	0.88	0.89	0.89	0.90	0.90	0.90	0.90	0.89	0.89	0.88	0.87	0.86	0.84	0.82
32	0.92	0.93	0.94	0.96	0.97	0.98	0.98	0.99	0.99	0.99	0.99	0.98	0.97	0.96	0.95	0.93	0.92	0.90
33	1.01	1.02	1.03	1.05	1.06	1.07	1.07	1.08	1.08	1.08	1.07	1.07	1.06	1.04	1.03	1.01	1.00	0.98
34	1.10	1.11	1.13	1.14	1.15	1.16	1.16	1.17	1.17	1.16	1.16	1.15	1.14	1.13	1.11	1.09	1.07	1.05
35	1.19	1.21	1.22	1.23	1.24	1.25	1.25	1.26	1.26	1.25	1.25	1.24	1.23	1.21	1.19	1.17	1.15	1.13
36	1.29	1.30	1.31	1.33	1.34	1.34	1.35	1.35	1.35	1.34	1.34	1.33	1.31	1.29	1.28	1.25	1.23	1.20
37	1.39	1.40	1.41	1.42	1.43	1.44	1.44	1.44	1.44	1.43	1.43	1.41	1.40	1.38	1.36	1.33	1.31	1.28
38	1.49	1.50	1.51	1.52	1.53	1.53	1.54	1.54	1.53	1.53	1.52	1.50	1.48	1.46	1.44	1.42	1.39	1.36
39	1.59	1.60	1.61	1.62	1.63	1.63	1.63	1.63	1.63	1.62	1.61	1.59	1.57	1.55	1.52	1.50	1.47	1.43
40	1.69	1.70	1.71	1.72	1.73	1.73	1.73	1.73	1.72	1.71	1.70	1.68	1.66	1.63	1.61	1.58	1.54	1.51

A.1.3. Total Solids and Refractive Index correlations
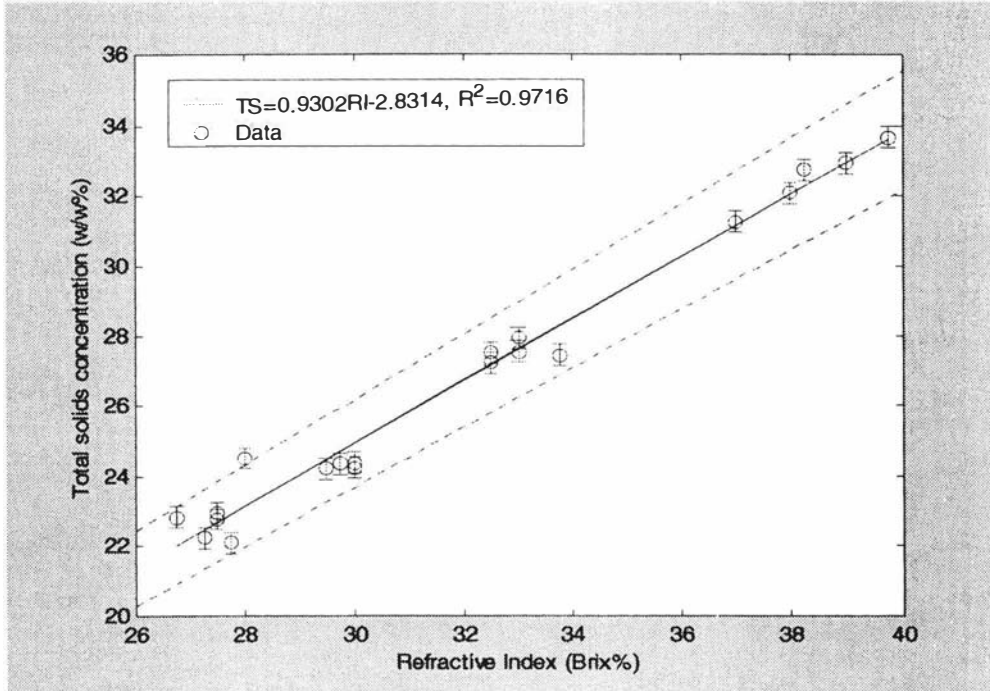
Figure A.1.3: RI calibration against total solids with WPC-1
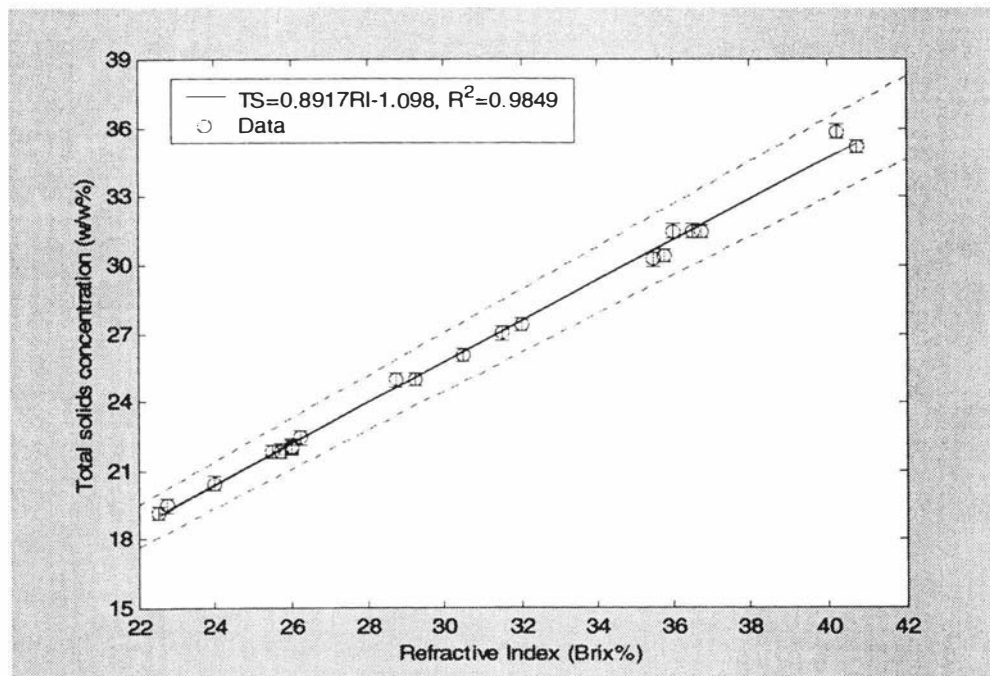
Figure A.1.4: RI calibration against total solids with WPC-2
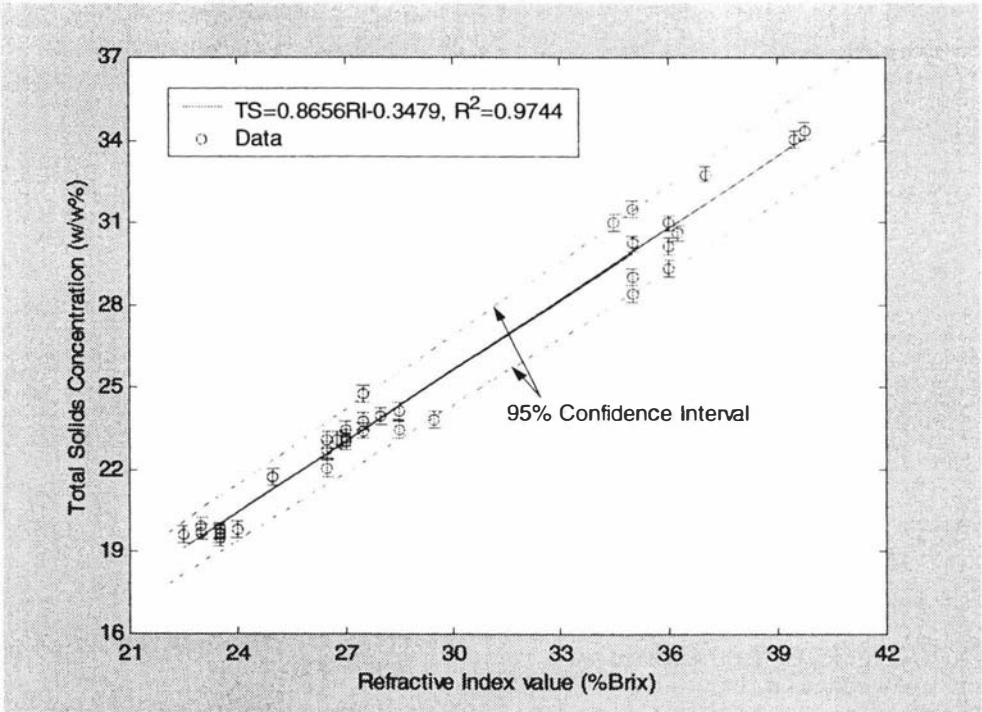
Figure A.1.5: RI calibration against total solids with WPC-3
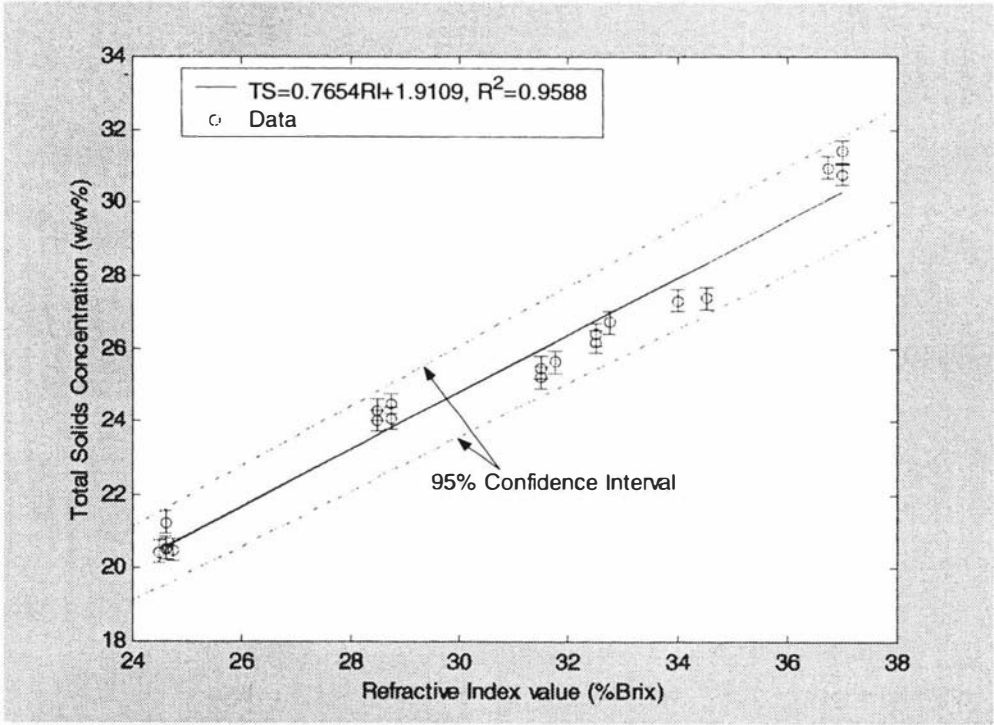
Figure A.1.6: RI calibration against total solids with WPI

(A.2) Samples preparation

Results

SAMPLE 8981, % native whey protein

Protein Species	NZDRI Sample number	Sample Description	Native Protein Measure #1	Native Protein Measure #2	Native Protein Average
β—lactoglobulin	26582	8981 Finished product	96.0	98.4	97.2
	26580	8981 Evaporator Feed	95.6	98.6	97.1
	26581	8981 Dryer feed	98.0	98.2	98.1
α—lactalbumin	26582	8981 Finished product	95.0	99.5	97.2
	26580	8981 Evaporator Feed	96.6	99.8	98.2
	26581	8981 Dryer feed	98.1	100.0	99.0
Lactoferrin	26582	8981 Finished product	Insufficient in sample for analysis		
	26580	8981 Evaporator Feed	Insufficient in sample for analysis		
	26581	8981 Dryer feed	Insufficient in sample for analysis		
bovine serum albumin	26582	8981 Finished product	96.8	97.2	97.0
	26580	8981 Evaporator Feed	99.3	97.9	98.6
	26581	8981 Dryer feed	98.7	98.4	98.5
Immunoglobulin G	26580	8981 Evaporator Feed	Insufficient in sample for analysis		
	26580	8981 Evaporator Feed	Insufficient in sample for analysis		
	26581	8981 Dryer feed	Insufficient in sample for analysis		

SAMPLE 3102, % native whey protein

Protein Species	NZDRI Sample number	Sample Description	Native Protein Measure #1	Native Protein Measure #2	Native Protein Average
β-lactoglobulin	26579	3102 Finished product	99.5	95.6	97.5
	26577	3102 Evaporator Feed	95.6	92.9	94.2
	26578	3102 Dryer feed	97.4	98.1	97.7
α-lactalbumin	26579	3102 Finished product	97.3	95.3	96.3
	26577	3102 Evaporator Feed	95.3	94.3	94.8
	26578	3102 Dryer feed	95.5	97.2	96.3
lactoferrin	26579	3102 Finished product	31.8	28.6	30.2
	26577	3102 Evaporator Feed	25.3	27.4	26.3
	26578	3102 Dryer feed	28.0	31.2	29.6
bovine serum albumin	26579	3102 Finished product	57.0	53.7	55.4
	26577	3102 Evaporator Feed	56.2	60.2	58.2
	26578	3102 Dryer feed	57.8	64.8	61.3
Immunoglobulin G	26579	3102 Finished product	20.1	13.4	16.8
	26577	3102 Evaporator Feed	12.4	16.1	14.2
	26578	3102 Dryer feed	11.7	21.1	16.4

Page 4 of 5

241

(A.3) Composition variability in the feed whey

A.3.1 Seasonal variation of composition in the milk

The seasonal variation in the composition of milk is associated with several factors: Nutritional factors, availability and quality of pasture, physiological changes associated with the stage of lactation and pathological factors. Though the milk composition (protein, fat and lactose) changes throughout the year, the proportion of the milk components (protein to fat ratio) is maintained by standardising the incoming milk at dairy industries. But the changes in the individual proteins (casein and whey proteins) components of the milk are not adjusted. Martin et al. (1998) have studied the factors that influence the milk compositions in New Zealand and the variation of composition of the important components of milk are shown in figure A.3.1.
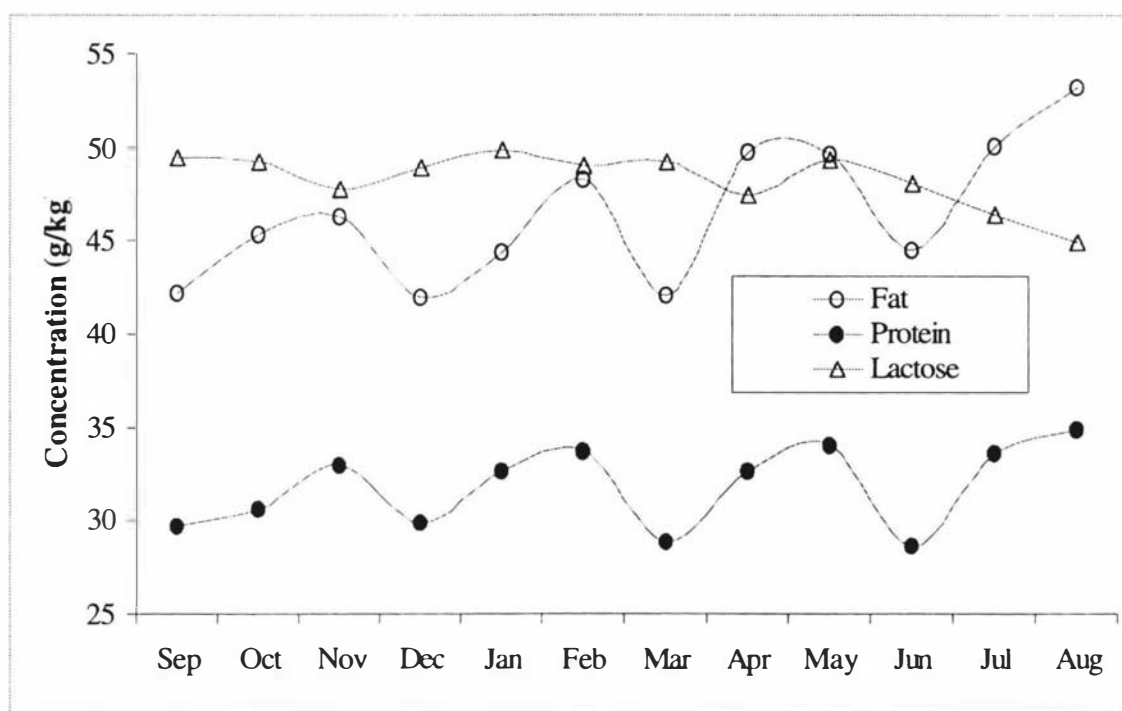
Figure A.3.1: Seasonal variation of composition in the supply milk

A.3.2 Composition variation in the final product

The compositions (fat and protein) of the final product tested on different days and in different months are shown in figure A.3.2 and A.3.3. The testing were done at the whey product laboratory (Fonterra-Ingredients, Whareroa, New Zealand) using the Infraliser. Figures show that there is no direct link between the milk compositions and the final product compositions. This is because several process steps take place between the raw milk and the whey powder process. The important ones are the Ultrafiltration and the Ion exchange processes where the milk components are separated. The figures also show that the variation in each component is not significant; protein is within $\pm 1\%$ with WPI and $\pm 2\%$ with WPC whereas the fat is within $\pm 1\%$ with WPC and within $\pm 0.15\%$ with WPI. The changes of composition over the time was neglected as the changes were too small to cause significant influence on the measurements.
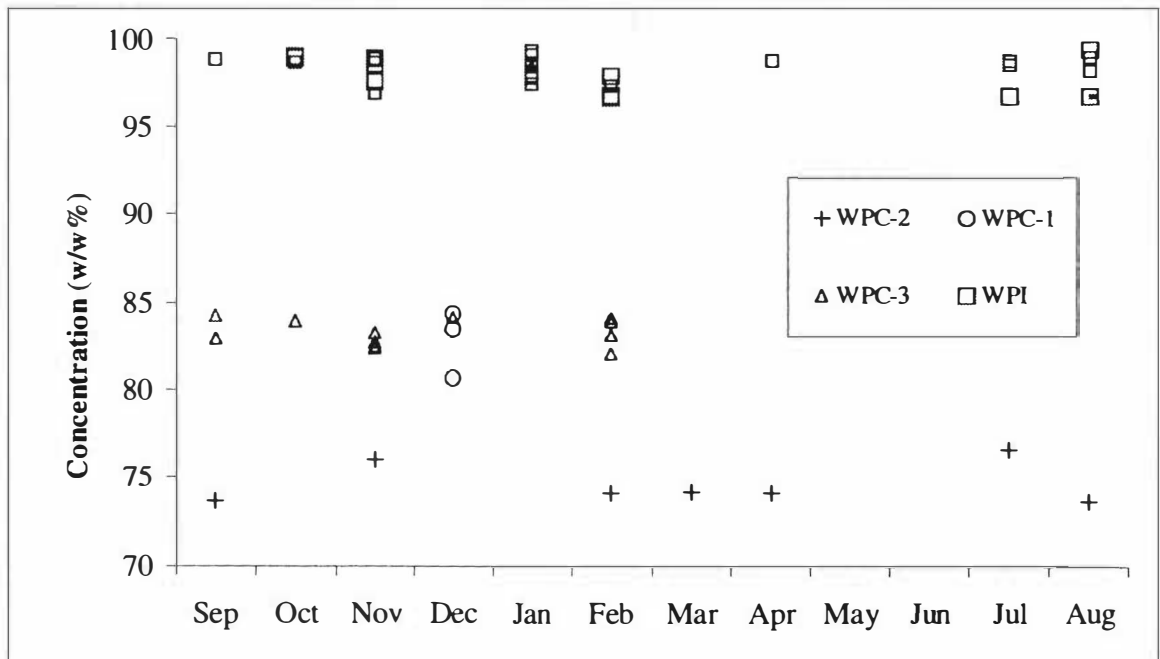
Figure A.3.2: The variation of protein content in the whey powder
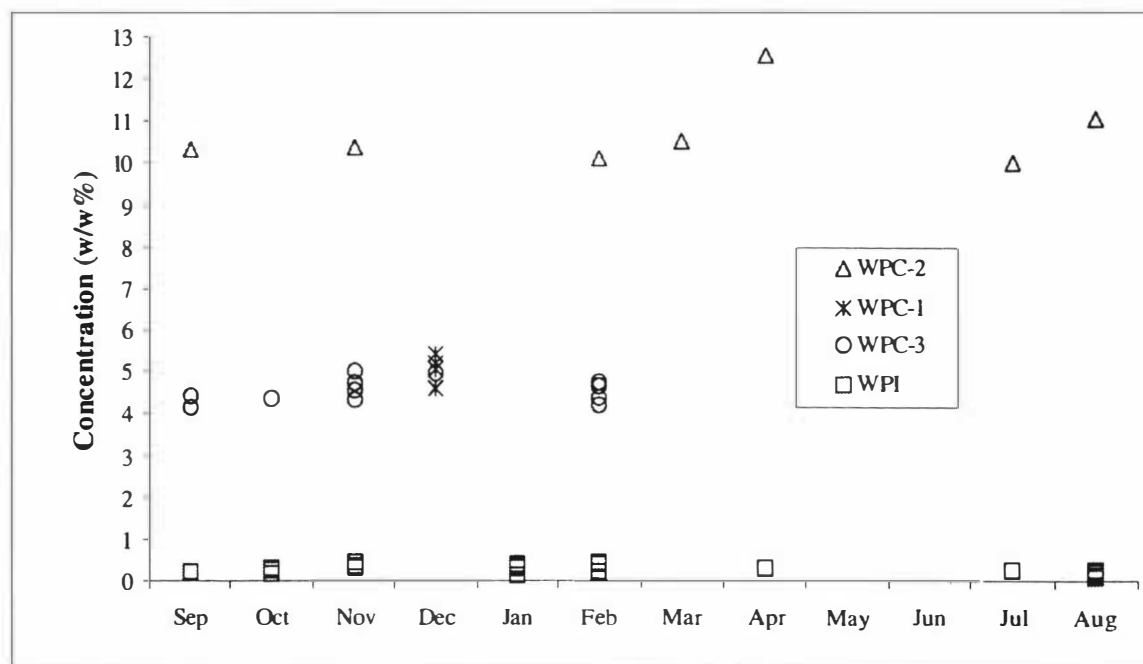
Figure A.3.3: The variation of fat content in the whey powder

(A.4) Density

A.4.1 Principles of measurement

The density can be measured quickly and easily using a device called a hydrometer, which makes use of the principle of flotation. If an object floats in a liquid, the principle of flotation states that the mass of the object is identically equal to the mass of liquid it displaces. The hydrometer is a cylindrical device with markings on the side. If the same hydrometer is placed in several different liquids, it will float at various depths, depending on the density of the liquid. If the liquid is very dense, the floating hydrometer will not be immersed very far (figure A.4.1). If the liquid is less dense, the hydrometer will float lower in the liquid, because more a greater volume of liquid must be displaced to displace the same mass. Once the hydrometer has been calibrated, comparing the level of the surface of the liquid with the markings on the side of the hydrometer allows for the direct measurement of the density.

244
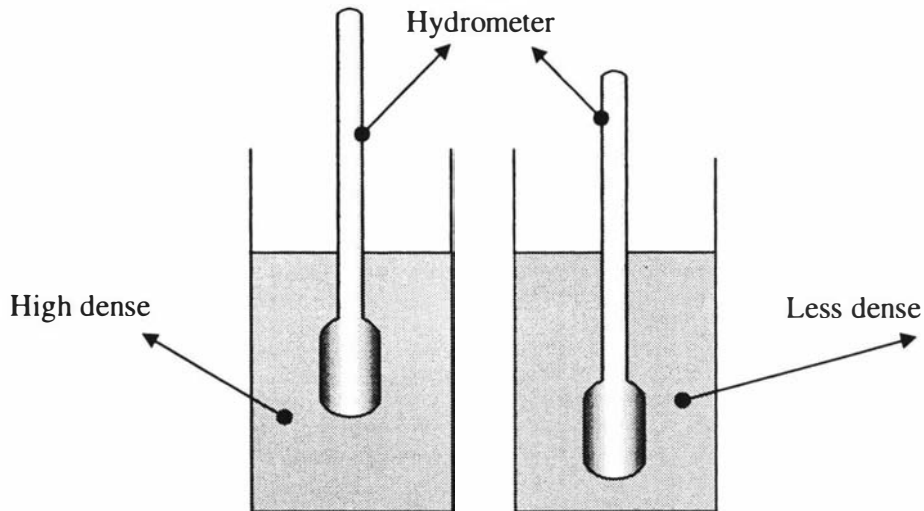
Figure A.4.1: Principle of density measurements

A.4.2 Calibration and temperature corrections

Calibration

To calibrate the density hydrometer, the measuring cylinder was filled with distilled water at 20°C. The hydrometer was put into water and given a spin. The value at which the hydrometer scale settled was noted at this temperature. This procedure was repeated several times at different temperatures and the average values were obtained as the deviation from the expected values. The expected values of density of water at different temperatures obtained from Perry and Green (1984).

Temperature correction

Hydrometers were calibrated at 20°C and the corrections for water at different temperatures are shown in table A.4.1. The corrections with other hydrometers were assumed to be the same.

Table A.4.1: Hydrometer reading correction for temperature

Temperature (^{o}C)	Density corrections (kg/m^3)
10	- 1.3
15	-0.5
20	0.0
25	0.5
29	1.0
35	2.0
40	4.0
50	5.1
60	6.7

A.4.3 Measurement Data (WPC-3)

Run Number	Temperature (°C)	Total Solids (w/w%)	Density (kg/m^3)
1	20	5	1012.2
		10	1024.9
		15	1039.3
		20	1051.3
		25	1070.2
	30	5	1009.2
		10	1020.5
		15	1037.5
		20	1048.5
		25	1066.6
	40	5	1006.5
		10	1018.2
		15	1034.0
		20	1045.0
		25	1062.2
	50	5	1002.5
		10	1016.1
		15	1029.4
		20	1042.9
		25	1058.2
	60	5	997.8
		10	1011.8
		15	1024.9
		20	1040.2
		25	-

Run Number	Temperature (°C)	Total Solids (w/w%)	Density (kg/m³)
2	20	5	1011.8
		10	1024.3
		15	1040.5
		20	1051.2
		25	1070.5
	30	5	1009.0
		10	1020.9
		15	1037.2
		20	1048.7
		25	1066.2
	40	5	1006.0
		10	1018.7
		15	1033.5
		20	1046.4
		25	1062.4
	50	5	1002.2
		10	1015.4
		15	1028.7
		20	1043.5
		25	1058.4
	60	5	997.3
		10	1011.2
		15	1024.7
		20	1039.8
		25	-

Run Number	Temperature (°C)	Total Solids (w/w%)	Density (kg/m³)
3	20	5	1012.4
		10	1024.9
		15	1039.1
		20	1051.1
		25	1069.7
	30	5	1010.1
		10	1020.0
		15	1037.8
		20	1049.1
		25	1066.4
	40	5	1006.2
		10	1019.1
		15	1034.2
		20	1045.4
		25	1062.6
	50	5	1001.7
		10	1015.8
		15	1027.8
		20	1043.1
		25	1058.4
	60	5	998.1
		10	1010.9
		15	1023.9
		20	1039.5
		25	1054.0

A.4.4 Measurement Data (WPI)

Run Number	Temperature (°C)	Total Solids (w/w%)	Density (kg/m³)
1	20	5 10 15 20 25	1012.8 1026.5 1040.0 1053.7 1067.6
	30	5 10 15 20 25	1008.9 1023.5 1037.0 1051.2 1066.0
	40	5 10 15 20 25	1006.5 1020.1 1033.8 1046.1 1063.4
	50	5 10 15 20 25	1003.5 1016.8 1030.1 1043.2 1059.5
	60	5 10 15 20 25	998.7 1012.8 1026.5 1040.7 1055.2

Run Number	Temperature (°C)	Total Solids (w/w%)	Density (kg/m³)
2	20	5 10 15 20 25	1012.0 1027.5 1040.9 1054.2 1068.2
	30	5 10 15 20 25	1007.7 1023.9 1037.8 1051.6 1065.5
	40	5 10 15 20 25	1006.8 1020.7 1034.8 1046.8 1063.9
	50	5 10 15 20 25	1003.8 1015.4 1030.8 1043.8 1060.2
	60	5 10 15 20 25	997.9 1013.0 1026.9 1040.1 1055.9

Run Number	Temperature (°C)	Total Solids (w/w%)	Density (kg/m³)
3	20	5	1013.9
		10	1026.0
		15	1041.5
		20	1054.6
		25	1068.9
	30	5	1009.4
		10	1024.5
		15	1038.5
		20	1050.8
		25	1066.5
	40	5	1007.7
		10	1021.3
		15	1033.2
		20	1045.7
		25	1063.0
	50	5	1004.4
		10	1017.5
		15	1031.4
		20	1044.0
		25	1059.0
	60	5	998.6
		10	1013.8
		15	1027.7
		20	1040.8
		25	1056.7

A.4.5 Regression Analysis (WPC-3)

Factorial Design

```
General Factorial Design

Factors:    2      Factor Levels: 5, 5
Runs:      75      Replicates:    3, blocked on replicates
```

Regression Analysis: Density versus Temp, Solids

```
The regression equation is
Density = 1005 - 0.342 Temp + 2.8 Solids

Predictor          Coef      SE Coef          T         P
Constant        1004.74         0.55    1836.07     0.000
Temp           -0.34163      0.01053     -33.25     0.000
Solids          2.80480      0.02106     134.14     0.000

S = 1.290      R-Sq = 99.6%      R-Sq(adj) = 99.6%
```

A.4.6 Regression model (WPI)

Factorial Design

```
General Factorial Design

Factors:    2      Factor Levels: 5, 5
Runs:      75      Replicates:    3, blocked on replicates
```

Regression Analysis: Density versus Temp, Solids
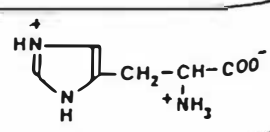
```
The regression equation is
Density = 1005.3 - 0.359 Temp + 2.837 TS

Predictor          Coef      SE Coef          T         P
Constant        1005.17         0.40    2535.93     0.000
Temp          -0.359331     0.007631     -44.15     0.000
TS              2.83707      0.01526     183.27     0.000

S = 0.9346     R-Sq = 99.8%      R-Sq(adj) = 99.8%
```
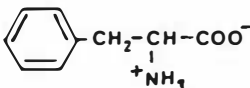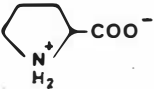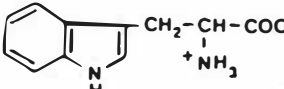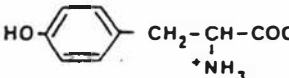
α-Lactalbumin B

```
                          10                              20
H.Glu-Gln-Leu-Thr-Lys-Cys-Glu-Val-Phe-Arg-Glu-Leu-Lys-Asp-Leu-Lys-Gly-Tyr-Gly-Gly-

                          30                              40
Val-Ser-Leu-Pro-Glu-Trp-Val-Cys-Thr-Thr-Phe-His-Thr-Ser-Gly-Tyr-Asp-Thr-Glu-Ala-

                          50                              60
Ile-Val-Glu-Asn-Asn-Gln-Ser-Thr-Asp-Tyr-Gly-Leu-Phe-Gln-Ile-Asn-Asn-Lys-Ile-Trp-

                          70                              80
Cys-Lys-Asn-Asp-Gln-Asp-Pro-His-Ser-Ser-Asn-Ile-Cys-Asn-Ile-Ser-Cys-Asp-Lys-Phe-

                          90                             100
Leu-Asn-Asn-Asp-Leu-Thr-Asn-Asn-Ile-Met-Cys-Val-Lys-Lys-Ile-Leu-Asp-Lys-Val-Gly-

                         110                             120
Ile-Asn-Tyr-Trp-Leu-Ala-His-Lys-Ala-Leu-Cys-Ser-Glu-Lys-Leu-Asp-Gln-Trp-Leu-Cys-

          123
Glu-Lys-Leu.OH
```

β-Lactoglobulin B

```
                          10                              20
H Leu-Ile-Val-Thr-Gln-Thr-Met-Lys-Gly-Leu-Asp-Ile-Gln-Lys-Val-Ala-Gly-Thr-Trp-Tyr-

                          30                              40
Ser-Leu-Ala-Met-Ala-Ala-Ser-Asp-Ile-Ser-Leu-Leu-Asp-Ala-Gln-Ser-Ala-Pro-Leu-Arg-

                          50                              60
Val-Tyr-Val-Glu-Glu-Leu-Lys-Pro-Thr-Pro-Glu-Gly-Asp-Leu-Glu-Ile-Leu-Leu-Gln-Lys-

                          70                              80
Trp-Glu-Asn-Gly-Glu-Cys-Ala-Gln-Lys-Lys-Ile-Ile-Ala-Glu-Lys-Thr-Lys-Ile-Pro-Ala-

                          90                             100
Val-Phe-Lys-Ile-Asp-Ala-Leu-Asn-Glu-Asn-Lys-Val-Leu-Val-Leu-Asp-Thr-Asp-Tyr-Lys-

                         110                             120
Lys-Tyr-Leu-Leu-Phe-Cys-Met-Glu-Asn-Ser-Ala-Glu-Pro-Glu-Gln-Ser-Leu-Ala-Cys-Gln-

                         130                             140
Cys-Leu-Val-Arg-Thr-Pro-Glu-Val-Asp-Asp-Glu-Ala-Leu-Glu-Lys-Phe-Asp-Lys-Ala-Leu-

                         150                             160
Lys-Ala-Leu-Pro-Met-His-Ile-Arg-Leu-Ser-Phe-Asn-Pro-Thr-Gln-Leu-Glu-Glu-Gln-Cys-

          162.
His-Ile.OH
```

Amino acid			Molecular Weight	Chemical name	Structure
name	Symbol 3 letters or 1 letter				
Alanine	Ala	A	89.1	α-amino-propionic acid	$CH_3-CH-COO^-$ $\quad +NH_3$
Arginine	Arg	R	174.2	α-amino-δ-ureinovalerianic acid	$H_2N-C-NH-(CH_2)_3-CH-COO^-$ $\quad +NH_2 \quad\quad +NH_3$
Asparagine	Asn	N	132.1	amide of Asp	$H_2N-C-CH_2-CH-COO^-$ $\quad\; O \quad\quad +NH_3$
Aspartic acid	Asp	D	133.1	α-amino-succinic acid	$^-O-C-CH_2-CH-COO^-$ $\quad\;\; O \quad\quad +NH_3$
Cysteine	Cys	C	121.1	α-amino-β-mercaptopropionic acid	$HS-CH_2-CH-COO^-$ $\quad\quad +NH_3$
Glutamine	Glu	Q	146.1	amide of Glu	$H_2N-C-(CH_2)_2-CH-COO^-$ $\quad\;\; O \quad\quad +NH_3$
Glutamic acid	Glu	E	147.1	α-amino-glutaric acid	$^-O-C-(CH_2)_2-CH-COO^-$ $\quad\;\; O \quad\quad +NH_3$
Glycine	Gly	G	75.1	α-amino-acetic acid	$H-CH-COO^-$ $\quad +NH_3$
Histidine	His	H	155.2	α-amino-β-imidazol propionic acid	$CH_2-CH-COO^-$ $\quad\quad +NH_3$
Isoleucine	Ile	I	131.2	α-amino-β-methyl valerianic acid	$CH_3-CH_2-CH-CH-COO^-$ $\quad\quad CH_3 \;\, +NH_3$

255

(Continued)

Amino acid			Molecular Weight	Chemical name	Structure
name	Symbol 3 letters or 1 letter				
Leucine	Leu	L	131.2	α-amino-isocaproic acid	$CH_3-CH-CH_2-CH-COO^-$ with CH_3 and $^+NH_3$
Lysine	Lys	K	146.2	α-ε-diamino-caproic acid	$NH_2-(CH_2)_4-CH-COO^-$ with $^+NH_3$
Methionine	Met	M	149.2	α-amino-ᵟ-methyl thiol-n-butyric acid	$CH_3-S-(CH_2)_2-CH-COO^-$ with $^+NH_3$
Phenylalanine	Phe	F	165.2	α-amino-β-phenyl propionic acid	⬡$-CH_2-CH-COO^-$ with $^+NH_3$
Proline	Pro	P	115.1	pyrrolidine-2-carboxylic acid	(pyrrolidine ring) $-COO^-$ with N^+H_2
Serine	Ser	S	105.1	α-amino-β-hydroxy propionic acid	$HO-CH_2-CH-COO^-$ with $^+NH_3$
Threonine	Thr	T	119.1	α-amino-β-hydroxy-n-butyric acid	$CH_3-CH-CH-COO^-$ with OH and $^+NH_3$
Tryptophan	Trp	W	204.2	α-amino-β-3-indolyl-propionic acid	(indole ring) $-CH_2-CH-COO^-$ with $^+NH_3$
Tyrosine	Tyr	Y	181.2	α-amino-β-(ρ-hydroxy-phenyl propionic) acid	$HO-$⬡$-CH_2-CH-COO^-$ with $^+NH_3$
Valine	Val	V	117.1	α-amino-isovalerianic acid	$CH_3-CH-CH-COO^-$ with CH_3 and $^+NH_3$

(A.5) Viscosity

A.5.1 Principles of measurement

Rheomat viscometer

The Rheomat viscometer operates by the principle of rotation of a cylinder (spindle) which is submerged in the substance to be analysed, measuring the resistance of the substance at a pre-set speed or at varying speed (figure A.5.1). The resulting resistance or torque is the measurement of the flow viscosity. The greater the resistance of the product to be determined, the greater the viscosity. Based on the speed and the characteristics of the spindle, the torque is calculated and a direct reading of the viscosity is provided in mPa .s. The viscometers are equipped with different types of spindles and speeds which provide a wide range of measurement of viscosity.
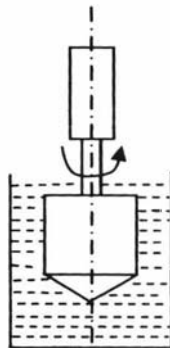
Figure A.5.1: Principle of Rheomat rotational viscometer

Capillary tube

The liquid in this type of viscometer runs through the capillary by its own weight. The liquid level above the exit orifice slowly decreases during the time, which consequently causes the flow rate to drop. This gradual change of flow rate also means a non-constant shear rate. This then means that the viscosity value measured cannot be linked to one defined shear rate but to a shear rate range.

A.5.2 Calibration

Rheomat viscometer

The Rheomat viscometer readings with Whole milk and Whey product were checked against the readings obtained from the capillary tube viscometer. The figure A.5.2 shows the concentrate viscosity measured using both viscometers. The concentrate behaves like Newtonian fluids at low total solids and therefore, the shear rate applied was not a problem in the testing.
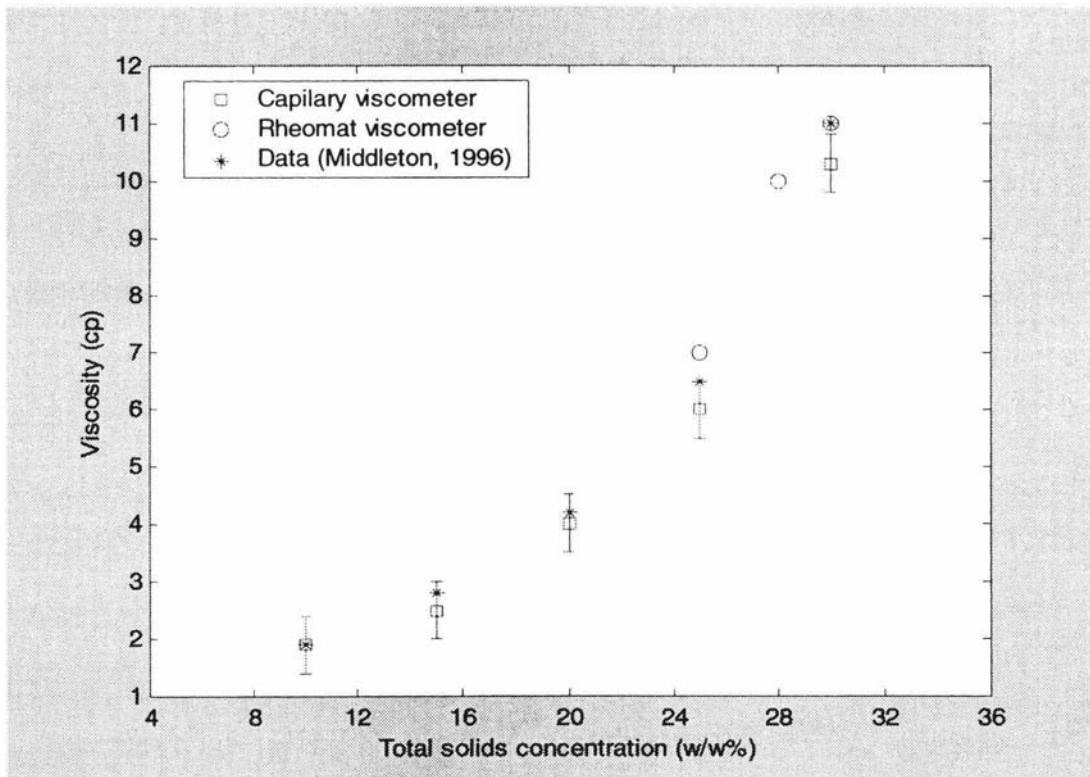
Figure A.5.2: Viscosity of whole milk with different viscometers at 22°C

Capillary tube

The capillary tube viscometer is calibrated against the viscosity of water. The flow time was measured at different temperatures with water and this is used in the viscometer model to estimate the product viscosity. The model relating the viscosity and density of both water and product is shown below.

$$\mu_p = \left(\frac{\rho_p}{\rho_w}\right) \cdot \left(\frac{\tau_p}{\tau_w}\right) \cdot \mu_w$$

A.5.3 Rheological behaviour of whey products

The Rheological behaviour of liquids can be categorised in to two major types: Newtonian and Non-Newtonian. With Newtonian liquids, the shear stress is independent of the shear rate thus the viscosity of the liquid is independent to the shear rate. With Non-Newtonian liquids, the shear stress depends upon the shear rate and therefore the viscosity is dependent on the shear rate. The figure A.5.3 shows the flow curves of all possible Newtonian and Non-Newtonian liquids (Schramm, 1981).
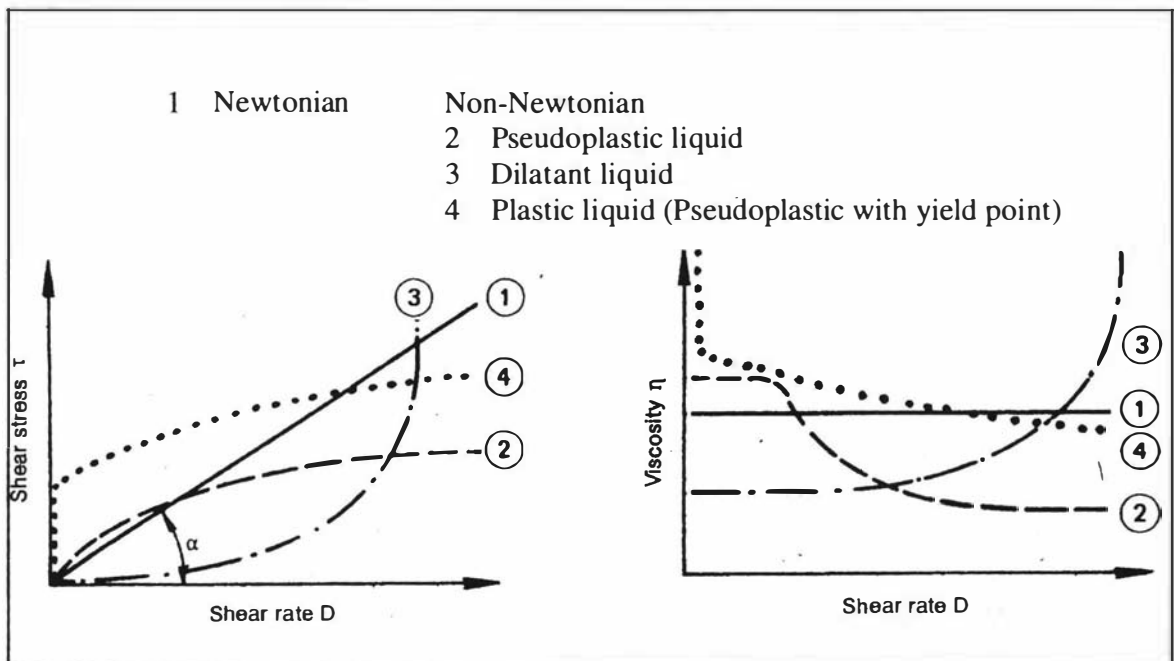
Figure A.5.3: Various types of flow behaviour

To categorise the type of behaviour of the whey concentrates, the flow curve for each types of concentrate was drawn and shown in figure A.5.4. The WPC-2 and WPC-3 product whey show Non-Newtonian behaviour whereas all other products and the feeds behave like Newtonian liquids at evaporator operating temperatures.

Therefore, the viscosity model developed using the experimental data is strongly depend upon the shear rate with WPC-2 and WPC-3 and less dependant with all other products at the evaporator operating conditions.
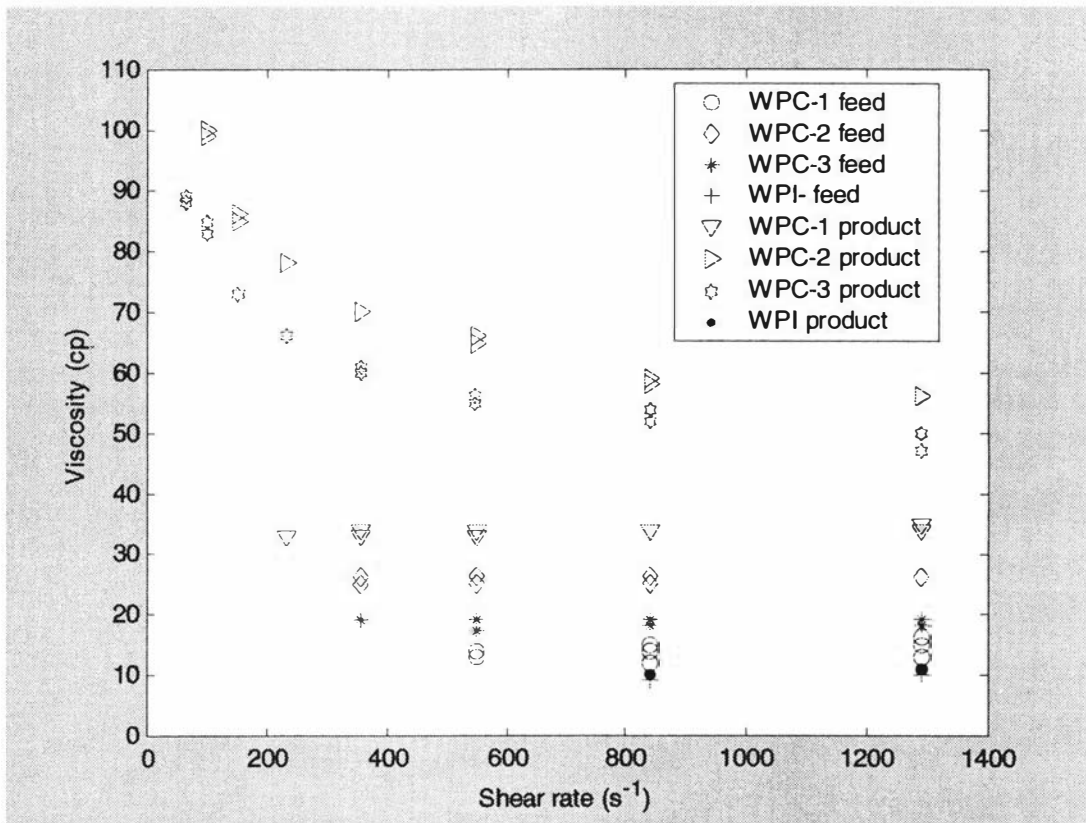
Figure A.5.4: Flow curves with whey products at evaporator operating conditions

A.5.4 Measurement Data (WPC-3) – Low Shear

Run Number	Temperature (°C)	Total Solids (w/w%)	Viscosity (cp)	Log(Viscosity)
1	20	10	7.01	1.947
		15	12.98	2.563
		20	20.00	2.995
		25	30.00	3.401
		30	60.00	4.094
		35	120.00	4.787
	30	10	5.50	1.704
		15	8.10	2.091
		20	14.97	2.706
		25	26.00	3.258
		30	44.00	3.784
		35	88.00	4.477
	40	10	4.25	1.446
		15	8.50	2.140
		20	10.00	2.302
		25	17.00	2.833
		30	37.00	3.610
		35	68.00	4.219
	50	10	3.30	1.193
		15	6.40	1.856
		20	10.00	2.302
		25	17.00	2.833
		30	31.00	3.433
		35	56.00	4.025

Run Number	Temperature (°C)	Total Solids (w/w %)	Viscosity (cp)	Log(Viscosity)
2	20	10	7.34	1.993
		15	13.50	2.602
		20	23.00	3.135
		25	29.00	3.367
		30	58.00	4.060
		35	116.00	4.753
	30	10	5.75	1.749
		15	9.87	2.289
		20	17.85	2.882
		25	25.00	3.218
		30	45.00	3.806
		35	87.00	4.465
	40	10	4.42	1.486
		15	8.24	2.109
		20	12.24	2.504
		25	18.00	2.890
		30	38.00	3.637
		35	66.00	4.189
	50	10	3.21	1.166
		15	6.24	1.830
		20	12.25	2.505
		25	17.00	2.833
		30	30.00	3.401
		35	55.00	4.007

Run Number	Temperature (°C)	Total Solids (w/w%)	Viscosity (cp)	Log(Viscosity)
3	20	10	6.87	1.927
		15	14.00	2.639
		20	23.50	3.157
		25	30.00	3.401
		30	62.00	4.127
		35	118.00	4.770
	30	10	5.62	1.726
		15	10.25	2.327
		20	18.87	2.937
		25	26.00	3.258
		30	44.00	3.784
		35	89.00	4.488
	40	10	4.38	1.477
		15	8.64	2.156
		20	13.54	2.605
		25	16.00	2.772
		30	37.00	3.610
		35	67.00	4.204
	50	10	3.34	1.205
		15	6.48	1.868
		20	12.87	2.554
		25	16.00	2.772
		30	32.00	3.465
		35	57.00	4.043

A.5.5 Measurement Data (WPC-3) – High Shear

Run Number	Temperature (°C)	Total Solids (w/w%)	Viscosity (cp)	Log(Viscosity)
1	20	20	19	2.944
		25	33	3.496
		30	56	4.025
		35	86	4.454
	30	20	14	2.639
		25	24	3.178
		30	40	3.688
		35	66	4.189
	40	20	11	2.397
		25	18	2.890
		30	31	3.433
		35	49	3.891
	50	20	10	2.302
		25	13	2.564
		30	23	3.135
		35	37	3.610

Run Number	Temperature (°C)	Total Solids (w/w%)	Viscosity (cp)	Log(Viscosity)
2	20	20	18	2.890
		25	34	3.526
		30	55	4.007
		35	85	4.442
	30	20	15	2.708
		25	24	3.178
		30	39	3.663
		35	65	4.174
	40	20	12	2.484
		25	17	2.833
		30	30	3.401
		35	50	3.912
	50	20	9	2.197
		25	12	2.484
		30	22	3.091
		35	38	3.637

Run Number	Temperature (°C)	Total Solids (w/w%)	Viscosity (cp)	Log(Viscosity)
3	20	20	19	2.944
		25	33	3.496
		30	58	4.060
		35	87	4.465
	30	20	14	2.639
		25	23	3.135
		30	40	3.688
		35	65	4.174
	40	20	11	2.397
		25	17	2.833
		30	31	3.433
		35	48	3.871
	50	20	10	2.302
		25	12	2.484
		30	23	3.135
		35	39	3.663

A.5.6 Measurement Data (WPI) –Low shear

Run Number	Temperature (°C)	Total Solids (w/w%)	Viscosity (cp)	Log(Viscosity)
1	20	15	1.48	0.392
		20	1.89	0.636
		25	2.70	0.993
	30	15	1.20	0.182
		20	1.54	0.432
		25	2.15	0.765
	40	15	0.99	-0.010
		20	1.30	0.262
		25	1.75	0.559
	50	15	0.78	-0.248
		20	1.05	0.049
		25	1.40	0.336
2	20	15	1.49	0.399
		20	1.91	0.647
		25	2.75	1.012
	30	15	1.25	0.223
		20	1.52	0.419
		25	2.13	0.756

Run Number	Temperature (°C)	Total Solids (w/w%)	Viscosity (cp)	Log(Viscosity)
2	40	15	0.97	-0.030
		20	1.35	0.300
		25	1.79	0.582
	50	15	0.75	-0.288
		20	1.12	0.113
		25	1.44	0.365
3	20	15	1.45	0.372
		20	1.87	0.626
		25	2.79	1.026
	30	15	1.28	0.247
		20	1.58	0.457
		25	2.18	0.779
	40	15	1.01	0.009
		20	1.38	0.322
		25	1.76	0.565
	50	15	0.77	-0.261
		20	1.09	0.086
		25	1.47	0.385

A.5.7 Measurement Data (WPI)- High shear

Run Number	Temperature (°C)	Total Solids (w/w%)	Viscosity (cp)	Log(Viscosity)
1	20	15	9	2.197
		20	11	2.398
		25	15	2.708
	25	15	8	2.079
		20	10	2.303
		25	13	2.565
	30	15	7	1.946
		20	9	2.197
		25	12	2.485
	35	15	6	1.792
		20	8	2.079
		25	11	2.398
	40	15	5	1.609
		20	8	2.079
		25	11	2.398
	45	15	5	1.609
		20	7	1.946
		25	11	2.398
	50	15	5	1.609
		20	7	1.946
		25	10	2.303

A.5.8 Regression model (WPC-3)

Medium Shear

Factorial Design

```
General Factorial Design

Factors:    2      Factor Levels: 4, 6
Runs:      72      Replicates:    3, blocked on replicates
```

Regression Analysis: Density versus Temp, Solids

```
The regression equation is
ln(vis) = 1.34 - 0.0233 Temp + 0.108 TS

Predictor         Coef     SE Coef          T         P
Constant       1.33933     0.05444      24.60     0.000
Temp          -0.023350    0.001156    -20.20     0.000
TS             0.107772    0.001514     71.21     0.000

S = 0.1097      R-Sq = 98.8%     R-Sq(adj) = 98.7%
```

High Shear

Factorial Design

```
General Factorial Design

Factors:    2      Factor Levels: 4, 4
Runs:      48      Replicates:    3, blocked on replicates
```

Regression Analysis: Density versus Temp, Solids

```
The regression equation is
log(vis) = 1.55 - 0.0281 Temp + 0.0993 TS

Predictor         Coef     SE Coef          T         P
Constant       1.54815     0.05233      29.59     0.000
Temp          -0.0280884   0.0007911   -35.51     0.000
TS             0.099305    0.001582     62.76     0.000

S = 0.06128     R-Sq = 99.1%     R-Sq(adj) = 99.1%
```

A.5.9 Regression model (WPI)

Low Shear

Factorial Design

```
Factors:    2     Factor Levels: 4, 3
Runs:      36     Replicates:    3, blocked on replicates
```

Regression Analysis: Density versus Temp, Solids

```
The regression equation is
log(vis) = - 0.100 - 0.0204 Temp + 0.0595 TS

Predictor        Coef      SE Coef          T          P
Constant      -0.10038      0.03280      -3.06      0.004
Temp         -0.0204413    0.0004973     -41.10      0.000
TS            0.059489      0.001362      43.68      0.000

S = 0.03336     R-Sq = 99.1%     R-Sq(adj) = 99.0%
```

High Shear

Factorial Design

```
General Factorial Design

Factors:    2     Factor Levels: 7, 3
Runs:      21     Replicates:    1
```

Regression Analysis: Density versus Temp, Solids

```
The regression equation is
log(vis) = 1.46 - 0.0163 Temp + 0.0630 TS

Predictor        Coef      SE Coef          T          P
Constant       1.45661      0.09198      15.84      0.000
Temp         -0.016344      0.001507     -10.84      0.000
TS            0.063022      0.003692      17.07      0.000

S = 0.06906     R-Sq = 95.8%     R-Sq(adj) = 95.3%
```

(A.6) Advancing contact angle and surface tension

A.6.1 Principles of measurement

Sessile Drop Profile Method

The contact angle of a sessile drop (figure A.6.1) can be determined indirectly by measurement of its dimensions. For sessile drops that have significant curvature, the contact angle is related by,

$$\cos \theta_a = 1 - 2\left\{\frac{h_s}{2a} - \frac{a}{3r}\left[\frac{\left(1 - \cos^3 \frac{\theta_a}{2}\right)}{\sin \frac{\theta_a}{2}}\right]^2\right\}$$

Where, $a = \left[\dfrac{\sigma_v}{(\rho_l - \rho_v)g}\right]^{\frac{1}{2}}$

     a- capillary number

     r- Radius of the sessile drop

     R_o- Radius of curvature

     h_s- Height of sessile drop

     ρ_v -*Density* of vapour

     ρ_l -*Density* of liquid
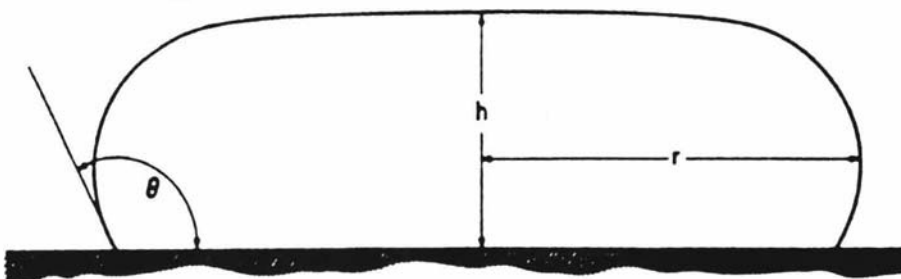
Fig A.6.1: Profile of liquid drop on a flat solid surface

Capillary rise on a vertical Plate

The capillary rises on a vertical plate as a method of measuring contact angle. As shown in Fig (A.6.2) the meniscus at a partially immersed plate rises to a definite height, if θ is finite. The equation which relate the height to the contact angle and the liquid properties is given by,

$$Sin\ \theta_a = 1 - \left(\frac{h}{\left[\frac{\sigma_v}{(\rho_l - \rho_v)g} \right]^{\frac{1}{2}}} \right)^2$$
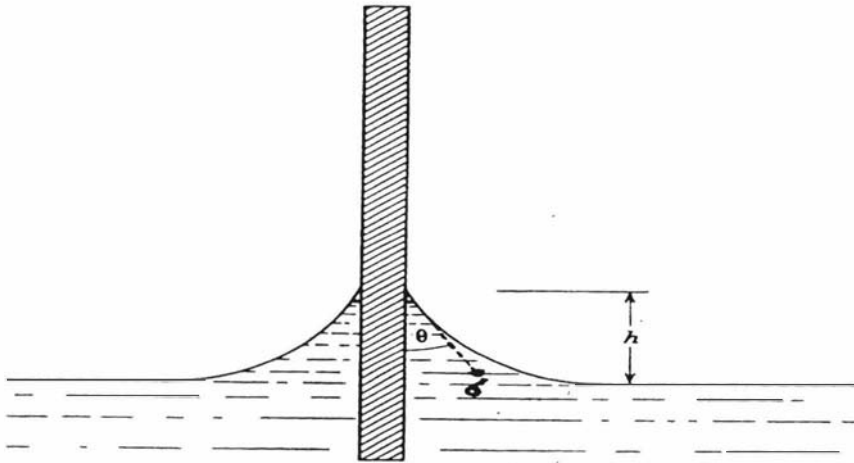
Fig.A.6.2 Capillary rise on a vertical solid plate

A.6.2 Measurement Data (WPC-3)

Run Number	Temperature (°C)	Total Solids (w/w%)	h_c/H_s (mm)	r (cm)	Contact Angle (°)	Surface tension (Nm^{-2})
1	20	10	0.87 / 2.40	2.50	66.25	0.0449
		15	1.00 / 2.38	2.55	63.44	0.0481
		20	1.20 / 2.32	2.45	59.13	0.0522
		25	1.28 / 2.27	2.25	57.17	0.0539
	30	10	0.89 / 2.38	2.35	65.63	0.0446
		15	1.14 / 2.31	2.35	62.09	0.0501
		20	1.33 / 2.25	2.40	58.18	0.0556
		25	1.38 / 2.23	2.55	55.21	0.0567
	40	10	0.94 / 2.37	2.45	64.55	0.0462
		15	1.12 / 2.35	2.35	60.82	0.0508
		20	1.26 / 2.22	2.30	57.07	0.0519
		25	1.46 / 2.23	2.50	53.89	0.0597
	50	10	0.98 / 2.35	2.25	63.51	0.0464
		15	1.15 / 2.29	2.65	59.83	0.0507
		20	1.34 / 2.26	2.50	56.15	0.0563
		25	1.44 / 2.21	2.45	53.09	0.0584

Run Number	Temperature (^{o}C)	Total Solids (w/w%)	h_c/H_s (mm)	r (cm)	Contact Angle (^{o})	Surface tension (Nm^{-2})
2	20	10	0.89 / 2.44	2.45	66.11	0.0464
		15	0.97 / 2.34	2.65	62.75	0.0463
		20	1.15 / 2.31	2.35	59.91	0.0504
		25	1.33 / 2.25	2.45	56.20	0.0557
	30	10	0.93 / 2.44	2.45	65.28	0.0474
		15	1.20 / 2.34	2.45	61.30	0.0528
		20	1.33 / 2.23	2.30	58.95	0.0549
		25	1.36 / 2.23	2.30	55.44	0.0558
	40	10	0.95 / 2.39	2.35	64.47	0.0469
		15	1.12 / 2.32	2.40	60.58	0.0500
		20	1.28 / 2.25	2.55	57.09	0.0537
		25	1.42 / 2.20	2.50	54.23	0.0576
	50	10	1.00 / 2.35	2.55	63.20	0.0473
		15	1.15 / 2.26	2.60	59.55	0.0498
		20	1.34 / 2.25	2.55	56.07	0.0561
		25	1.47 / 2.18	2.45	53.21	0.0584

Run Number	Temperature (^{o}C)	Total Solids (w/w%)	h_c/H_s (mm)	r (cm)	Contact Angle (^{o})	Surface tension (Nm^{-2})
3	20	10	0.872.41	2.55	67.33	0.0452
		15	1.002.34	2.65	63.15	0.0471
		20	1.202.31	2.35	58.99	0.0518
		25	1.332.26	2.35	56.26	0.0559
	30	10	0.992.40	2.45	65.77	0.0478
		15	1.202.32	2.40	61.71	0.0521
		20	1.152.29	2.30	58.05	0.0526
		25	1.372.23	2.30	55.28	0.0561
	40	10	0.94 / 2.39	2.35	64.67	0.0467
		15	1.12 / 2.33	2.50	60.69	0.0504
		20	1.28 / 2.22	2.30	56.72	0.0525
		25	1.44 / 2.23	2.50	54.21	0.0591
	50	10	1.002.36	2.60	63.29	0.0476
		15	1.132.26	2.60	59.92	0.0493
		20	1.382.26	2.50	55.48	0.0575
		25	1.472.20	2.60	53.47	0.0592

A.6.3 Measurement Data (WPI)

Run Number	Temperature (°C)	Total Solids (w/w%)	h_c/H_s (mm)	r (cm)	Contact Angle (°)	Surface tension (Nm^{-2})
1	20	10	1.00 / 2.43	2.40	63.79	0.0450
		15	1.20 / 2.37	2.50	59.58	0.0512
		20	1.33 / 2.25	2.45	56.20	0.0557
		25	1.59 / 2.28	2.60	52.44	0.0672
	30	10	0.97 / 2.34	2.65	62.75	0.0463
		15	1.28 / 2.37	2.50	58.18	0.0560
		20	1.41 / 2.32	2.60	55.59	0.0591
		25	1.61 / 2.21	2.45	51.38	0.0653
	40	10	1.1 / 2.34	2.52	61.17	0.0500
		15	1.29 / 2.28	2.50	57.18	0.0548
		20	1.44 / 2.25	2.58	54.44	0.0614
		25	1.70 / 2.22	2.40	50.16	0.0695
	50	10	1.13 / 2.31	2.32	60.28	0.0498
		15	1.39 / 2.32	2.80	55.98	0.0614
		20	1.45 / 2.21	2.25	53.75	0.0587
		25	1.59 / 1.99	2.5	49.29	0.0691

Run Number	Temperature (°C)	Total Solids (w/w%)	h_c/H_s (mm)	r (cm)	Contact Angle (°)	Surface tension (Nm⁻²)
2	20	10	1.002.42	2.50	63.75	0.0451
		15	1.222.41	2.45	59.56	0.0513
		20	1.332.25	2.40	56.18	0.0556
		25	1.612.28	2.60	52.14	0.0678
	30	10	0.952.39	2.35	62.47	0.0469
		15	1.282.41	2.45	58.52	0.0568
		20	1.432.34	2.55	55.45	0.0586
		25	1.632.25	2.50	51.51	0.0674
	40	10	1.112.34	2.52	60.98	0.0504
		15	1.282.30	2.60	57.58	0.0564
		20	1.432.23	2.47	54.36	0.0588
		25	1.752.22	2.60	49.55	0.0715
	50	10	1.142.31	2.32	60.09	0.0501
		15	1.382.32	2.80	56.45	0.0610
		20	1.472.19	2.55	53.35	0.0588
		25	1.602.00	2.55	49.28	0.0687

Run Number	Temperature (^{o}C)	Total Solids (w/w%)	h_c/H_s (mm)	r (cm)	Contact Angle (^{o})	Surface tension (Nm^{-2})
3	20	10	1.002.40	2.55	63.60	0.0449
		15	1.202.41	2.45	59.91	0.0509
		20	1.332.26	2.35	56.26	0.0559
		25	1.592.28	2.60	52.44	0.0672
	30	10	0.972.38	2.55	62.04	0.0474
		15	1.212.32	2.35	58.91	0.0547
		20	1.412.32	2.60	55.59	0.0618
		25	1.592.21	2.45	51.37	0.0646
	40	10	1.122.34	2.52	60.79	0.0506
		15	1.292.32	2.35	57.50	0.0570
		20	1.422.2	2.45	54.22	0.0575
		25	1.712.20	2.50	49.86	0.0693
	50	10	1.142.31	2.08	59.99	0.0498
		15	1.382.34	2.50	56.24	0.0613
		20	1.452.18	2.45	53.53	0.0578
		25	1.601.99	2.5	49.15	0.0679

A.6.4 Regression model

WPC-3

Factorial Design

```
General Factorial Design

Factors:   2     Factor Levels: 4, 4
Runs:     48     Replicates:    3, blocked on replicates
```

Regression Analysis: C.angle versus Temp, TS

```
The regression equation is
C.angle = 75.6 - 0.111 Temp - 0.685 TS

Predictor        Coef     SE Coef         T         P
Constant      75.5901      0.2572    293.92     0.000
Temp        -0.111405    0.005068    -21.98     0.000
TS           -0.68545     0.01014    -67.62     0.000

S = 0.3926      R-Sq = 99.1%      R-Sq(adj) = 99.1%
```

Regression Analysis: S.tension versus Temp, TS

```
The regression equation is
S.tension = 0.0357 +0.000097 Temp +0.000726 TS

Predictor        Coef     SE Coef         T         P
Constant   0.0357221   0.0009059     39.43     0.000
Temp       0.00009692  0.00001785     5.43     0.000
TS         0.00072550  0.00003570    20.32     0.000

S = 0.001383    R-Sq = 90.8%      R-Sq(adj) = 90.4%
```

WPI

Factorial Design

```
General Factorial Design

Factors:   2     Factor Levels: 4, 4
Runs:     48     Replicates:    3, blocked on replicates
```

Regression Analysis: C.angle versus Temp, TS

```
The regression equation is
C.angle = 72.9 - 0.109 Temp - 0.727 TS
```

```
Predictor        Coef      SE Coef          T         P
Constant      72.9013       0.2285     319.09     0.000
Temp        -0.109489     0.004502     -24.32     0.000
TS          -0.726801     0.009005     -80.71     0.000

S = 0.3487       R-Sq = 99.4%      R-Sq(adj) = 99.3%
```

Regression Analysis: S.tension versus Temp, TS

```
The regression equation is
S.tension = 0.0303 +0.000160 Temp + 0.00124 TS
```

```
Predictor        Coef      SE Coef          T         P
Constant     0.030272     0.001569      19.29     0.000
Temp       0.00016008   0.00003092       5.18     0.000
TS         0.00124083   0.00006185      20.06     0.000

S = 0.002395    R-Sq = 90.5%      R-Sq(adj) = 90.1%
```

A.7 Literature models

Buma's model

The regression model for the density of whey concentrates as a function of temperature was developed and shown in (2.1). The equation is applicable for the concentrates between 20 and 40% (w/w) and at temperatures of 20-60°C. The composition of the whey used for the measurements was lactose-73.8%, protein-12.6%, minerals-7.9%, moisture 1.56% and fat-4.14%.

$$\rho = 985.8 + 4.853 \cdot w_{TS} - 0.325 \cdot T$$

Where,

w_{TS} - Total solids concentration (w/w%)

T - Temperature (°C)

Model developed from property data (Heldman and Singh, 2001)

The models for the WPI and WPC-3 developed from the thermal property data for food compositions (protein, fat, water, carbohydrate and minerals). The regression models applicable for concentration range from 5 to 40% and at temperatures from 10 to 60°C. The food models were not specifically developed for milk or whey products and those were developed to apply to any kind of food of specified compositions.

WPI

$$\rho = 1003 - 0.317 \times T + 3.42 \times w_{TS}$$

$$k = 0.583 + 0.00123 \times T - 0.00341 \times w_{TS}$$

$$Cp = 4160 + 0.541 \times T - 21.4 \times w_{TS}$$

WPC-3

$$\rho = 1002 - 0.311 \times T + 3.78 \times w_{TS}$$

$$k = 0.584 + 0.00119 \times T - 0.00343 \times w_{TS}$$

$$Cp = 4160 + 0.492 \times T - 22.1 \times w_{TS}$$

Where,
k - Thermal conductivity (W/m. K)
Cp - Specific heat capacity (J/kg. K)

Murakami and Okos models

Density:

$$\frac{1}{\rho} = \sum_i \frac{w_i}{\rho_i}$$

Where, w_i - mass fraction of component in the milk mixture (kg/kg)
     ρ_i - density of component in the milk mixture (kg/m^3)

ρ - density of the milk mixture (kg/m^3)

V_{milk} - milk specific volume, volume that a unit mass occupies (m^3/kg)

V_i - specific volume of a milk component (m^3/kg)

The following specific densities have been given by Murakami and Okos (1989).

$$\rho_{water} = 997.18 + 3.1439x10^{-1}T - 3.7574x10^{-3}T^2, \qquad \rho_{fat} = 925.59 - 0.31046T,$$

$$\rho_{lact} = 1599.1 - 0.31046T, \qquad \rho_{salt} = 2423.8 - 0.28063T, \qquad \rho_{prot} = 1329.9 - 0.5184T$$

Thermal conductivity:

The thermal conductivity can be estimated using the following equations (Murakami and Okos, 1989).

$$k = \sum \phi_i.k_i, \qquad \phi_i = \frac{w_i}{\rho_i \sum \dfrac{w_i}{\rho_i}} = \frac{w_i.\rho}{\rho_i}$$

Where, k - thermal conductivity of the milk mixture (W/m.K)

k_i - thermal conductivity of component i in the milk mixture (W/m.K)

ϕ_i - volume fraction of the component in mixture (kg/kg)

ρ_i - density of component in mixture (kg/m^3).

ρ - density of the milk mixture (kg/m^3)

The density of the milk mixture is determined using the equations shown earlier. The specific thermal conductivities are given by the following equations (Murakami and Okos, 1989).

$$k_{water} = 0.5711 + 1.73x10^{-3}T - 6.704x10^{-6}T^2,$$

$$k_{fat} = 0.1807 + 2.7604x10^{-4}T - 1.7749x10^{-7}T^2 \text{(A.10)}$$

$$k_{prot} = 0.1788 + 1.958x10^{-3}T - 2.718x10^{-6}T^2,$$

$$k_{lact} = 0.2014 + 1.3874x10^{-3}T - 4.3312x10^{-6}T^2 \text{(A.12)}$$

$$k_{salt} = 0.3296 + 1.4011x10^{-3}T - 2.9069x10^{-6}T^2$$

Specific heat capacity:

The heat capacity of an ideal mixture is given by equation (A.16) (Murakina and Okos, 1989).

$$C_p = \sum w_i . C_{p,i}$$

The specific heat capacities of the milk components are given by the following equations.

$$C_{p\,water} = 4.21660729 - 2.35427x10^{-3}T + 3.9274488x10^{-5}.T^2 - 1.994188x10^{-7}T^3 + 4.8844x10^{-10}T^4$$

$$C_{pfat} = 1.848533088 + 8.258845x10^{-3}T - 4.97689x10^{-5}T^2, \qquad C_{pprot} = 2.219$$

$$C_{plact} = 1.256, \qquad C_{psalt} = 2.9301$$

Adam Miloslav et al. model

The viscosity, specific heat capacity and thermal conductivity models shown in equation (2.8) to (3.0) are developed for the whey concentrates. The compositions of the product for which the models were developed were not available. The equation (2.8) is applicable at temperatures 5-65°C and concentration up to 40% and the equation (2.9) temperatures 5-80°C and concentration from 7-26.5%. The thermal conductivity equation in (3.0) is valid for 10% concentration and the temperature range from 20-80°C.

$$\mu = 1.099 + \frac{0.2371}{\left(1 - \dfrac{w_{TS}}{100}\right)^{9.836}} \times e^{-0.03827 \times T}$$

$$Cp = 4200 + 0.31093 \times T - 25.77 \times w_{TS} + 0.0784 \times T \times w_{TS}$$

$$k = 0.647 - 0.00164 \times T + 0.0000553 \times T^2$$

Snoeren's model

Snoeren (1982) carried out experiments to find the volume fractions of milk components and shown that the equation (3.1) that can be applied to milk concentrates.

$$\mu = \mu_{ref} \left[1 + \frac{1.25\phi_t}{\left(1 - \dfrac{\phi_t}{\phi_m} \right)} \right]^2$$

Where, $\phi_t = w_{TS} \rho_{con} \sum_i x_x v_i$

Snoeren further postulate a theoretical relationship given in (3.2) to calculate the maximum volume fraction in the milk concentrate.

$$\phi_m = \left(\left(x_{cp} v_{cp} + x_{wp} v_{wp} \right) + x_f v_f \right) w_{max} \rho_{max}$$

Where,

v_i - Voluminosity of ith component (m^3/kg)

ϕ_i - Volume fraction of ith component (-)

ϕ_m - Maximum volume fraction (-)

μ_{ref} - Solvent dynamic viscosity (cp)

w_{max} - Maximum concentration before gel (w/w)

ρ_{max} - Density of the maximum concentration (kg/m^3)

ρ_{con} - Density of the whey concentrates (kg/m^3)

x_{cp} - Dry matter fraction of the casein protein in the whey concentrate (w/w)

x_{wp} - Dry matter fraction of the whey protein in the whey concentrate (w/w)

x_f - Dry matter fraction of the fat in the whey concentrate (w/w)

Appendix B: Model derivation

(B.1) Distribution plate

Flow through orifice

Consider the flow through a single orifice in the distribution plate (figure 6.1), from the Bernoulli's equation ($\frac{P}{\rho g} + \frac{U^2}{2g} + Z = k$). Applying Bernoulli's equation at the orifice surface,

$$\frac{P_1}{\rho g} + \frac{u_1^2}{2g} + z_1 = \frac{P_2}{\rho g} + \frac{u_2^2}{2g} + z_2 \tag{B.1}$$

Substituting $u_1 = \frac{q}{A_1}$, $u_2 = \frac{q}{A_2}$, $P_1 - P_2 = \Delta P$, $z_1 = t_p$ and $z_2 = 0$ into equation (B.1) and rearranged to get equation (B.2).

$$q = \frac{A_2 \left(\frac{2\Delta P}{\rho} + 2t_p g \right)^{0.5}}{\left(1 - \beta^2 \right)^{0.5}} \tag{B.2}$$

Where, $\beta = \left(\frac{A_2}{A_1} \right)^2$

Substituting $q_d = C_d q$, $\Delta P = \rho g h_d$ and $Q_d = n q_d$ into equation (B.2) gives the discharge flow from the orifice and given by,

$$Q_d = \frac{n C_d A_2 \left(2g \left(h_d + t_p \right) \right)^{0.5}}{\left(1 - \beta^2 \right)^{0.5}} \tag{B.3}$$

(B.2) Preheat/ Vacuum condenser

Temperature models

The condenser model is developed from the energy balance around infinitesimal cross section of the condenser tube. From the energy balance (heat of accumulation = net heat flow in- net heat flow out) across the element (figure 6.2) is given by the equation (B.4).

$$\frac{\partial\left[\rho \cdot A \cdot Cp \cdot T_{cond}(x,t)\Delta x\right]}{\partial t} = M_{cond}(t) \cdot Cp \cdot T_{cond}(x,t) + dq(x,t) - M_{cond}(t) \cdot Cp \cdot T_{cond}((x+dx),t) \quad (B.4)$$

Substituting $\rho \cdot A = \dfrac{M_{cond}(t)}{v_{cond}(t)}$ in equation (B.4) and dividing by $\dfrac{M_{cond}(t) \cdot Cp \cdot dx}{v_{cond}(t)}$ gives the

equation shown in (B.5).

$$\frac{\partial T_{cond}(x,t)}{\partial t} + v_{cond}(t) \cdot \frac{\partial T_{cond}(x,t)}{\partial x} = \left(\frac{v_{cond}(t)}{M_{cond}(t) \cdot Cp \cdot dx}\right) dq(x,t) \qquad (B.5)$$

Substituting $\dfrac{M_{cond}(t)}{v_{cond}(t)} = \rho \cdot A$, $\quad dq = U \cdot A \cdot [T_{sh}(t) - T_{cond}(x,t)]$ and $\quad A \cdot dx = V_{cond}$ into (B.5)

produces the equation (B.6).

$$\frac{\partial T_{cond}(x,t)}{\partial t} + v_{cond}(t)\frac{\partial T_{cond}(x,t)}{\partial x} = \frac{U \cdot A}{\rho \cdot Cp \cdot V_{cond}}[T_{sh}(t) - T_{cond}(x,t)] \qquad (B.6)$$

Equation (B.6) is linearised, substituted $\dfrac{\rho Cp V_{cond}}{UA} = \tau_{TC}$ and $v_{cond} = \dfrac{M_{cond}}{\rho \cdot A}$ to get (B.7).

$$\frac{\partial T_{cond}(x,t)}{\partial t} + v_{cond}^{o} \frac{\partial T_{cond}(x,t)}{\partial x} = \frac{1}{\tau_{TC}}[T_{sh}(t) - T_{cond}(x,t)] - \left(\frac{\left(T_{sh}^{o} - T_{in}^{o}\right)e^{\frac{-x}{\tau_{TC} \cdot v_{cond}^{o}}}}{\tau_{TC} \cdot M_{cond}^{o}}\right) \cdot M_{cond}(t) \qquad (B.7)$$

Taking Laplace transforms of (B.7) and rearranged to get (B.8)

$$\frac{dT_{cond}(x,s)}{dx} + \frac{(\tau_{TC} \cdot s + 1)}{v_{cond}^{o} \cdot \tau_{TC}} T_{cond}(x,s) = \frac{1}{v_{cond}^{o} \cdot \tau_{TC}} T_{sh}(s) - \left(\frac{\left(T_{sh}^{o} - T_{in}^{o}\right)e^{\frac{-x}{\tau_{TC} \cdot v_{cond}^{o}}}}{\tau_{TC} \cdot M_{con}^{o} \cdot v_{cond}^{o}}\right) \cdot M_{cond}(s) \qquad (B.8)$$

Integrating (B.8) using Integrating factor method ($I.F = \exp\left[\dfrac{(\tau_{TC} \cdot s + 1)}{v_{cond}^{o} \cdot \tau_{TC}} \cdot x\right]$) and the

integral can get to the format shown in (B.9).

$$\int_{T_{in}}^{T_{out}} d\left[\exp\left[\frac{(\tau_{TC} \cdot s + 1)}{v_{cond}^{o} \cdot \tau_{TC}} \cdot x\right] \cdot T_{cond}(x,s)\right] = \frac{T_{sh}(s)}{v_{cond}^{o} \cdot \tau_{TC}} \int_{0}^{L} \exp\left[\frac{(\tau_{TC} \cdot s + 1)}{v_{cond}^{o} \cdot \tau_{TC}} \cdot x\right] \cdot dx$$

$$- \left(\frac{\left(T_{sh}^{o} - T_{in}^{o}\right) \cdot M_{cond}(s)}{\tau_{TC} \cdot M_{cond}^{o} \cdot v_{cond}^{o}}\right) \int_{0}^{L} \exp\left[\frac{(\tau_{TC} \cdot s + 1)}{v_{cond}^{o} \cdot \tau_{TC}} \cdot x\right] \cdot e^{\frac{-x}{\tau_{TC} \cdot v_{cond}^{o}}} \cdot dx \qquad (B.9)$$

Integrating (B.9) and reduced to give (B.10).

$$T_{out}(s)=T_{dum}(s)+e^{\frac{\tau_{RT}}{\tau_{TC}}}\cdot e^{-\tau_{RT}\cdot s}\cdot T_{in}(s)-\frac{\tau_{RT}\left(T_{sh}^{o}-T_{in}^{o}\right)}{\tau_{TC}\cdot M_{cond}^{o}}\cdot e^{\frac{\tau_{RT}}{\tau_{TC}}}\cdot M_{dum}(s) \tag{B.10}$$

Where, $\tau_{RT}=\dfrac{\rho V_{cond}}{M_{cond}}$ and

$$\frac{\left[1-e^{\frac{\tau_{RT}}{\tau_{TC}}}\cdot e^{-\tau_{RT}\cdot s}\right]}{\left(\tau_{TC}\cdot s+1\right)}\cdot T_{sh}(s)=T_{dum}(s)\ ,\ \frac{\left[1-e^{-\tau_{RT}\cdot s}\right]}{\tau_{RT}\cdot s}\cdot M_{cond}(s)=M_{dum}(s) \tag{B.11}$$

The inverse Laplace transform of equation (B.11) and converting equation (B.10) into time domain gives the models for the exit temperature from the condenser as shown in equations (B.12 to B.14).

$$T_{out}(t)=T_{dum}(t)+e^{\frac{\tau_{RT}}{\tau_{TC}}}T_{in}(t-\tau_{RT})-\frac{\tau_{RT}\left(T_{sh}^{0}-T_{in}^{0}\right)e^{\frac{\tau_{RT}}{\tau_{TC}}}}{M_{cond}^{0}\tau_{TC}}M_{dum}(t) \tag{B.12}$$

$$\tau_{TC}\frac{dT_{dum}(t)}{dt}=-T_{dum}(t)+T_{sh}(t)-e^{\frac{\tau_{RT}}{\tau_{TC}}}T_{sh}(t-\tau_{RT}) \tag{B.13}$$

$$\tau_{RT}\frac{dM_{dum}(t)}{dt}=M_{cond}(t)-M_{cond}(t-\tau_{RT}) \tag{B.14}$$

Heat flow through condenser tubes

Total heat flow though condenser tubes is given by the integral equation (B.15).

$$q_{cond}(t)=\frac{1}{L}\int_{0}^{L}U\cdot A\cdot[T_{sh}(t)-T_{cond}(x,t)]\cdot dx \tag{B.15}$$

Expanding the right hand side of the equation (B.15) and differentiating both sides with respect to time gives the equation (B.16).

$$\frac{dq_{cond}(t)}{dt}=U\cdot A\cdot\frac{dT_{sh}(t)}{dt}-\frac{U\cdot A}{L}\int_{0}^{L}\frac{\partial T_{cond}(x,t)}{\partial t}\cdot dx \tag{B.16}$$

Substituting equation (B.6) into (B.16) and expanding the integral gives equation (B.17).

$$\frac{dq_{cond}(t)}{dt}=U\cdot A\cdot\frac{dT_{sh}(t)}{dt}-\left\{\frac{U\cdot A}{L}\int_{0}^{L}\frac{(T_{sh}(t)-T_{cond}(x,t))}{\tau_{TC}}-\frac{U\cdot A}{L}\int_{0}^{L}v_{cond}(t)\cdot\frac{\partial T_{cond}(x,t)}{\partial x}\cdot dx\right\} \tag{B.17}$$

The integration of (B.17) after substituting (B.15), $v_{cond}(t) = \dfrac{M_{cond}(t)}{\rho \cdot A}$ and $\tau_{RT} = \dfrac{\rho V_{cond}}{M_{cond}}$ will

produce the differential equation for heat flow through the condenser tubes which I shown in (B.18).

$$\frac{dq_{cond}(t)}{dt} = U \cdot A \cdot \frac{dT_{sh}(t)}{dt} - \frac{1}{\tau_{TC}} \cdot q_{cond}(t) + \frac{U \cdot A}{\tau_{RT}} \left[T_{out}(t) - T_{in}(t) \right] \tag{B.18}$$

(B.3) Evaporation

The equation (B.19) to (B.21) shows the mass flow balance, solids content balance and energy balance across the finite element shown in figure 6.3.

$$\frac{\partial \left[\rho(x,t) \cdot A(x,t) \cdot \Delta x \right]}{\partial t} = M(x,t) - M(x+dx,t) - dM_{evap}(x,t) \tag{B.19}$$

$$\frac{\partial \left[\rho(x,t) \cdot A(x,t) \cdot \Delta x \cdot w(x,t) \right]}{\partial t} = M(x,t) \cdot w(x,t) - M(x+dx,t) \cdot w(x,t) \tag{B.20}$$

$$\frac{\partial \left[\rho(x,t) \cdot A(x,t) \cdot Cp(w(x,t)) \cdot T_f(x,t) \right]}{\partial t} = M(x,t) \cdot Cp(w(x,t)) \cdot T_f(x,t) + dq(x,t)$$

$$- M(x+dx,t) \cdot Cp(w(x+dx,t)) \cdot T_f(x+dx,t) - \left[\lambda + Cp_w \cdot T_f(x,t) \right] dM_{evap}(x,t) \tag{B.21}$$

Substituting $\rho(x,t) \cdot A(x,t) = \dfrac{M(x,t)}{v}$ into equations (B.19), (B.20) and (B.21) with the

constant velocity assumption, equations (B.22), (B.23) and (B.24) are produced.

$$\frac{1}{v} \cdot \frac{\partial M(x,t)}{\partial t} + \frac{\partial M(x,t)}{\partial x} = \frac{\partial M_{evap}(x,t)}{\partial x} \tag{B.22}$$

$$\frac{1}{v} \cdot \frac{\partial \left[M(x,t) \cdot w(x,t) \right]}{\partial t} + \frac{\partial \left[M(x,t) \cdot w(x,t) \right]}{\partial x} = 0 \tag{B.23}$$

$$\frac{1}{v} \cdot \frac{\partial \left[M(x,t) \cdot Cp(w(x,t)) \cdot T_f(x,t) \right]}{\partial t} + \frac{\partial \left[M(x,t) \cdot Cp(w(x,t)) \cdot T_f(x,t) \right]}{\partial x}$$

$$= U(w(x,t)) \cdot \pi \cdot d \cdot n \cdot \left[T_s(x,t) - T_e(x,t) \right] - \left[\lambda + Cp_w \cdot T_f(x,t) \right] \frac{\partial M_{evap}(x,t)}{\partial x} \tag{B.24}$$

Mass flow out from the tube

Expanding the equation (B.24), substituting (B.22) and $Cp = Cp_w - Cp_{TS} \cdot w(x,t)$ will produce the equation (B.25).

$$M(x,t) \cdot Cp(w(x,t)) \left[\frac{1}{v} \cdot \frac{\partial T_f(x,t)}{\partial t} + \frac{\partial T_f(x,t)}{\partial x} \right] + \lambda \cdot \frac{\partial M_{evap}(x,t)}{\partial x}$$

$$= U(w(x,t)) \cdot \pi \cdot d \cdot n \cdot [T_s(x,t) - T_e(x,t)] \tag{B.25}$$

If we assume negligible thermal inertia then the equation (B.25) is reduced to the form in (B.26).

$$\lambda \cdot \frac{\partial M_{evap}(x,t)}{\partial x} = U(w(x,t)) \cdot \pi \cdot d \cdot n \cdot [T_s(x,t) - T_e(x,t)] \tag{B.26}$$

Substituting equation (B.26) in to the equation (B.22) will give equation (B.27).

$$\frac{1}{v} \cdot \frac{\partial M(x,t)}{\partial t} + \frac{\partial M(x,t)}{\partial x} = \frac{U(w(x,t)) \cdot \pi \cdot d \cdot n \cdot [T_s(x,t) - T_e(x,t)]}{\lambda} \tag{B.27}$$

The heat flow through the tube wall is given by (B.28) and can be integrated with the assumption of uniform heat transfer. Thus the equation (B.27) can be modified to (B.29).

$$q_{shell}(t) = \int_0^L U(w(x,t)) \cdot \pi \cdot d \cdot n \cdot [T_s(x,t) - T_e(x,t)] dx \tag{B.28}$$

$$\frac{1}{v} \cdot \frac{\partial M(x,t)}{\partial t} + \frac{\partial M(x,t)}{\partial x} = \frac{q_{shell}(t)}{\lambda \cdot L} \tag{B.29}$$

Transferring (B.29) into Laplace domain gives,

$$\frac{dM(x,s)}{dx} + \frac{s}{v} M(x,s) + k(s) = 0 \tag{B.30}$$

Where $k(s) = \dfrac{q_{shell}(s)}{\lambda \cdot L}$

Integrating (B.30) as shown in (B.31) to get (B.32). Converting back to time domain substituting $k(s)$ produces (B.33).

$$\int_{M_d(s)}^{M_e(s)} \frac{dM(x,s)}{\left(\frac{s}{v}M(x,s)+k(s)\right)} = -\int_0^L dx \tag{B.31}$$

$$\frac{s}{v} \cdot M_e(s)+k(s) = \left[\frac{s}{v} \cdot M_d(s)+k(s)\right] \cdot e^{\frac{L\cdot s}{v}} \tag{B.32}$$

$$M_e(t) = M_d(t-\tau_e)-M_{tubes}(t) \tag{B.33}$$

Where $\dfrac{dM_{tubes}(t)}{dt} = \dfrac{1}{\lambda \cdot \tau_e}\left[q_{shell}(t)-q_{shell}(t-\tau_e)\right]$ and $\tau_e = \dfrac{L}{v}$

Solids in the flow out from the tube

The equation describing the solids content of the product exiting the tube is derived here.

Taking Laplace transform of the equation (B.23) and rearranging to get (B.34).

$$\frac{d[M(x,s)\cdot w(x,s)]}{dx} = -\frac{s}{v}\cdot M(x,s)\cdot w(x,s) \tag{B.34}$$

Substituting $M(x,s)\cdot w(x,s) = V(x)$ and integrating equation (B.34) as shown in (B.35) will produce (B.36).

$$\int_{V_d(s)}^{V_e(s)} \frac{dV}{V} = -\frac{s}{v}\int_0^L dx \text{ Where, } V_d(s) = M_d(s)w_d(s) \text{ and } V_e = M_e(s)w_e(s) \tag{B.35}$$

$$V_e(s) = V_d(s)\cdot e^{-s\tau_e} \text{ Where } \tau_e = \frac{L}{v} \tag{B.36}$$

Converting back the equation (B.36) into time domain and substituting (B.35) will produce the equation (B.37) for the solids exiting the tube. Substituting (B.33) into (B.37) and can be rearrange to get to the form (B.38) for the solids exiting the tube.

$$M_e(t)\cdot w_e(t) = M_d(t-\tau_e)\cdot w_d(t-\tau_e) \tag{B.37}$$

$$w_e(t) = \frac{M_d(t-\tau_e)\cdot w_d(t-\tau_e)}{[M_d(t-\tau_e)-M_{tubes}(t)]} \tag{B.38}$$

Appendix C: Physical models

C.1 Surface energy losses heat transfer coefficients

Natural convection (McAdams, 1958)

The heat transfer coefficient for the heat losses from the evaporator surfaces, effects, shells, and the condensers, U_l, can be approximated by the convective heat transfer coefficient, h_c, which is estimated by (converted into SI units from McAdams, 1958, Guoxin Luo, 1998)

$$U_l = 1.3123 (\Delta T_c)^{1/3} \tag{C.1}$$

Where

U_l - Heat transfer coefficient ($W/m^2.K$)

ΔT_c - Temperature difference between the ambient and the hot surface ($°C$).

Natural convection (Holman 1989)

$$Nu^{1/2} = 0.825 + \frac{0.387 (Gr\,\mathrm{Pr})^{1/6}}{\left[1 + \left(\dfrac{0.492}{\mathrm{Pr}}\right)^{9/16}\right]^{8/27}} \tag{C.2}$$

Where, $Nu = 0.1(Gr\,\mathrm{Pr})^{1/3}$, $Nu = \dfrac{hL}{k}$, $Gr = \dfrac{g\beta(T_w - T_a)L^3\rho^2}{\mu^2}$ and $\mathrm{Pr} = \dfrac{\mu C_p}{k}$

Nu - Nusselt number (-)

Gr - Grashof number (-)

Pr   - Prandtl number (-)

h - Losses heat transfer coefficient (W m^{-2} K^{-1})

L - Length of the evaporator effect surface (m)

k - Thermal conductivity of air (W m^{-1} K^{-1})

g - Gravitational acceleration (m s^{-2})

β - Coefficient of volumetric expansion (K^{-1})

T_w - Temperature of the evaporator surface ($^{\circ}$C)

T_a - Room temperature ($^{\circ}$C)

μ - Viscosity of air (kg m^{-1} s^{-1})

ρ - Density of air (kg m^{-3})

C_p - Specific heat capacity of air (J kg^{-1} K^{-1})

The shell of the condensers are at 50°C, 44°C and 40°C where as the effects are at 44°C and 40°C. The heat loss is significant from the condenser compared to the losses from the effects as the room temperature is 30°C. It is assumed that the heat losses from the evaporator surfaces is by natural convection and using these numbers can estimate convection film temperature $\left(T_f = \dfrac{50+30}{2} = 40^{\circ}C\right)$ and the properties of the air $\left(\beta = \dfrac{1}{T_f} = 0.0032 K^{-1}, k = 0.0278 Wm^{-1}K^{-1}, \text{Pr} = 0.7193\right)$. The length of the evaporator surfaces is approximately 12 m and therefore the Grashof number $\left(Gr = 2.624 \times 10^{11}\right)$. The natural convection heat transfer coefficient estimated from equation C.1 and C.2 are 3.5621 and 2.44 W m^{-2} K^{-1} respectively.

C.2 Falling-film heat transfer coefficients

There are many theoretical models available for the heat transfer coefficient for evaporating and condensing liquid in the literature (Billet, 1989; Perry and Green, 1984; Minton, 1986; Coulson and Rechardson, 1991). Since falling-films are most often initially Laminar, wavy laminar and then transition or turbulent, different models for different flow regime are needed for the analysis. As theoretical model predictions significantly deviate from the actual values, researchers (Chun and Seban, 1972; Jebson and Iyer, 1991; Mackereth, 1993; Chen, 1997; Winchester, 2000) have corrected the coefficients in the models using the experimental data. The falling-film models used in the literature are listed below.

Bouman et. al (1993)

Bouman applied Nusselt theory to estimate the condensing film heat transfer coefficient shown in equation C.3. Then the equation C.4 is used to estimate the boiling milk heat transfer coefficient knowing the overall heat transfer coefficient. These models were used for a wetting flow range of 300 - 1000 kg m^{-1} h^{-1} and thus the Reynolds number in the range 10 – 2000.

$$Nu = 0.693 \, \mathrm{Re}^{-\frac{1}{3}} \tag{C.3}$$

Where, $Nu = \dfrac{\alpha_s \left(\mu^2 g^{-1} \rho^{-2} \right)^{1/3}}{k}$, $\mathrm{Re} = \dfrac{4\Gamma}{\mu}$

$$h_o = \dfrac{1}{\dfrac{1}{\alpha_p} + \dfrac{\delta_w}{\lambda_w} + \dfrac{1}{\alpha_s}} \tag{C.4}$$

Γ - Wetting flow rate (kg m^{-1} s^{-1})

h_o - Overall heat transfer coefficient (W m^{-2} K^{-1})

α_p - Condensing steam heat transfer coefficient (W m^{-2} K^{-1})

α_s - Boiling milk heat transfer coefficient (W m^{-2} K^{-1})

λ_w - Thermal conductivity of tube material (W m^{-1} K^{-1})

δ_w - Tube thickness (m)

Unterberge and Edwards (1965)

The heat transfer coefficient of the falling-film evaporation for water was investigated. The Reynolds number range of the flow was between 160 and 600. It was assumed that the flow range in the laminar region and the equation used for estimating the evaporating film and the condensing steam film heat transfer coefficient is shown in C.3.

Chun and Seban

The heat transfer coefficients correlations developed for water using experimental data by Chun and Seban (1972) are well-known equations, widely used in falling-film evaporator design and recommended in the previous studies (Mill, 1995; Berntsson and Asblad, 1991; Stuhltrager, 1995; Mackereth, 1993). Chun and seban's correlations are valid only for a

narrow range of Prandtl numbers (1.7 to 5.7) and Reynolds numbers between 320 to 21,000. The equation developed by Chun and seban are shown in C.5 to C.7.

$$Nu = \left(\frac{3}{4}\mathrm{Re}\right)^{\frac{-1}{3}} \qquad \mathrm{Re} < 30, \text{ Laminar} \tag{C.5}$$

$$Nu = 0.822\,\mathrm{Re}^{-0.22} \qquad 30 < \mathrm{Re} < \mathrm{Re}_{tr}, \text{ Wavy laminar} \tag{C.6}$$

$$Nu = 3.8 \times 10^{-3}\,\mathrm{Re}^{0.4}\,\mathrm{Pr}^{0.65} \qquad \mathrm{Re}_{tr} < \mathrm{Re}, \text{ Turbulent} \tag{C.7}$$

Where, $Nu = \dfrac{h\left(v^2 / g\right)^{1/3}}{k}$, $\mathrm{Re} = \dfrac{4\Gamma}{\mu}$

Christopher (2001)

The following heat transfer coefficient correlations were used for evaporating orange juice in a falling-film evaporator. No data on the accuracy of the correlations or heat transfer coefficient values were listed. The steam side coefficient calculated by the equation C.8 and C.9 and the evaporating heat transfer coefficient calculated by equation C.10.

$$h = \frac{1.13 \times k_l}{L}\left(\frac{\rho_l(\rho_l - \rho_v)g\lambda L^3}{\mu_l k_l \Delta T}\right)^{\frac{1}{4}} \quad \text{for laminar flow} \tag{C.8}$$

$$h = \frac{0.0077 \times k_l}{L}\left(\frac{\rho_l g L^3}{\mu_l^2}\right)^{\frac{1}{3}}(\mathrm{Re})^{0.4} \quad \text{for turbulent flow} \tag{C.9}$$

$$h = \frac{k_l}{L}(1.3 + 128D)(\mathrm{Pr})_l^{0.9}(\mathrm{Re})_l^{0.23}(\mathrm{Re})_v^{0.34}\left(\frac{\rho_l}{\rho_v}\right)^{0.25}\left(\frac{\mu_v}{\mu_l}\right) \tag{C.10}$$

Where,

ρ_l - Liquid density (kg m^{-3})

ρ_v - Vapour density (kg m^{-3})

L - Vertical height of tubes (m)

μ_l - Liquid viscosity (Pa. s)

μ_v - Vapour viscosity (Pa. s)

k_l - Liquid thermal conductivity (W m^{-1} K^{-1})

ΔT - Temperature different across the tube wall (K)

λ - Latent heat (J kg^{-1})

Choudhary (1996)

Under the trickle film condition, which prevails, when the Reynolds number is less than 300, the value of heat transfer coefficient, on the inside of a evaporator tube is calculated from equation C.11 and the evaluation of heat transfer coefficient on the condensing side is using the equation C.12. The Reynolds number of the concentrate in the evaporator is between 65 and 125.

$$h = 0.9 \, \mathrm{Re}^{\frac{-1}{3}} \, k \left(\frac{\mu^2}{\rho^{-2} g} \right)^{\frac{-1}{3}} \tag{C.11}$$

$$h = 0.943 \left(\frac{k^3 \delta^2 g \lambda}{\mu \Delta T L} \right)^{0.25} \tag{C.12}$$

Alhusseini (1998)

Alhusseini et al. (1998) have carried out experiments and showed that the Chun and seban's correlations are valid only for a narrow range of Prandtl numbers (1.7 to 5.7) and the equations developed by Alhusseini et al. that applied for wide range of Prandtl numbers are shown in C.13 and C.14.

$$Nu_l = \left(\frac{3 \cdot \mathrm{Re}}{4} \right)^{\frac{-1}{3}} \qquad\qquad \mathrm{Re} < 30 \text{ (Laminar)} \tag{C.13}$$

$$Nu_{wl} = 2.65 \, \mathrm{Re}^{(-0.158)} \, Ka^{0.0563} \qquad 30 < \mathrm{Re} < \mathrm{Re}_t \text{ (Wavy Laminar)} \tag{C.14}$$

Where,

$$\mathrm{Re}_t = 5800 \cdot \mathrm{Pr}^{(-1.06)}, Nu = \frac{h}{k} \left(\frac{\mu^2}{\rho^2 \cdot g} \right)^{\frac{1}{3}}, \mathrm{Re} = \frac{4 \cdot \Gamma}{\mu}, \; \mathrm{Pr} = \frac{\mu \cdot Cp}{k} \text{ and } Ka = \frac{g \mu^4}{\rho \sigma^3}$$

Nu - Nusselt number (-)

Re   - Reynolds number (-)

Pr   - Prandtl number (-)

Ka   - Kapitza number (-)

h   - Film heat transfer coefficient (W/m^2. K)

μ - Viscosity of the fluid (Pa. s)

k   - Thermal Conductivity of the tube material (W/m. K)

g   - Acceleration due to gravity (ms^{-2})

Falling-film model selection

The operating range of Reynolds number in the whey products evaporator is shown in Figure C.1. Prandtl number is between 3 and 5 for water and between 100 and 500 for products. The evaporator operating in the wavy laminar regime (as shown in Figure C.2) and therefore the models developed for turbulent film were ignored. The laminar heat transfer coefficient model used in the literature is similar and only two researchers (Alhusseini et. al, 1998; Chun and Seban, 1972) have published work on the wavy falling-film models. These wavy model predictions were compared in Figure C.3. It can be seen from Figure C.3 that there is significant deviation between the two wavy falling-film models. Alhusseini's model shows higher nusselt number with products than with water and this is contradiction to the experimental data. Therefore, Chun and Seban falling-film model is used in this work.
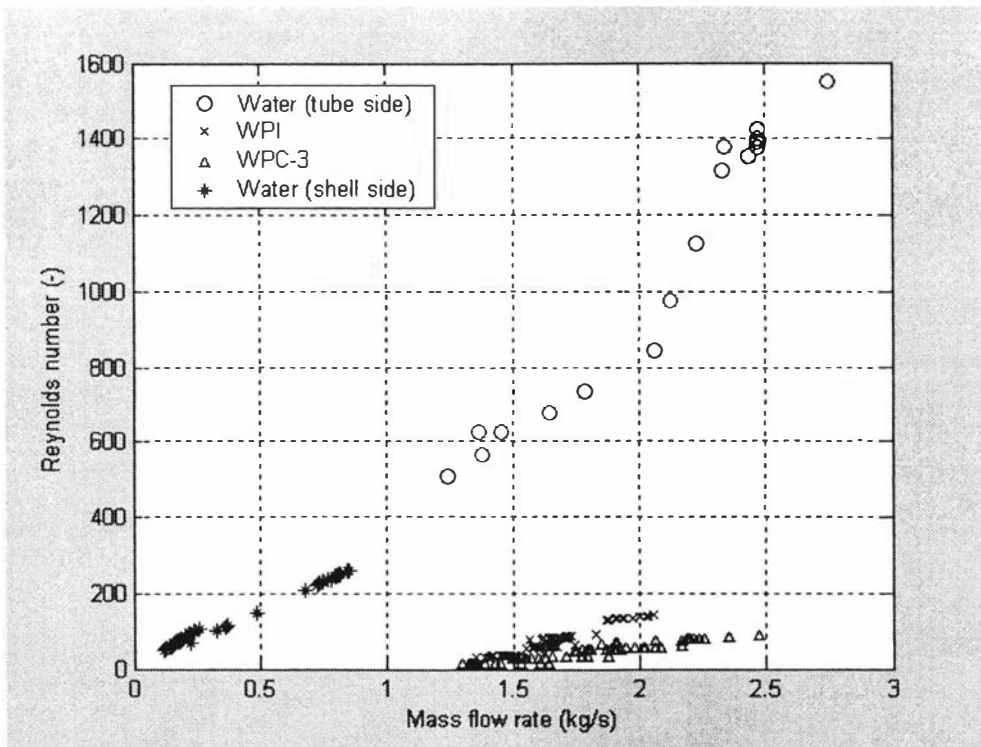
Figure C. 1: Reynolds number as a function of mass flow rate for current whey evaporator operating conditions
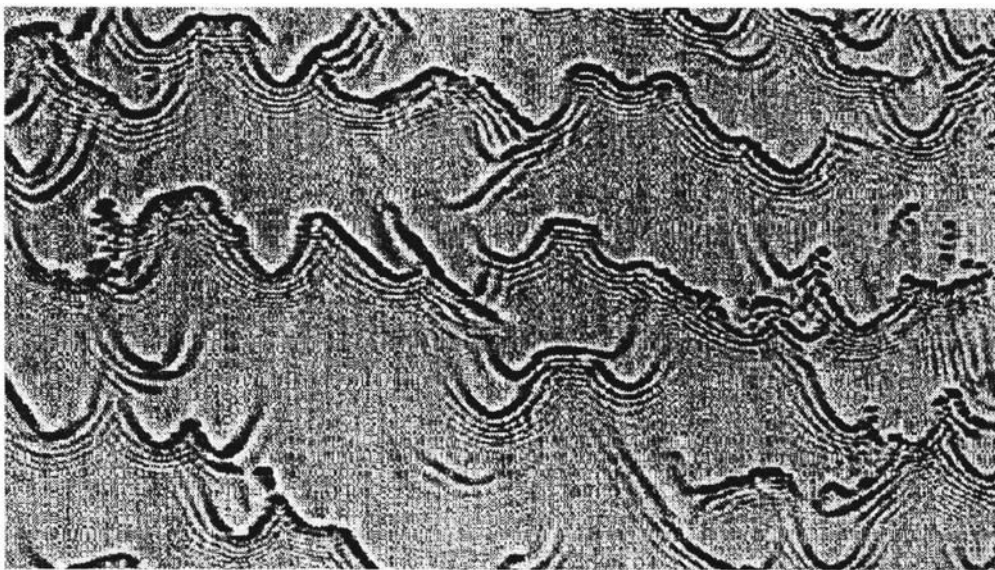
Figure C. 2: Wavy falling-film at Reynolds number 280. (Mills A (1995), "Heat and Mass Transfer")

299
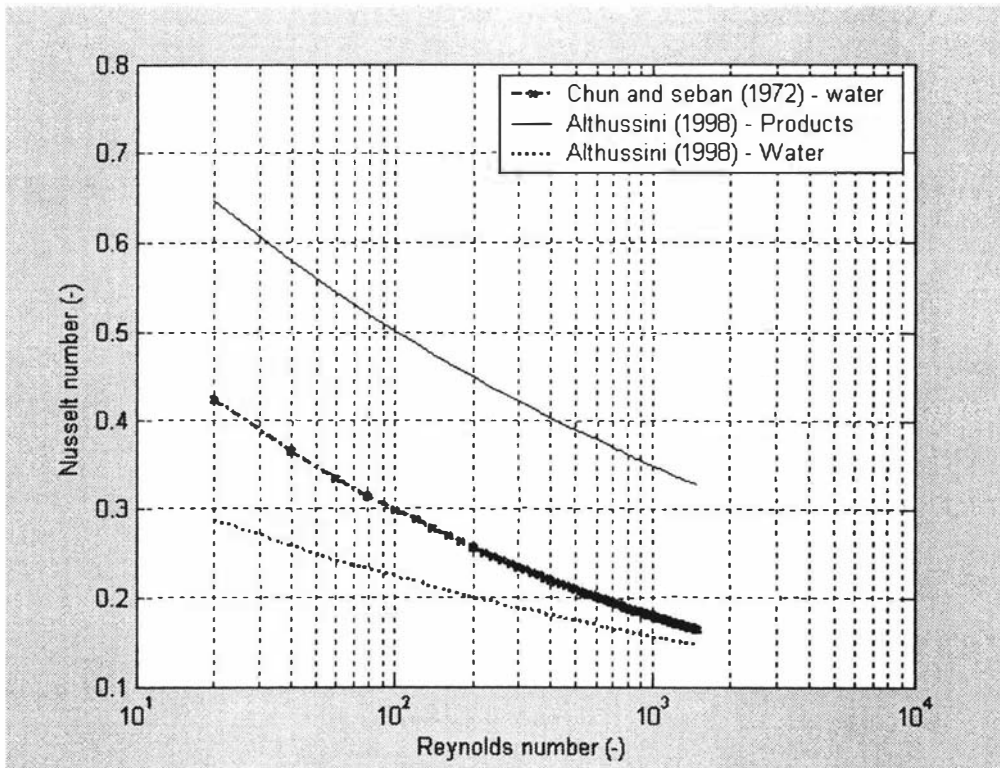
Figure C. 3: Comparison of wavy falling-film models

C.3 Boiling point elevation

When a solute is added to a solvent, the vapour pressure of the solvent is less than the vapour pressure above the pure solvent. The boiling point of a solution, then, will be greater than the boiling point of the pure solvent because the solution will need to be heated to a higher temperature in order for the vapour pressure to become equal to the external pressure (i.e., the boiling point). The boiling point elevation of milk concentrates was estimated using the model given in (C.15). It was derived by Castellan (1964) and widely used in the concentration process applications (Mackereth, 1993; Trinh, 1997; Winchester, 2000).

$$\Delta T_{BPE} = \frac{1}{\left[\dfrac{1}{T_{sat}} + \dfrac{R \cdot \ln(1 - x_{sol})}{\lambda} \right]} - T_{sat} \tag{C.15}$$

Where,

$$x_{sol} = \frac{b_{TS}.w_{TS}}{[1 + (b_{TS} - 1)w_{TS}]} \text{ and } b_{TS} = \sum_i \frac{M_{water}}{M_i} x_i$$

ΔT_{BPE} - Boiling point elevation (^{o}C)

T_{sat} - Saturation temperature of boiling water (^{o}C)

R - Gas constant (J/kg. K)

x_{sol} - Molar concentration of dissolved particles (mol/mol)

M_i - Molecular weight (kg/kmol)

λ - Latent heat of vaporisation (J/kg. K)

C.4 Pressure drop

The uncertainty and complexity of the flow patterns encountered with two-phase flow in tubes make the prediction of pressure drop difficult. Anthony suggested a simple method (C.16 to C.22) to estimate the pressure drop along the falling-film assuming the velocity of each phase is the same.

$$\frac{dP}{dx} = \left(\frac{dP}{dx}\right)_F + \left(\frac{dP}{dx}\right)_G + \left(\frac{dP}{dx}\right)_M \tag{C.16}$$

$$\left(\frac{dP}{dx}\right)_F = -\frac{f \cdot G^2}{D \cdot 2\rho} \tag{C.17}$$

$$\left(\frac{dP}{dx}\right)_G = -\rho g \tag{C.18}$$

$$\left(\frac{dP}{dx}\right)_M = \left(\frac{G}{\rho}\right)^2 \frac{d\rho}{dz} \tag{C.19}$$

$$\rho = m\rho_v + (1-m)\rho_l. \tag{C.20}$$

$$\frac{1}{\mu_r} = \frac{m}{\mu_v} + \frac{1-m}{\mu_l} \tag{C.21}$$

$$Re = \frac{GD}{\mu_r} \text{ And } f = \frac{64}{Re} \tag{C.22}$$

Where,

Subscripts F, G and M refer to pressure gradients due to wall friction, gravity and momentum changes respectively.

$\left(\dfrac{dP}{dx}\right)$ - Pressure gradient along the falling-film (Pa/m)

G - Mass flow rate of liquid per unit area (kg/m^2.s)

ρ - Density of the two phase flow (kg/m^3)

f - Friction factor (-)

m - Mass fraction of the component (-)

C.5 Affect of vapour drag on the heat transfer coefficient

The effect of vapour velocity on the heat transfer coefficient was first derived by Shekriladze and Gomelauri (1966) for laminar falling-film flow and later revised and recommended by Mills (1995). The model shown in (C.23) gives the percentage change in the heat transfer coefficient due to vapour drag effect at different location and at different velocities. It is assumed that the change in heat transfer coefficient follows the same relation with the vapour flow for the wavy laminar falling-film flow. Vapour drag is estimated under laminar conditions and assumed the same with wavy laminar conditions (Anthony book did the same). The methodology and the calculations involved are shown in Figure C.4.

$$HTC_{drag} = -c_1 \times v^2 + c_2 \times v - c_3 \tag{C.23}$$

Where, $c_1 = \dfrac{5 \times L^2}{10^5} - 0.0003 \times L + 0.0009$, $c_2 = 0.0078 \times L^2 - 0.0305 \times L + 0.3237$,

$c_3 = \dfrac{9 \times L^2}{10^5} - 0.0012 \times L + 0.0076$

L - Length of the tube (m), SL - Number of falling film elements in the simulation (-)
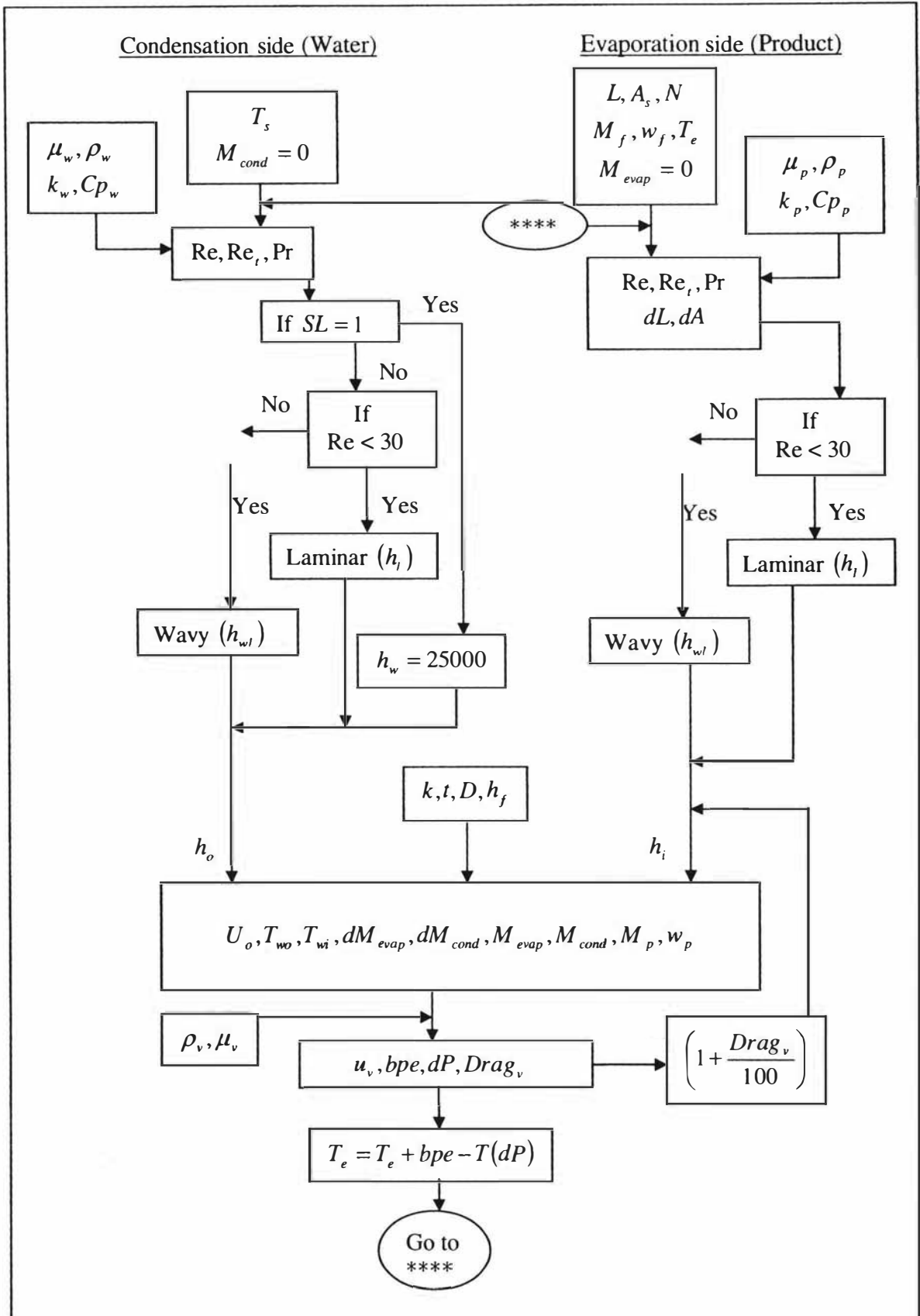
Figure C.4: Methodology for estimating Falling-film heat transfer coefficient

C.6 Residence time measurements

The laboratory falling-film residence time measurements data are listed in Table C.1.

Table 1: Falling-film residence time measurement data

Product	Solids	Temperature	Viscosity	Flow rate	No of frames
Water	0	18	1	180	9,9
		20	1	230	9,9
Whole milk	9.8	22		150	8,9
	10.4	24.5		200	9,9
Whole milk	20.6	21		145	9,10
	21.2	24.5		180	9,10

C.7 Film break-down

Hartley and Murgatroyd force criteria

Hartley and Murgatroyd have presented several analyses of the criteria for film break-up. Their force criterion considers the stability of dry patches (Figure C.5) on a vertical plate. To permit the existence of a stable dry patch, the upward forces on the film at the stagnation point of a dry patch must exceed those required to sustain the pressure difference across the liquid/vapour interface. This pressure difference will increase as the peripheral flow (mass flow per unit width) increases. The maximum peripheral flow, Γ ($kgm^{-1}s^{-1}$), at which dry patches are stable, is shown to be given by:

$$\Gamma = 1.69\left(\frac{\mu\rho}{g}\right)^{\frac{1}{5}}\left(\sigma(1-Cos\theta_a)\right)^{\frac{3}{5}} \tag{C.24}$$

Where

μ -Liquid viscosity ($kgm^{-1}s^{-1}$)

ρ -Liquid density (kgm^{-3})

σ   -Surface tension (Nm^{-1})

θ_a -Advancing contact angle (^{o})

g   -Acceleration due to gravity (ms^{-2})
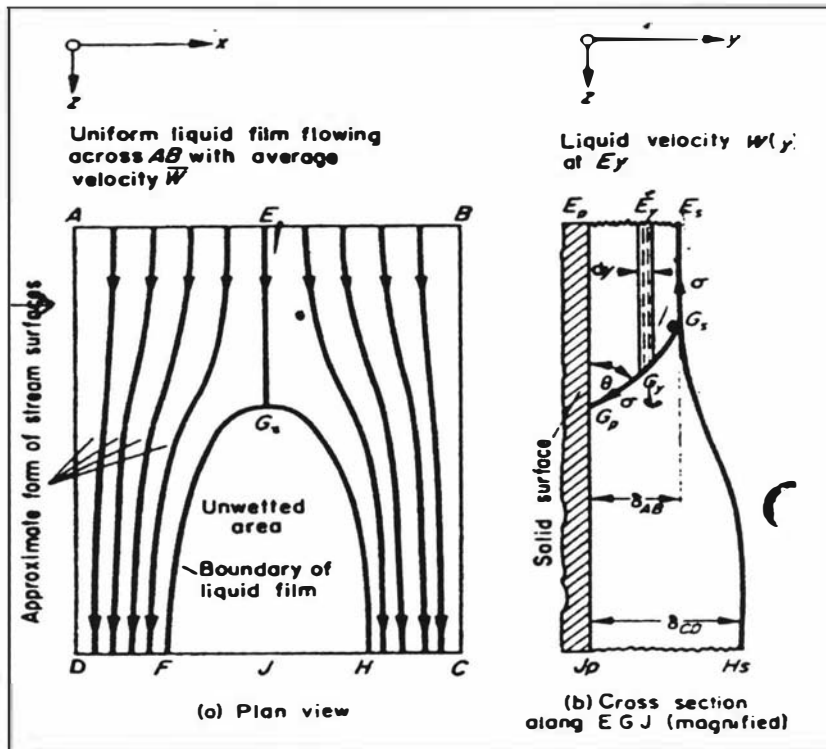
Figure C.5: Dry patch formation in liquid layers flowing over a solid body
International Journal of Heat and Mass Transfer, 1964, vol.7, pp1004

To avoid dry patches becoming stable and hence the likely onset of fouling, the peripheral flows in the evaporator tubes should exceed this threshold value. Previous experimental studies (Paramalingam, 1999) on minimum flow revealed that the Hartley and Murgatroyd (1964) model predicts the minimum flow well at low concentrations but overestimates at high concentrations of milk. Figure C.6 shows the predicted flows using the Hartley and Murgatroyd (1964) model and measured minimum flows. The Hoke and Chen (1992) model will be shown to eliminate this discrepancy at high concentration.
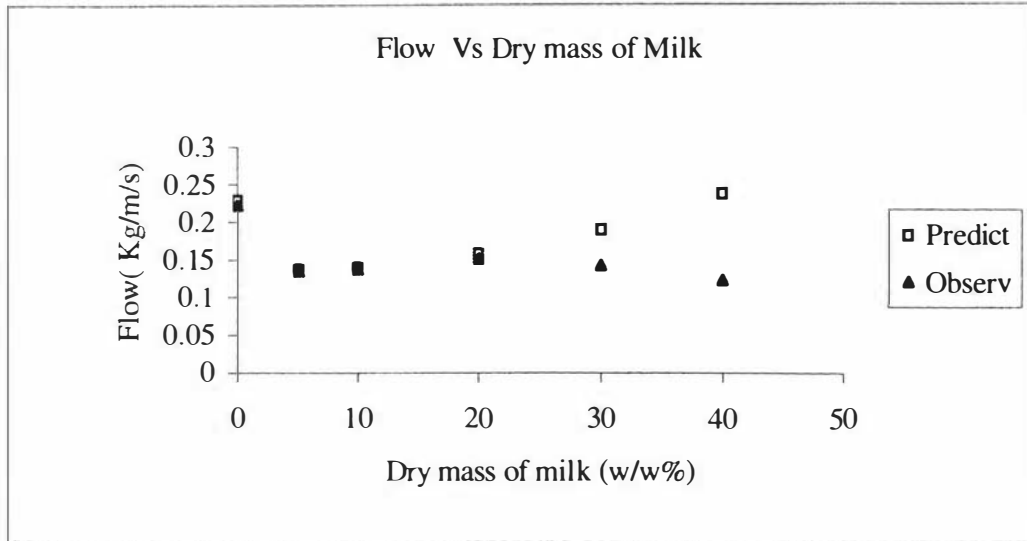
Figure C.6: Comparison of observed and predicted minimum flow

Paramalingam, *Dip.Tech.Dissertation, 1999, Massey University, Palmerston North, NZ*

Hoke and Chen force criteria

The Hartley and Murgatroyd (1964) model assumes that the wall shear force cancels the weight of the liquid above the dry patch. This is not true at high concentrations because Hoke and Chen (1992) relax this assumption by adding extra terms to incorporate wall shear and the weight. The film thickness and the minimum liquid loading equations of the Hartley and Murgatroyd model are modified to:

$$\sigma[1 - \cos(\theta)] = \frac{\rho.g}{4}\left[\frac{\delta}{1 - \cos(\theta)}\right]^2 [2.\theta - \sin(2.\theta)] + \frac{\rho^3.g^2.\delta^5}{15.\mu^2} \tag{C.25}$$

And $\quad \Gamma_{H\&C} = \frac{\rho^2.g.\delta^3}{3.\mu} \tag{C.26}$

The symbols are the same as for the Hartley and Murgatroyd equation. Figure C.7 shows the predicted flows using the Hoke and Chen (1992) model and the measured minimum flows.
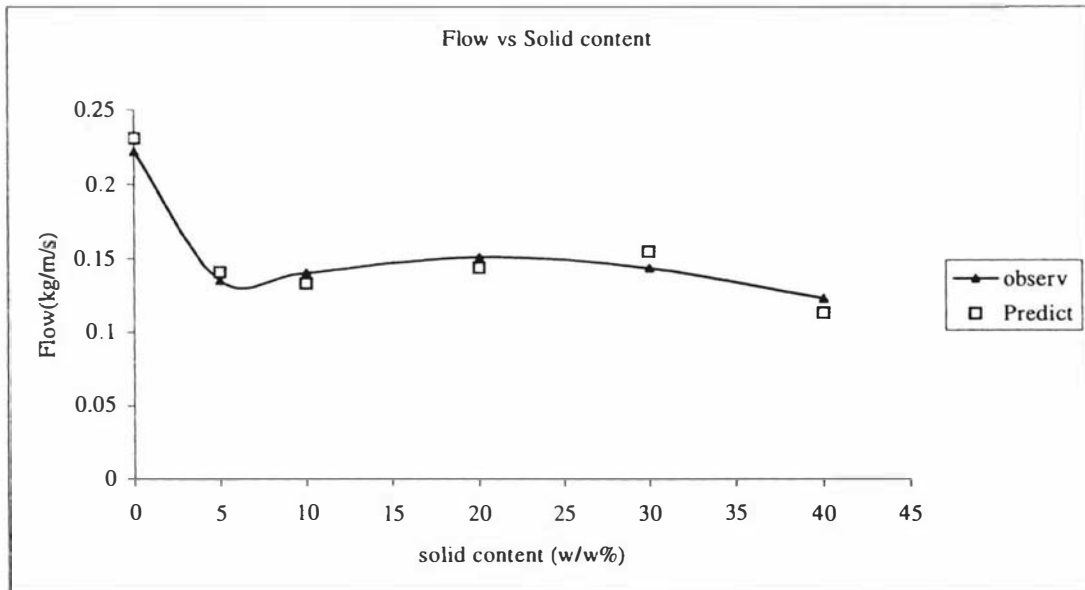
Figure C.7: Comparison of observed and predicted minimum flow

Winchester, PhD thesis, 2000, Massey University, Palmerston North, NZ

Appendix D: Evaporator Geometries

Evaporator Geometries
WPC

First Evaporator Pass				Third Evaporator Pass		
$L_1 =$	12 m	Length of evaporator tubes.		$L_3 =$	12 m	Length of evaporator tubes.
$D_1 =$	0.05 m	Diameter of evaporator tubes.		$D_3 =$	0.05 m	Diameter of evaporator tubes.
$n_1 =$	74	Number of evaporator tubes.		$n_3 =$	84	Number of evaporator tubes.
$np_1 =$	89	Number of distribution plate holes		$np_3 =$	92	Number of distribution plate holes
$dp_1 =$	0.0075 m	Diameter of distribution plate holes		$dp_3 =$	0.0075 m	Diameter of distribution plate holes
$P_1 =$	11.62 m	Perimeter of evaporator tubes		$P_3 =$	13.19 m	Perimeter of evaporator tubes
$As_1 =$	139.5 m^2	Surface area of evaporator tubes		$As_3 =$	158.3 m^2	Surface area of evaporator tubes
$Ah_1 =$	0.0039 m^2	Surface area of distribution plate holes		$Ah_3 =$	0.0041 m^2	Surface area of distribution plate holes
$Ad_1 =$	0.3350 m^2	Surface area of distribution plate		$Ad_3 =$	0.3848 m^2	Surface area of distribution plate
V	1.7436			V	1.9792	

Second Evaporator Pass.				Vacuum Condenser		
$L_2 =$	12 m	Length of evaporator tubes.		$L_c =$	24 m	Length of condenser tubes.
$D_2 =$	0.05 m	Diameter of evaporator tubes.		$n_c =$	18	Number of condenser tubes.
$n_2 =$	65	Number of evaporator tubes.		$D_c =$	0.030 m	Diameter of condenser tubes.
$np_2 =$	80	Number of distribution plate holes		V	0.305363	
$dp_2 =$	0.0075 m	Diameter of distribution plate holes				
$P_2 =$	10.21 m	Perimeter of evaporator tube s				
$As_2 =$	122.5 m^2	Surface area of evaporator tubes		Preheat condenser - 1,2,3- identical		
$Ah_2 =$	0.0035 m^2	Surface area of distribution plate holes		$L_c =$	18 m	Length of condenser tubes.
$Ad_2 =$	0.3011 m^2	Surface area of distribution plate		$n_c =$	6	Number of condenser tubes.
V	1.5315			$D_c =$	0.020 m	Diameter of condenser tubes.
				A	6.78672 m2	
				V	0.033929 m3	

Whey Products Evaporator Online Computer Tagnames

Tag	Units	Description
WPFT1001	M^3/hr	Evaporator feed flow
WPFT1001SP	M^3/hr	Evaporator feed flow set point
WPLT1002	%	Evaporator feed tank level
WPLT1002SP	%	Evaporator feed tank level set point
WPTT1011	°C	TVR first effect temperature
WPTT1005	°C	TVR second effect temperature
WPPT1004	kPa	TVR first effect shell pressure
WPDT1010	Kg/m^3	TVR product density
WPDT1010SP	Kg/m^3	TVR product density set point

Appendix E: Evaporator simulations

E.1 Physical properties

The Matlab codes shown below are to calculate the properties of the casein whey protein concentrates.

E.1.1 Density

```
Wf0=0;N=1000;Wf=0;Wi=(0.5-Wf0)/N;
for n=1:N,
    Wf=Wf0+Wi*n;
    wfn(n)=Wf;
T0=40;
xf=6/100;xl=7.5/100;xp=82.5/100;xs=4/100;
xcp=0.04*xp;xawp=(xp-xcp)*0.4;xbwp=(xp-xcp)*0.6;
Dw=1001.3-0.2423*T0-0.0004*T0^2;
Df=925.58-0.1553*T0;Dl=1599.1-0.31046*T0;
Ds=2800-0.28063*T0; Dap=1464.4-1.2103*T0;
Dbp=1378.1-1.1451*T0; Dcp=1317.3-0.4141*T0;
ats=1-Dw*xl/Dl-Dw*xcp/Dcp-Dw*xawp/Dap-Dw*xbwp/Dbp-Dw*xf/Df-Dw*xs/Ds;
y(n)=Dw/(1-ats*Wf);
n=n+1;
end
```

E.1.2 Viscosity

```
% viscosity of lactic whey concentrates
%at 1290 s-1 apply within 0.2 to 0.4% TS
% reason above 38% is maximum TS concentration
Wf0=0;
N=50;
Wf=0;
Wi=(0.42-Wf0)/N;
for n=1:N,
    %Wf=Wf0+Wi*n;
    wfn(n)=Wf;
T0=40;

%compositions
xf=4.5/100;xl=7.5/100;xp=83/100;xs=5/100;xcp=0.05*xp;xawp=(xp-
xcp)*0.3;xbwp=(xp-xcp)*0.7;

%density of solution
Dw=1001.3-0.2423*T0-0.0004*T0^2;
Df=925.58-0.1553*T0;
Dl=1599.1-0.31046*T0;
Ds=2800-0.28063*T0;
Dap=1464.4-1.2103*T0;
Dbp=1378.1-1.1451*T0;
Dcp=1317.3-0.4141*T0;
```

```
ats=1-Dw*xl/Dl-Dw*xcp/Dcp-Dw*xawp/Dap-Dw*xbwp/Dbp-Dw*xf/Df-Dw*xs/Ds;
Dsol=Dw/(1-ats*Wf);
ds(n)=Dsol;

%viscosity of lactose solution
wl=xl*Wf/(1-Wf+xl*Wf);
ll(n)=wl;
MuS=exp(0.326-0.0226*T0+0.0457*wl*100);
ls(n)=MuS;

%voluminosity-experimental
vcp=3.57*0.001;
vnwp=1.07*0.001;
vdwp=3.09*0.001;
vf=1.11*0.001;

vap=0.706*0.001;
vbp=0.751*0.001;

%maximum volume fraction
TSm=0.5; %  (w/w%)
Dm=1152; %kg/m3
FiM=((xcp*vcp+(xp-xcp)*vnwp)+xf*vf)*TSm*Dm;
fm(n)=FiM;

%volume fractions
FiCp=Wf*Dsol*xcp*vcp;
FiWdp=Wf*Dsol*(xp-xcp)*0.04*vdwp;

FiWnp=Wf*Dsol*(xp-xcp)*0.96*vnwp;
%FiWap=Wf*Dsol*(xp-xcp)*0.96*0.3*vap;
%FiWbp=Wf*Dsol*(xp-xcp)*0.96*0.7*vbp;
Fifat=Wf*Dsol*xf*vf;

FiT=(FiCp+FiWnp+FiWdp+Fifat);
%FiT=(FiCp+FiWap+FiWbp+FiWdp+Fifat);
ft(n)=FiT;

%Low shear
y(n)=MuS*(1+1.25*5*FiT/(1-FiT/FiM))^2;

n=n+1;
Wf=Wf0+Wi*n;
end
```

E.1.3 Thermal conductivity

```
Wf0=0;
N=1000;
Wf=0;
Wi=(0.5-Wf0)/N;
for n=1:N,
    Wf=Wf0+Wi*n;
    wfn(n)=Wf;
T0=10;
```

```
%xf=0.3/100;xl=0.2/100;xp=97.5/100;xs=2/100;xcp=0.04*xp;xawp=(xp-
xcp)*0.3;xbwp=(xp-xcp)*0.7;

%whole milk 0.79
xf=27.7/100;xl=38.4/100;xp=27.9/100;xs=6/100;xcp=0.8*xp;xawp=(xp-
xcp)*0.3;xbwp=(xp-xcp)*0.7;

%high fat denatur is 15 percentage
%high fat modified compositions- SHOULD PUT ACCURATE COMPOSITIONS FOR
BETTER PREDICTIONS 0.7
%xf=12/100;xl=7.5/100;xp=75/100;xs=5.5/100;xcp=0.041*xp;xawp=(xp-
xcp)*0.3;xbwp=(xp-xcp)*0.7;

%xf=15/100;xl=7.5/100;xp=72/100;xs=5.5/100;xcp=0.041*xp;xawp=(xp-
xcp)*0.3;xbwp=(xp-xcp)*0.7;

%lactic 0.7
%xf=6/100;xl=7.5/100;xp=82/100;xs=4.5/100;xcp=0.041*xp;xawp=(xp-
xcp)*0.3;xbwp=(xp-xcp)*0.7;

Dw=1001.3-0.2423*T0-0.0004*T0^2;

Df=925.58-0.1553;
Dl=1599.1-0.31046*T0;
Ds=2800-0.28063*T0;

Dap=1464.4-1.2103*T0;
Dbp=1378.1-1.1451*T0;
Dcp=1317.3-0.4141*T0;

ats=1-Dw*xl/Dl-Dw*xcp/Dcp-Dw*xawp/Dap-Dw*xbwp/Dbp-Dw*xf/Df-Dw*xs/Ds;
D=Dw/(1-ats*Wf);


Kw=0.5672+1.7e-3*T0-6e-6*T0^2;
Kf=0.1807+2.7604e-4*T0-1.7749e-7*T0^2;
Kl=0.2014+1.3874e-3*T0-4.3312e-6*T0^2;
Ks=0.3296+1.4011e-3*T0-2.9069e-6*T0^2;

Kap=0.2024-3e-4*T0;
Kbp=0.1997-3e-4*T0;
Kcp=0.1797-3e-4*T0;


Kts=Kcp*xcp/Dcp+Kap*xawp/Dap+Kbp*xbwp/Dbp+Kl*xl/Dl+Ks*xs/Ds+Kf*xf/Df-
Kw/Dw;

y(n)=D*(Kw/Dw+Kts*Wf);
n=n+1;
end
```

E.1.4 Specific heat capacity

```
Wf0=0;
N=1000;
Wf=0;
Wi=(0.5-Wf0)/N;
for n=1:N,
    Wf=Wf0+Wi*n;
    wfn(n)=Wf;
T0=40;

xf=6/100;xl=7.5/100;xp=82/100;xs=4.5/100;xcp=0.041*xp;xawp=(xp-
xcp)*0.3;xbwp=(xp-xcp)*0.7;

CPw=4226.6-2.4917*T0+3.54e-2*T0^2-1e-4*T0^3;
CPf=1932.2+4.6209*T0;
CPl=1256;
CPs=2930.1;

CPap=2630.3-2.4668*T0+0.0116*T0^2;
CPbp=2592.8-2.342*T0+0.0118*T0^2;
CPcp=2183.8-2.7901*T0+0.014*T0^2;


CPts=CPw-CPl*xl-CPap*xawp-CPbp*xbwp-CPcp*xcp-CPf*xf-CPs*xs;
y(n)=(CPw-CPts*Wf);
n=n+1;
end
```

E.2 Steady state simulations

The Matlab codes shown below are the whey evaporator complete steady state simulations.

E.2.1 Master file

```
%This file determines the steady state conditions of TVR Whey evaporator
%Inputs and constants are declared as global variables
global Ps Mf Wf Tf Ta CtoK Awater Bwater Cwater
global Avap Bvap Cvap LAMBDA RHO RHOO RHOT RHOTS
global Uel1 Ael1 Usl1 Asl1 Uel2 Ael2 Usl2 Asl2
global Avcon Vvcon Uvcon Mvccwi Tvccwi Tcons TTcons
global As1 As2 As3 Uo Uw Atvr Btvr Ctvr
global Upreh1 Upreh2 Upreh3 Apreh1 Apreh2 Apreh3 Uvcs Avcs
global Vpreh1 Vpreh2 Vpreh3 CPw CP ND Uphs1 Uphs2 Uphs3 Aphs1 Aphs2 Aphs3
global Te2
global Hsteam
Ps=9.6;%TVR steam pressure (bar)
Mf=2.75;%2.0625(7.5)1.788(6.5);%Mass    flow    of    feed    milk    to    the
evaporator(kg/s)
Tf=35;%Temperature of feed milk to the evaporator(oC)
Wf=0;%Feed total solids to the evaporator(w/w)
Ta=30;%Ambient temperature(oC)
Mvccwi=3.7;%Mass flow of coolant to the vacuum condenser(kg/s)
Tvccwi=17;%Temperature of coolant to the condenser(oC)
```

```
Te2=40;
Hsteam=(0.1219*Ps^3-3.3946*Ps^2+34.379*Ps+2648.2)*1000;


% Evaporator tubes geometry
% Number of tubes in each pass
Ntubes1=74;
Ntubes2=65;
Ntubes3=84;

% Diameter of tubes in each pass
Dtubes1=50/1000;
Dtubes2=50/1000;
Dtubes3=50/1000;

% Length of tubes in each pass
Ltubes1=12;
Ltubes2=12;
Ltubes3=12;

%Surface area of tubes for evaporation(m2)
As1=139.49;% calculate the average surface area based on inner and outer
diameter
As2=122.52;
As3=158.34;

% Number of distribution holes in each passes
Ndh1=89;
Ndh2=80;
Ndh3=102;

%Diameter of distribution holes
Ddh1=7.5/1000;
Ddh2=7.5/1000;
Ddh3=7.5/1000;

% Area of distribution holes{(pi*D^2/4)*Nh}m2 in each passes
Ah1=(3.14159*Ddh1^2/4)*Ndh1;
Ah2=(3.14159*Ddh2^2/4)*Ndh2;
Ah3=(3.14159*Ddh3^2/4)*Ndh3;

%Coefficient of discharge
Cd1=0.8;%depend on orifice size in distribution plate
Cd2=0.8;%same
Cd3=0.8;%same

% Diameter of evaporator column in each effect
%De01=1900/1000;
%De02=1200/1000;

%Diameter of the distribution plate
De01=0.950;
De02=0.6;
% Area of tube plate in each passes
Ad1=3.14159*De01^2/4*(Ndh1/(Ndh1+Ndh2));
Ad2=3.14159*De01^2/4*(Ndh2/(Ndh1+Ndh2));
Ad3=3.14159*De02^2/4;
```

```
% Constants in the model
CtoK=273.15;%conversion factor from celcius to kelvin
Awater=23.1748;
Bwater=3806.44;
Cwater=46.36;
Avap=10.5884;
Bvap=3680.109;
Cvap=41.6919;
LAMBDA=2340000;
ND=1.5;

% TVR compressor constants
%Atvr=2.129e-7;
%Btvr=58.434;
%Ctvr=0.971;

% HTC and losses areas
Uel1=10;%19.3;%should be corrected
Ael1=17.90115;
Uel2=17;%19.3;%should be corrected
Ael2=10.36679;
Usl1=13;%19.3;%should be corrected
Asl1=39.5892;
Usl2=10;%19.3;%shouldbe corrected
Asl2=31.29432;
Uphs1=17;%5;%should check
Aphs1=8.88;
Uphs2=10;%5;%should check
Aphs2=8.88;
Uphs3=13;%5;%should check
Aphs3=8.88;
Uvcs=17;%5;%should check
Avcs=12.35125;

% detail of preheat condenser
%Upreh1=1648;%should check
Apreh1=6.6954;
Vpreh1=0.033477;
%Upreh2=1648;%should check
Apreh2=6.6954;
Vpreh2=0.033477;
%Upreh3=1648;%should check
Apreh3=6.6954;
Vpreh3=0.033477;

% milk HTC parameters** have to incorporate the time and the milk
dependant factors
%Uo=2000;% should work on this
%Uw=-2360;%should do this as well

%density equations**** again deopend upon the milk type
%RHOO=1014;%should do
%RHOT=-0.5;%should do
%RHOTS=265;%should do

% Heat capacity
```

```
%CPw=4190;
%CP=4100;%should do
% detail of vacuum condenser
Uvcon=700;%should find
Avcon=40.72;%20.4423;%should check for other half of the tubes
Vvcon=0.15332;

%estimate the evap. temperatures of the evaporators
% these are the intial values for the estimationTe1s=52;

%for 40 Te2
Te1i=43;
Ts1i=48;

%for 44 Te2
%Te1i=46;
%Ts1i=55;

%options=optimset('MaxFunEvals',10000);

Yst=fsolve('wheyoptf',[Te1i Ts1i]);

Te1s=Yst(1);
Ts1s=Yst(2);

Te2s=Te2;

LAMBDAe1s=2.5132e+6-2.565e+3*Te1s;

% calculations
Ps1s=1e-5*exp(Awater-Bwater/(Ts1s+CtoK-Cwater));
Pe1s=1e-5*exp(Awater-Bwater/(Te1s+CtoK-Cwater));

% TVR compressor equations*** careful of the units here
Wcomp1s=LAMBDAe1s*44.37*ND^2*(Ps)^0.96/3600;%ND in cm and Ps in bar
Qfactors=0.37*exp(4.6*(log((Ps1s)/(Pe1s))/(log((Ps*100)/(Pe1s)))));%press
ures should be in KPa
Qcomp1s=Wcomp1s/Qfactors;


% preheat condensers

y1=phc1([Mf Wf Te2s Tf]);
Tprhc1s=y1(1);
htcph1s=y1(2);

y2=phc2([Mf Wf Te1s Tprhc1s]);
Tprhc2s=y2(1);
htcph2s=y2(2);

y3=phc3([Mf Wf Ts1s Tprhc2s]);
Tprhc3s=y3(1);
htcph3s=y3(2);
```

```
%put sensible heat or flash here
LAMBDAe1s=2.5132e+6-2.565e+3*Te1s;
CPf1s=cplw1([Wf Tprhc3s]);

if Tprhc3s<Te1s
   Sheats=Mf*CPf1s*(Te1s-Tprhc3s);
   Mflash1s=0;
else
   Mflash1s=Mf*CPf1s*(Tprhc3s-Te1s)/LAMBDAe1s;
   Sheats=0;
end

%new TS and flow after flash
Mfp1s=Mf-Mflash1s;
Wfp1s=Mf*Wf/Mfp1s;

y1=pass1([Mfp1s Wfp1s Te1s Ts1s]);
htc1=y1(1);
Mp1=y1(2);
Wp1=y1(3);
RTlf1=y1(4);
RTwlf11=y1(5);
RTwlf21=y1(6);


%recalculates the Wp and flow after sensible
Msheats=Sheats/LAMBDAe1s;
Mp1s=Mp1+Msheats;
%Wp1s=Mp1*Wp1/Mp1s;
Wp1s=Mf*Wf/Mp1s;
htc1s=htc1*(Mp1s-Mfp1s)/(Mp1s-Mfp1s);
Qshell1s=htc1s*As1*(Ts1s-Te1s);


y2=pass2([Mp1s Wp1s Te1s Ts1s]);
htc2s=y2(1);
Mp2s=y2(2);
Wp2s=y2(3);
RTlf2=y2(4);
RTwlf12=y2(5);
RTwlf22=y2(6);

Qshell2s=htc2s*As2*(Ts1s-Te1s);

%include the flash here
LAMBDAe2s=2.5132e+6-2.565e+3*Te2s;
CPf3s=cplw1([Wp2s Te1s]);

Mflash3s=Mp2s*CPf3s*(Te1s-Te2s)/LAMBDAe2s;
Mpf3s=Mp2s-Mflash3s;
%Wpf3=Mp2s*Wp2s/Mpf3;
Wpf3s=Mf*Wf/Mpf3s;

y3=pass3([Mpf3s Wpf3s Te2s Te1s]);
htc3s=y3(1);
Mp3s=y3(2);
Wp3s=y3(3);
```

```
RTlf3=y3(4);
RTwlf13=y3(5);
RTwlf23=y3(6);
Qshell3s=htc3s*As3*(Te1s-Te2s);

%vacuum condenser
Dw=1000;
CPw=4200;
tvcon=Dw*Vvcon/Mvccwi;
tfvcon=Dw*CPw*Vvcon/(Uvcon*Avcon);
Tvccwouts=Te2s-(Te2s-Tvccwi)*exp(-tvcon/tfvcon);

% Density of milk feed to each pass
Dmilk1=densitylw1([Wf Tprhc3s]);
Dmilk2=densitylw1([Wp1s Te1s]);
Dmilk3=densitylw1([Wp2s Te1s]);

% Height of liquid level above the distribution plate in each pass
hd1s=1/(2*9.81)*(Mf/(Dmilk1*Cd1*Ah1))^2;
hd2s=1/(2*9.81)*(Mp1s/(Dmilk2*Cd2*Ah2))^2;
hd3s=1/(2*9.81)*(Mp2s/(Dmilk3*Cd3*Ah3))^2;

% Mass of water evaporated in each pass
Mtubes1s=Qshell1s/LAMBDAe1s;
Mtubes2s=Qshell2s/LAMBDAe1s;
Mtubes3s=Qshell3s/LAMBDAe2s;

% Initial values assignments
Wfs=Wf;
Tfs=Tf;
Mfs=Mf;
Tvccwis=Tvccwi;


%energy flows
Qfeed1s=cplw1([Wf Tprhc3s])*Mf*(Tprhc3s-Te1s);
Qfeed3s=Mp2s*cplw1([Wp2s Te1s])*(Te1s-Te2s);
Qshelle1s=Qshell1s+Qshell2s;
Qshelle2s=Qshell3s;
Qpreh1s=Mf*cplw1([Wf Tf])*(Tprhc1s-Tf);
Qpreh2s=Mf*cplw1([Wf Tprhc1s])*(Tprhc2s-Tprhc1s);
Qpreh3s=Mf*cplw1([Wf Tprhc2s])*(Tprhc3s-Tprhc2s);
QlossE1s=((Uel1*Ael1)+(Usl2*Asl2)+(Uphs2*Aphs2))*(Te1s-Ta);
QlossS1s=((Usl1*Asl1)+(Uphs3*Aphs3))*(Ts1s-Ta);
QlossE2s=((Uel2*Ael2)+(Uphs1*Aphs1)+(Uvcs*Avcs))*(Te2s-Ta);
Wcomps=(Hsteam-CPw*Ts1s)*(Wcomp1s/LAMBDA);
Qcomps=Qcomp1s-((Qcomp1s/LAMBDA)*CPw*(Ts1s-Te1s));
%Qvcons=Mvccwi*CPw*(Tvccwouts-Tvccwi);
Qvcons=Qshelle2s-Qpreh1s;
```

E.2.2 Function files

Pass-1

```
function y1=pass1(x)

% all depend upon the temp. diff,  the mass flow and the fouling
coefficient
Mf0=x(1);%14.18;
Wf0=x(2);%0.12;
Tsv=x(3);%65;
Tss=x(4);%68.333;


Nt=74;
Ast=139.49;%surface area in the first pass
L=12;%length of tube
Kw=16.3;%conductivity of tube wall
tw=0.0015;%thickness of tube wall
Ac=3.142*(0.05)^2*74/4;
Dt=0.05;
Pmt=3.142*0.05*74;

LAMBDAe=2.5132e+6-2.565e+3*Tsv;%2343000;% latent heat of vapourisation
LAMBDAs=2.5132e+6-2.565e+3*Tss;%2336000;% latent heat of vapourisation

Dw=-0.0004*Tss^2-0.2423*Tss+1001.3;
Vw=(-9e-10*Tss^5+2e-7*Tss^4-2e-5*Tss^3+0.0013*Tss^2-
0.0597*Tss+1.8106)*0.001;
Kwt=-6e-6*Tss^2+0.0017*Tss+0.5672;
CPw=(-1e-7*Tss^3+4e-5*Tss^2-0.0025*Tss+4.2266)*1000;
STw=-0.0002*Tss+0.0778;


N=10;

Mp=Mf0;% mass flow (kg/s)
Wp=Wf0;%dry matter (w/w%)
Vwater=Vw; % viscosity of water (kg/m/s)
Dwater=Dw; % density of water (kg/m3)
Kwater=Kwt; % thermal conductivity of water(w/m.k)
CPwater=CPw;%heat capacity of water (J/kg.k)

% input variables declaration

TTlf=0;
TTwlf1=0;
TTwlf2=0;


Mevap=0;
Mcond=0.001;
HTC=0;
PDET=0;
PDECT=0;
BPECT=0;
drag=1.05;
```

```
SL=1;
dA=Ast/N;
dL=L/N;
%PDTE=0.5;
%PDTS=0.3;
BPE0=bpe([Wf0 Tsv]);
Ts=Tss;
Te=Tsv+BPE0;%  (Tef=Te+PD-BPE)0.5oC  increse  at  top  due  to  pressure  drop
and minus the BPE at the end of the tube

% loop for hi & ho calculations
    % Evaporation side heat transfer coefficient

    for SL=1:N,

        % Physical properties
    Vmilk=viscositylw2([Wp Te]);
    VM(SL)=Vmilk;
    Dmilk=densitylw1([Wp Te]);
    DM(SL)=Dmilk;
    Kmilk=conductlw1([Wp Te]);
    KM(SL)=Kmilk;
    CPmilk=cplw1([Wp Te]);
    CPM(SL)=CPmilk;
    STmilk=0.045;


    %Dimensionless calculations for milk
    Remilk=4*Mp/Pmt/Vmilk;
    REM(SL)=Remilk;
    %ReLWM=0.392*((STmilk/Dmilk/9.81)^0.5*(9.81*Dmilk/Vmilk)^(1/3))^0.75;
    %Prmilk=Vmilk*CPmilk/Kmilk; %put the equation
    %PRM(SL)=Prmilk;
    %ReWTM=5800*Prmilk^(-1.06);% put the equation
    %REWTM(SL)=ReWTM;
    HFmilk=(Vmilk^2/Dmilk^2/9.81)^(1/3)/Kmilk;

    %laminar
    %him=(1+drag/100)*(0.75*Remilk)^(-1/3)/HFmilk;
    %HIM(SL)=him;

    %wavy
    him=(1+drag/100)*0.822*(Remilk)^(-0.22)/HFmilk;
    HIM(SL)=him;


    %condensation side heat transfer coefficient

% dimensionless calculations for water
    Rewater=4*Mcond/Pmt/Vwater;
    STwater=0.072;

%ReLWW=0.392*((STwater/Dwater/9.81)^0.5*(9.81*Dwater/Vwater)^(1/3))^0.75;
    %Prwater=Vwater*CPwater/Kwater;
    %ReWTW=5800*Prwater^(-1.06);
    REW(SL)=Rewater;
    HFwater=(Vwater^2/Dwater^2/9.81)^(1/3)/Kwater;
```

```
    % conditions for h0 calculations
        %how=0.822*(Rewater)^(-0.22)/HFwater;
    %HOW(SL)=how;

    %how=(0.75*Rewater)^(-1/3)/HFwater;
    how=0.822*(Rewater)^(-0.22)/HFwater;
    HOW(SL)=how;

    % calculation of Twi and Two
% steam condensate range 1500-5000 and boiling organics 2500- fouling
coefficient
    if SL == 1
        Two=Ts;
        Twi=(Kw*Ts/tw+him*Te)/(him+Kw/tw);

%hov=1/((0.052*log(0.052/0.050)/2/Kw)+(0.052/0.050/him)+0.052/0.05/10
    %0000);%with a value for the ho
        hov=1/((0.052*log(0.052/0.050)/2/Kw)+(0.052/0.050/him));% no hi anf
fc value
    else
        Two=((how/him+how*tw/Kw)*Ts+Te)/(1+how*tw/Kw+how/him);
        Twi=Two-how*tw*(Ts-Two)/Kw;

%hov=1/(1/how+1/100000+(0.052*log(0.052/0.050)/2/Kw)+(0.052/0.050/him)+0.
052/0.05/100000);
        hov=1/(1/how+(0.052*log(0.052/0.050)/2/Kw)+(0.052/0.050/him));%   no
fc
    end

% overall heat transfer coefficient
    HOV1(SL)=hov;
    HTC=HTC+hov;
    dMevap=hov*dA*(Ts-Te)/LAMBDAe;
    dMcond=hov*dA*(Ts-Te)/LAMBDAs;
    Mp=Mp-dMevap;
    MPM1(SL)=Mp;
    Mevap=Mevap+dMevap;
    MEM(SL)=Mevap;
    Mcond=Mcond+dMcond;
    Wpp=Wp;
    Wp=Mf0*Wf0/Mp;
    WPM1(SL)=Wp;


    %residence time calculations
    %laminar film thickness
    FTlf=0.91*(4*Vmilk*Mp/Dmilk^2/9.81/Pmt)^(1/3);
    ftlf(SL)=FTlf;

    %wavy flow film thickness- theorey
    FTwlf1=0.8434*(4*Vmilk*Mp/Dmilk^2/9.81/Pmt)^(1/3);
    ftwlf1(SL)=FTwlf1;

    %wavy flow film thickness- exp
    FTwlf2=0.805*(4*Vmilk*Mp/Dmilk^2/9.81/Pmt)^(0.368);
    ftwlf2(SL)=FTwlf2;
```

```
%velocity
VLF=(Mp/3.1416/Dt/Dmilk/FTlf/Nt);
vlf(SL)=VLF;

VWLF1=(Mp/3.1416/Dt/Dmilk/FTwlf1/Nt);
vwlf1(SL)=VWLF1;

VWLF2=(Mp/3.1416/Dt/Dmilk/FTwlf2/Nt);
vwlf2(SL)=VWLF2;

%R.times
Tlf=dL/VLF;
TTlf=TTlf+Tlf;

Twlf1=dL/VWLF1;
TTwlf1=TTwlf1+Twlf1;

Twlf2=dL/VWLF2;
TTwlf2=TTwlf2+Twlf2;

    %vapour density
    Dvapour=exp(10.5884-(3680.109/(Te+273.17-41.6919)));
    Vvapour=1.07e-5;

    % evaporation side temp. modification
    % Boiling point elevation

    %BPEc=bpe([Wp Te])-bpe([Wpp Te]);
    BPEc=bpe([Wp Te])-bpe([Wpp Te]);

    BPe(SL)=bpe([Wp Te]);
    BPEC(SL)=BPEc;
    BPECT=BPECT+BPEc;
    BPET(SL)=BPECT;

    %pressure drop
    Vvelocity=Mevap/Dvapour/Ac;
    VV1(SL)=Vvelocity;
    drag=2.8662*Vvelocity;
    DRAG(SL)=drag;
    VD(SL)=drag;
    Rev=Dvapour*Vvelocity*Dt/Vvapour;
    REV(SL)=Rev;
    Fv=0.079/Rev^0.25;
    Vshear=0.5*Fv*Dvapour*Vvelocity^2;
    VS(SL)=Vshear;
    PDE=4*Vshear*dL/Dt;%pressure drop along dL distance( 10 times for
turbulent flow)
    PDET=PDET+PDE;
    PD(SL)=PDE;
    Pe=TtoP(Te);
    Tet=PtoT(Pe-PDE);
    PDEc=Te-Tet;
    PDEC(SL)=PDEc;
    PDECT=PDECT+PDEc;
```

```
    %effect temp
    Te=Te+BPEc-PDEc;
    TE(SL)=Te;
    sl(SL)=SL;
    SL=SL+1;
end
yf=HTC/N;
ys=Mp;
yt=Wp;
ylf=TTlf;
ywlf1=TTwlf1;
ywlf2=TTwlf2;

y1=[yf;ys;yt;ylf;ywlf1;ywlf2];
```

Pass-2
```
function y2=pass2(x)
% all depend upon the temp. diff,   the   mass   flow   and   the   fouling
coefficient
Mf0=x(1);%14.18;
Wf0=x(2);%0.12;
Tsv=x(3);%65;
Tss=x(4);%68.333;


Nt=65;
Ast=122.52;%surface area in the first pass
L=12;%length of tube
Kw=16.3;%conductivity of tube wall
tw=0.0015;%thickness of tube wall
Ac=3.142*(0.05)^2*65/4;
Dt=0.05;
Pmt=3.142*0.05*65;

LAMBDAe=2.5132e+6-2.565e+3*Tsv;%2343000;% latent heat of vapourisation
LAMBDAs=2.5132e+6-2.565e+3*Tss;%2336000;% latent heat of vapourisation

Dw=-0.0004*Tss^2-0.2423*Tss+1001.3;
Vw=(-9e-10*Tss^5+2e-7*Tss^4-2e-5*Tss^3+0.0013*Tss^2-
0.0597*Tss+1.8106)*0.001;
Kwt=-6e-6*Tss^2+0.0017*Tss+0.5672;
CPw=(-1e-7*Tss^3+4e-5*Tss^2-0.0025*Tss+4.2266)*1000;
STw=-0.0002*Tss+0.0778;


N=10;

Mp=Mf0;% mass flow (kg/s)
Wp=Wf0;%dry matter (w/w%)
Vwater=Vw; % viscosity of water (kg/m/s)
Dwater=Dw; % density of water (kg/m3)
Kwater=Kwt; % thermal conductivity of water(w/m.k)
CPwater=CPw;%heat capacity of water (J/kg.k)
```

```
% input variables declaration
TTlf=0;
TTwlf1=0;
TTwlf2=0;
Mevap=0;
Mcond=0.001;
HTC=0;
PDET=0;
PDECT=0;
BPECT=0;
drag=1.05;
SL=1;
dA=Ast/N;
dL=L/N;
%PDTE=0.5;
%PDTS=0.3;
BPE0=bpe([Wf0 Tsv]);
Ts=Tss;
Te=Tsv+BPE0;% (Tef=Te+PD-BPE)0.5oC increse at top due to pressure drop
and minus the BPE at the end of the tube

% loop for hi & ho calculations
    % Evaporation side heat transfer coefficient

    for SL=1:N,

    % Physical properties
    Vmilk=viscositylw2([Wp Te]);
    VM(SL)=Vmilk;
    Dmilk=densitylw1([Wp Te]);
    DM(SL)=Dmilk;
    Kmilk=conductlw1([Wp Te]);
    KM(SL)=Kmilk;
    CPmilk=cplw1([Wp Te]);
    CPM(SL)=CPmilk;
    STmilk=0.045;


    %Dimensionless calculations for milk
    Remilk=4*Mp/Pmt/Vmilk;
    REM(SL)=Remilk;
    %ReLWM=0.392*((STmilk/Dmilk/9.81)^0.5*(9.81*Dmilk/Vmilk)^(1/3))^0.75;
    %Prmilk=Vmilk*CPmilk/Kmilk; %put the equation
    %PRM(SL)=Prmilk;
    %ReWTM=5800*Prmilk^(-1.06);% put the equation
    %REWTM(SL)=ReWTM;
    HFmilk=(Vmilk^2/Dmilk^2/9.81)^(1/3)/Kmilk;

    %laminar
    %him=(1+drag/100)*(0.75*Remilk)^(-1/3)/HFmilk;
    %HIM(SL)=him;

    %wavy
    him=(1+drag/100)*0.822*(Remilk)^(-0.22)/HFmilk;
    HIM(SL)=him;
```

```
%condensation side heat transfer coefficient

% dimensionless calculations for water
   Rewater=4*Mcond/Pmt/Vwater;
   STwater=0.072;

%ReLWW=0.392*((STwater/Dwater/9.81)^0.5*(9.81*Dwater/Vwater)^(1/3))^0.75;
   %Prwater=Vwater*CPwater/Kwater;
   %ReWTW=5800*Prwater^(-1.06);
   REW(SL)=Rewater;
   HFwater=(Vwater^2/Dwater^2/9.81)^(1/3)/Kwater;

   % conditions for h0 calculations

   %how=0.822*(Rewater)^(-0.22)/HFwater;
   %HOW(SL)=how;

   %how=(0.75*Rewater)^(-1/3)/HFwater;
   how=0.822*(Rewater)^(-0.22)/HFwater;
   HOW(SL)=how;

% calculation of Twi and Two
% steam condensate range 1500-5000 and boiling organics 2500- fouling
coefficient
   if SL == 1
      Two=Ts;
      Twi=(Kw*Ts/tw+him*Te)/(him+Kw/tw);

%hov=1/((0.052*log(0.052/0.050)/2/Kw)+(0.052/0.050/him)+0.052/0.05/10
      %0000);%with a value for the ho
      hov=1/((0.052*log(0.052/0.050)/2/Kw)+(0.052/0.050/him));% no hi anf
fc value
   else
      Two=((how/him+how*tw/Kw)*Ts+Te)/(1+how*tw/Kw+how/him);
      Twi=Two-how*tw*(Ts-Two)/Kw;

%hov=1/(1/how+1/100000+(0.052*log(0.052/0.050)/2/Kw)+(0.052/0.050/him)+0.
052/0.05/100000);
      hov=1/(1/how+(0.052*log(0.052/0.050)/2/Kw)+(0.052/0.050/him));%   no
fc
   end
% overall heat transfer coefficient
   HOV1(SL)=hov;
   HTC=HTC+hov;
   dMevap=hov*dA*(Ts-Te)/LAMBDAe;
   dMcond=hov*dA*(Ts-Te)/LAMBDAs;
   Mp=Mp-dMevap;
   MPM1(SL)=Mp;
   Mevap=Mevap+dMevap;
   MEM(SL)=Mevap;
   Mcond=Mcond+dMcond;
   Wpp=Wp;
   Wp=Mf0*Wf0/Mp;
   WPM1(SL)=Wp;
```

```
%residence time calculations
%laminar film thickness
FTlf=0.91*(4*Vmilk*Mp/Dmilk^2/9.81/Pmt)^(1/3);
ftlf(SL)=FTlf;

%wavy flow film thickness- theorey
FTwlf1=0.8434*(4*Vmilk*Mp/Dmilk^2/9.81/Pmt)^(1/3);
ftwlf1(SL)=FTwlf1;

%wavy flow film thickness- exp
FTwlf2=0.805*(4*Vmilk*Mp/Dmilk^2/9.81/Pmt)^(0.368);
ftwlf2(SL)=FTwlf2;

%velocity

VLF=(Mp/3.1416/Dt/Dmilk/FTlf/Nt);
vlf(SL)=VLF;

VWLF1=(Mp/3.1416/Dt/Dmilk/FTwlf1/Nt);
vwlf1(SL)=VWLF1;

VWLF2=(Mp/3.1416/Dt/Dmilk/FTwlf2/Nt);
vwlf2(SL)=VWLF2;

%R.times
Tlf=dL/VLF;
TTlf=TTlf+Tlf;

Twlf1=dL/VWLF1;
TTwlf1=TTwlf1+Twlf1;

Twlf2=dL/VWLF2;
TTwlf2=TTwlf2+Twlf2;

    %vapour density
    Dvapour=exp(10.5884-(3680.109/(Te+273.17-41.6919)));
    Vvapour=1.07e-5;

    % evaporation side temp. modification
    % Boiling point elevation

    %BPEc=bpe([Wp Te])-bpe([Wpp Te]);
    BPEc=bpe([Wp Te])-bpe([Wpp Te]);

    BPe(SL)=bpe([Wp Te]);
    BPEC(SL)=BPEc;
    BPECT=BPECT+BPEc;
    BPET(SL)=BPECT;

    %pressure drop
    Vvelocity=Mevap/Dvapour/Ac;
    VV1(SL)=Vvelocity;
    drag=2.8662*Vvelocity;
    DRAG(SL)=drag;
    VD(SL)=drag;
    Rev=Dvapour*Vvelocity*Dt/Vvapour;
    REV(SL)=Rev;
```

327

```
   Fv=0.079/Rev^0.25;
   Vshear=0.5*Fv*Dvapour*Vvelocity^2;
   VS(SL)=Vshear;
   PDE=4*Vshear*dL/Dt;%pressure  drop  along  dL  distance(  10  times  for
turbulent flow)
   PDET=PDET+PDE;
   PD(SL)=PDE;
   Pe=TtoP(Te);
   Tet=PtoT(Pe-PDE);
   PDEc=Te-Tet;
   PDEC(SL)=PDEc;
   PDECT=PDECT+PDEc;

   %effect temp
   Te=Te+BPEc-PDEc;
   TE(SL)=Te;
   sl(SL)=SL;
   SL=SL+1;
end
yf=HTC/N;
ys=Mp;
yt=Wp;
ylf=TTlf;
ywlf1=TTwlf1;
ywlf2=TTwlf2;

y2=[yf;ys;yt;ylf;ywlf1;ywlf2];


Pass-3
function y3=pass3(x)

% all depend upon the temp. diff,   the  mass  flow  and  the  fouling
coefficient
Mf0=x(1);%14.18;
Wf0=x(2);%0.12;
Tsv=x(3);%65;
Tss=x(4);%68.333;


Nt=84;
Ast=158.34;%surface area in the first pass
L=12;%length of tube
Kw=16.3;%conductivity of tube wall
tw=0.0015;%thickness of tube wall
Ac=3.142*(0.05)^2*84/4;
Dt=0.05;
Pmt=3.142*0.05*84;

LAMBDAe=2.5132e+6-2.565e+3*Tsv;%2343000;% latent heat of vapourisation
LAMBDAs=2.5132e+6-2.565e+3*Tss;%2336000;% latent heat of vapourisation

Dw=-0.0004*Tss^2-0.2423*Tss+1001.3;
Vw=(-9e-10*Tss^5+2e-7*Tss^4-2e-5*Tss^3+0.0013*Tss^2-
0.0597*Tss+1.8106)*0.001;
Kwt=-6e-6*Tss^2+0.0017*Tss+0.5672;
CPw=(-1e-7*Tss^3+4e-5*Tss^2-0.0025*Tss+4.2266)*1000;
STw=-0.0002*Tss+0.0778;
```

```
N=10;
Mp=Mf0;% mass flow (kg/s)
Wp=Wf0;%dry matter (w/w%)
Vwater=Vw; % viscosity of water (kg/m/s)
Dwater=Dw; % density of water (kg/m3)
Kwater=Kwt; % thermal conductivity of water(w/m.k)
CPwater=CPw;%heat capacity of water (J/kg.k)

% input variables declaration

TTlf=0;
TTwlf1=0;
TTwlf2=0;
Mevap=0;
Mcond=0.001;
HTC=0;
PDET=0;
PDECT=0;
BPECT=0;
drag=1.05;
SL=1;
dA=Ast/N;
dL=L/N;
%PDTE=0.5;
%PDTS=0.3;
BPE0=bpe([Wf0 Tsv]);
Ts=Tss;
Te=Tsv+BPE0;% (Tef=Te+PD-BPE)0.5oC increse at top due to pressure drop
and minus the BPE at the end of the tube

% loop for hi & ho calculations
   % Evaporation side heat transfer coefficient

   for SL=1:N,

      % Physical properties
   Vmilk=viscpositylw2([Wp Te]);
   VM(SL)=Vmilk;
   Dmilk=densitylw1([Wp Te]);
   DM(SL)=Dmilk;
   Kmilk=conductlw1([Wp Te]);
   KM(SL)=Kmilk;
   CPmilk=cplw1([Wp Te]);
   CPM(SL)=CPmilk;
   STmilk=0.045;


   %Dimensionless calculations for milk
   Remilk=4*Mp/Pmt/Vmilk;
   REM(SL)=Remilk;
   %ReLWM=0.392*((STmilk/Dmilk/9.81)^0.5*(9.81*Dmilk/Vmilk)^(1/3))^0.75;
   %Prmilk=Vmilk*CPmilk/Kmilk; %put the equation
   %PRM(SL)=Prmilk;
   %ReWTM=5800*Prmilk^(-1.06);% put the equation
   %REWTM(SL)=ReWTM;
```

```
    HFmilk=(Vmilk^2/Dmilk^2/9.81)^(1/3)/Kmilk;

    %laminar
    %him=(1+drag/100)*(0.75*Remilk)^(-1/3)/HFmilk;
    %HIM(SL)=him;

    %wavy
    him=(1+drag/100)*0.822*(Remilk)^(-0.22)/HFmilk;
    HIM(SL)=him;


%condensation side heat transfer coefficient
% dimensionless calculations for water
    Rewater=4*Mcond/Pmt/Vwater;
    STwater=0.072;

%ReLWW=0.392*((STwater/Dwater/9.81)^0.5*(9.81*Dwater/Vwater)^(1/3))^0.75;
    %Prwater=Vwater*CPwater/Kwater;
    %ReWTW=5800*Prwater^(-1.06);
    REW(SL)=Rewater;
    HFwater=(Vwater^2/Dwater^2/9.81)^(1/3)/Kwater;

    % conditions for h0 calculations

    %how=0.822*(Rewater)^(-0.22)/HFwater;
    %HOW(SL)=how;

    %how=(0.75*Rewater)^(-1/3)/HFwater;
    how=0.822*(Rewater)^(-0.22)/HFwater;
    HOW(SL)=how;

    % calculation of Twi and Two
% steam condensate range 1500-5000 and boiling organics 2500- fouling
coefficient
    if SL == 1
       Two=Ts;
       Twi=(Kw*Ts/tw+him*Te)/(him+Kw/tw);

%hov=1/((0.052*log(0.052/0.050)/2/Kw)+(0.052/0.050/him)+0.052/0.05/10
    %0000);%with a value for the ho
       hov=1/((0.052*log(0.052/0.050)/2/Kw)+(0.052/0.050/him));% no hi anf
fc value
    else
       Two=((how/him+how*tw/Kw)*Ts+Te)/(1+how*tw/Kw+how/him);
       Twi=Two-how*tw*(Ts-Two)/Kw;

%hov=1/(1/how+1/100000+(0.052*log(0.052/0.050)/2/Kw)+(0.052/0.050/him)+0.
052/0.05/100000);
       hov=1/(1/how+(0.052*log(0.052/0.050)/2/Kw)+(0.052/0.050/him));%   no
fc
    end
% overall heat transfer coefficient
    HOV1(SL)=hov;
    HTC=HTC+hov;
    dMevap=hov*dA*(Ts-Te)/LAMBDAe;
    dMcond=hov*dA*(Ts-Te)/LAMBDAs;
    Mp=Mp-dMevap;
```

```
   MPM1(SL)=Mp;
   Mevap=Mevap+dMevap;
   MEM(SL)=Mevap;
   Mcond=Mcond+dMcond;              .
   Wpp=Wp;
   Wp=Mf0*Wf0/Mp;
   WPM1(SL)=Wp;


   %residence time calculations
   %laminar film thickness
   FTlf=0.91*(4*Vmilk*Mp/Dmilk^2/9.81/Pmt)^(1/3);
   ftlf(SL)=FTlf;

   %wavy flow film thickness- theorey
   FTwlf1=0.8434*(4*Vmilk*Mp/Dmilk^2/9.81/Pmt)^(1/3);
   ftwlf1(SL)=FTwlf1;

   %wavy flow film thickness- exp
   FTwlf2=0.805*(4*Vmilk*Mp/Dmilk^2/9.81/Pmt)^(0.368);
   ftwlf2(SL)=FTwlf2;

%velocity

VLF=(Mp/3.1416/Dt/Dmilk/FTlf/Nt);
vlf(SL)=VLF;

VWLF1=(Mp/3.1416/Dt/Dmilk/FTwlf1/Nt);
vwlf1(SL)=VWLF1;

VWLF2=(Mp/3.1416/Dt/Dmilk/FTwlf2/Nt);
vwlf2(SL)=VWLF2;

%R.times
Tlf=dL/VLF;
TTlf=TTlf+Tlf;

Twlf1=dL/VWLF1;
TTwlf1=TTwlf1+Twlf1;

Twlf2=dL/VWLF2;
TTwlf2=TTwlf2+Twlf2;

   %vapour density
   Dvapour=exp(10.5884-(3680.109/(Te+273.17-41.6919)));
   Vvapour=1.07e-5;

   % evaporation side temp. modification
   % Boiling point elevation

   %BPEc=bpe([Wp Te])-bpe([Wpp Te]);
   BPEc=bpe([Wp Te])-bpe([Wpp Te]);

   BPe(SL)=bpe([Wp Te]);
   BPEC(SL)=BPEc;
   BPECT=BPECT+BPEc;
   BPET(SL)=BPECT;
```

```
    %pressure drop
    Vvelocity=Mevap/Dvapour/Ac;
    VV1(SL)=Vvelocity;
    drag=2.8662*Vvelocity;
    DRAG(SL)=drag;
    VD(SL)=drag;
    Rev=Dvapour*Vvelocity*Dt/Vvapour;
    REV(SL)=Rev;
    Fv=0.079/Rev^0.25;
    Vshear=0.5*Fv*Dvapour*Vvelocity^2;
    VS(SL)=Vshear;
    PDE=4*Vshear*dL/Dt;%pressure  drop  along  dL  distance(  10  times  for
turbulent flow)
    PDET=PDET+PDE;
    PD(SL)=PDE;
    Pe=TtoP(Te);
    Tet=PtoT(Pe-PDE);
    PDEc=Te-Tet;
    PDEC(SL)=PDEc;
    PDECT=PDECT+PDEc;

    %effect temp
    Te=Te+BPEc-PDEc;
    TE(SL)=Te;
    sl(SL)=SL;
    SL=SL+1;
end
yf=HTC/N;
ys=Mp;
yt=Wp;
ylf=TTlf;
ywlf1=TTwlf1;
ywlf2=TTwlf2;

y3=[yf;ys;yt;ylf;ywlf1;ywlf2];
```

E.3 Control simulations

The Matlab codes shown below are the whey evaporator complete linear dynamic

simulations.

E.3.1 Master file

```
% THIS FILE DETERMINES THE TRANSFER FUNCTIONS FOR THE WPC TVR EVAPORATOR-
PRDUCT LACTIC WHEY
%variables declaration
global Awater Bwater Cwater CtoK LAMBDAs LAMBDA1 LAMBDA2 ND Psteam Tph1
Tf Wf Mf Tpc1 TTpc1 Tpc2 TTpc2 Tpc3 TTpc3 Uph2 Uph3 Aph2 Aph3 CPp
global U1 U2 U3 As1 As2 As3 Te2 Ta Uel1 Ael1 Usl1 Asl1 Uphs2 Aphs2 Uphs3
Aphs3 Hsteam
global Usl2 Asl2

% Input variables
Mf=2.167;                                                    %   Feed
to evaporator (kg/s)- 7.4m3/hr at 1054kg/m3
Wf=0.20;                                                     %   Feed
dry matter to evaporator (w/w)(feed density 1054kg/m3)
Tf=20;                                                       %   Feed
temperature  to  the  2nd  PHC  (current  value  and  will  change  after
modifications 20-25 C)
Psteam=10.6;                                                 %   Steam
supply pressure to evaporator (bar)

%Constants-Assumption
Ta=30;
Te2=40;


% Properties
Dpf=1054;
Dppc2=Dpf-3;
Dppc3=Dppc2-4;
CPp=3800;
CPw=4200;
Hsteam=(0.1219*Psteam^3-3.3946*Psteam^2+34.379*Psteam+2648.2)*1000;


% condensers
Vpc1=0.034;
Vpc2=0.034;
Vpc3=0.034;
Aph1=6.787;
Aph2=6.787;
Aph3=6.787;
Uph2=1000;           % to have flash with high viscous 300;
Uph3=1600;           % 600;
Uph1=300;

Tpc1=Vpc1*Dpf/Mf;
```

```
TTpc1=CPp*Dpf*Vpc1/(Uph1*Aph1);
TTpc2=CPp*Dppc2*Vpc2/(Uph2*Aph2);
Tpc2=Vpc2*Dppc2/Mf;
TTpc3=CPp*Dppc3*Vpc3/(Uph3*Aph3);
Tpc3=Vpc3*Dppc3/Mf;

% Evaporator passes
U1=2000;%650;
U2=800;
U3=500;%650;
As1=230;%139.49;
As2=135;%122.52;
As3=100;%158.34;

% HTC and losses areas
Uel1=10;
Ael1=17.9;
Usl1=13;
Asl1=39.6;
Uphs2=10;
Aphs2=8.88;
Uphs3=13;
Aphs3=8.88;
Usl2=10;
Asl2=31.29432;


%Constants
CtoK=273.15;
Awater=23.1748;
Bwater=3806.44;
Cwater=46.36;
LAMBDAs=2375000;
LAMBDA1=2400000;
LAMBDA2=2411000;
ND=1.5;

% Distribution plate
Ad1=0.335;
Ad2=0.3011;
Ad3=0.3848;
Ah1=0.0039;
Ah2=0.0035;
Ah3=0.0041;
Cd=0.8;
g=9.81;


% residence time
Tfd=75;%residence time from feed to 1st distribution plate
Tff1=27;%27residence time in the first pass
Tp1d2=30;% pumping delay between pass1 and 2nd distribution plate
Tff2=34;%34residence time in the 2nd pass
Tp2d3=30;%pumping delay between pass2 and 3rd distribution plate
Tff3=57;%57residence time in the 3rd pass
```

```
%Ted=200;%(maximum delay)
%Tp=20;

% DETERMINE THE EVAPORATOR STEADY STATE OPERATING CONDITIONS
x=fsolve('steadyop',[43,48]);
Te=x(1);
Ts=x(2);

%steady state operating conditions

Tph1=Te2-(Te2-Tf)*exp(-Tpc1/TTpc1);
Tph2=Te-(Te-Tph1)*exp(-Tpc2/TTpc2);
Tph3=Ts-(Ts-Tph2)*exp(-Tpc3/TTpc3);
Qph2=Uph2*Aph2*(Tph2-Tph1);
Qph3=Uph3*Aph3*(Tph3-Tph2);

Mflash1=Mf*CPp*(Tph3-Te)/LAMBDA1;
Md1=Mf-Mflash1;
Wd1=Mf*Wf/Md1;
Mtubes1=U1*As1*(Ts-Te)/LAMBDA1;
Mp1=Md1-Mtubes1;
Wp1=Mf*Wf/Mp1;

Md2=Mp1;
Wd2=Wp1;
Mtubes2=U2*As2*(Ts-Te)/LAMBDA1;
Mp2=Md2-Mtubes2;
Wp2=Mf*Wf/Mp2;

Mflash2=Mp2*CPp*(Te-Te2)/LAMBDA2;
Md3=Mp2-Mflash2;
Wd3=Mf*Wf/Md3;
Mtubes3=U3*As3*(Te-Te2)/LAMBDA2;
Mp3=Md3-Mtubes3;
Wp3=Mf*Wf/Mp3;

Dp1=densitylw1([Wd2 Te]);
Dp2=densitylw1([Wd3 Te2]);

hd1=1/(2*9.81)*(Md1/(Dppc3*Cd*Ah1))^2;
hd2=1/(2*9.81)*(Md2/(Dp1*Cd*Ah2))^2;
hd3=1/(2*9.81)*(Md3/(Dp2*Cd*Ah3))^2;


% DETERMINE THE LINEAR VERSIONS OF THE NON-LINEAR DIFFERENTIAL EQUATIONS

% TVR compressor linear constants
alpha1=(44.37*0.96*ND^2*(Hsteam-CPw*Ts))/3600;
alpha2=-(44.37*ND^2*CPw*(Psteam)^0.96/3600);

K0=(44.37*ND^2/3600/0.4)*(Hsteam-CPw*(Ts-Te))*(Psteam)^(-0.04);
K1b=(Ts+273.15-Cwater)*((Te+273.15-Cwater)*log(Psteam*10^5)-
Awater*(Te+273.15-Cwater)+Bwater);
K1=exp(-4.6*Bwater*(Ts-Te)/K1b);

beta1b=(Ts+273.15-Cwater)*((Te+273.15-Cwater)*log(Psteam*10^5)-
Awater*(Te+273.15-Cwater)+Bwater)^2;
```

335

```
beta1=K0*K1*(0.96+(4.6*Bwater*(Ts-Te)*(Te+273.15-Cwater))/beta1b);

K2=(44.37*ND^2/3600/0.4)*(Psteam)^0.96;
beta2b=((Te+273.15-Cwater)*log(Psteam*10^5)-Awater*(Te+273.15-
Cwater)+Bwater)*(Ts+273.15-Cwater)^2;
beta2=-K1*K2*(CPw+((Hsteam-CPw*(Ts-Te))*4.6*Bwater*((Ts+273.15-Cwater)-
(Ts-Te)))/beta2b);

K3t=(Ts-Te)*(log(Psteam*10^5)-Awater)+((Te+273.15-
Cwater)*log(Psteam*10^5)-Awater*(Te+273.15-Cwater)+Bwater);
K3b=((Te+273.15-Cwater)*log(Psteam*10^5)-Awater*(Te+273.15-
Cwater)+Bwater)^2;
K3=K3t/K3b;
beta3=K1*K2*(CPw+(Hsteam-CPw*(Ts-Te))*(4.6*Bwater*K3/(Ts+273.15-
Cwater)));


% Distribution plate linear coefficients
%1st plate
AHD1=(LAMBDA1-CPp*(Tph3-Te))/(Ad1*Dppc3*LAMBDA1);
AHD2=CPp*Mf/(LAMBDA1*Ad1*Dppc3);
AHD3=CPp*Mf/(LAMBDA1*Ad1*Dppc3);
Thd1=Md1*Ad1/((Cd*Ah1)^2*g*Dppc3);

Twd1o=Mf*Ad1/((Cd*Ah1)^2*2*g*Dppc3);
Twd1=Ad1*Dppc3*hd1/Mf;


%2nd plate
AHD4=1/(Ad2*Dp2);
Thd2=Md2*Ad2/((Cd*Ah2)^2*g*Dp1);
Twd2o=Mp1*Ad2/((Cd*Ah2)^2*2*g*Dp1);
Twd2=Ad2*Dp1*hd2/Mp1;


%3rd plate
AHD5=(LAMBDA2-CPp*(Te-Te2))/(Ad3*Dp2*LAMBDA2);
AHD6=CPp*Mp2/(LAMBDA2*Ad3*Dp2);
Thd3=Md3*Ad3/((Cd*Ah3)^2*g*Dp2);
Twd3o=Mp2*Ad3/((Cd*Ah3)^2*2*g*Dp2);
Twd3=Ad3*Dp2*hd3/Mp2;


%Evaporator shell linear coefficients
MIS=2.311*1e+6;%1.311*10e+6;
TTS=MIS/(beta2+alpha2-(U1*As1+U2*As2)-Usl1*Asl1);
a1=(beta1+alpha1)/MIS;a2=(beta3+U1*As1+U2*As2)/MIS;
a3=(-1/MIS);

% Evaporator effect linear coefficients
MIE=3.1033*1e+6;
TTE=MIE/(CPp*Mf+(U1*As1+U2*As2+U3*As3)+beta3+Uel1*Ael1);
b1=CPp*(Tph3-Te)/MIE;b2=(U1*As1+U2*As2-beta2)/MIE;
b3=(-beta1/MIE);b4=CPp*Mf/MIE;b5=(-1/MIE);

%Preheat condensers linear coefficients
Tpc1=Vpc1*Dpf/Mf;
```

```
TTpc1=CPp*Dpf*Vpc1/(Uph1*Aph1);
TTpc2=CPp*Dppc2*Vpc2/(Uph2*Aph2);
Tpc2=Vpc2*Dppc2/Mf;
TTpc3=CPp*Dppc3*Vpc3/(Uph3*Aph3);
Tpc3=Vpc3*Dppc3/Mf;
ACond1=-((Te2-Tf)*exp(-Tpc1/TTpc1))/Mf/TTpc1;
ACond2=-((Te-Tph1)*exp(-Tpc2/TTpc2))/Mf/TTpc2;
ACond3=-((Ts-Tph2)*exp(-Tpc3/TTpc3))/Mf/TTpc3;

%extra
WD1F=(Wf-Wd1+CPp*Wd1*(Tph3-Te)/LAMBDA1)/Mf;


%hd1 wd1 Ts Te Tph1 Tph2 Tph3 qph2 qph3 Tsd Ted Tph1d Tph2d

A=[(-1/Thd1) 0 0 AHD2 0 0 -AHD2 0 0 0 0 0 0;
   0 (-(LAMBDA1-CPp*(Tph3-Te))/LAMBDA1/Twd1) 0 (-CPp*Wd1/LAMBDA1/Twd1) 0
0 (CPp*Wd1/LAMBDA1/Twd1) 0 0 0 0 0 0;
   0 0 (1/TTS) a2 0 0 0 0 a3 0 0 0 0;
   0 0 b2 (-1/TTE) 0 0 b4 b5 0 0 0 0 0;
   0 0 0 0 (-1/TTpc1) 0 0 0 0 0 0 0 0;
   0 0 0 (1/Tpc2) 0 (-1/Tpc2) 0 0 0 0 (-exp(-Tpc2/TTpc2)/TTpc2) (exp(-
Tpc2/TTpc2)/TTpc2) 0;
   0 0 (1/TTpc3) 0 0 0 (-1/TTpc3) 0 0 (-exp(-Tpc3/TTpc3)/TTpc3) 0 0
(exp(-Tpc3/TTpc3)/TTpc3);
   0 0 (Uph2*Aph2*b2) (-Uph2*Aph2/TTE) 0 (Uph2*Aph2/Tpc2) (Uph2*Aph2*b4)
(Uph2*Aph2*b5-1/TTpc2) 0 0 0 (-Uph2*Aph2/Tpc2) 0;
   0  0  (Uph3*Aph3/TTS)  (Uph3*Aph3*a2)  0  0  (Uph3*Aph3/Tpc3)  0
(Uph3*Aph3*a3-1/TTpc3) 0 0 0 (-Uph3*Aph3/Tpc3);
   0 0 (2/Tpc3-1/TTS) -a2 0 0 0 0 -a3 (-2/Tpc3) 0 0 0;
   0 0 -b2 (2/Tpc2+1/TTE) 0 0 -b4 -b5 0 0 (-2/Tpc2) 0 0;
   0 0 0 0 (2/Tpc2+1/TTpc1) 0 0 0 0 0 0 (-2/Tpc2) 0;
   0 0 0 (-1/TTpc2) 0 (2/Tpc3+1/TTpc2) 0 0 0 0 (exp(-Tpc2/TTpc2)/TTpc2)
(-exp(-Tpc2/TTpc2)/TTpc2) (-2/Tpc3)];


% Psteam Mf Mfp1 Mfp1p2 Mfd wfd Tfp1

B=[0 0 0 0 AHD1 0 0;
   0 0 0 0 (WD1F/Twd1) (1/Twd1) 0;
   a1 0 0 0 0 0 0;
   b3 0 0 0 b1 0 0;
   0 ACond1 -ACond1 0 0 0 (exp(-Tpc1/TTpc1)/TTpc1);
   0 0 ACond2 -ACond2 0 0 0;
   0 0 0 ACond3 -ACond3 0 0;
   (Uph2*Aph2*b3) 0 0 0 (Uph2*Aph2*b1) 0 0;
   (Uph3*Aph3*a1) 0 0 0 0 0 0;
   -a1 0 0 0 0 0 0;
   -b3 -b1 0 0 0 0 0;
   0 -ACond1 ACond1 0 0 0 (-exp(-Tpc1/TTpc1)/TTpc1);
   0 0 -ACond2 ACond2 0 0 0];


% Md1(hd1) wd1 (Ts-Te) Te
C=[(Ad1*Dppc3/Thd1) 0 0 0 0 0 0 0 0 0 0 0 0;
```

```
       0  1  0  0  0  0  0  0  0  0  0  0  0;
       0  0  1 -1  0  0  0  0  0  0  0  0  0;
       0  0  0  1  0  0  0  0  0  0  0  0  0];


D=zeros(4,7);% out put no. of rows and input no. of colums
Gsys=ss(A,B,C,D);
%Gsys=minreal(TF(sys),0.001);

% transfer functions

%PASS-1
Gint=tf(1,[1 0]);
[NUM1 DEN1]=pade(Tff1,5);
sysp1=TF(NUM1, DEN1);
Gtubes1=(U1*As1/Tff1/LAMBDA1)*(1-sysp1)*Gint;
gama1=Wd1*Mtubes1/(Md1-Mtubes1)^2;gama2=Md1/(Md1-
Mtubes1);gama3=Md1*Wd1/(Md1-Mtubes1)^2;

H1=TF({1      0     -1;-gama1    gama2    gama3},{[1]      [1]      [1];[1]      [1]
[1]},'iodelay',[Tff1 0 0;Tff1 Tff1 0]);
sysH1=pade(H1,[],[],[1 0 0;1 1 0]);

%PASS-2
H21=TF({1 0;0  1},{[Thd2  1]   [1];[1]   [Twd2  1]},'iodelay',[Tp1d2  0  ;0
Tp1d2]);
Gc1=1;Gc2=1;
H21c=TF({1 0;0 1},{[Thd2 1] [1];[1] [Twd2 1]});

sysH21=pade(H21,[],[],[1 0;0 1]);
[NUM2 DEN2]=pade(Tff2,5);
sysp2=TF(NUM2, DEN2);
Gtubes2=(U2*As2/Tff2/LAMBDA1)*(1-sysp2)*Gint;
gama4=Wd2*Mtubes2/(Md2-Mtubes2)^2;gama5=Md2/(Md2-
Mtubes2);gama6=Md2*Wd2/(Md2-Mtubes2)^2;
H22=TF({1      0     -1;-gama4    gama5    gama6},{[1]      [1]      [1];[1]      [1]
[1]},'iodelay',[Tff2 0 0;Tff2 Tff2 0]);
H22c=TF({1 0 -1;-gama4 gama5 gama6},{[1] [1] [1];[1] [1] [1]});

sysH22=pade(H22,[],[],[1 0 0;1 1 0]);

%PASS-3
ff1=(LAMBDA2-CPp*Te+CPp*Te2)/LAMBDA2;ff2=-CPp*Mp2/LAMBDA2;
F1=((Wp2-Wd3)+CPp*(Te-Te2)*Wd3/LAMBDA2)/Mp2;F2=(1-CPp*(Te-
Te2)/LAMBDA2);F3=CPp*Wd3/LAMBDA2;F4=1;
H31=TF({ff1 0 ff2;F1 F4 F3},{[Thd3 1]   [1]   [Thd3 1];[Twd3 F2]   [Twd3 F2]
[Twd3 F2]},'iodelay',[Tp2d3 0 Tp2d3;Tp2d3 Tp2d3 0]);
Ge1=ff1;Ge2=ff2;Ge3=F1;Ge4=F4;Ge5=F3;
H31c=TF({ff1 0 ff2;F1 F4 F3},{[Thd3 1]   [1]   [Thd3 1];[Twd3 F2]   [Twd3 F2]
[Twd3 F2]});


sysH31=pade(H31,[],[],[1 0 1;1 1 0]);
[NUM3 DEN3]=pade(Tff3,5);
sysp3=TF(NUM3, DEN3);
Gtubes3=(U3*As3/Tff3/LAMBDA2)*(1-sysp3)*Gint;
```

```
gama7=Wd3*Mtubes3/(Md3-Mtubes3)^2;gama8=Md3/(Md3-
Mtubes3);gama9=Md3*Wd3/(Md3-Mtubes3)^2;
H32=TF({1     0     -1;-gama7     gama8     gama9},{[1]     [1]     [1];[1]     [1]
[1]},'iodelay',[Tff3 0 0;Tff3 Tff3 0]);
sysH32=pade(H32,[],[],[1 0 0;1 1 0]);

%feed delay--MAKE FEED DELAY ZERO TO GET THE TRUE RESPONSE Tfd=0
Hf=TF({1 0 0 0;0 1 0 0;0 1 0 0;0 1 0 0;0 1 0 0;0 0 1 0;0 0 0 1},{[1] [1]
[1] [1];[1]     [1]     [1]     [1];[1]     [1]     [1]     [1];[1]     [1]     [1]
[1];[1]     [1]     [1]     [1];[1]     [1]     [1]     [1]},'iodelay',[0 0 0 0;0 0 0 0;0 Tpc1 0
0;0 (Tpc1+Tpc2) 0 0;0 Tfd 0 0;0 0 Tfd 0;0 0 0 Tpc1]);
sysHf=pade(Hf,[],[],[1 0 0 0;0 1 0 0;0 1 0 0;0 1 0 0;0 1 0 0;0 0 1 0;0 0
0 1]);



%Cascade loop transfer functions- METHOD-2

% feed to pass3 (G3)
H1m=TF({1 0 -1},{[1] [1] [1]},'iodelay',[Tff1 0 0]);
sysH1m=pade(H1m,[1 0 0]);

H21m=TF({1;0},{[Thd2 1];[1]},'iodelay',[Tp1d2; 0]);
sysH21m=pade(H21m,[],[],[1;0]);



%Cascade loop transfer functions- METHOD-2

% feed to pass3 (G3)
Gtot=append(sysHf,Gsys,Gtubes1,sysH1m,sysH21m,Gtubes2,sysH22,sysH31,Gtube
s3,sysH32);
Qt=[5 1;6 2;7 3;8 4;9 5;10 6;11 7;12 10;13 8;14 9;15 12;16 13;17 10;18
14;19 15;20 16;21 17;22 18;23 11;24 11;25 19;26 20;27 21];
input=[1 2 3 4];
output=[22 23];
GtotC=minreal(connect(Gtot,Qt,input,output));

% feed to pass1(G1 and Gd)
Gp1=append(sysHf,Gsys,Gtubes1,sysH1);
Qp1=[5 1;6 2;7 3;8 4;9 5;10 6;11 7;12 10;13 8;14 9;15 12];
inp1=[1 2 3 4];
outp1=[13 14];
Gp1C=minreal(connect(Gp1,Qp1,inp1,outp1));

%pass1 to pass3(G2)
Gp1p2=append(sysHf,Gsys,sysH21,Gtubes2,sysH22,sysH31,Gtubes3,sysH32);
Qp1p2=[5 1;6 2;7 3;8 4;9 5;10 6;11 7;14 10;15 12;16 13;17 14;18 15;19
16;20 11;21 11;22 17;23 18;24 19];
inp1p2=[1 2 3 4 12 13];
outp1p2=[20 21];
Gp1p2C=minreal(connect(Gp1p2,Qp1p2,inp1p2,outp1p2));


%transfer functions
G1=Gp1C(2,1);%G1=wp1/Psteam
G2=Gp1p2C(2,6);%G2=Wp3/Wp1
G3=GtotC(2,1);%G3=Wp3/Psteam
```

```
Gd=Gp1C(2,3);%Gd=wp1/wf


%%CASCADE CONTROLLER DESIGN

%inner loop controller design

%Tintegral_i=25000;
Kp_i=85;%150;
C_i=Kp_i;%ss(TF(Kp_i*[1 1/Tintegral_i],[1 0]));

%Tintegral_i=2000;
%Kp_i=85;%150;
%C_i=ss(TF(Kp_i*[1 1/Tintegral_i],[1 0]));


L_i=C_i*G1;
figure(1);bode(G1)
figure(2);bode(L_i)
S_i=minreal(feedback(1,L_i));
figure(3);bode(S_i);
T_i=minreal(feedback(L_i,1));
figure(4);bode(T_i)
figure(5);time=[0:0.1:200]';step(T_i,time)
%figure(6);time=[0:0.1:200]';step(Gd*S_i,time)

%Gd=gama2*Gsys(2,6);
figure(6);time=[0:0.1:200]';step(Gd*S_i,time)


%outer loop controller design

G_o=minreal(C_i*S_i*(G1*G2+G3));
Gd_o=minreal(Gd*S_i*(G2-C_i*G3));
Tintegral_o=73;%165;%73;
Kp_o=0.3;%0.25;%0.65;
C_o=TF(Kp_o*[1 1/Tintegral_o],[1 0]);
L_o=C_o*G_o;
figure(7);bode(G_o);
figure(8);bode(L_o);
S_o=feedback(1,L_o);
figure(9);bode(S_o);
T_o=feedback(L_o,1);
figure(10);bode(T_o);
figure(11);time=[0:0.1:1000]';step(T_o,time);
figure(12);time=[0:0.1:1000]';step(Gd_o*S_o,time);

%SINGLE LOOP CONTROLLER DESIGN

G4=G3+G2*G1;
Tintegral=200;%160;
Kp=30;%40;
C=TF(Kp*[1 1/Tintegral],[1 0]);
L=C*G4;
figure(13);bode(G4);
figure(14);bode(L);
S=feedback(1,L);
```

```
figure(15);bode(S);
T=feedback(L,1);
figure(16);bode(T);
figure(17);time=[0:0.1:1000]';step(T,time);

Gd_single=Gd*G2;
figure(18);time=[0:0.1:1000]';step(Gd_single*S,time);

figure (19);step(Gd_o*S_o,'.',Gd_single*S,'--',time);
```

E.3.2 Function file

```
% function file to determine the steady state temperatures
function y=steadyop(x)

Te=x(1);
Ts=x(2);

% variable declarations
global Awater Bwater Cwater CtoK LAMBDAs LAMBDA1 LAMBDA2 ND Psteam Tph1
Tf Wf Mf Tpc1 TTpc1 Tpc2 TTpc2 Tpc3 TTpc3 Uph2 Uph3 Aph2 Aph3 CPp
global U1 U2 U3 As1 As2 As3 Te2 Ta Uel1 Ael1 Usl1 Asl1 Uphs2 Aphs2 Uphs3
Aphs3 Hsteam
global Usl2 Asl2



% TVR compressor equations
Ps=1e-5*exp(Awater-Bwater/(Ts+CtoK-Cwater));
Pe=1e-5*exp(Awater-Bwater/(Te+CtoK-Cwater));
Wcomp1=LAMBDAs*44.37*ND^2*(Psteam)^0.96/3600;
Qfactor=0.40*exp(4.6*(log((Ps)/(Pe))/(log((Psteam)/(Pe)))));
Qcomp1=Wcomp1/Qfactor;
Wcomp=(Hsteam-CPp*Ts)*(Wcomp1/LAMBDAs);
Qcomp=Qcomp1-((Qcomp1/LAMBDAs)*CPp*(Ts-Te));

% preheat condensers (2 and 3)
Tph1=Te2-(Te2-Tf)*exp(-Tpc1/TTpc1);
Tph2=Te-(Te-Tph1)*exp(-Tpc2/TTpc2);
Tph3=Ts-(Ts-Tph2)*exp(-Tpc3/TTpc3);

% product flow and dry matter calculations
Mevap1=U1*As1*(Ts-Te)/LAMBDA1;
Mevap2=U2*As2*(Ts-Te)/LAMBDA1;
Mevap3=U2*As3*(Te-Te2)/LAMBDA2;
Mp2=Mf-Mevap1-Mevap2;

%energy flows
Qshellp1=Mevap1*LAMBDA1;
Qshellp2=Mevap2*LAMBDA1;
Qshellp3=Mevap3*LAMBDA2;
Qfeed1=CPp*Mf*(Tph3-Te);
Qfeed3=Mp2*CPp*(Te-Te2);
Qshelle1=Qshellp1+Qshellp2;
Qshelle2=Qshellp3;
```

341

```
Qph2=Uph2*Aph2*(Tph2-Tph1);
Qph3=Uph3*Aph3*(Tph3-Tph2);
QlossE1=((Uel1*Ael1)+(Usl2*Asl2)+(Uphs2*Aphs2))*(Te-Ta);
QlossS1=((Usl1*Asl1)+(Uphs3*Aphs3))*(Ts-Ta);

% optimisation
y1=Qfeed1+Qshelle1-Qcomp-Qshelle2-Qph2-QlossE1;
y2=Qcomp+Wcomp-Qshelle1-Qph3-QlossS1;

y(1)=y1;
y(2)=y2;
```

E.3.3 Transfer functions

Out put from Ga

$$
\begin{bmatrix} M_d \\ w_d \\ (T_s - T_e) \\ T_e \end{bmatrix} = \begin{bmatrix} \dfrac{A_{d1}\rho_{d1}}{\tau_{hd1}} & 0 & 0 & 0 & 0 & 0 & 0 & 0 & 0 & 0 & 0 & 0 & 0 \\ 0 & 1 & 0 & 0 & 0 & 0 & 0 & 0 & 0 & 0 & 0 & 0 & 0 \\ 0 & 0 & 1 & -1 & 0 & 0 & 0 & 0 & 0 & 0 & 0 & 0 & 0 \\ 0 & 0 & 0 & 1 & 0 & 0 & 0 & 0 & 0 & 0 & 0 & 0 & 0 \end{bmatrix} \begin{bmatrix} h_{d1} \\ w_{d1} \\ T_s \\ T_e \\ T_{ph1} \\ T_{ph2} \\ T_{ph3} \\ q_{ph2} \\ q_{ph3} \\ T_{sd} \\ T_{ed} \\ T_{ph1d} \\ T_{ph2d} \end{bmatrix}
$$

Gtubes l

$$
\frac{M_{tubes1}(s)}{(T_s - T_e)(s)} = \left(\frac{U_{s1} A_{s1}}{\tau_{p1} \lambda_1} \right) \left[\frac{1 - e^{-\tau_{p1} \cdot s}}{\tau_{p1} \cdot s} \right]
$$

System Gb

$$\begin{bmatrix} M_{p1}(s) \\ w_{p1}(s) \end{bmatrix} = \begin{bmatrix} e^{-\tau_{p1}s} & 0 & -1 \\ -\gamma_1 e^{-\tau_{p1}s} & \gamma_2 e^{-\tau_{p1}s} & \gamma_3 \end{bmatrix} \begin{bmatrix} M_{d1}(s) \\ w_{d1}(s) \\ M_{tubes1}(s) \end{bmatrix}$$

System Gc

$$\begin{bmatrix} M_{d2}(s) \\ w_{d2}(s) \end{bmatrix} = \begin{bmatrix} \dfrac{e^{-\tau_{p1d2}s}}{(\tau_{hd2}s+1)} & 0 \\ 0 & \dfrac{e^{-\tau_{p1d2}s}}{(\tau_{wd2}s+1)} \end{bmatrix} \begin{bmatrix} M_{p1}(s) \\ w_{p1}(s) \end{bmatrix}$$

Gtubes2

$$\frac{M_{tubes2}(s)}{(T_s - T_e)(s)} = \left(\frac{U_{s2} A_{s2}}{\tau_{p2} \lambda_1} \right) \left[\frac{1 - e^{-\tau_{p2} \cdot s}}{\tau_{p2} \cdot s} \right]$$

System Gd

$$\begin{bmatrix} M_{p2}(s) \\ w_{p2}(s) \end{bmatrix} = \begin{bmatrix} e^{-\tau_{p2}s} & 0 & -1 \\ -\gamma_4 e^{-\tau_{p2}s} & \gamma_5 e^{-\tau_{p2}s} & \gamma_6 \end{bmatrix} \begin{bmatrix} M_{d2}(s) \\ w_{d2}(s) \\ M_{tubes2}(s) \end{bmatrix}$$

System Ge

Let,

$$F_1 = \frac{w_{p2}^o - w_{d3}^o + \dfrac{Cp_p w_{d3}^o (T_e^o - T_{e2})}{\lambda_2}}{M_{p2}^o}, \; F_2 = 1 - \frac{Cp_p (T_e^o - T_{e2})}{\lambda_2}, \; F_3 = \frac{Cp_p w_{d3}^o}{\lambda_2}$$

$$
\begin{bmatrix} M_{d3}(s) \\ w_{d3}(s) \end{bmatrix} = \begin{bmatrix} \dfrac{\left(\lambda_2 - CP_{p2}\left(T_e^o - T_{e2}\right)\right)e^{-\tau_{p2d3}s}}{\lambda_2\left(\tau_{hd3}s+1\right)} & 0 & \dfrac{-CP_{p2}M_{p2}^o}{\lambda_2\left(\tau_{hd3}s+1\right)} \\ \dfrac{F_1 \cdot e^{-\tau_{p2d3}s}}{\left(\tau_{wd3}s+F_2\right)} & \dfrac{e^{-\tau_{p2d3}s}}{\left(\tau_{wd3}s+F_2\right)} & \dfrac{F_3}{\left(\tau_{wd3}s+F_2\right)} \end{bmatrix} \begin{bmatrix} M_{p2}(s) \\ w_{p2}(s) \\ T_e(s) \end{bmatrix}
$$

Gtubes3

$$
\frac{M_{tubes3}(s)}{T_e(s)} = \left(\frac{U_{s3}A_{s3}}{\tau_{p3}\lambda_2}\right)\frac{\left[1-e^{-\tau_{p3}\cdot s}\right]}{\tau_{p3}\cdot s}
$$

$$
\begin{bmatrix} M_{p3}(s) \\ w_{p3}(s) \end{bmatrix} = \begin{bmatrix} e^{-\tau_{p3}s} & 0 & -1 \\ -\gamma_7 e^{-\tau_{p3}s} & \gamma_8 e^{-\tau_{p3}s} & \gamma_9 \end{bmatrix} \begin{bmatrix} M_{d3}(s) \\ w_{d3}(s) \\ M_{tubes3}(s) \end{bmatrix}
$$

Three pass- Linear dynamic model of TVR evaporator $\left(T_{e2}^{st} = T_{e2}\ \text{and}\ P_{steam}^{st} = P_{steam}\right)$

$$
\begin{bmatrix}
\dot h_{d1} \\ \dot w_{d1} \\ \dot T_s \\ \dot T_e \\ \dot T_{ph1} \\ \dot T_{ph2} \\ \dot T_{ph3} \\ \dot q_{ph2} \\ \dot q_{ph3} \\ \dot T_{sd} \\ \dot T_{ed} \\ \dot T_{ph1d} \\ \dot T_{ph2d}
\end{bmatrix}
=
\begin{bmatrix}
\frac{-1}{\tau_{hd1}} & 0 & 0 & \frac{Cp_p M_f^o}{\lambda_1 A_{d1}\rho_{d1}} & 0 & 0 & \frac{-Cp_p M_f^o}{\lambda_1 A_{d1}\rho_{d1}} & 0 & 0 & 0 & 0 & 0 & 0 \\[6pt]
0 & \frac{-\left(\lambda_1 - Cp_p\left(T_{ph3}^o - T_{e1}^o\right)\right)}{\lambda_1 \tau_{wd1}} & 0 & \frac{-Cp_p w_{d1}^o}{\lambda_1 \tau_{wd1}} & 0 & 0 & \frac{Cp_p w_{d1}^o}{\lambda_1 \tau_{wd1}} & 0 & 0 & 0 & 0 & 0 & 0 \\[6pt]
0 & 0 & \frac{1}{\tau_{TS}} & a_2 & 0 & 0 & 0 & 0 & a_3 & 0 & 0 & 0 & 0 \\[6pt]
0 & 0 & b_2 & \frac{-1}{\tau_{Te1}} & 0 & 0 & b_4 & b_5 & 0 & 0 & 0 & 0 & 0 \\[6pt]
0 & 0 & 0 & 0 & \frac{-1}{\tau_{TPC1}} & 0 & 0 & 0 & 0 & 0 & 0 & 0 & 0 \\[6pt]
0 & 0 & 0 & \frac{1}{\tau_{TPC2}} & 0 & \frac{-1}{\tau_{TPC2}} & 0 & 0 & 0 & 0 & \frac{-e^{\left(\frac{-\tau_{PC2}}{\tau_{TPC2}}\right)}}{\tau_{TPC2}} & \frac{e^{\left(\frac{-\tau_{PC2}}{\tau_{TPC2}}\right)}}{\tau_{TPC2}} & 0 \\[8pt]
0 & 0 & \frac{1}{\tau_{TPC3}} & 0 & 0 & 0 & \frac{-1}{\tau_{TPC3}} & 0 & 0 & \frac{-e^{\left(\frac{-\tau_{PC3}}{\tau_{TPC3}}\right)}}{\tau_{TPC3}} & 0 & 0 & \frac{e^{\left(\frac{-\tau_{PC3}}{\tau_{TPC3}}\right)}}{\tau_{TPC3}} \\[8pt]
0 & 0 & U_{ph2}A_{ph2}b_2 & \frac{-U_{ph2}A_{ph2}}{\tau_{Te1}} & 0 & \frac{U_{ph2}A_{ph2}}{\tau_{PC2}} & U_{ph2}A_{ph2}b_4 & \left(U_{ph2}A_{ph2}b_5 - \frac{1}{\tau_{TPC2}}\right) & 0 & 0 & 0 & \frac{-U_{ph2}A_{ph2}}{\tau_{PC2}} & 0 \\[8pt]
0 & 0 & \frac{U_{ph3}A_{ph3}}{\tau_{TS}} & U_{ph3}A_{ph3}a_2 & 0 & 0 & \frac{U_{ph3}A_{ph3}}{\tau_{PC3}} & 0 & \left(U_{ph3}A_{ph3}a_3 - \frac{1}{\tau_{TPC3}}\right) & 0 & 0 & 0 & \frac{-U_{ph3}A_{ph3}}{\tau_{PC3}} \\[8pt]
0 & 0 & \left(\frac{2}{\tau_{PC3}} - \frac{1}{\tau_{TS}}\right) & -a_2 & 0 & 0 & 0 & 0 & -a_3 & \frac{-2}{\tau_{PC3}} & 0 & 0 & 0 \\[8pt]
0 & 0 & -b_2 & \left(\frac{2}{\tau_{PC2}} + \frac{1}{\tau_{Te1}}\right) & 0 & 0 & -b_4 & -b_5 & 0 & 0 & \frac{-2}{\tau_{PC2}} & 0 & 0 \\[8pt]
0 & 0 & 0 & 0 & \left(\frac{2}{\tau_{PC2}} + \frac{1}{\tau_{TPC1}}\right) & 0 & 0 & 0 & 0 & 0 & 0 & \frac{-2}{\tau_{PC2}} & 0 \\[8pt]
0 & 0 & 0 & \frac{-1}{\tau_{TPC2}} & 0 & \left(\frac{2}{\tau_{PC3}} + \frac{1}{\tau_{TPC2}}\right) & 0 & 0 & 0 & 0 & \frac{e^{\left(\frac{-\tau_{PC2}}{\tau_{TPC2}}\right)}}{\tau_{TPC2}} & \frac{-e^{\left(\frac{-\tau_{PC2}}{\tau_{TPC2}}\right)}}{\tau_{TPC2}} & \frac{-2}{\tau_{PC3}}
\end{bmatrix}
\begin{bmatrix}
h_{d1} \\ w_{d1} \\ T_s \\ T_e \\ T_{ph1} \\ T_{ph2} \\ T_{ph3} \\ q_{ph2} \\ q_{ph3} \\ T_{sd} \\ T_{ed} \\ T_{ph1d} \\ T_{ph2d}
\end{bmatrix}
$$

$$
+ \begin{bmatrix}
0 & 0 & 0 & 0 & \dfrac{\lambda_1 - C_{p_p}\left(T_{ph3}^o - T_{e1}^o\right)}{\lambda_1 A_{d1}\rho_{d1}} & 0 & 0 \\[3ex]
0 & 0 & 0 & 0 & \dfrac{\lambda_1\left(w_f^o - w_{d1}^o\right) + C_{p_p}w_{d1}^o\left(T_{ph3}^o - T_{e1}^o\right)}{M_f^o \lambda_1 \tau_{wd1}} & \dfrac{1}{\tau_{wd1}} & 0 \\[3ex]
a_1 & 0 & 0 & 0 & 0 & 0 & 0 \\[1ex]
b_3 & 0 & 0 & 0 & b_1 & 0 & 0 \\[1ex]
0 & \dfrac{-\left(T_{e2}-T_f^o\right)e^{\left(\frac{-\tau_{PC1}}{\tau_{TPC1}}\right)}}{M_f^o \tau_{TPC1}} & \dfrac{\left(T_{e2}-T_f^o\right)e^{\left(\frac{-\tau_{PC1}}{\tau_{TPC1}}\right)}}{M_f^o \tau_{TPC1}} & 0 & 0 & 0 & \dfrac{e^{\left(\frac{-\tau_{PC1}}{\tau_{TPC1}}\right)}}{\tau_{TPC1}} \\[3ex]
0 & 0 & \dfrac{-\left(T_e^o - T_{ph1}^o\right)e^{\left(\frac{-\tau_{PC2}}{\tau_{TPC2}}\right)}}{M_f^o \tau_{TPC2}} & \dfrac{\left(T_e^o - T_{ph1}^o\right)e^{\left(\frac{-\tau_{PC2}}{\tau_{TPC2}}\right)}}{M_f^o \tau_{TPC2}} & 0 & 0 & 0 \\[3ex]
0 & 0 & 0 & \dfrac{-\left(T_s^o - T_{ph2}^o\right)e^{\left(\frac{-\tau_{PC3}}{\tau_{TPC3}}\right)}}{M_f^o \tau_{TPC3}} & \dfrac{\left(T_s^o - T_{ph2}^o\right)e^{\left(\frac{-\tau_{PC3}}{\tau_{TPC3}}\right)}}{M_f^o \tau_{TPC3}} & 0 & 0 \\[3ex]
U_{ph2}A_{ph2}b_3 & 0 & 0 & 0 & U_{ph2}A_{ph2}b_1 & 0 & 0 \\[1ex]
U_{ph3}A_{ph3}a_1 & 0 & 0 & 0 & 0 & 0 & 0 \\[1ex]
-a_1 & 0 & 0 & 0 & 0 & 0 & 0 \\[1ex]
-b_3 & -b_1 & 0 & 0 & 0 & 0 & 0 \\[1ex]
0 & \dfrac{\left(T_{e2}-T_f^o\right)e^{\left(\frac{-\tau_{PC1}}{\tau_{TPC1}}\right)}}{M_f^o \tau_{TPC1}} & \dfrac{-\left(T_{e2}-T_f^o\right)e^{\left(\frac{-\tau_{PC1}}{\tau_{TPC1}}\right)}}{M_f^o \tau_{TPC1}} & 0 & 0 & 0 & \dfrac{-e^{\left(\frac{-\tau_{PC1}}{\tau_{TPC1}}\right)}}{\tau_{TPC1}} \\[3ex]
0 & 0 & \dfrac{\left(T_e^o - T_{ph1}^o\right)e^{\left(\frac{-\tau_{PC2}}{\tau_{TPC2}}\right)}}{M_f^o \tau_{TPC2}} & \dfrac{-\left(T_e^o - T_{ph1}^o\right)e^{\left(\frac{-\tau_{PC2}}{\tau_{TPC2}}\right)}}{M_f^o \tau_{TPC2}} & 0 & 0 & 0
\end{bmatrix}
\begin{bmatrix}
P_{steam} \\ M_f \\ M_{fp1} \\ M_{fp1p2} \\ M_{fd} \\ w_{fd} \\ T_{fp1}
\end{bmatrix}
$$